2019

Deciphering the receptor kinase FERONIA: Functions and underlying mechanisms

Hongqing Guo
Iowa State University

Deciphering the receptor kinase FERONIA: Functions and underlying mechanisms

by

Hongqing Guo

A dissertation submitted to the graduate faculty

in partial fulfillment of the requirement for the degree of

DOCTOR OF PHILOSOPHY

Major: Genetics

Program of Study Committee:
Jo Anne Powell-Coffman, Co-major Professor
Steve A. Whitham, Co-major Professor
Gwyn A. Beattie
Drena L. Dobbs
Patrick S. Schnable

The student author, whose presentation of the scholarship herein was approved by the program of study committee, is solely responsible for the content of this dissertation.
The Graduate College will ensure this dissertation is globally accessible and will not permit alterations after a degree is conferred.

Iowa State University

Ames, Iowa

2019

TABLE OF CONTENTS

ACKNOWLEDGMENTS

I would like to thank my major professors, Prof. Jo Anne Powell-Coffman and Prof. Steve Whitham, and my POS Committee members, Prof. Gwyn Beattie, Prof. Drena Dobbs and Prof. Patrick Schnable. Thank you for your encouragement and guidance.

I want to thank the past and current members in the Yin Lab. Jiani Chen, Zhouli Xie, Trevor Nolan, Hao Jiang, Ping Wang and Sean McLaughlin, the undergraduate assistant and soon-to-be IG2 graduate student. The lab is like a second home for me, and you guys have made it warm and very much livable.

A special thank you to Yanhai Yin for providing resources for my research. You have made this journey fun and enjoyable.

I also want to thank the collaborators, Sanzhen Liu and Patrick Schnable from the Schnable lab in the Department of Agronomy and the Plant Science Institute, Rebecca Hansen and Young-Jin Lee from the Lee lab in the Department of Chemistry, Gaoyuan Song, Christian Montes-Serey and Justin Walley from the Walley lab in the Department of Plant Pathology, Ching-Yi Liao and Diane Bassham from the Bassham lab from the Department of GDCB.

A special thank you to Linda Wild. Thank you for all your help through the years. You are one of the most dedicated and hardest working people I have ever met.

This journey would not be possible without my children on board. Thank you Peter Yin and Kimberly Yin for your love and inspiration. You are kind, loving, strong and independent. I am so proud of the very persons you have become!

Lastly, I want to thank my parents who have just celebrated their 90th Birthdays. Happy Birthday, Mom and Dad! This is for you. Decades later and one ocean away today, I still agree with my Dad on this one: “the sky’s the limit!”

ABSTRACT

FERONIA, a plasmamembrane-localized receptor kinase, is expressed ubiquitously except for in the pollen tube, and plays vital roles in many aspects of a plant's life. Loss-of-function *fer* mutant displays stunted growth, altered biotic and abiotic stress responses and compromised female fertility. In the past decade, ligands, co-receptors, and many signaling components have been identified to shine light on the regulatory mechanisms. However, a comprehensive signaling network underlying FER-mediated diverse processes is still lacking.

To this end, and also to facilitate the discovery of novel FER-mediated pathways, we carried out transcriptomic, proteomic and phosphoproteomic analyses. From the transcriptome analysis, we discovered that FER is a major negative regulator of plant hormone Jasmonic acid (JA) signaling, and the G-box binding site for MYC2, a major transcription factor (TF) and positive regulator in the JA pathway, is enriched in the promoters of FER-regulated genes. Further genetics, biochemistry and cell biology experiments reveal that FER phosphorylates and destabilizes MYC2 to inhibit JA signaling and MYC2-mediated host plant susceptibility, which establishes FER as a positive regulator in bacterial pathogen defense. RALF23, a rapid alkalization factor and a peptide ligand for FER, functions through FER to negatively contribute to bacterial defense.

The Gene Ontology analysis of the proteome validates previous findings such as negative regulation of FER on JA and Abscisic acid (ABA) pathways, and supports a role of FER in maintaining nutrient and energy homeostasis. The phosphoproteomics data analysis identified a group of TFs that potentially carry out diverse functions, including Brassinosteroid (BR)-regulated growth and ABA-mediated stress responses.

The omics data analysis has revealed two novel FER-mediated processes, ER body formation and autophagy. FER negatively regulates ER body formation likely through the ER body TF NAI1 and ER body-associated protein NAIP2. FER also negatively regulates autophagy likely by functioning in a complex with heterotrimeric SnRK1 kinase and TOR kinase. SnRK1 positively and TOR negatively regulate autophagy at the early induction stage. FER inhibits SnRK1 likely by phosphorylating and destabilizing the SnRK1 regulatory subunit KINβ1, and activates TOR likely through the activation of a small GTPase, ROP2.

The dissertation research establishes FERONIA receptor kinase as a positive regulator in bacterial defense and provides a ligand-receptor-transcription factor (RALF23-FER-MYC2) signaling module as the underlying molecular mechanism. Further studies on FER and the newly identified candidate substrate TFs will provide new insights into the molecular interplay of many FER-mediated processes. The discovery of the two novel FER-mediated pathways, ER body formation and autophagy, will further expand our understanding of how FERONIA, a plasmamembrane-localized receptor kinase, regulates diverse biological processes through a plant's life.

CHAPTER 1

GENERAL INTRODUCTION

FERONIA MEDIATES PLANT GROWTH DEVELOPMENT AND STRESS RESPONSES

1.1 Overview of FER and Family Members

FERONIA (FER), named after the Etruscan goddess of fertility, is a CrRLK1 (*Catharanthus reseus* receptor-like kinase 1)-family receptor kinase (Schulze-Muth et al., 1996), with a signal peptide and an extracellular domain (ECD), one transmembrane domain and an intracellular Serine/Threonine kinase domain (ICD). The ECD contains two malectin-like domains (MLD) that have been shown to bind carbohydrates in animal systems (Lindner et al., 2012). *FER* gene is expressed ubiquitously in all plant tissues except for pollen in Arabidopsis and is involved in diverse biological processes. Accordingly, FER has been identified as a critical regulator in many biological pathways. FER is required for pollen tube rupture during fertilization (Escobar-Restrepo et al., 2007; Huck et al., 2003). In a *fer* loss-of-function mutant, the pollen tube fails to rupture when it reaches the ovule, resulting in female infertility. FER transcripts are also induced by brassinosteroids (BRs) and required for optimal vegetative growth. Loss-of-function *fer* mutant displays compromised cell elongation and a severe dwarf phenotype (Guo et al., 2009a). In a forward genetic screen for ethylene-responsive mutations, FER has been identified as a negative regulator in the ethylene signaling pathway, with *fer* mutants showing hypersensitivity to ethylene treatment (Deslauriers and Larsen, 2010). FER has also been identified via yeast-two hybrid screening using a guanine exchange factor, ROPGEF1, as bait (Duan et al., 2010).

Subsequently, FER has been shown to be involved in many more biological processes, such as powdery mildew and Fusarium fungal defense (Kessler et al., 2010; Masachis et al., 2016), abscisic acid (ABA) signaling and cold, heat, salt and osmotic stress responses (Chen et al., 2016; Yu et al., 2012), bacterial pathogen defense (Keinath et al., 2010; Stegmann et al., 2017), mechanical signal transduction (Shih et al., 2014), ethylene biosynthesis (Mao et al., 2015), starch biosynthesis (Yang et al., 2015), seed size control (Yu et al., 2014), cell wall integrity maintenance during salt stress (Feng et al., 2018), slat stress regulation (Zhao et al., 2018), pavement cell morphogenesis (Lin, 2018) and vacuole expansion regulation during root cell elongation (Dunser et al., 2019).

FER belongs to a family of 17 members, many of which have been characterized with overlapping and/or distinct functions. *THESEUS1* (*THE1*) was identified in a genetic suppressor screen to rescue the cell elongation defect in *cesa6* (*cellulose synthase 6*) null mutant, and proposed to be a cell wall integrity sensor (Hematy et al., 2007). *THE1* is also involved in lateral root initiation (Gonneau et al., 2018). *HERCULES1 Receptor Kinase 1* (*HERK1*) and *HERK2*, along with *FER,* are induced by BRs through BR-induced transcription factor BES1, and are positively involved in plant growth (Guo et al., 2009a; Guo et al., 2009b). ANXUR1/ANXUR2, closest homologs of FER, function in pollen growth and control the timing of pollen tube rupture (Boisson-Dernier et al., 2013; Boisson-Dernier et al., 2009; Ge et al., 2017; Miyazaki et al., 2009). Interestingly, they have also been found to play negative roles in bacterial pathogen defense through a genetic suppressor screen for altered *pWRKY46-LUC* reporter, where WRKY46 is a transcription factor regulating plant immunity-related gene expression (Mang et al., 2017). BUDDHA's PAPER SEAL 1 (BUPS1) and BUPS2 function together with ANXUR1/ANXUR2 to control pollen tube integrity (Ge et al., 2017).

Another CrRLK1 family member, ERULUS (ERU)/CAP1 (cytoplasmic Ca2+-associated protein kinase 1) is required for root hair growth. The loss of function mutant *eru/cap1* displays root hair growth defects (Bai et al., 2014) due to disrupted tip-focused cytoplasmic calcium oscillation (Kwon et al., 2018). ERU/CAP1 has also been shown to regulate pollen tube growth and targeting to ovule. Pollen tube in the *eru* mutant grows more slowly on low Ca^{2+}-containing medium, and the mutant has lowered fertilization rate likely due to the skewed guidance for ovule-targeted growth (Schoenaers et al., 2017). The same group later showed that ERU regulates auxin-mediated root hair development and that ERU is a direct target of transcription factors ARF7 and ARF19 in the auxin signaling pathway (Schoenaers et al., 2018). Moreover, the phosphorylation of FER and proton ATPases 1/2 (AHA1/2) are altered in *eru* mutant. While Serine (S)701 in FER has decreased phosphorylation in *eru,* S904 in AHA1/2 has significantly increased phosphorylation, which might provide the underlying mechanism for ERU-regulated root hair development, in addition to that FER and proton ATPase function to regulate root elongation (Haruta et al., 2014).

CURVY1 plays a role in trichome and pavement cell morphogenesis. Interestingly, faster growth, early flowering and more seed production were also observed in a *cvy1* loss-of-function mutant, in addition to the distorted trichome and misshaped pavement cells (Gachomo et al., 2014).

There are still seven family members without known functions. Further studies are needed for their functional characterization.

1.2 Mechanisms Underlying FER Regulation of Biological Processes

With all the diverse functions described so far, it has become increasingly clear that FER and its family members can sense multiple stimuli and utilize different partners and cellular components to carry out their diverse missions. In the past decade, great strides have been made in identifying signaling components that mediate FER functions in plant growth development, abiotic stress responses, plant immunity and reproduction. Here, I summarize the findings in the context of these specific processes (Fig 1.1).

1.2.1 Plant Growth and Development

FER is required for multiple growth and developmental processes. FER is required for shoot growth but negatively regulates root elongation (Haruta et al., 2014). Although the mechanisms by which FER regulates shoot growth remain to be determined, the mechanisms of FER in the regulation of root elongation, root hair and leaf pavement cell development have begun to be established and are summarized here (Figure 1.1-path1).

Root Elongation

In FER-regulated root elongation, peptide hormone RALF1 (Rapid Alkalization Factor 1) functions as FER ligand (Haruta et al., 2008). RALF1 binding stimulates FER phosphorylation, which in turn leads to the increase of cytosolic Ca^{2+} and the inhibitory phosphorylation of proton ATPase 2 (AHA2) at Serine 899, leading to alkalization of the extracellular matrix and inhibition of cell elongation (Haruta et al., 2014). It is important to point out that other RALFs such as RALF22 and RALF23 function to inhibit FER functions, which will be discussed later.

RALF1 was first identified as a 5-KD peptide that can induce the increase of cytosolic Ca^{2+} in tobacco, and the tomato homolog caused arrested root growth and development during seed germination (Pearce et al., 2001). It was so named due to its ability to rapidly alkalize the medium of the suspension cells. In Arabidopsis, there are at least 34 members in the RALF family. The functional mature peptides of the RALFs are about 50 amino acids in length and cysteine rich, with four or more cysteine residues (Murphy and De Smet, 2014; Srivastava et al., 2009; Stegmann et al., 2017).

During root elongation, FER also interacts with potential co-receptors, namely cell wall proteins LRX3/4/5 that sense cell wall status to restrict vacuole enlargement during cell elongation (Dunser et al., 2019). The *lrx3/4/5* and *fer* mutants have constitutively enlarged vacuoles. The LRXs (leucine-rich-repeat extensins) are cell wall proteins, with 11 of them in Arabidopsis. While LRXs1-7 are mostly expressed in vegetative tissues, LRXs 8-11 are mostly expressed in pollen (Zhao et al., 2018). LRR domain presumably binds to proteins and the more diverse extensin domain binds to cell wall components (Draeger et al., 2015).

In summary, FER perceives RALF1 to regulate proton ATPase and FER interacts with LRX co-receptors to negatively regulate root elongation (Figure 1.1-path1). The ligands and partners of FER in positively regulating shoot growth remain to be identified and characterized.

Root Hair Development

In root hair development, FER activates ROP2 (small GTPase) through the interaction with ROPGEF1 (ROP Guanine exchange factor), which leads to the activation of NADPH oxidases such as ROBHs (Respiratory Burst Oxidase Homologs) and ROS (Reactive Oxygen Species) production, and results in normal root hair development (Duan et al., 2010). Constitutive root

hair rupture and scarce root hair in the *fer* mutant support that FER is required for root hair development.

ROPs (Rho GTPases of plants) are a family of eleven small monomeric GTP binding proteins that plays versatile roles in mediating extracellular signaling. They shuttle from GDP-bound inactive state to GTP-bound active state that is mediated by ROPGEFs (ROP GTP exchange factors) and relay cell signals to the effector proteins (Etienne-Manneville and Hall, 2002; Feiguelman et al., 2018). There are fourteen ROPGEFs in Arabidopsis.

FER also directly interacts with RIPK (RPM1-induced protein kinase) to regulate root hair development, and FER and RIPK mutually phosphorylate each other in a RALF1-dependent manner. A *ripk* loss-of-function mutant mimics *fer*, in that it produces short root hairs (Du et al., 2016). RIPK, a receptor-like cytoplasmic kinase (RLCK), belongs to the RLCK-VII family. FER therefore activates ROP and NADPH oxidase to generate ROS to induce root hair growth, which also involves a RALF1-FER-RIPK signaling module (Figure 1.1-path1).

Leaf Pavement Cell Morphogenesis

In leaf pavement cell morphogenesis, FER appears to use pectins as ligands. Pectins, a group of galacturonan-based polysaccharides, are an important part of the cell wall along with cellulose and hemicellulose. They constitute up to 35% of the primary cell wall in dicots. They exist in various methylesterified states, likely regulated by pectin methylesterase and pectin methylesterase inhibitors, and crosslinked states (Wormit and Usadel, 2018). FER interacts with de-methylesterified pectin through the MALA domain (the Malectin-like domain proximal to N-terminus of FER extracellular domain), which leads to the interaction with ROPGEF14 and

subsequent activation of ROP6 (Lin, 2018). Misshapen leaf pavement cells in the *fer* mutant support a positive role of FER in regulating their morphogenesis.

1.2.2 Abiotic Stress

FER is involved in the regulation of abiotic stress responses (Figure 1.1-path 2). In FER-mediated salt stress response, FER perceives pectin through the extracellular domain, likely as a signal of the cell wall status under salt stress, and elicits cell-specific transient increase Ca^{2+} to respond accordingly to the stress and facilitate cell wall recovery after salt stress (Feng et al., 2018).

In the meantime, cell wall protein LRXs can interact with ligand RALF22/23 (Zhao et al., 2018). Zhao et al proposed a model, in that the interaction of LRXs and RALF22/23 restricts the inhibitory effects of the RLAFs over FER under normal growth. The salt stress promotes RALF22/23 mature peptides production by S1P, resulting in the RALF22/23 and FER interaction, which might lead to RALF22/23-induced endocytosis of FER to down regulate the receptor function (Zhao et al., 2018). Loss-of-function *fer* and overexpression of *RALF22* and *RALF23* result in hypersensitivity to salt stress, supporting a positive role of FER in regulating salt stress.

FER also regulates responses to other abiotic stresses such as heat, cold and osmotic stresses. Although the signaling components in these pathways are not clear, the negative regulation of FER on ABA signaling might be responsible to some extent. FER activates ROP11 through interacting with ROPGEF1/4/10, which subsequently activates ABI2 (ABA-insensitive 2) to inhibit ABA signaling (Chen et al., 2016; Yu et al., 2012). The observation that mutant *fer* is hypersensitive to ABA supports some of the findings, especially the role of FER in regulating

osmotic stress. ABI2, a protein phosphatase 2C, functions as a co-receptor of ABA and is a negative regulator in ABA signaling pathway (Cutler et al., 2010). ABI2 was later found to interact with FER directly and dephosphorylate FER to down regulate its kinase activity, serving as a feedback mechanism (Chen et al., 2016).

Stomatal signaling can be a form of stress response. AGB1, the Arabidopsis G-protein beta subunit 1 in the heterotrimeric GTP binding proteins, was shown to be in the same complex with FER, and this complex is involved in the RALF1-mediated stomatal events (Yu et al., 2018). The authors further showed that AGB1, the only beta subunit, three out of the four alpha subunits, and all three gamma subunits participate in RALF1-mediated stomatal signaling, inhibiting stomatal opening and promoting stomatal closure, which conceivably regulates stress responses.

1.2.3 Plant Immunity

In response to bacterial pathogens, FER functions as a scaffold to facilitate the complex formation of the immune receptors FLS2/EFR and co-receptor BAK1 (Figure 1.1-path 3), which is required for pathogen-associated molecular pattern-triggered immunity (PTI). FLS2 (Flagellin-sensitive 2) and EFR (EF-TU receptor) are plasmamembrane-localized leucine-rich-repeat (LRR) receptor kinases. They perceive Flagellin and elongation factor TU, respectively, from invading bacterial pathogens and trigger PTI. BAK1 (BRI1–Associated Kinase 1), initially identified in the BR signaling pathway, serves as a co-receptor for many plasmamembrane-localized receptor kinases, such as the growth-related receptor kinase BRI1 (Brassinosteroid Insensitive 1) and the immune receptor kinases FLS2 and EFR.

RALF23 is processed to a functional mature peptide upon pathogen infection and functions through FER to reduce the complex formation and hence the immune response (Stegmann et al., 2017). Both loss-of-function *fer* and overexpression of *RALF23* are hypersensitive to bacterial pathogen infection, supports a positive role of FER and negative role of RALF23 in bacterial defense.

In a separate study, FER homologs ANX1/2, originally established to be involved in pollen tube integrity (see below), were found to constantly associate with FLS2 and BAK1. The perception of flagellin by FLS2 promotes association of ANX1/2 with BAK1, resulting in the inhibition of FLS2, which categorizes ANX1/2 as negative regulators in plant immunity (Mang et al., 2017).

RALF peptide orthologs are encoded in some plant fungal pathogens (Thynne et al., 2017). Upon infection of the root fungal pathogen *Fusarium oxysporum*, *Fusarium* RALF (F-RALF) released from the pathogen is perceived by FER in the host plant. This perception leads to extracellular alkalization likely due to FER-mediated inhibitory phosphorylation of proton ATPases. The alkalinized host tissue promotes fungal pathogen proliferation (Masachis et al., 2016). Mutant *fer* is resistant to *Fusarium oxysporum* infection. FER-mediated powdery mildew infection is also likely due to similar mechanism (Kessler et al., 2010). The fact that the *fer* mutant is resistant to both *Fusarium oxysporum* and powdery mildew infection supports a negative role of FER in fungal pathogen defense (Figure 1.1-path 3).

1.2.4 Female and Male Reproduction

In plant reproduction, FER and its close homologs ANX1/2 are involved in the female and male reproduction processes, respectively (Figure 1.1-path 4). In the female gametophyte, the ovule,

FER regulates ROS production and specific Ca^{2+} signatures to promote pollen tube rupture when it arrives at the ovule (Duan et al., 2014; Escobar-Restrepo et al., 2007). In the male gametophyte, the pollen tube, pollen-specific FER homologs ANX1/2 and BUPS1/2 perceive pollen-specific ligands RALF4/19 to maintain normal pollen growth and integrity. Pollen-specific LRXs can also interact with RALF4/19, which may in turn function through the receptor kinases to maintain pollen tube wall integrity (Ge et al., 2017; Mecchia et al., 2017).

The newly proposed "Ligand Switch Model" explains the fertilization processes nicely (Ge et al., 2017). When pollen reaches the ovule, the ovule RALF34 out-competes RALF4/19 for binding to the receptors ANX1/2 and BUPS1/2. The outcome of RALF34 interaction with the receptors leads to pollen tube rupture and release of the sperm cells for fertilization. The fertilization process involves cell death of one synergid cell and rupture of the pollen tube. It is tempting to speculate that FER and its homologs ANX1/2 and BUPS1/2 maintain cell integrity in synergid cell and pollen, respectively, through interacting with tissue-specific RALFs or LRXs. When they meet physically during fertilization, FER and ANX1/2 and BUPS1/2 can switch ligands and change their downstream signaling output from maintaining cell integrity to cell rupture and death.

There are several more components that are involved in FER and ANX1/2-mediated reproduction, although detailed functional mechanisms remain to be elucidated (Figure 1.1-path 4).

NTA (NORTIA), a plasmamembrane protein with seven transmembrane domains, belongs to the MLO family (Mildew resistance locus O). The *nta* mutant has similar failed pollen tube rupture and reduced female fertility as the *fer* mutant (Kessler et al., 2010).

TUN (TURAN) and EVN (EVAN) have been shown to play a role in the fertilization process. TUN encodes a uridine diphosphate glycosyltransferase and EVN is a dolichol kinase; both are localized in the ER and possibly function in protein N-glycosylation. Loss-of-function mutants display failed pollen-tube rupture during fertilization. TUN is suggested to be required for glycosylation and stabilization of ANX1/2 (Lindner et al., 2015).

ENs 11/12/13/14/15 (early nodulin-like proteins) have been described as a group of GPI (glycosylphosphatidylinositol)-anchored proteins. EN14 and 15 express strongly in the ovule, and a loss-of-function *en11-15* mutant displayed strong female infertility due to failed pollen tube rupture during fertilization (Hou et al., 2016). The authors further showed that EN14 strongly interacts with the FER extracellular domain. Interestingly, the ENs also contain a plastocyanin-like domain (plastocyanin is a copper-containing protein involved in electron transfer) that may bring more diversity to the FER-mediated signaling in the ovule.

AUN1/2 (ATUNIS1/2) are nucleocytoplasmic phosphatases**.** They were identified as negative regulators to suppress ANX1/2 and FER-mediated tip growth in pollen tube and root hair. Their substrate and the exact functional mechanism need to be further characterized (Franck et al., 2018).

MRI (MYRIS) was identified through an *anx1/2* suppressor screen (Boisson-Dernier et al., 2015). It is a receptor-like cytoplasmic kinase (RLCK) from superfamily RLCK-VIII, and has been shown to function as a positive regulator in pollen tube and root hair cell wall integrity. Loss-of-function mutant *mri* displays constitutive pollen tube and root hair rupture (Liao et al., 2016).

FER Co-receptors LRE (LORELEI) and LLG1 (LRE-like GPI-anchored protein)

LRE and LLG1 are homologous glycosylphosphatidylinositol (GPI)-anchored proteins, that are expressed in female gametophyte and vegetative tissue, respectively. Similar to a *fer* mutant, a loss-of-function *lre* mutant displays failed pollen tube rupture upon arrival at the ovule and female infertility (Capron et al., 2008). The *llg1* mutant is almost indistinguishable from the *fer* mutant in growth phenotype (Li et al., 2015). Li et al further showed that LRE and LLG1 interact with FER through the FER extracellular juxtadomain and the interaction is required for the translocation of FER to the plasmamembrane from the ER. The ligand RALF1 can bind to the FER-LLG1 complex, suggesting that LLG1 functions as a co-receptor of FER.

LLG1 has also been identified as a positive regulator of plant immunity in a genetic suppressor screen (Shen et al., 2017). The authors propose that LLG1 associates with and regulates the immune receptors FLS2 and EFR to regulate FLS2 abundance and ligand-mediated degradation. Since LRE/LLG1 are required for proper FER plasmamembrane localization, it is conceivable that they are involved in most FER-mediated processes (Figure 1.1-path 3).

1.3 Perspectives

FER is one of the most functionally versatile receptor kinases. It is involved in the regulation of plant growth and development, response to abiotic and biotic stresses and plant reproduction. Great progress has been made to elucidate the underlying mechanisms of this regulation, and many interacting proteins and functional components have been identified, including ligands, co-receptors and downstream protein components. However, there is a large void in terms of FER regulation over the nuclear events. In a *fer* mutant, thousands of genes are either up- or down-

regulated, raising the possibility that FER functions to regulate gene expression. However, how FER-mediated signals are transduced to nuclear gene expression regulation is not known. To fill this knowledge gap and also to facilitate the discovery of novel functions of FER, I carried out quantitative transcriptome, proteome and phosphoproteome analyses of a *fer* mutant. The omics data identified several transcription factors that mediate FER functions, and also revealed previously unknown functions of FER. The new findings are presented in this dissertation.

1.4 Dissertation Organization

This dissertation summarizes up my work on receptor kinase FERONIA function and underlying mechanisms in *Arabidopsis* since fall 2013 when I became a Ph.D. student in the Interdepartmental Genetics and Genomics (IG2) graduate major.

Chapter 1 provides a comprehensive overview on FERONIA receptor kinase and its family members, including the identification of founding members, their potential ligands, co-receptors and downstream signaling components, and how they function together to regulate important signaling pathways and biological processes.

Chapter 2 establishes FER receptor kinase as a positive regulator in plant defense against bacterial pathogens via *fer* transcriptome analysis. We also established the underlying mechanism: FER phosphorylates and destabilizes MYC2, the master regulator in JA signaling, and downregulates the pathogen-mediated host susceptibility. Furthermore, we found RALF23, a ligand for FER, functions through FER and MYC2 to negatively regulate plant immunity. The findings were published in Current Biology (Guo et al., 2018).

Chapter 3 carried out the analyses of the quantitative proteomics and phosphoproteomics of the *fer* mutant. The data analysis supports that FER is a critical regulator in plant growth and stress responses, and that the candidate substrate TFs might account for some of the underlying mechanisms. The omics data also helped identify new functions of FER. FER negatively regulates ER body formation likely through NAI1 and NAIP2, and FER functions in a complex with SnRK1 and TOR to regulate plant growth and autophagy. The omics data analysis has opened up new revenues for future studies of FERONIA function and underlying mechanisms.

Chapter 4 summarizes the conclusions and provides discussions and future directions originated from the studies in this dissertation.

Included in Appendix is a manuscript that I contributed to and was published in Plant Journal (Hansen et al., 2019). FER regulates diverse biological processes but the underlying mechanisms are not fully understood. To better understand how FER carries out its function, Hansen et al. (2019) set out to analyze metabolites, especially the ones increased in *fer* mutant. Using a direct-infusion Fourier-transformed ion cyclotron resonance (FTICR)-MS approach, Arabidopsides were found to be significantly enriched in *fer.* Arabidopsides are family of oxylipins that are hydrophilic molecules from the oxidation of polyunsaturated fatty acids. They further found that wounding increased the levels of Arabidopsides, using a quadruple time-of-flight (Q-TOF) MS by direct injection and LC-MS/MS. The Arabidopside A was later isolated from the *fer* mutant and it displayed root growth inhibitory activity. While WT seedling roots were inhibited by 20 uM Arabidopside A, the *fer* mutant was insensitive. Using matrix-assisted laser desorption/ionization MS imaging (MALDI-MSI), the authors further showed that Arabidopsides are highly abundant around wounding sites and localized in the chloroplasts.

1.5 References

Bai, L., Ma, X., Zhang, G., Song, S., Zhou, Y., Gao, L., Miao, Y., and Song, C.P. (2014). A Receptor-Like Kinase Mediates Ammonium Homeostasis and Is Important for the Polar Growth of Root Hairs in Arabidopsis. Plant Cell *26*, 1497-1511.

Boisson-Dernier, A., Franck, C.M., Lituiev, D.S., and Grossniklaus, U. (2015). Receptor-like cytoplasmic kinase MARIS functions downstream of CrRLK1L-dependent signaling during tip growth. Proc Natl Acad Sci U S A *112*, 12211-12216.

Boisson-Dernier, A., Lituiev, D.S., Nestorova, A., Franck, C.M., Thirugnanarajah, S., and Grossniklaus, U. (2013). ANXUR receptor-like kinases coordinate cell wall integrity with growth at the pollen tube tip via NADPH oxidases. PLoS Biol *11*, e1001719.

Boisson-Dernier, A., Roy, S., Kritsas, K., Grobei, M.A., Jaciubek, M., Schroeder, J.I., and Grossniklaus, U. (2009). Disruption of the pollen-expressed FERONIA homologs ANXUR1 and ANXUR2 triggers pollen tube discharge. Development *136*, 3279-3288.

Capron, A., Gourgues, M., Neiva, L.S., Faure, J.E., Berger, F., Pagnussat, G., Krishnan, A., Alvarez-Mejia, C., Vielle-Calzada, J.P., Lee, Y.R.*, et al.* (2008). Maternal control of male-gamete delivery in Arabidopsis involves a putative GPI-anchored protein encoded by the LORELEI gene. Plant Cell *20*, 3038-3049.

Chen, J., Yu, F., Liu, Y., Du, C., Li, X., Zhu, S., Wang, X., Lan, W., Rodriguez, P.L., Liu, X.*, et al.* (2016). FERONIA interacts with ABI2-type phosphatases to facilitate signaling cross-talk between abscisic acid and RALF peptide in Arabidopsis. Proc Natl Acad Sci U S A *113*, E5519-5527.

Cutler, S.R., Rodriguez, P.L., Finkelstein, R.R., and Abrams, S.R. (2010). Abscisic acid: emergence of a core signaling network. Annu Rev Plant Biol *61*, 651-679.

Deslauriers, S.D., and Larsen, P.B. (2010). FERONIA is a key modulator of brassinosteroid and ethylene responsiveness in Arabidopsis hypocotyls. Mol Plant *3*, 626-640.

Draeger, C., Ndinyanka Fabrice, T., Gineau, E., Mouille, G., Kuhn, B.M., Moller, I., Abdou, M.T., Frey, B., Pauly, M., Bacic, A.*, et al.* (2015). Arabidopsis leucine-rich repeat extensin (LRX) proteins modify cell wall composition and influence plant growth. BMC Plant Biol *15*, 155.

Du, C., Li, X., Chen, J., Chen, W., Li, B., Li, C., Wang, L., Li, J., Zhao, X., Lin, J.*, et al.* (2016). Receptor kinase complex transmits RALF peptide signal to inhibit root growth in Arabidopsis. Proc Natl Acad Sci U S A *113*, E8326-E8334.

Duan, Q., Kita, D., Johnson, E.A., Aggarwal, M., Gates, L., Wu, H.M., and Cheung, A.Y. (2014). Reactive oxygen species mediate pollen tube rupture to release sperm for fertilization in Arabidopsis. Nat Commun *5*, 3129.

Duan, Q., Kita, D., Li, C., Cheung, A.Y., and Wu, H.M. (2010). FERONIA receptor-like kinase regulates RHO GTPase signaling of root hair development. Proc Natl Acad Sci U S A *107*, 17821-17826.

Dunser, K., Gupta, S., Herger, A., Feraru, M.I., Ringli, C., and Kleine-Vehn, J. (2019). Extracellular matrix sensing by FERONIA and Leucine-Rich Repeat Extensins controls vacuolar expansion during cellular elongation in Arabidopsis thaliana. EMBO J. 38, e100353

Escobar-Restrepo, J.M., Huck, N., Kessler, S., Gagliardini, V., Gheyselinck, J., Yang, W.C., and Grossniklaus, U. (2007). The FERONIA receptor-like kinase mediates male-female interactions during pollen tube reception. Science *317*, 656-660.

Etienne-Manneville, S., and Hall, A. (2002). Rho GTPases in cell biology. Nature *420*, 629-635.

Feiguelman, G., Fu, Y., and Yalovsky, S. (2018). ROP GTPases Structure-Function and Signaling Pathways. Plant Physiol *176*, 57-79.

Feng, W., Kita, D., Peaucelle, A., Cartwright, H.N., Doan, V., Duan, Q., Liu, M.C., Maman, J., Steinhorst, L., Schmitz-Thom, I.*, et al.* (2018). The FERONIA Receptor Kinase Maintains Cell-Wall Integrity during Salt Stress through Ca(2+) Signaling. Curr Biol *28*, 666-675 e665.

Franck, C.M., Westermann, J., Burssner, S., Lentz, R., Lituiev, D.S., and Boisson-Dernier, A. (2018). The Protein Phosphatases ATUNIS1 and ATUNIS2 Regulate Cell Wall Integrity in Tip-Growing Cells. Plant Cell *30*, 1906-1923.

Gachomo, E.W., Jno Baptiste, L., Kefela, T., Saidel, W.M., and Kotchoni, S.O. (2014). The Arabidopsis CURVY1 (CVY1) gene encoding a novel receptor-like protein kinase regulates cell morphogenesis, flowering time and seed production. BMC Plant Biol *14*, 221.

Ge, Z., Bergonci, T., Zhao, Y., Zou, Y., Du, S., Liu, M.C., Luo, X., Ruan, H., Garcia-Valencia, L.E., Zhong, S.*, et al.* (2017). Arabidopsis pollen tube integrity and sperm release are regulated by RALF-mediated signaling. Science *358*, 1596-1600.

Gonneau, M., Desprez, T., Martin, M., Doblas, V.G., Bacete, L., Miart, F., Sormani, R., Hematy, K., Renou, J., Landrein, B.*, et al.* (2018). Receptor Kinase THESEUS1 Is a Rapid Alkalinization Factor 34 Receptor in Arabidopsis. Curr Biol *28*, 2452-2458 e2454.

Guo, H., Li, L., Ye, H., Yu, X., Algreen, A., and Yin, Y. (2009a). Three related receptor-like kinases are required for optimal cell elongation in Arabidopsis thaliana. Proc Natl Acad Sci U S A *106*, 7648-7653.

Guo, H., Nolan, T.M., Song, G., Liu, S., Xie, Z., Chen, J., Schnable, P.S., Walley, J.W., and Yin, Y. (2018). FERONIA Receptor Kinase Contributes to Plant Immunity by Suppressing Jasmonic Acid Signaling in Arabidopsis thaliana. Curr Biol *28*, 3316-3324 e3316.

Guo, H., Ye, H., Li, L., and Yin, Y. (2009b). A family of receptor-like kinases are regulated by BES1 and involved in plant growth in Arabidopsis thaliana. Plant Signal Behav *4*, 784-786.

Hansen, R.L., Guo, H., Yin, Y., and Lee, Y.J. (2019). FERONIA mutation induces high levels of chloroplast-localized Arabidopsides which are involved in root growth. Plant J *97*, 341-351.

Haruta, M., Monshausen, G., Gilroy, S., and Sussman, M.R. (2008). A cytoplasmic Ca2+ functional assay for identifying and purifying endogenous cell signaling peptides in Arabidopsis seedlings: identification of AtRALF1 peptide. Biochemistry *47*, 6311-6321.

Haruta, M., Sabat, G., Stecker, K., Minkoff, B.B., and Sussman, M.R. (2014). A peptide hormone and its receptor protein kinase regulate plant cell expansion. Science *343*, 408-411.

Hematy, K., Sado, P.E., Van Tuinen, A., Rochange, S., Desnos, T., Balzergue, S., Pelletier, S., Renou, J.P., and Hofte, H. (2007). A receptor-like kinase mediates the response of Arabidopsis cells to the inhibition of cellulose synthesis. Curr Biol *17*, 922-931.

Hou, Y., Guo, X., Cyprys, P., Zhang, Y., Bleckmann, A., Cai, L., Huang, Q., Luo, Y., Gu, H., Dresselhaus, T.*, et al.* (2016). Maternal ENODLs Are Required for Pollen Tube Reception in Arabidopsis. Curr Biol *26*, 2343-2350.

Huck, N., Moore, J.M., Federer, M., and Grossniklaus, U. (2003). The Arabidopsis mutant feronia disrupts the female gametophytic control of pollen tube reception. Development *130*, 2149-2159.

Keinath, N.F., Kierszniowska, S., Lorek, J., Bourdais, G., Kessler, S.A., Shimosato-Asano, H., Grossniklaus, U., Schulze, W.X., Robatzek, S., and Panstruga, R. (2010). PAMP (pathogen-associated molecular pattern)-induced changes in plasma membrane compartmentalization reveal novel components of plant immunity. J Biol Chem *285*, 39140-39149.

Kessler, S.A., Shimosato-Asano, H., Keinath, N.F., Wuest, S.E., Ingram, G., Panstruga, R., and Grossniklaus, U. (2010). Conserved molecular components for pollen tube reception and fungal invasion. Science *330*, 968-971.

Kwon, T., Sparks, J.A., Liao, F., and Blancaflor, E.B. (2018). ERULUS Is a Plasma Membrane-Localized Receptor-Like Kinase That Specifies Root Hair Growth by Maintaining Tip-Focused Cytoplasmic Calcium Oscillations. Plant Cell *30*, 1173-1177.

Li, C., Yeh, F.L., Cheung, A.Y., Duan, Q., Kita, D., Liu, M.C., Maman, J., Luu, E.J., Wu, B.W., Gates, L.*, et al.* (2015). Glycosylphosphatidylinositol-anchored proteins as chaperones and co-receptors for FERONIA receptor kinase signaling in Arabidopsis. Elife *4*.

Liao, H.Z., Zhu, M.M., Cui, H.H., Du, X.Y., Tang, Y., Chen, L.Q., Ye, and Zhang, X.Q. (2016). MARIS plays important roles in Arabidopsis pollen tube and root hair growth. J Integr Plant Biol *58*, 927-940.

Lin, W.T., W.; Anderson C.T.; and Yang, Z. (2018). FERONIA's sensing of cell wall pectin activates ROP GTPase signaling in Arabidopsis. bio Rxiv, 269647.

Lindner, H., Kessler, S.A., Muller, L.M., Shimosato-Asano, H., Boisson-Dernier, A., and Grossniklaus, U. (2015). TURAN and EVAN mediate pollen tube reception in Arabidopsis Synergids through protein glycosylation. PLoS Biol *13*, e1002139.

Lindner, H., Muller, L.M., Boisson-Dernier, A., and Grossniklaus, U. (2012). CrRLK1L receptor-like kinases: not just another brick in the wall. Curr Opin Plant Biol *15*, 659-669.

Mang, H., Feng, B., Hu, Z., Boisson-Dernier, A., Franck, C.M., Meng, X., Huang, Y., Zhou, J., Xu, G., Wang, T.*, et al.* (2017). Differential Regulation of Two-Tiered Plant Immunity and Sexual Reproduction by ANXUR Receptor-Like Kinases. Plant Cell *29*, 3140-3156.

Mao, D., Yu, F., Li, J., Van de Poel, B., Tan, D., Li, J., Liu, Y., Li, X., Dong, M., Chen, L.*, et al.* (2015). FERONIA receptor kinase interacts with S-adenosylmethionine synthetase and suppresses S-adenosylmethionine production and ethylene biosynthesis in Arabidopsis. Plant Cell Environ *38*, 2566-2574.

Masachis, S., Segorbe, D., Turra, D., Leon-Ruiz, M., Furst, U., El Ghalid, M., Leonard, G., Lopez-Berges, M.S., Richards, T.A., Felix, G.*, et al.* (2016). A fungal pathogen secretes plant alkalinizing peptides to increase infection. Nat Microbiol *1*, 16043.

Mecchia, M.A., Santos-Fernandez, G., Duss, N.N., Somoza, S.C., Boisson-Dernier, A., Gagliardini, V., Martinez-Bernardini, A., Fabrice, T.N., Ringli, C., Muschietti, J.P.*, et al.* (2017). RALF4/19 peptides interact with LRX proteins to control pollen tube growth in Arabidopsis. Science *358*, 1600-1603.

Miyazaki, S., Murata, T., Sakurai-Ozato, N., Kubo, M., Demura, T., Fukuda, H., and Hasebe, M. (2009). ANXUR1 and 2, sister genes to FERONIA/SIRENE, are male factors for coordinated fertilization. Curr Biol *19*, 1327-1331.

Murphy, E., and De Smet, I. (2014). Understanding the RALF family: a tale of many species. Trends Plant Sci *19*, 664-671.

Pearce, G., Moura, D.S., Stratmann, J., and Ryan, C.A., Jr. (2001). RALF, a 5-kDa ubiquitous polypeptide in plants, arrests root growth and development. Proc Natl Acad Sci U S A *98*, 12843-12847.

Schoenaers, S., Balcerowicz, D., Breen, G., Hill, K., Zdanio, M., Mouille, G., Holman, T.J., Oh, J., Wilson, M.H., Nikonorova, N.*, et al.* (2018). The Auxin-Regulated CrRLK1L Kinase

ERULUS Controls Cell Wall Composition during Root Hair Tip Growth. Curr Biol *28*, 722-732 e726.

Schoenaers, S., Balcerowicz, D., Costa, A., and Vissenberg, K. (2017). The Kinase ERULUS Controls Pollen Tube Targeting and Growth in Arabidopsis thaliana. Front Plant Sci *8*, 1942.

Schulze-Muth, P., Irmler, S., Schroder, G., and Schroder, J. (1996). Novel type of receptor-like protein kinase from a higher plant (Catharanthus roseus). cDNA, gene, intramolecular autophosphorylation, and identification of a threonine important for auto- and substrate phosphorylation. J Biol Chem *271*, 26684-26689.

Shen, Q., Bourdais, G., Pan, H., Robatzek, S., and Tang, D. (2017). Arabidopsis glycosylphosphatidylinositol-anchored protein LLG1 associates with and modulates FLS2 to regulate innate immunity. Proc Natl Acad Sci U S A *114*, 5749-5754.

Shih, H.W., Miller, N.D., Dai, C., Spalding, E.P., and Monshausen, G.B. (2014). The receptor-like kinase FERONIA is required for mechanical signal transduction in Arabidopsis seedlings. Curr Biol *24*, 1887-1892.

Srivastava, R., Liu, J.X., Guo, H., Yin, Y., and Howell, S.H. (2009). Regulation and processing of a plant peptide hormone, AtRALF23, in Arabidopsis. Plant J *59*, 930-939.
Stegmann, M., Monaghan, J., Smakowska-Luzan, E., Rovenich, H., Lehner, A., Holton, N., Belkhadir, Y., and Zipfel, C. (2017). The receptor kinase FER is a RALF-regulated scaffold controlling plant immune signaling. Science *355*, 287-289.

Wormit, A., and Usadel, B. (2018). The Multifaceted Role of Pectin Methylesterase Inhibitors (PMEIs). Int J Mol Sci *19*.

Yang, T., Wang, L., Li, C., Liu, Y., Zhu, S., Qi, Y., Liu, X., Lin, Q., Luan, S., and Yu, F. (2015). Receptor protein kinase FERONIA controls leaf starch accumulation by interacting with glyceraldehyde-3-phosphate dehydrogenase. Biochem Biophys Res Commun *465*, 77-82.

Yu, F., Li, J., Huang, Y., Liu, L., Li, D., Chen, L., and Luan, S. (2014). FERONIA receptor kinase controls seed size in Arabidopsis thaliana. Mol Plant *7*, 920-922.

Yu, F., Qian, L., Nibau, C., Duan, Q., Kita, D., Levasseur, K., Li, X., Lu, C., Li, H., Hou, C.*, et al.* (2012). FERONIA receptor kinase pathway suppresses abscisic acid signaling in Arabidopsis by activating ABI2 phosphatase. Proc Natl Acad Sci U S A *109*, 14693-14698.

Yu, Y., Chakravorty, D., and Assmann, S.M. (2018). The G Protein beta-Subunit, AGB1, Interacts with FERONIA in RALF1-Regulated Stomatal Movement. Plant Physiol *176*, 2426-2440.

Zhao, C., Zayed, O., Yu, Z., Jiang, W., Zhu, P., Hsu, C.C., Zhang, L., Tao, W.A., Lozano-Duran, R., and Zhu, J.K. (2018). Leucine-rich repeat extensin proteins regulate plant salt tolerance in Arabidopsis. Proc Natl Acad Sci U S A *115*, 13123-13128.

1.6 Figures

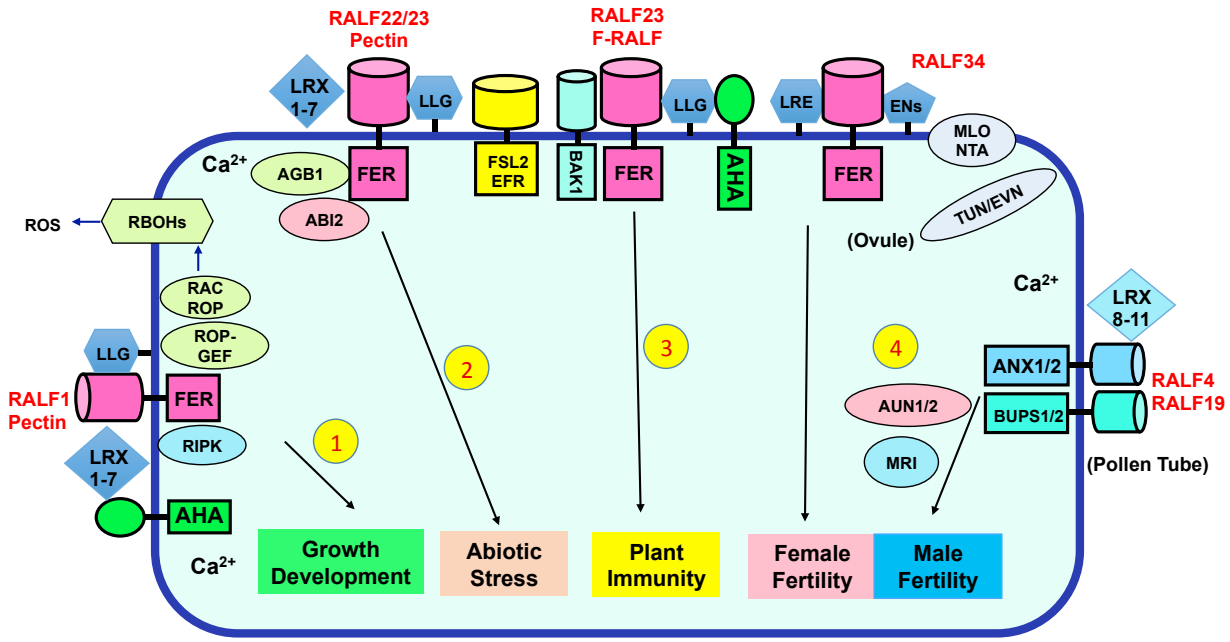

Figure 1.1: FER signaling Pathways during Plant Growth and Development, Stress Responses and Reproduction. (1) Peptide ligand RALF1 interacts with FER and likely regulates FER kinase activity, leading to inactivation of AHA (*Arabidopsis* proton ATPases) and inhibition of root growth. Pectin and FER coreceptor LRX 1-7 likely participate in the process as well. On the other hand, FER activates ROPGEFs, ROPs and RBOH as well as RIPK kinase to promote root hair development. (2) RALF22/23 as well as pectin function through FER, LRXs and AGB1 and ABI2 to regulate responses to abiotic stresses such as salt, cold, heat and osmotic stresses. (3) RALF23 acts through FER, coreceptor BAK1 and PAMP receptor FLS2/EFR to regulate plant immunity against bacterial pathogens. Fusarium RALF (F-RALF) acts through FER to inhibit AHA, which results in alkalization of the infection sites and promotion of fungal

pathogen infection. (4) FER functions with coreceptor LRE and ENs in the ovule to promote pollen rupture and therefore control female fertility. Seven-transmembrane protein MLO and the TUN/EVN proteins are also involved in FER function related to fertility. On the other hand, the close FER homologs ANX1/2 and BUPS1/2 perceive RALF4/19 to regulate pollen tube function and male fertility. Many other proteins are identified that contribute to the process, such as AUN1/2 and MRI, but the mechanisms of their action remain to be fully established.

CHAPTER 2

FERONIA RECEPTOR KINASE CONTRIBUTES TO PLANT IMMUNITY BY SUPPRESSING JASMONIC ACID SIGNALING IN *ARABIDOPSIS THALIANA*

A paper published in Current Biology

Hongqing Guo[1*], Trevor M. Nolan[1], Gaoyuan Song[2], Sanzhen Liu[3,4, 5], Zhouli Xie[1], Jiani Chen[1], Patrick S. Schnable[3,4], Justin W. Walley[2] and Yanhai Yin[1]*

[1]Department of Genetics, Development and Cell Biology; Iowa State University

[2]Department of Plant Pathology and Microbiology; Iowa State University

[3]Department of Agronomy, Iowa State University

[4]Data2Bio LLC, Ames, Iowa 50011-3650, USA.

[5]Present address: Department of Plant Pathology, Kansas State University, Manhattan, Kansas 66506-5502, USA (S.L.)

*Correspondence and requests for materials should be addressed to Y.Y. (email: yin@iastate.edu) and H.G. (hguo@iastate.edu).

Department of Genetics, Development and Cell Biology, Iowa State University, 1111 WOI Road, Ames, Iowa 50011-1085, USA

Keywords: FERONIA, receptor kinase, MYC2, transcription factor, plant immunity, signaling, phosphorylation, Arabidopsis, Jasmonic acid, hormone

2.1 Abstract

Bacterial pathogens use effectors and phytotoxins to facilitate infection of host plants. Coronatine (COR) is one of the phytotoxins produced in bacterial pathogens such as *Pseudomonas syringae* pv. tomato DC3000 (pst DC3000). COR structurally and functionally mimics the active form of the plant hormone jasmonic acid (JA), JA-isoleucine (JA-Ile), and can hijack the host JA-signaling pathway to achieve host disease susceptibility [1]. COR utilizes the transcription factor MYC2, a master regulator of JA signaling, to activate NAC transcription factors, which functions to inhibit accumulation of salicylic acid (SA) and thus compromise host immunity [2]. It has been demonstrated that SA can antagonize JA signaling through NONEXPRESSOR of PATHOGENESIS-RELATED GENE1 (NPR1) [3], and downstream transcription factors TGAs [4] and WRKYs [5, 6]. However, the detailed mechanism by which host plants counteract COR-mediated susceptibility is largely unknown. Here we show that the receptor kinase FERONIA (FER) functions to inhibit JA/COR-signaling by phosphorylating and destabilizing MYC2, thereby positively regulating immunity. Conversely, the peptide ligand RALF23 acts through FER to stabilize MYC2 and elevate JA signaling, negatively contributing to plant immunity. Our results establish the RALF23-FER-MYC2 signaling module and provide a previously unknown mechanism by which host plants utilize FER signaling to counteract COR-mediated host disease susceptibility.

2.2 Introduction

FER belongs to the CrRLKL1 family of receptor-like kinases and functions in various biological processes, including plant growth, development, hormone signaling, biotic and abiotic stress responses [7-17]. Several family members are involved in sensing cell wall integrity, mechanical sensing and pollen tube function [18-24]. A few components in FER-mediated signaling have been described, including peptides RALF1 [25] and RALF23 [26] that function as ligands for FER, and LORELEI (LRE)/LORELEI-LIKE-GPI-ANCHORED PROTEIN 1(LLG1) which are FER coreceptors [27]. In addition, FER regulates guanine nucleotide exchange factor 1 (RopGEF1) and ROP/RAC GTPases, which activates PP2C phosphatase ABI2 to inhibit plant hormone abscisic acid (ABA) signaling [10]. ABI2 dephosphorylates FER, likely as a feedback regulation mechanism [9]. The downstream signaling components, especially transcription factors mediating FER functions, are largely unknown [13, 22, 25].

2.3 Results

2.3.1 FER receptor kinase functions upstream of MYC2 to regulate JA signaling

To understand how FER functions to regulate plant growth and reveal other processes regulated by FER, we performed global gene expression studies with *fer* mutants. RNA-seq analysis indicated that 6,995 genes are differentially expressed (*fer*-DE genes, $q<0.05$), with 3,127 up-regulated and 3,868 down-regulated genes in the *fer* mutant, respectively (Fig. 2.1A,

Dataset1 and Dataset 2). In order to better understand FER-mediated signaling, we compared *fer*-DE genes with plant hormone-regulated genes. When compared to the genes regulated by growth-promoting hormones including brassinosteroids (BRs), auxin (IAA) and cytokinin (CK) [28, 29], close correlations were revealed between *fer*-DE genes and genes regulated by BRs (Fig. 2S1A). Specifically, 29.6% of BR-induced genes are down-regulated in *fer* and 25.5% BR-repressed genes are up-regulated in *fer*, which supports our previous finding that FER is positively involved in BR-regulated plant growth [16].

When compared to the genes regulated by stress-related hormones Abscisic Acid (ABA), Salicylic Acid (SA), ethylene (ACC), Jasmonic Acid (JA) and Coronatine (COR) [29-31], a greater degree of overlap was observed between genes up-regulated in *fer* and ABA-, JA- and COR-induced genes; and between genes down-regulated in *fer* and ABA-, JA- and COR-repressed genes than the overlap with growth-related hormones (Fig. 2.1A). These results indicate that ABA-, JA- and COR-regulated gene expression is promoted in the *fer* mutant. For example, 59.8% (482/806 genes) of JA-induced genes are up-regulated in *fer* and 44% (309/701 genes) of JA-repressed genes are down-regulated in the mutant (Fig. 2.1A). We also tested whether JA-responsive gene expression was altered in *fer* by testing several JA-induced genes via RT-qPCR analysis, using 10-day-old seedlings without or with 100uM JA treatment. These experiments confirmed that JA-induced genes are constitutively up-regulated in *fer,* although the additional increase after JA treatment varied among the genes tested (Fig.2.1B-2.1E).

It is well known that COR, a phytotoxin from bacterial pathogens such as pst DC3000*,* is structurally similar to JA-Ile and can activate JA signaling in host plants to achieve host susceptibility [1]. Comparison of *fer*-DE genes and COR-regulated genes shows that more than 75% (713/944 genes) of COR-regulated genes are altered in *fer* mutant in a highly similar

manner. For example, 472 out of 597 COR-induced genes are differentially expressed in *fer*, more than 97% of which (457/472 genes) are up-regulated in *fer*. Likewise, 241 of 347 COR-repressed genes are differentially expressed in *fer,* 85% of which are down-regulated in the mutant (205/241 genes) (Fig. 2.1F, Fig. 2S1B). These global gene expression profiles indicate that JA/ COR signaling is up-regulated in the *fer* mutant. A recent report showed that *fer* is more sensitive to DC3000 COR^- and proposed a positive role of FER in PAMP-triggered immunity (PTI) [26]. Our results indicate that *fer* is also more susceptible to wild-type DC3000 (Fig. 2.1G). Given the striking changes of JA- and COR-regulated genes in *fer* it is also conceivable that elevated JA/COR signaling renders *fer* mutant more prone to bacterial pathogen infection.

The large number of genes mis-regulated in *fer* suggests that FER regulates diverse biological processes through transcriptional reprogramming; however, knowledge of transcription factors downstream of FER is limited. In order to elucidate the transcription factors involved in controling *fer*-DE genes, we conducted promoter analysis. These results revealed that the G-box sequence is highly enriched in the promoters of *fer*-DE genes (Fig. 2S1C, Dataset 3). The G-box exists in many JA target genes and is a binding site for MYC2, a major positive regulator mediating JA/COR signaling [32], suggesting that FER regulates JA- and COR-regulated genes through MYC2. To test the potential interaction of FER and MYC2, we generated a *fer myc2* double mutant and found that *myc2* mutation can suppress the *fer* stunted growth phenotype, with longer leaf petioles in the double mutant compared to that of *fer* (Fig. 2.1H, 2.1I). The partial suppression of *fer* growth phenotype by *myc2* implies that FER regulates additional factors that contribute to growth. While *myc2* mutants are less-sensitive to JA in both roots and shoots, *fer* is hypersensitive to JA. *myc2* suppressed *fer* hypersensitivity to JA in *fer myc2* (Fig. 2.1J, Fig. 2S1D-H). Additionally, bacterial infection assays showed that *myc2*

suppressed the elevated susceptibility of *fer* to DC3000 in the *fer myc2* double mutant (Fig. 2.1K). These results are consistent with the previous studies indicating that *myc2* is more resistant to bacterial infection [33]. Together, our genetic studies demonstrate that MYC2 functions downstream of FER and at least partially accounts for the positive role of FER in bacterial defense responses.

2.3.2 FER interacts with and phosphorylates MYC2

The genetic interaction of *FER* and *MYC2* led us to test if there is a physical interaction between the corresponding proteins. We first tested direct interactions between FER kinase domain (FERK) and MYC2 by GST pulldown assays (Fig. 2.2A-B, Fig. 2S2A-B). GST-FERK can directly interact with full-length MYC2, as well as its amino (N)-terminus (aa 1-251), but barely or not with carboxyl (C)-terminus (aa 440-623) and the middle region (aa 252-339). Next, the FER-MYC2 interaction was confirmed *in vivo* by Co-immunoprecipitation (Co-IP) and Bimolecular Fluroescence Complementation (BiFC). For these experiments, we employed FERm-GFP, the mutant FER-GFP, in which the kinase activity is abolished with K565R mutation [17]. The mutation allowed FERm-GFP and MYC2-FLAG to express at higher levels in *N. benthamiana* (Fig. S2C), thus we used FERm-GFP here for both Co-IP and the following BiFC experiment. A similar approach has been used to detect interaction between ABI5 and its ubiquitin ligase, KEG since the interaction could only be detected with mutant KEG [34]. Although the reason for stabilization of FER-GFPm is not known, it is possible that similar to flagellin receptor FLS2 [35], FER also goes through endocytosis and subsequent degradation upon ligand perception and subsequent activity, which would explain the lower protein level of FER-GFP compared to that of the inactive FERm-GFP. When co-expressed in *N. benthamiana*

leaves, Co-IP experiments showed that MYC2-FLAG immunoprecipitated with anti-FLAG antibody is associated with FERm-GFP (Fig. 2.2C). Furthermore, BiFC assays with FERm-YFPN and MYC2-YFPC confirmed the interaction between these two proteins and indicated that FER and MYC2 interaction occurs in the cytoplasm (Fig. 2.2D).

The interaction between FER and MYC2 prompted us to test if FER kinase can phosphorylate MYC2. *In vitro* kinase assays showed that FERK indeed phosphorylates the full-length as well as the N-terminus (N) and Middle (M) region of MYC2 (Fig. 2.2E, Fig. 2S2D, 2S2E). To test if FER phosphorylates MYC2 *in vivo*, we generated an anti-MYC2 antibody that recognizes the middle region of MYC2. The antibody recognizes MYC2 in both whole-cell extract and in nuclear protein from wild-type (WT) plants but the signal corresponding to MYC2 protein is absent in *myc2* mutants (Fig. 2S2F). The MYC2 protein from both WT and *fer* mutant was immunoprecipitated by anti-MYC2 antibody. Western blotting with anti-phosphoserine antibody showed that MYC2 was phosphorylated in WT, and that phosphorylation was reduced in *fer* mutant (Fig. 2.2F), suggesting that MYC2 is phosphorylated by FER in vivo.

To determine the effect of FER phosphorylation on MYC2, we examined the MYC2 protein stability in both WT and *fer* mutant with cycloheximide (CHX) treatments. The half-life of MYC2 in WT was around 60 minutes, while the half-life of the protein was over 120 minutes in *fer* (Fig. 2.2G). Similar results were obtained when we co-expressed MYC2-FLAG with FER-GFP or FERm-GFP. Co-expression of FER, but not FERm, clearly reduced MYC2 protein levels (Fig. 2S2C). These results support the conclusion that FER functions to destabilize MYC2 protein.

We then mapped the FER phosphorylation sites on MYC2 using *in vitro* phosphorylated MYC2N and MYC2M via mass spectrometry. In total, 36 possible FER phosphorylation sites

were identified, including 6 sites in which phosphorylation was localized to a specific amino acid (Table 2S1). We chose 12 sites that are mostly conserved among different species (Table 2S2, Fig. 2.2B) for further mutational analysis. Mutations of these sites to Alanine (MYC2 NM^{A12}) largely reduced the FERK phosphorylation of MYC2 N-terminal and middle (NM) domain (Fig. 2.3A).

2.3.3 FER phosphorylation of MYC2 destabilizes MYC2

To further test the effect of the FER phosphorylation of MYC2 on its stability, we generated a mutant form of full length MYC2, $MYC2^{A12}$, and obtained stable transgenic Arabidopsis plants expressing $MYC2^{A12}$-FLAG. To test the phosphorylation status of $MYC2^{A12}$ in the transgenic plants, immunoprecipitation was carried out with anti-FLAG and the IP product was treated with alkaline phosphatase and resolved on a Phos-tag gel, which leads to slower migration of phosphorylated proteins (Fig. 2.3B). Two forms of MYC2 were observed after blotting with anti-MYC2 antibody both of which shifted downwards after phosphatase treatment in the WT MYC2-FLAG, consistent with phosphorylation of MYC2. On the other hand, the effect of the phosphatase treatment on $MYC2^{A12}$-FLAG was minimal (Fig. 2.3B), suggesting that the mutated amino acids are involved in MYC2 phosphorylation *in vivo*. The different mobility of the two MYC2 forms is likely due to post-translational modifications in addition to phosphorylation since both bands were still present after phosphatase treatments.

Next, we carried out cyclohexamide treatment with the transgenic lines, which showed that MYC2-FLAG has a half-life between 30 and 60 minutes (Fig. 2.3C) while MYC2 ^{A12}-FLAG is more stable with a half-life of around 90 minutes (Fig. 2.3D). Similar observations were made in transient assays in *N. benthamiana*. While MYC2 is clearly reduced by co-expression with

FER (Fig. 2S2G, lanes 2, 6, 10), stabilization of MYC2^{A12} was observed (Fig. 2S2G, lanes 4, 8,12). Compared to MYC2, the stability of MYC2^{A12} was increased 2.7 to 5.3 fold (Fig. 2S2H). Furthermore, treatment with the kinase inhibitor K252a promoted MYC2 accumulation (Fig. 2S2I), confirming that MYC2 stability is related to its phosphorylation.

In order to rule out the possibility that the mutations in MYC2 ^{A12} rendered the protein dysfunctional, we tested response to JA and pst DC3000 in the MYC2 transgenic lines. Similar to *MYC2-FLAGox*, *MYC2 ^{A12}-FLAGox* also showed hypersensitivity to JA treatment (Fig. 2.3E, Fig. 2S3A-D), and increased pst DC3000 growth (Fig. 2S3E), compared to WT plants, suggesting that MYC2 ^{A12} is functional in mediating JA responses. Taken together, these data suggest that FER phosphorylation of MYC2 is at least in part responsible for MYC2 destabilization.

With the knowledge that FER phosphorylates and destabilizes MYC2, we hypothesized that the elevated susceptibility of *fer* mutant to pst DC3000 is due to increased levels of MYC2. To test the hypothesis, we infiltrated WT, *fer* and *myc2* mutant plants with pst DC3000 and examined their MYC2 levels. In WT plants, nuclear MYC2 level is very low and accumulated after bacterial infection, reaching the highest level at 48 hours post infiltration and declining at 72 hours, with a 35% reduction relative to that of 48 hours (Fig. 2.3F, lanes 1-4). Interestingly, MYC2 accumulated significantly more in *fer* mutant and accumulated even more after bacterial infection, to the highest level at 48 hours post infiltration with a small decline at 72 hours (Fig. 2.3F, lanes 5-8), consistent with the prolonged half-life of MYC2 in *fer.* As expected, MYC2 was not detected in loss-of-function *myc2* mutants (Fig. 2.3F, lanes 9-12), and FER is absent from *fer* (Fig. 2.3F, lanes 5-8, Fig. 2S3F). Similar defense responses and MYC2 protein changes were also observed in the *amiRNA* knock down line of FER, *FERamiRNA* [16] (Fig. 2S3G-H),

confirming that these phenotypes were due to the absence of FER in the *fer* mutants. Furthermore, in transgenic plants expressing FER-GFP, MYC2 induction is greatly reduced 48 hours after pst DC3000 infection, compared to that of WT (Fig. 2S3I-J). Taken together, these results demonstrate that *pst* DC3000 infection induces MYC2 protein in host plants, and FER phosphorylates and destabilizes MYC2 to alleviate the pathogen-mediated host disease susceptibility. The increased MYC2 protein levels both prior and after pathogen infection in *fer* are likely at least partially responsible for its compromised immunity.

2.3.4 RALF23 functions through FER to regulate MYC2 and JA signaling

The peptide hormone RALF1 has been shown to function as ligand for FER [25]. RALF23 is a homolog of RALF1 and is negatively involved in plant growth [36]. In order to test ligand/receptor relationship of RALF23 and FER, we generated *RALF23ox fer* plants, where *RALF23* is overexpressed in *fer* mutant. *RALF23ox fer* showed a similar growth phenotype to *fer*, indicating that the function of RALF23 is dependent on FER (Fig. 2.4A, Fig. 2S4A).

During the course of our study, FER was reported to function as a scaffold protein for PAMP receptors and play a positive role in PTI and plant immunity, and that RALF23 functions through FER to negatively regulate PTI and plant immunity [26]. To test if RALF23 is also involved in MYC2 regulation and JA signaling, we carried out JA response using root growth assays. Similar to the elevated JA sensitivity of *fer*, *RALF23ox* root growth is also hypersensitive to JA treatment (Fig. 2.4B, Fig.2S3A, 3D and Fig. 2S4B-C). A bacterial infection assay showed that *RALF23ox* accumulated more bacteria than that of WT (Fig. 2.4C), in line with the increased MYC2 protein level in *RALF23ox* (Fig. 2.4D). Moreover, analysis of JA target gene expression in *RALF23ox* showed that some target genes such as *RD26* and *TAT* displayed similar pattern of

JA response to that in *fer* (Fig. 2.4E-F, compare with Fig.2.1B-C), with higher basal expression and additional increase in expression upon JA treatment. Other genes such as *VSP1* and *PDF1.2*, showed increased induction after JA treatment (Fig. 2.4G-H), although these genes had a lower absolute expression level in *RALF23ox* compared to WT (Fig. 2S4D-E). This phenomenon might be due to complex interactions between FER, MYC2 and other transcription factors in JA target gene regulation. For example, MYC2 and ORA59 negatively regulate each other, and potentially negatively regulate each other's target genes (e.g. VSP1 and PDF1.2) [37].

In order to rule out compensatory effects regarding MYC2 levels in *RALF23ox* plants, we tested the short-term effect of RALF23 on MYC2 stability in *N. benthamiana*. *RALF23-MYC*, used for generating *RALF23ox,* was co-infiltrated with *FER-GFP, MYC2-FLAG* and *S1P-YFP*. S1P, SITE-1 PROTEASE, is required for the production of active RALF23 peptide [26, 36]. Consistent with the increased MYC2 levels in *RALF23ox* plants, accumulation of MYC2-FLAG was observed 48 hours post co-infiltration with *RALF23-MYC*, compared to vector only control (Fig. 2.4I, Fig. 2S4F-G). These results demonstrate that both short-term and long-term RALF23 expression lead to increased MYC2 protein accumulation.

To test the effect of RALF23 on MYC2 phosphorylation, we conducted immunoprecipitation with anti-MYC2 from cytoplasmic proteins of *RALF23ox* along with WT and *fer,* treated with pst DC3000 for 48 hours. Since FER interacts with MYC2 in the cytoplasm, we reasoned that we can observe FER-specific MYC2 phosphorylation in cytoplasmic proteins in a less biased way, and pathogen treatment increases MYC2 level so we can circumvent the problem caused by the potential high instability of FER-phosphorylated MYC2. After resolved on a Phos-tag gel, the MYC2 IP showed two distinct forms that are shifted down after alkaline phosphatase treatment, suggesting that MYC2 is phosphorylated and likely exists in two

different forms (Fig. 2S4H), consistent with what we observed with MYC2-FLAG (Fig. 2.3B). The portion of phosphorylated MYC2 protein is decreased in *fer* compared to the non-cytoplasmic MYC2, indicating the phosphorylation is FER-specific. Interestingly, there is only one form of phosphorylated MYC2 observed in *RALF23ox* and the portion of phosphorylated MYC2 is also decreased compared to that of WT, indicating that RALF23 inhibited MYC2 phosphorylation. The difference between *RALF23ox* and *fer* might be due to RALF23's regulation on FER homologs that are potentially involved in MYC2 phosphorylation as well. The results suggest that RALF23 functions through FER to play a positive role in JA signaling and negative role in plant immunity by suppressing FER function and elevating MYC2 levels. We also observed that FER protein level is decreased in *RALF23ox* transgenic plants, which provides another form of regulation of FER by RALF23 (Fig. 2S4I).

2.4 Conclusions and Discussion

In summary, our results demonstrate that FER negatively regulates JA/COR signaling and positively contributes to plant immunity, which establishes FER as a critical regulator of JA/COR signaling and provides a novel mechanism that host plants possess to counteract COR-mediated MYC2 elevation (Fig. 2S4J) and disease susceptibility. It has recently been reported that RALF23 functions through FER to negatively regulate PTI and plant immunity [26]. It is conceivable that RALF23/FER-mediated signaling pathway employs different means to regulate both host plant disease susceptibility through MYC2 and defense responses through PTI. Our study thus establishes a more comprehensive signaling pathway from a peptide ligand

(RALF23), to its receptor (FER) and downstream transcription factor (MYC2) in the regulation of JA/COR signaling and plant responses to bacterial pathogen infection (Fig. 2.4J).

In addition to FER's role as a negative regulator in JA signaling, our global gene expression data also indicate that FER functions to suppress many other hormone-regulated stress responses. It has been reported that FER suppresses ABA signaling through the activation of ABI2 but how FER regulates SA and ethylene signaling is not clear. We have also shown that FER is positively involved in plant growth, in cooperation with growth-related hormones such as BRs, but the detailed mechanism remains to be elucidated. Future studies of the crosstalk between FER signaling and hormonal pathways will reveal more complete mechanisms by which FER regulates plant growth and stress responses.

2.5 Acknowledgements

HG would like to thank Prof. Jo Anne Powell-Coffman and Prof. Steve Whitham for guidance and encouragement, Dr. Bing Yang for pst DC3000, Dr. Ping He for pst DC3000 COR^-. The research is supported by grants from NSF (IOS-1257631), NIH (1R01GM120316-01A1), and by Plant Sciences Institute at Iowa State University.

2.6 Author Contributions

HG and YY conceived the project. HG performed most of the genetic, molecular and biochemical experiments. TN performed confocal microscopy experiments, gene expression comparisons and assisted with mapping MYC2 phosphorylation sites. SL and PSS performed RNAseq analysis. GS and JWW performed mass spectrometry and analysis. XZ performed GST

pulldown assay and JC generated FER antibody. All authors contributed to analysis of corresponding data. HG wrote the paper with edits from other co-authors.

2.7 Methods

Plant Materials and Growth Conditions

The Arabidopsis accession Columbia-0 was used as WT in all experiments. T-DNA insertion mutants *fer*-4 (GABI_106A06) and *myc2* (Salk_061267), were obtained from the Arabidopsis Biological Resource Center (ABRC) [38]. The *fer-4* mutant is referred as *fer* in this manuscript. The *fer myc2* double mutant was generated by crossing *fer* to *myc2*. *RALF23ox* was produced previously [36]. The *fer RALF23ox* was generated by crossing *fer* to *RALF23ox*. For all experiments involving Arabidopsis plants, seeds were sterilized with 70% ethanol containing 0.1% triton and germinated on 1/2MS plates with 1% sucrose and 0.8% agar.

RNA-seq

For global gene expression profiling, 12-day-old seedlings were transferred to soil and grown at 22ºC with 75% humidity under short day conditions with an 8-hour light and 16-hour dark cycle in a growth chamber. After 3 more weeks, leaf tissues were collected and RNA was isolated using Trizol (Invitrogen) following the manufacturer's protocol. The RNA samples were then purified using RNeasy kit (Qiagen) following the manufacturer's protocol. RNA-seq was performed at the DNA facility of Iowa State University with Illumina HiSeq 2000.

Bacterial pathogen growth and infiltration

Plants for the experiments were grown under same conditions as the ones for RNA sequencing. Bacterial pathogen strain used in this study was *Pseudomonas syringae* pv. tomato (*Pst)*

DC3000 and the Coronatine deficient strain, *pst* DC3000 Cor$^-$. The *Pst* DC3000 was grown on plates with King's B medium containing 30ug/ml Rifampin at 28ºC for 3 days before use, and pst DC3000 Cor$^-$ grown under same condition except the addition of 100ug/ul Ampicillin.

Bacterial pathogen accumulation experiments were done as described [39] with modifications. Briefly, *pst* DC3000 was scraped from the plate and resuspended in H2O, then diluted to an OD_{600} of 0.001 (about 10^6 colony forming unit or cfu/ml). The leaf infiltration was done with 1ml syringe without a needle on the abaxial side of the leaf. Usually 2-3 healthy and mature leaves per plant and 10-15 healthy plants were used per treatment. The infected plants were covered with a transparent plastic dome for 12 hours. Leaf discs (7mm in diameter) were collected with a hole puncher at indicated time points with 8-10 leaf discs per sample and three replicates per treatment. The leaf discs were ground in 0.5 ml sterile H2O, then the volume was brought up to 100 μl/disc with H2O, which was diluted serially (5 or 10 times for each dilution, 5-6 dilutions). Aliquots (10 μl) of each dilution were plated onto a grid of a gridded plate with King's B medium containing 30 μg/ml Rifampin and grown as described above. The numbers of bacterial colonies were counted and used to calculate the bacterial accumulation in plants (CFU/leaf disc). The average and standard deviation were derived from three replicates. The experiments were repeated more than three times and representative results are presented.

For MYC2 protein induction assay, pst DC3000 and pst DC3000 Cor$^-$ were diluted to OD600 of 0.001 and 0.1, respectively, in H2O, and H2O only served as control. Leaves were collected at indicated times after infiltration for total or nuclear protein extraction, followed by Western blotting detection.

Jasmonic acid treatment

For root growth inhibition assay, seeds of different genotypes were germinated on 1/2MS plates with 50μm Jasmonic acid (Sigma) or control. The plates were kept at 4°C for 4 days and placed vertically for 7-8 days under constant light. About 12-18 representative seedlings from each genotype on JA or control plate were placed on a fresh 1/2MS plate and subjected to scanning.

For shoot growth assay, seeds of different genotypes were sterilized and spotted on gridded plate to better control the density and plates were kept at 4°C for 4 days and then placed horizontally under constant light. Plates with seedlings were scanned two weeks later.

For qPCR experiments, 7-day-old seedlings grown on 1/2MS plates were transferred to 1ml liquid1/2MS medium in 24-well plates and incubated for 2 hours to minimize any mechanical touching effect. Then 1ml liquid 1/2MS containing 100uM JA or control was added to each well, to make the final JA concentration 50uM. Three replicates for each treatment of each genotype were collected 10 hours after the treatment. RNA was extracted as described above, and qPCR was performed using SYBR Green PCR master mix (Applied Biosystems) on the Stratagene Mx4000 real time PCR system.

Total protein and nuclear protein extraction

For total protein extraction from *Arabidopsis*, 100 mg tissues were collected and flash frozen in liquid nitrogen and ground directly in 300 μl of 2xSDS sample buffer (100 mM Tris-Cl, pH6.8, 4% (w/v) sodium dodecyl sulfate, 0.2% (w/v) bromophenol blue, 20% (v/v) glycerol and 200 mM dithiothreitol) before SDS-PAGE and western blotting. For transient expression in *Nicotiana benthamiana*, 5 leaf discs (7mm in diameter) were collected for each sample and flash frozen in liquid nitrogen and ground directly in 200 μl of 2xSDS sample buffer.

Nuclear protein extraction was carried out as described [40]. Briefly, half to one gram of tissue was collected and flash frozen in liquid Nitrogen and ground to powder. The powdered sample was then resuspended in the lysis buffer (20mM Tris-HCl pH7.4, 25% Glycerol, 20mM KCl, 2mM EDTA, 2.5mM $MgCl_2$, 250mM Sucrose, 1mM DTT and 1mM PMSF added right before use), and filtered through 0.45um mesh to a new tube and spun for 10 min at 1500xg at 4°C. The pellet was resuspended in the nuclei resuspension buffer (20mM Tris-HCl pH7.4, 25% Glycerol, 2.5mM $MgCl_2$) with 0.2% triton and spun for 10 min at 1500xg at 4°C. After two more washes, the nuclei were resuspended in the resuspension buffer without triton and spun for 10 min at 1500xg at 4°C. The pellet was then resuspanded in 2xSDS buffer and used in western blotting. Nuclei from 1 g of tissue was resuspended in 100 µl of 2xSDS buffer.

Antibody Production

Anti-MYC2 was generated against MBP fusion protein with middle domain of MYC2 (amino acids 251-440) and anti-FER was generated against MBP fusion protein with FER kinase domain (amino acids 470-895) in rabbits. The antibodies were purified with GST fusion proteins by affinity chromatography.

Protein half-life determination

This assay was carried out as described with modifications [41]. Briefly, seeds were germinated on 1/2MS plates vertically for 10 days. For WT and *fer*, seedlings were transferred to a 24 well plate containing 1/2MS liquid medium with 50µM MG132, and gently rocked for 16 hours. The seedlings were rinsed with fresh 1/2MS liquid medium 5 times, and supplied with fresh 1/2MS liquid medium containing 200µM Cycloheximide (CHX), DMSO as control. For *MYC2-FLAGox* and *MYC2^{A12}-FLAGox* transgenic plants, seedlings were incubated in 1ml 1/2MS medium for 2 hours to minimize any mechanical touching effect, and then 1ml 1/2MS containing 400 µM

CHX or DMSO was added. Seedlings were collected at the time points indicated in the Figs. 2G, 3C and 3D, and gently dabbed dry and flash frozen in liquid nitrogen. The samples were ground in 2xSDS sample buffer and used for western blotting. Protein half-life was estimated as the time when the protein level decreased to half of the amount compared to that of the control.

Transient expression assay in *Nicotiana benthamiana*

Nicotiana benthamiana seeds were germinated in soil and the seedlings were transferred to soil in individual pots. About two-month-old plants were used for the assays. Agrobacterial cultures carrying the genes of interest were grown in liquid LB medium with antibiotics in a 30°C shaker for 2 days. The cultures were spun down in 1.5ml microtubes at full speed for 1 minute. The Agrobacterium cells were resuspended in infiltration buffer (10mM $MgCl_2$, 10mM MES, pH 5.7, 200μM Acetosyringone). The density was measured at 600 nm wavelength and each Agrobacterium culture was diluted to final concentration of OD600 0.3 for infiltration. The leaf infiltration was done with 1ml syringe without needle on the abaxial side of the leaf.

BiFC Assay

BiFC assay was conducted using the N-or C-terminus of YFP [42] as decribed in [43]. FERm was fused to the upstream of YFP-N and MYC2 was fused to the upstream of YFP-C and transformed into *Agrobacterium tumefaciens*. The different combinations of *Agrobacterium* (Fig. 2D) were infiltrated into *Nicotiana benthamiana* leaves. After 48 hours, the YFP signal was detected using a Leica SP5 X MP confocal microscope with an HCS PL APO CS 20x0.7 oil objective. YFP was excited with a laser line of 514nm and detected from 530-560nm. Images were acquired with LAS AF software using identical settings for both specific interaction and controls.

Co-immunoprecipitation (Co-IP)

Agrobacteria carrying FERm-GFP and MYC2-FLAG were co-infiltrated into *Nicotiana benthamiana* leaves, co-infiltration of vector containing GFP only and MYC2-FLAG, vector containing FLAG only and FERm-GFP as controls. Leaf samples were collected two days after the infiltration. One gram of each sample was ground in liquid nitrogen and extracted with 2.5 ml IP buffer (10mM HEPEs pH7.5, 100mMNaCl, 1mM EDTA, 10% Glycerol, 0.5% NP-40) [44], with 1mM PMSF (phenylmethylsulfonyl fluoride, a serine protease inhibitor) and one pellet of the protease inhibitors/10ml from Roche. After 10 min rotation at 4°C, the mixture was centrifuged at 10,000 rpm for 10 min at 4°C and filtered through two layers of Miracloth (Millipore, Inc.). The IP was performed by adding 30µl of GFP-TRAP-MA (Chromotek) to the filtered plant extract, rotated at 4°C for 2 hours. The IP product was precipitated using a magnetic stand after a brief spin at 1000xg for one minute, and washed twice with IP buffer containing 0.5% NP-40 and twice with IP buffer without NP-40. The IP product was resuspended in 2xSDS buffer and resolved on SDS-PAGE gel. Anti-GFP and anti-FLAG antibody were used to detect FERm-GFP and MYC2-FLAG, respectively.

Immunoprecipitation (IP) and *in vivo* phosphorylation detection

For MYC2 phosphorylation in *Arabidopsis*, 8 grams of WT and 4 grams of *fer* 4-week old plants were collected and ground in liquid nitrogen. IP was carried out using 50ul anti-MYC2 antibody in 20ml IP buffer as described above, except that Halt protease and phosphatase inhibitor cocktail was used. 25ul Dynabeads Protein A (Invitrogen) was used to pull down anti-MYC2 antibody. Anti-MYC2 antibody and Anti-phosphoserine antibody (Sigma) were used to detect MYC2 and MYC2 phosphorylation, respectively.

For MYC2-FLAG and MYC2-FLAG^{A12} phosphorylation detection, the corresponding proteins were immunoprecipitated from transgenic plants overexpressing them using anti-FLAG-M2 magnetic beads. About 1 gram of leaf tissue of each genotype was collected from 4-week old plants, flash frozen and ground to powder. IP was carried out using a-FLAG M2 magnetic beads in 2.5ml IP buffer the same as described above, with 0.5% NP-40, 1mM PMSF and one pellet of the protease inhibitor/10ml from Roche, for 2 hours. The beads were collected with a magnetic stand, and washed with 50mM HEPES buffer (pH 7.5) 4 times. The beads were then resuspended in 100ul 1x phosphatase buffer. Half was taken to a new tube and 1.5ul phosphatase was added and the second half served as control. The reactions were incubated at 37°C with rotation for one hour and stopped by adding 10ul 6xSDS buffer. The reactions were resolved on a Phos-tag gel (Waco) and anti-MYC2 anitbodies were used for western blotting.

For IP with anti-MYC2 from cytoplasmic proteins, pst-DC3000-infiltrated leaves were collected and ground to powder in liquid nitrogen. Cytoplasmic protein was separated from non-cytoplasmic protein as described in the nuclear protein extraction. IP was carried out with the cytoplasmic portion, and the non-cytoplasmic portion was resuspended in 2XSDS buffer and used as control.

In vitro GST pull-down assay

GST pull-down assays were performed as described previously [41]. Briefly, FERK fused to glutathione-S- transferase (GST) were purified using glutathione HiCap Matrix (Qiagen). Different MYC2 fragments fused to maltose binding protein (MBP) were purified using amylose resin (NEB). Approximately 2μg of proteins were mixed into 1ml of pull-down buffer (50mM Tris-HCl, pH7.5, 200mM NaCl, 0.5% Trition X-100, 0.5mM β-mercaptoethanol, and protease inhibitor from Roche), and incubated at room temperature for 2 hours with rotation,

then 10ul of GST beads (washed twice using the pull down buffer) were added to each reaction and incubate the same condition for another 2 hours. The GST beads were spun down, washed 5 times with the pull down buffer, resuspended in 2XSDS buffer, resolved on 8% SDS-PAGE gel and detected by anti-MBP (NEB) antibody, 1% of each MBP fusion protein as input. The pulldown assays were repeated three times with similar results.

In vitro kinase assay and Mass Spectrometry to identify FER phosphorylation sites on MYC2

For in vitro kinase assays, GST, GST-MYC2, GST-MYC2N, GST-MYC2M (Fig. 2E), GST-MYC2NM and GST-MYC2NM^{A12} (Fig. 3A) proteins were mixed with GST-FERK in 20 μL kinase buffer (20 mM Tris, pH 7.5, 100 mM NaCl, 12 mM MgCl2 and 10μCi ^{32}P-γATP) as previously described [45] and incubated at room temperature for 1 hour. The reactions were stopped by the addition of 2xSDS sample buffer and resolved on 8% SDS-PAGE. The phosphorylation was detected using phosphoimager. For the control for GST-FERK specificity, GST-MYC2M (Fig. S2E) was mixed with GST or GST-FERK and kinase assay and phosphorylation detection were carried out as above.

Mass spectrometry analysis of phosphorylated proteins was carried out as described [43]. MBP-MYC2N and MBP-MYC2M were phosphorylated by GST-FERK in kinase buffer containing 10 mM ATP. Reactions without GST-FERK were used as controls. Samples were subjected to protein digestion using Glu-C (ThermoFisher) and Trypsin (Roche) and LC-MS/MS performed using a Thermo Scientific Q-Exactive high-resolution quadrupole Orbitrap mass spectrometer. The raw data were extracted and searched against the TAIR10 proteome using Spectrum Mill v4.01 (Agilent Technologies). Phosphorylation sites were localized to a particular

amino acid within a phosphopeptide using the variable modification localization (VML) score in Agilent's Spectrum Mill software [46].

Quantification and statistical analysis

RNA-seq data analysis

Raw RNA-seq reads were subjected to quality checking and trimming and then aligned to the Arabidopsis reference genome (TAIR10) using Genomic Short-read Nucleotide Alignment Program (GSNAP) [47] . The alignment coordinates of uniquely aligned reads for each sample were used to calculate the read depth of each annotated gene. These values were used to detect differential expression between WT and *fer* mutant samples. Two biological replicates were used for each genotype. The negative binomial QLSpline method implemented in the QuasiSeq package (http://cran.r-project.org/web/packages/QuasiSeq) was used to compute a p-value for each gene with minimum one average read across all the samples in the comparison. The 0.75 quantile of reads from each sample was used as the normalization factor [48]. The adjusted p-values (q-values) were converted from p-values using a multiple test controlling approach [49, 50]. To control the false discovery rate at the 5% level, genes with q-values smaller than 0.05 were declared to be differentially expressed. The raw RNA seq data was deposited and can be found using the following link: https://www.ncbi.nlm.nih.gov/biosample?LinkName=bioproject_biosample_all&from_uid=215313.

Venn diagrams were generated using Venny (http://bioinfogp.cnb.csic.es/tools/venny/). Comparisons of hormone [29-31] and *fer*-regulated genes were performed in R (version 3.3.0) using the *GeneOverlap* package (version 1.12.0; http://shenlab-sinai.github.io/shenlab-sinai/). P-values for intersections between gene lists were assessed using Fisher's exact test and visualized

with ComplexHeatmap. Clustering analysis of *fer* RNA-seq data was performed using the 'aheatmap' function of the NMF package in R (https://cran.r-project.org/web/packages/NMF/index.html) using log2 reads per million mapped reads (RPM) values. For identification of enriched promoter elements, 500bp promoter region of the selected 1277 *fer*-regulated genes (q<0.05 and >2 fold change), were bulk downloaded from TAIR and submitted to DREME [51] in the MEME Suite motif discovery (http://meme-suite.org/doc/dreme.html).

Root length measurement

The measurement of the root length was carried out using ImageJ. Statistical significance was calculated using Tukey HSD test. P-values less than 0.05 were considered significant.

Data and software availability

The raw RNA-seq data were deposited to NCBI and freely available at https://www.ncbi.nlm.nih.gov/biosample?LinkName=bioproject_biosample_all&from_uid=215313. The Mass spectrometry data is deposited to The MASSIVE database "ftp://MSV000080972@massive.ucsd.edu" with ID MSV000080972 and Password "MYC2". All other original data are available upon requests.

2.8 References

1. Xin, X.F., and He, S.Y. (2013). Pseudomonas syringae pv. tomato DC3000: a model pathogen for probing disease susceptibility and hormone signaling in plants. Annu Rev Phytopathol *51*, 473-498.

2. Zheng, X.Y., Spivey, N.W., Zeng, W., Liu, P.P., Fu, Z.Q., Klessig, D.F., He, S.Y., and Dong, X. (2012). Coronatine promotes Pseudomonas syringae virulence in plants by activating a signaling cascade that inhibits salicylic acid accumulation. Cell Host Microbe *11*, 587-596.

3. Spoel, S.H., Koornneef, A., Claessens, S.M., Korzelius, J.P., Van Pelt, J.A., Mueller, M.J., Buchala, A.J., Metraux, J.P., Brown, R., Kazan, K., et al. (2003). NPR1 modulates

cross-talk between salicylate- and jasmonate-dependent defense pathways through a novel function in the cytosol. Plant Cell *15*, 760-770.

4. Zander, M., La Camera, S., Lamotte, O., Metraux, J.P., and Gatz, C. (2010). Arabidopsis thaliana class-II TGA transcription factors are essential activators of jasmonic acid/ethylene-induced defense responses. Plant J *61*, 200-210.

5. Mao, P., Duan, M., Wei, C., and Li, Y. (2007). WRKY62 transcription factor acts downstream of cytosolic NPR1 and negatively regulates jasmonate-responsive gene expression. Plant Cell Physiol *48*, 833-842.

6. Li, J., Brader, G., and Palva, E.T. (2004). The WRKY70 transcription factor: a node of convergence for jasmonate-mediated and salicylate-mediated signals in plant defense. Plant Cell *16*, 319-331.

7. Yu, Y., Chakravorty, D., and Assmann, S.M. (2018). The G Protein beta-Subunit, AGB1, Interacts with FERONIA in RALF1-Regulated Stomatal Movement. Plant Physiol *176*, 2426-2440.

8. Feng, W., Kita, D., Peaucelle, A., Cartwright, H.N., Doan, V., Duan, Q., Liu, M.C., Maman, J., Steinhorst, L., Schmitz-Thom, I., et al. (2018). The FERONIA Receptor Kinase Maintains Cell-Wall Integrity during Salt Stress through Ca(2+) Signaling. Curr Biol *28*, 666-675 e665.

9. Chen, J., Yu, F., Liu, Y., Du, C., Li, X., Zhu, S., Wang, X., Lan, W., Rodriguez, P.L., Liu, X., et al. (2016). FERONIA interacts with ABI2-type phosphatases to facilitate signaling cross-talk between abscisic acid and RALF peptide in Arabidopsis. Proc Natl Acad Sci U S A *113*, E5519-5527.

10. Yu, F., Qian, L., Nibau, C., Duan, Q., Kita, D., Levasseur, K., Li, X., Lu, C., Li, H., Hou, C., et al. (2012). FERONIA receptor kinase pathway suppresses abscisic acid signaling in Arabidopsis by activating ABI2 phosphatase. Proc Natl Acad Sci U S A *109*, 14693-14698.

11. Kessler, S.A., Shimosato-Asano, H., Keinath, N.F., Wuest, S.E., Ingram, G., Panstruga, R., and Grossniklaus, U. (2010). Conserved molecular components for pollen tube reception and fungal invasion. Science *330*, 968-971.

12. Keinath, N.F., Kierszniowska, S., Lorek, J., Bourdais, G., Kessler, S.A., Shimosato-Asano, H., Grossniklaus, U., Schulze, W.X., Robatzek, S., and Panstruga, R. (2010). PAMP (pathogen-associated molecular pattern)-induced changes in plasma membrane compartmentalization reveal novel components of plant immunity. J Biol Chem *285*, 39140-39149.

13. Duan, Q., Kita, D., Li, C., Cheung, A.Y., and Wu, H.M. (2010). FERONIA receptor-like kinase regulates RHO GTPase signaling of root hair development. Proc Natl Acad Sci U S A *107*, 17821-17826.

14. Deslauriers, S.D., and Larsen, P.B. (2010). FERONIA is a key modulator of brassinosteroid and ethylene responsiveness in Arabidopsis hypocotyls. Mol Plant *3*, 626-640.

15. Guo, H., Ye, H., Li, L., and Yin, Y. (2009). A family of receptor-like kinases are regulated by BES1 and involved in plant growth in Arabidopsis thaliana. Plant Signal Behav *4*, 784-786.

16. Guo, H., Li, L., Ye, H., Yu, X., Algreen, A., and Yin, Y. (2009). Three related receptor-like kinases are required for optimal cell elongation in Arabidopsis thaliana. Proc Natl Acad Sci U S A *106*, 7648-7653.

17. Escobar-Restrepo, J.M., Huck, N., Kessler, S., Gagliardini, V., Gheyselinck, J., Yang, W.C., and Grossniklaus, U. (2007). The FERONIA receptor-like kinase mediates male-female interactions during pollen tube reception. Science *317*, 656-660.

18. Schoenaers, S., Balcerowicz, D., Breen, G., Hill, K., Zdanio, M., Mouille, G., Holman, T.J., Oh, J., Wilson, M.H., Nikonorova, N., et al. (2018). The Auxin-Regulated CrRLK1L Kinase ERULUS Controls Cell Wall Composition during Root Hair Tip Growth. Curr Biol *28*, 722-732 e726.

19. Mang, H., Feng, B., Hu, Z., Boisson-Dernier, A., Franck, C.M., Meng, X., Huang, Y., Zhou, J., Xu, G., Wang, T., et al. (2017). Differential Regulation of Two-Tiered Plant Immunity and Sexual Reproduction by ANXUR Receptor-Like Kinases. Plant Cell *29*, 3140-3156.

20. Ge, Z., Bergonci, T., Zhao, Y., Zou, Y., Du, S., Liu, M.C., Luo, X., Ruan, H., Garcia-Valencia, L.E., Zhong, S., et al. (2017). Arabidopsis pollen tube integrity and sperm release are regulated by RALF-mediated signaling. Science *358*, 1596-1600.

21. Shih, H.W., Miller, N.D., Dai, C., Spalding, E.P., and Monshausen, G.B. (2014). The receptor-like kinase FERONIA is required for mechanical signal transduction in Arabidopsis seedlings. Curr Biol *24*, 1887-1892.

22. Boisson-Dernier, A., Lituiev, D.S., Nestorova, A., Franck, C.M., Thirugnanarajah, S., and Grossniklaus, U. (2013). ANXUR receptor-like kinases coordinate cell wall integrity with growth at the pollen tube tip via NADPH oxidases. PLoS Biol *11*, e1001719.

23. Boisson-Dernier, A., Roy, S., Kritsas, K., Grobei, M.A., Jaciubek, M., Schroeder, J.I., and Grossniklaus, U. (2009). Disruption of the pollen-expressed FERONIA homologs ANXUR1 and ANXUR2 triggers pollen tube discharge. Development *136*, 3279-3288.

24. Hematy, K., Sado, P.E., Van Tuinen, A., Rochange, S., Desnos, T., Balzergue, S., Pelletier, S., Renou, J.P., and Hofte, H. (2007). A receptor-like kinase mediates the response of Arabidopsis cells to the inhibition of cellulose synthesis. Curr Biol *17*, 922-931.

25. Haruta, M., Sabat, G., Stecker, K., Minkoff, B.B., and Sussman, M.R. (2014). A peptide hormone and its receptor protein kinase regulate plant cell expansion. Science *343*, 408-411.

26. Stegmann, M., Monaghan, J., Smakowska-Luzan, E., Rovenich, H., Lehner, A., Holton, N., Belkhadir, Y., and Zipfel, C. (2017). The receptor kinase FER is a RALF-regulated scaffold controlling plant immune signaling. Science *355*, 287-289.

27. Li, C., Yeh, F.L., Cheung, A.Y., Duan, Q., Kita, D., Liu, M.C., Maman, J., Luu, E.J., Wu, B.W., Gates, L., et al. (2015). Glycosylphosphatidylinositol-anchored proteins as chaperones and co-receptors for FERONIA receptor kinase signaling in Arabidopsis. Elife *4*.

28. Ye, H., Liu, S., Tang, B., Chen, J., Xie, Z., Nolan, T.M., Jiang, H., Guo, H., Lin, H.Y., Li, L., et al. (2017). RD26 mediates crosstalk between drought and brassinosteroid signalling pathways. Nat Commun *8*, 14573.

29. Nemhauser, J.L., Hong, F., and Chory, J. (2006). Different plant hormones regulate similar processes through largely nonoverlapping transcriptional responses. Cell *126*, 467-475.

30. Pajerowska-Mukhtar, K.M., Wang, W., Tada, Y., Oka, N., Tucker, C.L., Fonseca, J.P., and Dong, X. (2012). The HSF-like transcription factor TBF1 is a major molecular switch for plant growth-to-defense transition. Curr Biol *22*, 103-112.

31. Thilmony, R., Underwood, W., and He, S.Y. (2006). Genome-wide transcriptional analysis of the Arabidopsis thaliana interaction with the plant pathogen Pseudomonas syringae pv. tomato DC3000 and the human pathogen Escherichia coli O157:H7. Plant J *46*, 34-53.

32. Kazan, K., and Manners, J.M. (2013). MYC2: the master in action. Mol Plant *6*, 686-703.

33. Laurie-Berry, N., Joardar, V., Street, I.H., and Kunkel, B.N. (2006). The Arabidopsis thaliana JASMONATE INSENSITIVE 1 gene is required for suppression of salicylic acid-dependent defenses during infection by Pseudomonas syringae. Mol Plant Microbe Interact *19*, 789-800.

34. Liu, H., and Stone, S.L. (2013). Cytoplasmic degradation of the Arabidopsis transcription factor abscisic acid insensitive 5 is mediated by the RING-type E3 ligase KEEP ON GOING. J Biol Chem *288*, 20267-20279.

35. Robatzek, S., Chinchilla, D., and Boller, T. (2006). Ligand-induced endocytosis of the pattern recognition receptor FLS2 in Arabidopsis. Genes Dev *20*, 537-542.

36. Srivastava, R., Liu, J.X., Guo, H., Yin, Y., and Howell, S.H. (2009). Regulation and processing of a plant peptide hormone, AtRALF23, in Arabidopsis. Plant J *59*, 930-939.

37. Wasternack, C., and Hause, B. (2013). Jasmonates: biosynthesis, perception, signal transduction and action in plant stress response, growth and development. An update to the 2007 review in Annals of Botany. Ann Bot *111*, 1021-1058.

38. Alonso, J.M., Stepanova, A.N., Leisse, T.J., Kim, C.J., Chen, H., Shinn, P., Stevenson, D.K., Zimmerman, J., Barajas, P., Cheuk, R., et al. (2003). Genome-wide insertional mutagenesis of Arabidopsis thaliana. Science *301*, 653-657.

39. Katagiri, F., Thilmony, R., and He, S.Y. (2002). The Arabidopsis thaliana-pseudomonas syringae interaction. Arabidopsis Book *1*, e0039.

40. Xu, F.a.C., C. (2012). Nuclear extraction from Arabidopsis thaliana. Bio-protocol *2*.

41. Jung, C., Zhao, P., Seo, J.S., Mitsuda, N., Deng, S., and Chua, N.H. (2015). PLANT U-BOX PROTEIN10 Regulates MYC2 Stability in Arabidopsis. Plant Cell *27*, 2016-2031.

42. Yu, X., Li, L., Li, L., Guo, M., Chory, J., and Yin, Y. (2008). Modulation of brassinosteroid-regulated gene expression by Jumonji domain-containing proteins ELF6 and REF6 in Arabidopsis. Proc Natl Acad Sci U S A *105*, 7618-7623.

43. Nolan, T.M., Brennan, B., Yang, M., Chen, J., Zhang, M., Li, Z., Wang, X., Bassham, D.C., Walley, J., and Yin, Y. (2017). Selective Autophagy of BES1 Mediated by DSK2 Balances Plant Growth and Survival. Dev Cell *41*, 33-46 e37.

44. Lu, D., Lin, W., Gao, X., Wu, S., Cheng, C., Avila, J., Heese, A., Devarenne, T.P., He, P., and Shan, L. (2011). Direct ubiquitination of pattern recognition receptor FLS2 attenuates plant innate immunity. Science *332*, 1439-1442.

45. Yin, Y., Wang, Z.Y., Mora-Garcia, S., Li, J., Yoshida, S., Asami, T., and Chory, J. (2002). BES1 accumulates in the nucleus in response to brassinosteroids to regulate gene expression and promote stem elongation. Cell *109*, 181-191.

46. Chalkley, R.J., and Clauser, K.R. (2012). Modification site localization scoring: strategies and performance. Mol Cell Proteomics *11*, 3-14.

47. Wu, T.D., and Nacu, S. (2010). Fast and SNP-tolerant detection of complex variants and splicing in short reads. Bioinformatics *26*, 873-881.

48. Bullard, J.H., Purdom, E., Hansen, K.D., and Dudoit, S. (2010). Evaluation of statistical methods for normalization and differential expression in mRNA-Seq experiments. BMC Bioinformatics *11*, 94.

49. Nettleton, D., Hwang, J.T.G., Caldo, R.A., and Wise, R.P. (2006). Estimating the number of true null hypotheses from a histogram of p-values. J. Agricultural, Biological, and Environmental Statistics *11*, 337-356.

50. Benjamini, Y., and Hochberg, Y. (1995). Controlling the false discovery rate: a practical and powerful approach to multiple testing. J. Roy. Statistical Society, Series B *57*, 289–300.

51. Bailey, T.L. (2011). DREME: motif discovery in transcription factor ChIP-seq data. Bioinformatics *27*, 1653-1659.

2.9 Figures

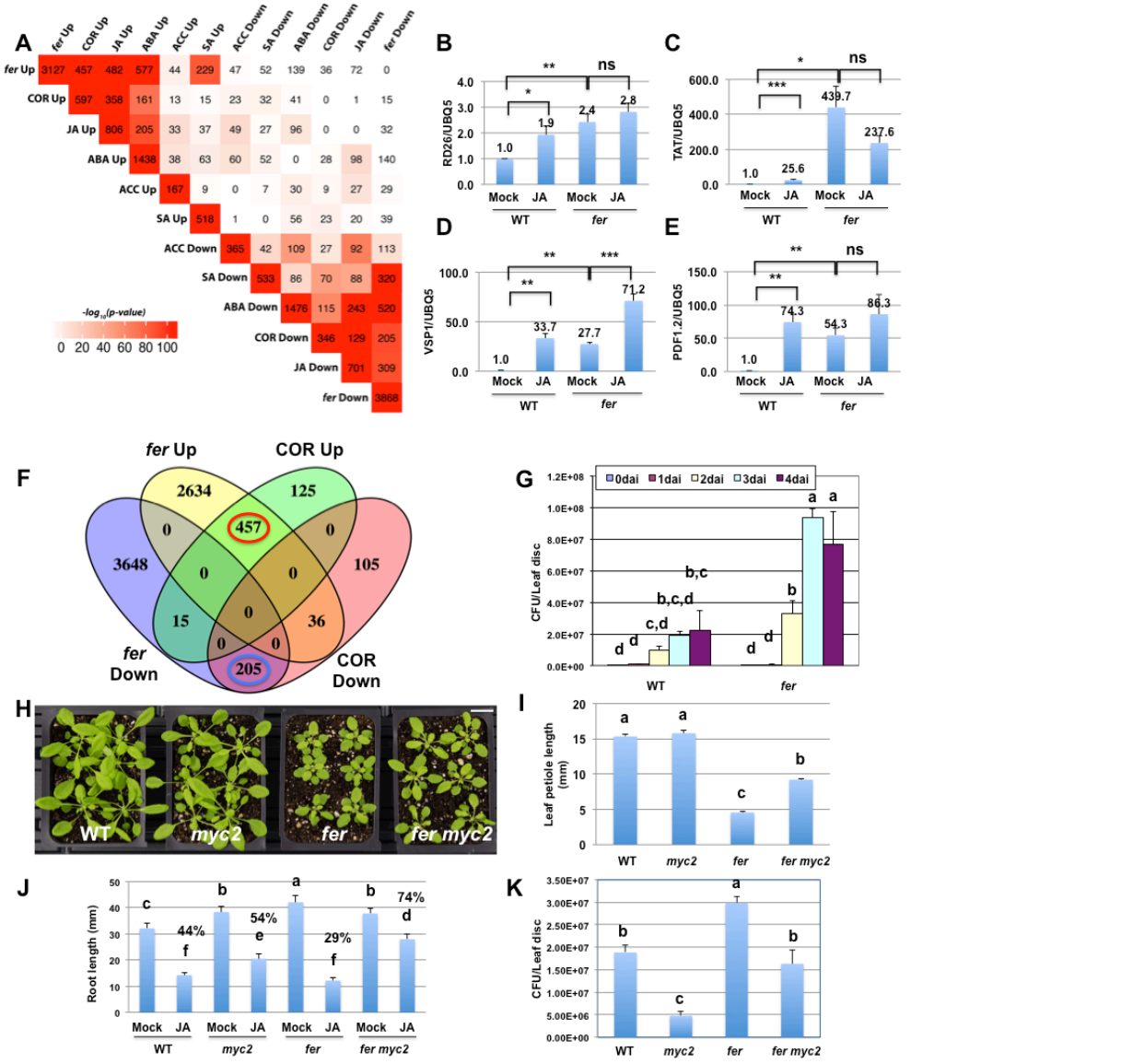

Figure 2.1: FER receptor kinase functions upstream of MYC2 to regulate JA signaling. **A,** Gene expression comparisons among *fer*-DEs and stress hormone-DEs. Color represents –log10 p-values from the indicated overlaps calculated from Fisher's exact test by GeneOverlap. The number of genes in each intersection is indicated. **B-E,** The up-regulation of several Jasmonic acid (JA)-induced genes in *fer* mutant and their JA induction were confirmed by qPCR. RNA

was prepared from 10-day-old WT or *fer* seedlings with or without 50uM JA for 10 hours, and qPCR was performed with indicated genes. Standard error was calculated based on 3 sets of samples per treatment, and student's t test was used to calculate the statistic significance. **F,** Venn diagram showing overlaps between Coronatine-induced (COR Up) or Coronatine-repressed genes (COR Down) and genes up- (f*er* Up) or down-regulated (fer Down) in *fer* mutant. The Coronatine-regulated genes were previously published [31] and genes differentially expressed in *fer* were determined by RNA-seq with 5-week-old WT and *fer* plants. **G,** *Pseudomonas synringae tomato* DC3000 accumulated more in *fer* mutant. The bacterium was infiltrated into 5-week-old plants and leaf discs were collected at different days after infiltration (dai). Bacterial accumulation was measured by Colony Forming Units (CFU) per leaf disc (n=3). The experiments were repeated more than 5 times with similar results [51]. **H-I,** Loss-of-function *myc2* mutant suppresses *fer* mutant phenotype in vegetative growth as shown with four-week-old plants of WT, *myc2*, *fer* and *fer myc2* double mutants. Bar in H represents 2 cm. (E) and quantification of the 5th leaf petioles length (n=15, F). **J,** The *myc2* mutant suppresses *fer* mutant phenotype in JA-inhibition of root growth. Seeds were germinated on 1/2MS medium with 50 □m JA or mock and root lengths were measured at 8 days. Averages and S.D. were derived from 10-12 seedlings. The experiments were repeated more than 3 times with similar results. **K,** The *myc2* mutant suppresses *fer* mutant phenotype in bacterial defense. The experiments were done as described in Fig. 1G. The experiments were repeated more than 3 times with similar results. Statistical significance was calculated using Tukey HSD test and P-values less than 0.05 were considered significant for Figs. 1G, I, J and K.

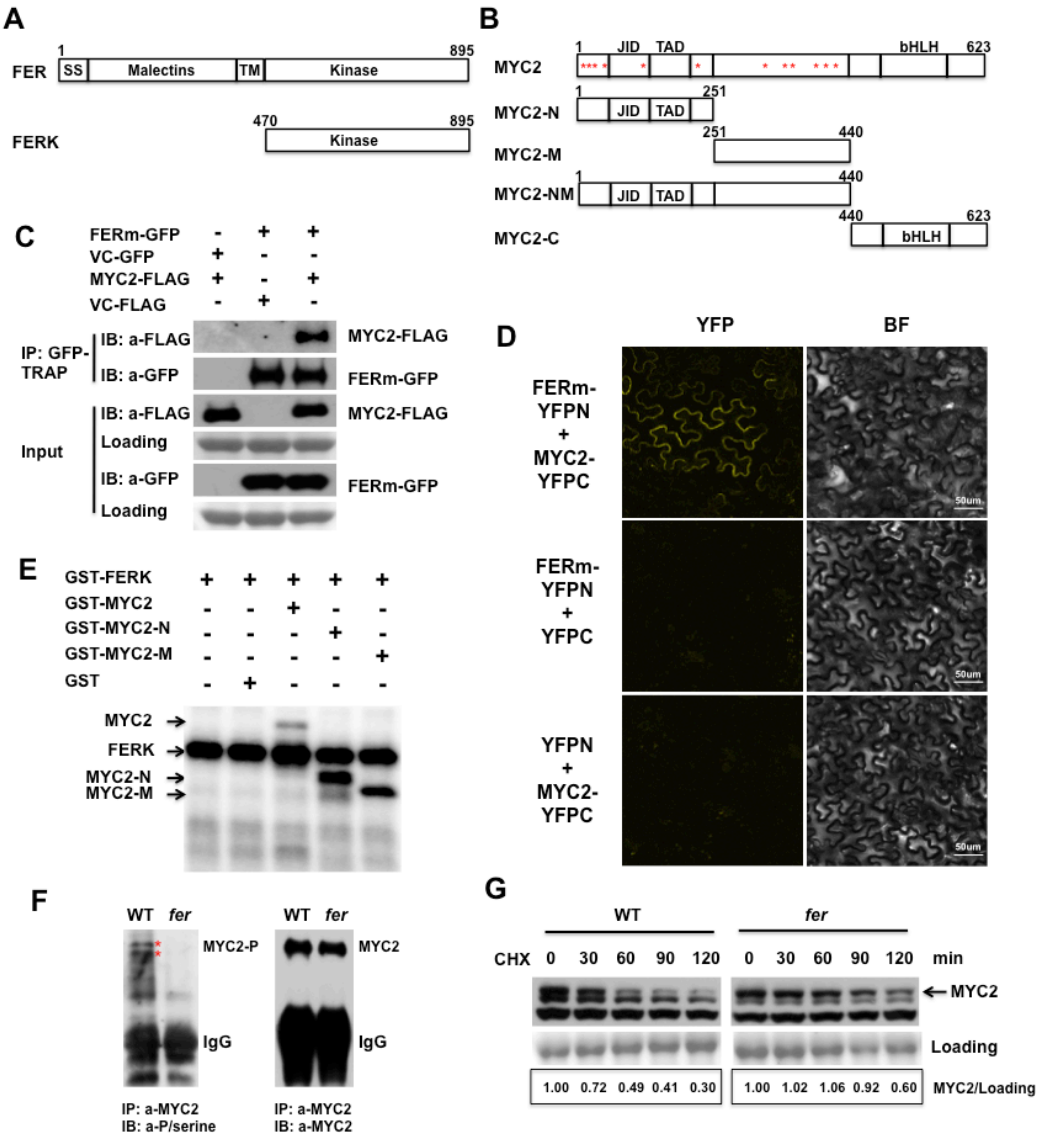

Figure 2.2: FER interacts with and phosphorylates MYC2. A-B, The domain structures of FER (**A**) and MYC2 (**B**) are shown. SS: Signal Sequence; TM: Transmembrane Domain; The Malectin domains in the extracellular region and FER kinase domain (FERK) are indicated. For MYC2, the amino (N), Middle (M) and Carboxyl (C) domains used in the study are indicated. While the C-terminal domain includes basic helix-loop-helix (bHLH) DNA binding motif, the N domain includes JAZ Interacting Domain (JID) and Transcription Activation Domain (TAD).

FER phosphorylation sites are indicted with *. **C,** FER interacts with MYC2 *in vivo*. MYC2-FLAG and FERm-GFP were co-expressed or each was co-expressed with vector only as controls in *N. benthamiana* leaves. Total protein was used for immunoprecipitation with GFP-TRAP-MA and detected with anti-GFP or anti-FLAG antibodies. The 1% input from each reaction is shown. **D.** BiFC assay further supports that FER interacts with MYC2 *in vivo*. MYC2 fused with YFP C-terminus and FERm fused with YFP N-terminus were co-expressed in *N. benthamiana* leaves, and reconstituted YFP signal was observed in the cytoplasm of epidermal cells. Bar represents 50 μm. **E.** FER kinase phosphorylates full-length, N- and M-domains of MYC2 in *in vitro* kinase assay. FERK autophosphorylation and various forms of phosphorylated MYC2 are indicated. **F.** MYC2 is phosphorylated in WT but the phosphorylation is reduced in *fer* mutant. MYC2 was immunoprecipitated from WT and *fer* using anti-MYC2 antibody, and anti-phosphoserine antibody was used to detect MYC2 phosphorylation (left panel). The detection with anti-MYC2 antibody serves as control (right panel). **G.** MYC2 has prolonged half-life in *fer* mutant. Ten-day-old seedlings were incubated with MG132 in liquid 1/2 MS medium for 16 hours to accumulate MYC2. Then the seedlings were washed 5 times with 1/2MS medium to remove MG132 and incubated with cycloheximide (CHX) for indicated times, and were collected and flash frozen. Total proteins were extracted and resolved on SDS-PAGE. MYC2 was detected by MYC2 antibody, Ponceau S staining is used as loading control. Quantification was carried out using ImageJ.

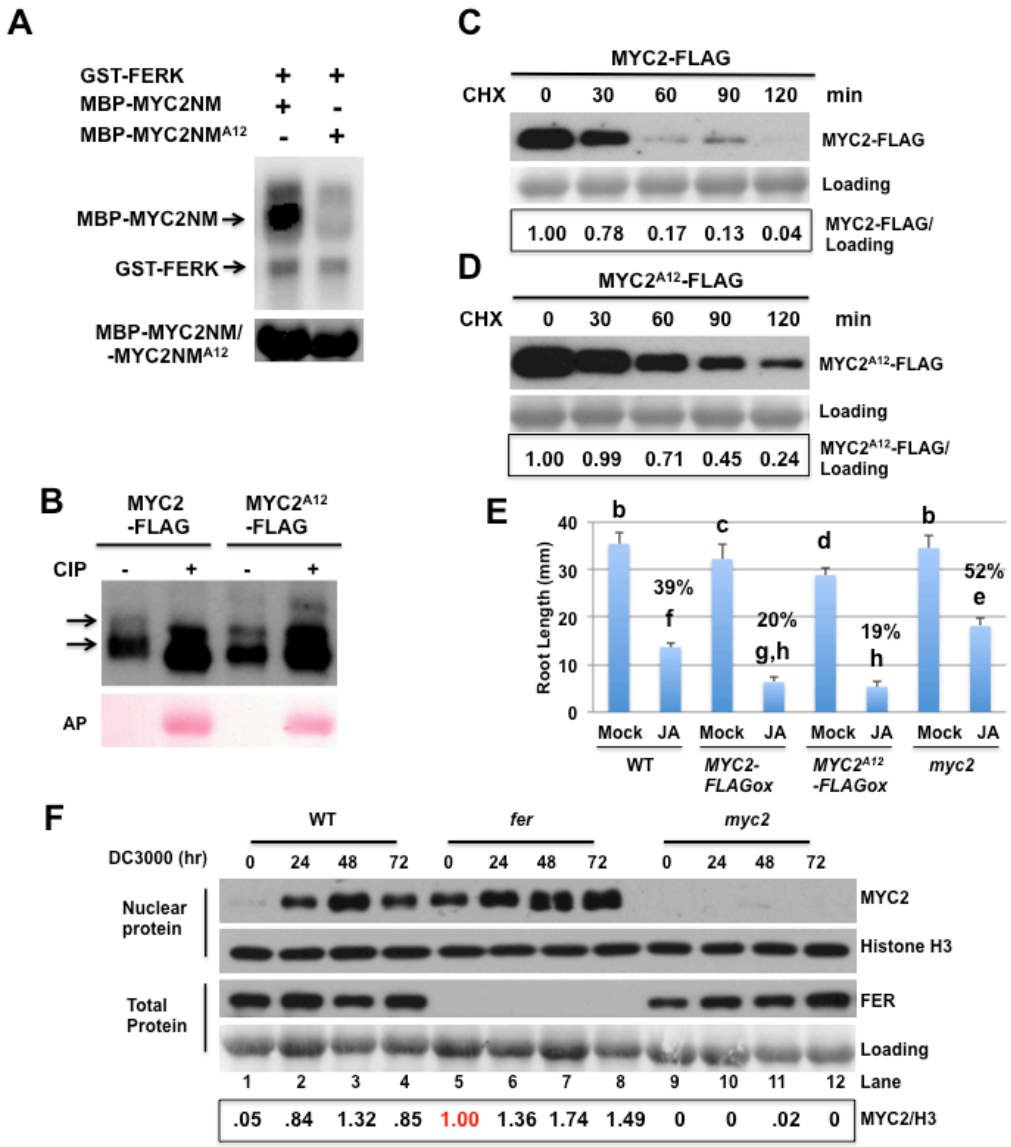

Figure 2.3: FER phosphorylation of MYC2 destabilizes MYC2. **A,** FER phosphorylation of MYC2NM (N- and Middle domains) is reduced when 12 mapped phosphorylation sites are mutated to Alanine, indicated as MYC2NM^{A12}. Phosphorylated MYC2NM and FERK autophosphorylation revealed by kinase assay with ^{32}P-gamma-ATP are indicated. The bottom panel indicates MYC2NM and MYC2NM^{A12} used in the assay. **B,** MYC2^{A12} phosphorylation is reduced *in vivo*. MYC2-FLAG and MYC2 ^{A12}-FLAG were immunoprecipitated from transgenic plants over-expressing the corresponding proteins, and the IP product was treated with

phosphatase and resolved on SDS-PAGE. There is a shift in the MYC2-FLAG while the shift in MYC2 ^{A12}-FLAG is minimal. **C-D,** MYC2^{A12} has prolonged half-life than that of WT MYC2. Ten-day-old transgenic plants *MYC2-FLAGox* (**C**) or *MYC2 ^{A12}-FLAGox* (**D**) were incubated with cycloheximide (CHX) for indicated times and were collected and flash frozen. Total proteins were extracted and resolved on SDS-PAGE. MYC2-FLAG and MYC2 ^{A12}-FLAG were detected by anti-FLAG antibody, Ponceau S staining is used as loading control. Quantification was carried out using ImageJ. **E,** Both *MYC2-FLAGox* and *MYC2 ^{A12}-FLAGox* are hypersensitive to JA in the root growth assay, indicating that MYC2^{A12} is still functional (n=14-18 plants). Statistical significance was calculated using Tukey HSD test and P-values less than 0.05 were considered significant. **F,** MYC2 protein accumulates in *fer* mutant. Five-week-old WT, *fer* and *myc2* plants were infiltrated with Pst DC3000 for indicated times. Total or nuclear proteins were prepared from each sample and the accumulation of MYC2 and FER was detected with anti-MYC2 or anti-FER antibody. Anti-Histone H3 and Ponceau S staining were used as loading controls. Quantification of MYC2 was carried out using ImageJ using Histone H3 as control.

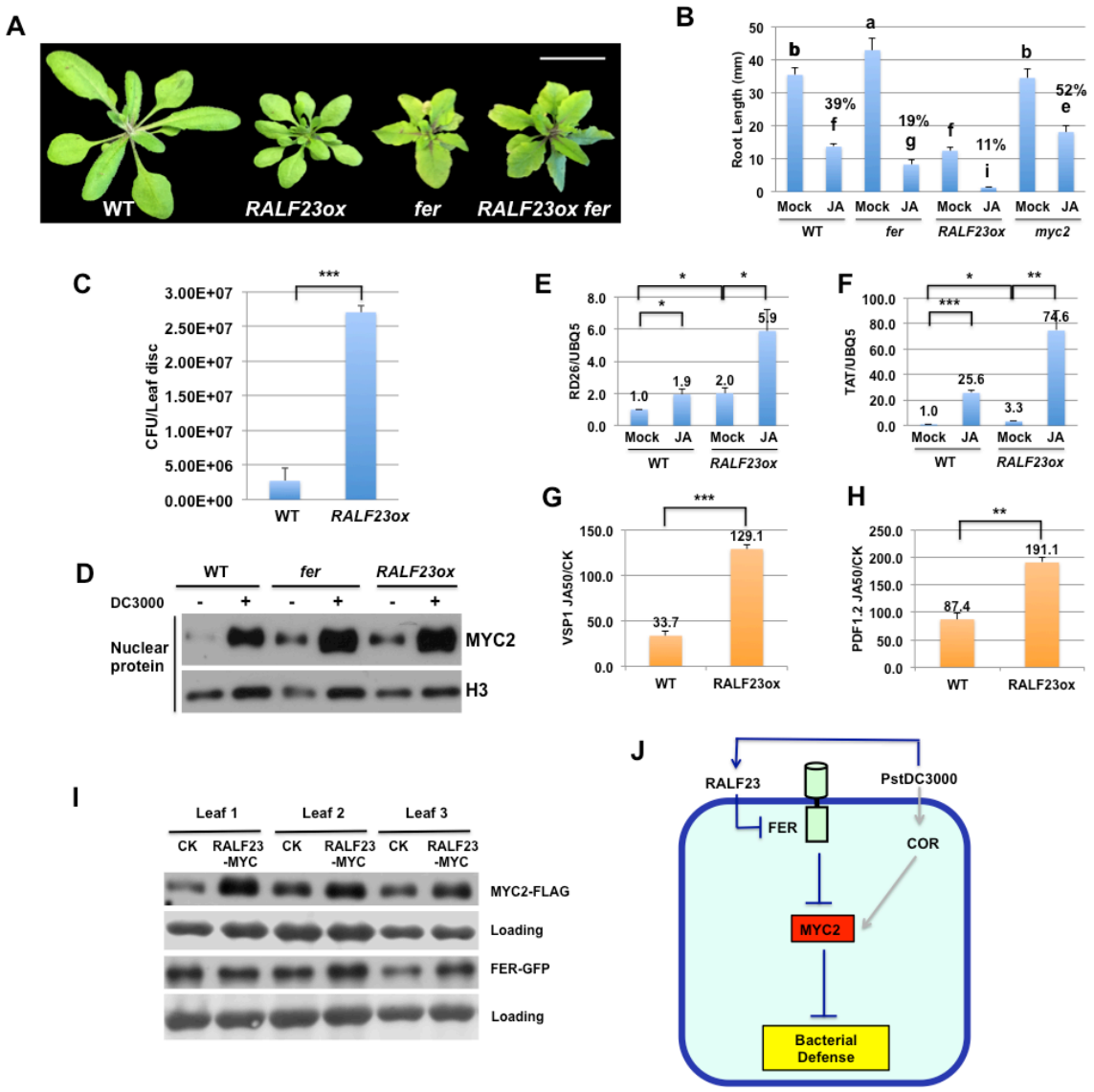

Figure 2.4: FER regulation of MYC2 and modulation by RALF23. **A,** Four-week-old plants show growth phenotypes of WT, *RALF23ox*, *fer* and *RALF23ox fer*. Bar represents 2 cm. **B,** *RALF23ox* plants are more sensitive to JA inhibition of root growth, Statistical significance was calculated using Tukey HSD test and P-values less than 0.05 were considered significant (n=14-18). **C,** *RALF23ox* plants are more susceptible to bacterial infection. The experiment is described in Fig. 1G. The statistical significance is evaluated by student t-test, p<0.0001 (***, n=3). The experiment was repeated three times with similar results. **D,** *RALF23ox* plants accumulate more

MYC2 in response to pst DC3000 than WT control. Four-week-old plants with indicated genotypes were infiltrated with Pst DC3000 for 2 days and nuclear protein was prepared and blotted with anti-MYC2 or Histone H3 antibodies. **E-H,** JA target gene expression analysis in RALF23ox shows that RALF23 plays an important role in JA signaling. RNA was prepared from 10-day-old WT or *fer* seedlings with or without 50uM JA, and qPCR was performed with indicated genes. The expression pattern of RD26 and TAT is similar to that in *fer* (E-F). Standard error was calculated based on 3 sets of samples per treatment, and Student's t test was used to calculate the statistic significance. **I,** Similar to the effect of RALF23 on MYC2 in *RALF23ox*, short term RALF23 treatment also promotes MYC2 stability. FER-GFP, MYC2-FLAG and S1P-YFP were co-expressed with RALF23 or vector only for 48 hours. Total protein was extracted from leaf discs and resolved on SDS-PAGE. All three leaves assayed showed elevated MYC2 level. **J,** A working model for FER and RALF23 regulation of MYC2 during pst DC3000 infection. FER phosphorylates and inhibits MYC2 to positively contribute to plant defense. RALF23 peptide, the processing of which is increased by bacterial infection, functions to inhibit FER receptor signaling hence negatively contributes to bacterial defense.

2.10 Supplemental Figures and Tables

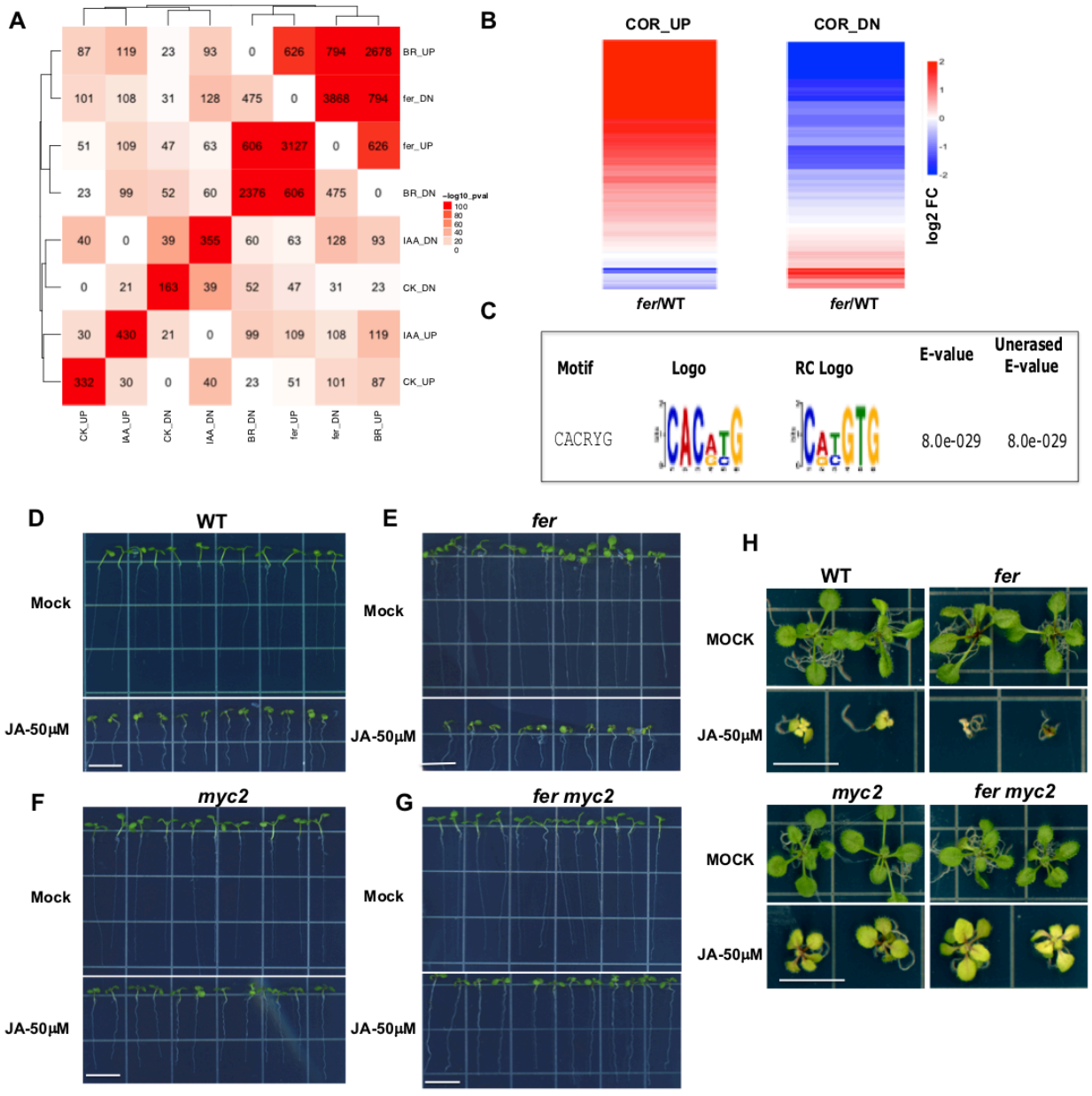

Figure 2S1. Loss of function of FER affects Brassinosteroid (BR)- and Coronatine-regulated gene expression and *myc2* suppresses *fer* phenotype. Related to Figure 2.1 and Data S1.

(A) Comparison of genes affected in *fer* with genes regulated by growth-related hormones brassinosteroid (BR), Auxin (IAA) and Cytokinin (CK). Color represents –log10 p-values from the indicated overlaps calculated from Fisher's exact test by GeneOverlap. (**B)** Clustering analysis indicates that most of the Coronatine-induced genes are constitutively up-regulated in *fer* (left panel) and a majority of the Coronatine-repressed genes are constitutively down-regulated in the mutant (right panel). (**C)** G-box promoter element is enriched in *fer*-DEs. Motif analysis of *fer*-DEs was carried out using DREME [51]. (**D-G)** WT, *fer, myc2 and fer myc2* seedlings growing in the absence or presence of JA show that *fer* is hypersensitive to JA treatment in root growth, supplemental to Figures 2.1J. (**H)** Seedlings growing in the absence or presence of JA show that *fer* is hypersensitive to JA treatment (the yellowing of leaf color and delayed growth), which is suppressed by *myc2*. The bars in D-H represent 1cm.

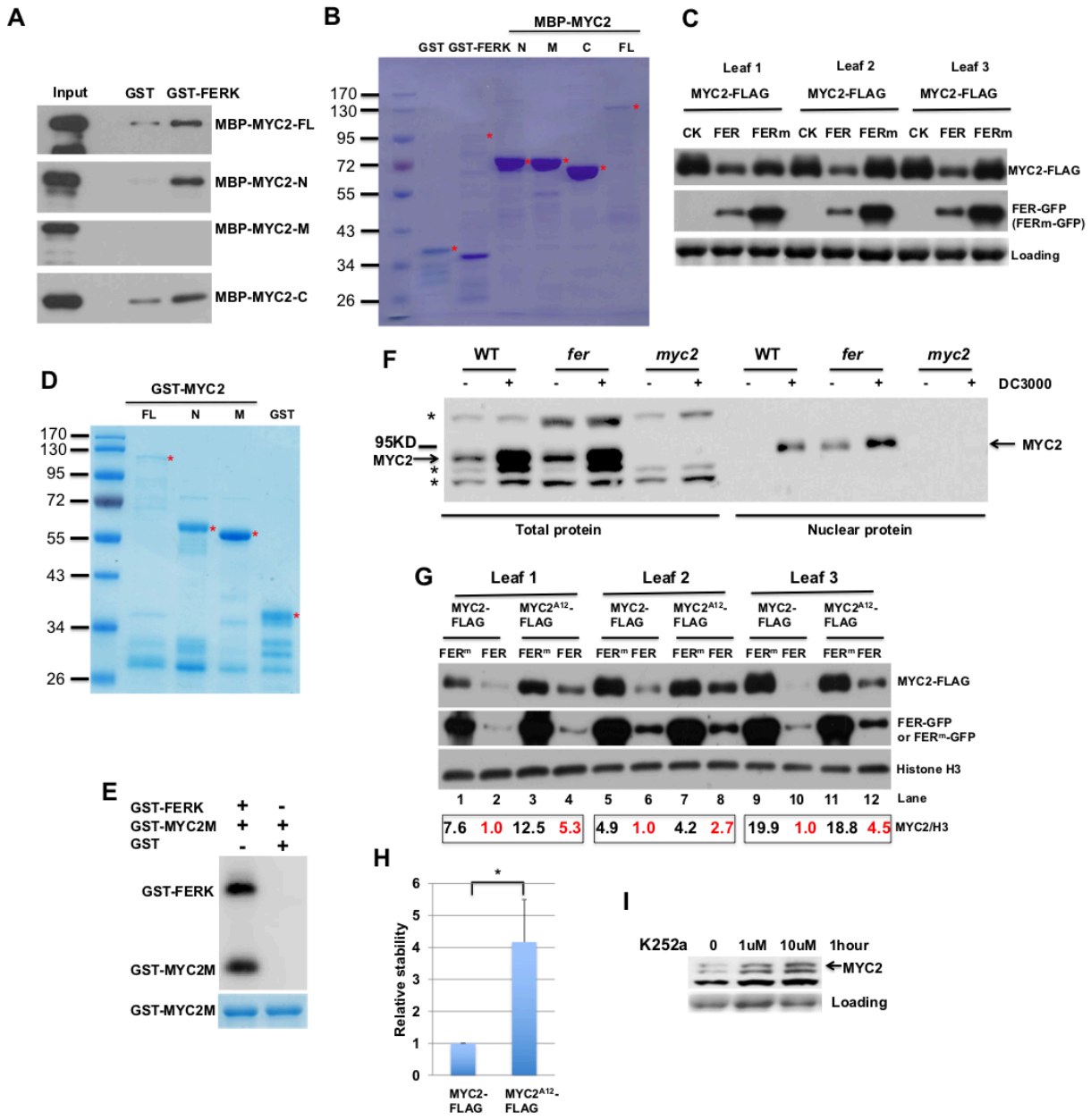

Figure 2S2. FER interacts with MYC2, phosphorylates and destabilizes MYC2. Related to Figure 2.2 and Figures 2.3C and 2.3D. (**A)** FER kinase domain interacts with MYC2 in vitro. GST or GST-FERK was used to pull down full-length (FL) or different regions (N, M or C) of MYC2 fused with MBP and detected with anti-MBP antibody. Inputs are shown with 1% of the corresponding protein in the pull-down assays. (**B)** Coomassie blue staining shows the recombinant proteins used in the GST pull-down in Figure 2S2A, and in vitro kinase assays

(GST and GST-FERK only) shown in Figure 2.2E, Figure 2.3A and Figure 2S2E. The proteins were expressed in E. coli and purified by GST or MBP affinity beads. The expected sizes of the proteins are indicated by *. (**C)** Co-expression of wild-type FER, but not the mutant form of FER (FERm), in which the kinase activity is abolished with K565R mutation, decreased MYC2 protein levels in tobacco. MYC2-FLAG is co-expressed with vector control (CK), FER-GFP or mutant FER (FERm -GFP). The total protein was prepared from leaf discs from three independent infiltrated leaves of *N. benthamiana* and immunoblotting analysis carried out with anti-FLAG and anti-GFP. Supplemental to Figure 2.2G. (**D)** Coomassie blue staining shows the recombinant proteins used for in vitro kinase assay shown in Figure 2.2E and Figure 2S2E. The proteins were expressed in E. coli and purified by GST affinity beads. The expected sizes of the proteins are indicated by *. (**E)** In vitro phosphorylation assay with GST-MYC2M as a substrate shows that GST-FERK has kinase activity while the reaction without FERK has no kinase activity, supplemental to Figure 2.2E. (**F)** Validation of MYC2 antibody in total protein and nuclear protein. The specific MYC2 band is indicated by arrows. Several MYC2-independent bands present in total protein are indicated by *. (**G** and **H)** $MYC2^{A12}$ is more stable than that of WT MYC2. Mutations of putative FER phosphorylation sites in MYC2 compromised FER regulation of MYC2. MYC2-FLAG or $MYC2^{A12}$-FLAG (in which 12 putative FER phosphorylation sites are mutated to Ala) were co-expressed with FER-GFP or FERm -GFP and the accumulation of proteins were detected as described in Figure 2S2C (G); the ratio of MYC2-FLAG over Histone H3 was calculated. The quantification of relative accumulation of $MYC2^{A12}$ is shown in H with significance by student's t-test, $p<0.015$ (n=3). Related to Figures 2.3C and 2.3D. (**I)** Kinase inhibitor K252a treatment promoted MYC2 accumulation, suggesting that phosphorylation negatively regulates MYC2 stability.

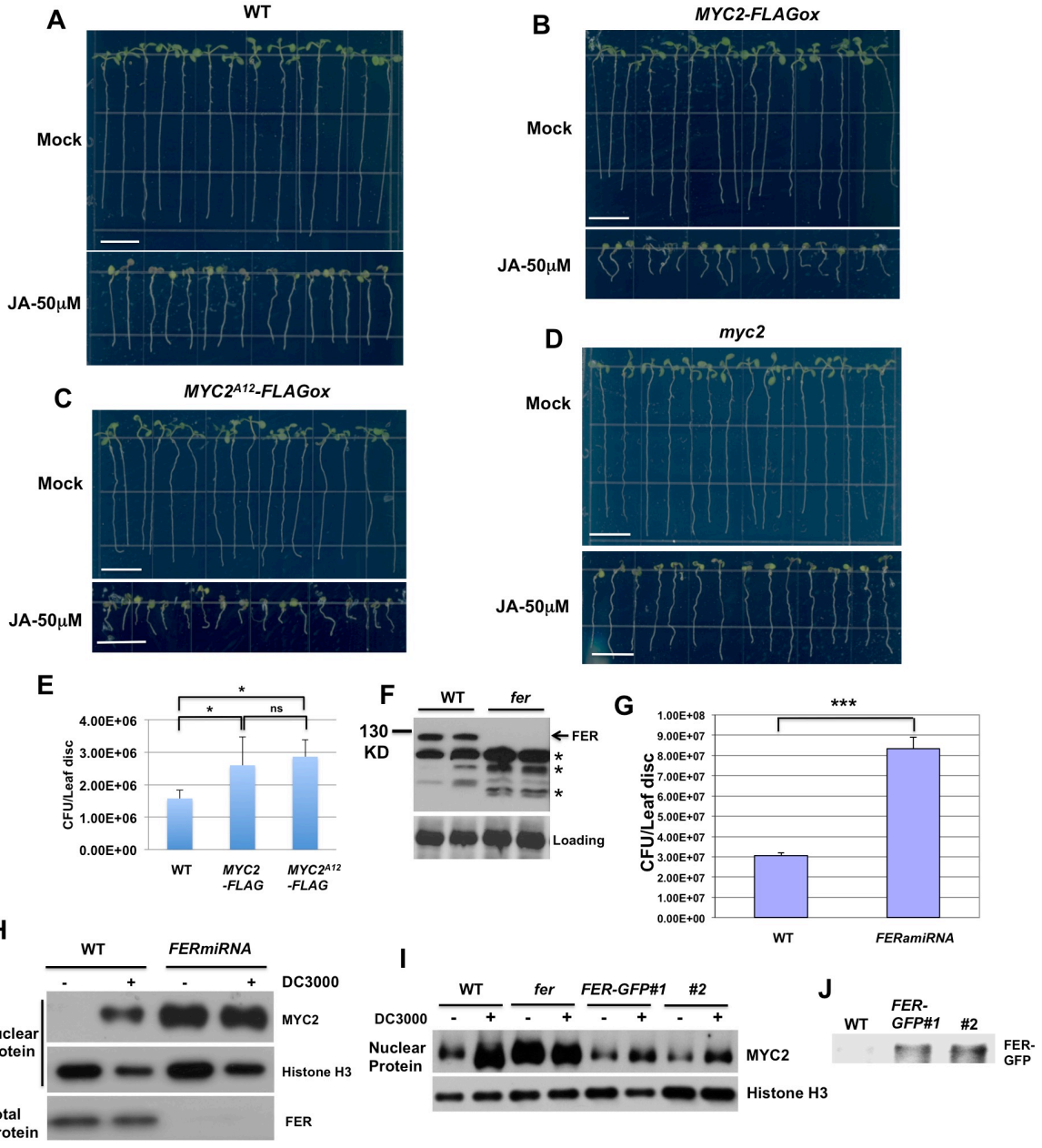

Figure 2S3. FER destabilizes MYC2 through phosphorylation. Related to Figure 2.3 and Figure 2.4B. (**A-D)** WT, *MYC2-FLAGox, MYC2*^{A12}*-FLAGox* and *myc2* seedlings growing in the absence or presence of JA show that both *MYC2*-FLAGox and *MYC2*^{A12}*-FLAGox* are hypersensitive to JA treatment in root growth, related to Figure 2.3E and Figure 2.4B. Bars in Figures 2S4A-D represent 1 cm. (**E)** Similar to *MYC2-FLAGox, MYC2*^{A12}*-FLAGox* is also more

sensitive to bacterial infection, allowed more bacterial growth than that of WT. The averages and S.D. were derived from 3 biological repeats, and the statistic significance was calculated by student's t-test (n=3), * denotes $p<0.05$, ns denotes not significant. (**F)** Anti-FER antibody generated in rabbit recognizes full length FER. * indicates non-specific bands. The antibody was produced in rabbit against MBP fusion of FER kinase domain. (**G)** The artificial miRNA knockdown mutant of *FER, FERmiRNA* [51] is more sensitive to pst DC3000 infection, accumulated more pathogen than WT control. The averages and S.D. were derived from 3 biological repeats, and the statistic significance was calculated by student's t-test (n=3), $p<0.001$ (***). (**H)** The corresponding MYC2 accumulation in *FERmiRNA* before and after pst DC3000 infection is similar to that of *fer* mutant. FER is not detectable with anti-FER in the *FERmiRNA* mutant. (**I** and **J)** Two lines of transgenic plants overexpressing *FER-GFP* accumulated less nuclear MYC2 both before and after 48 hours of pstDC3000 infection, compared to WT, suggesting that FER actively destabilizes MYC2 (I), and FER-GFP protein level in the transgenic plants is low but was detected by IP with anti-GFP (J).

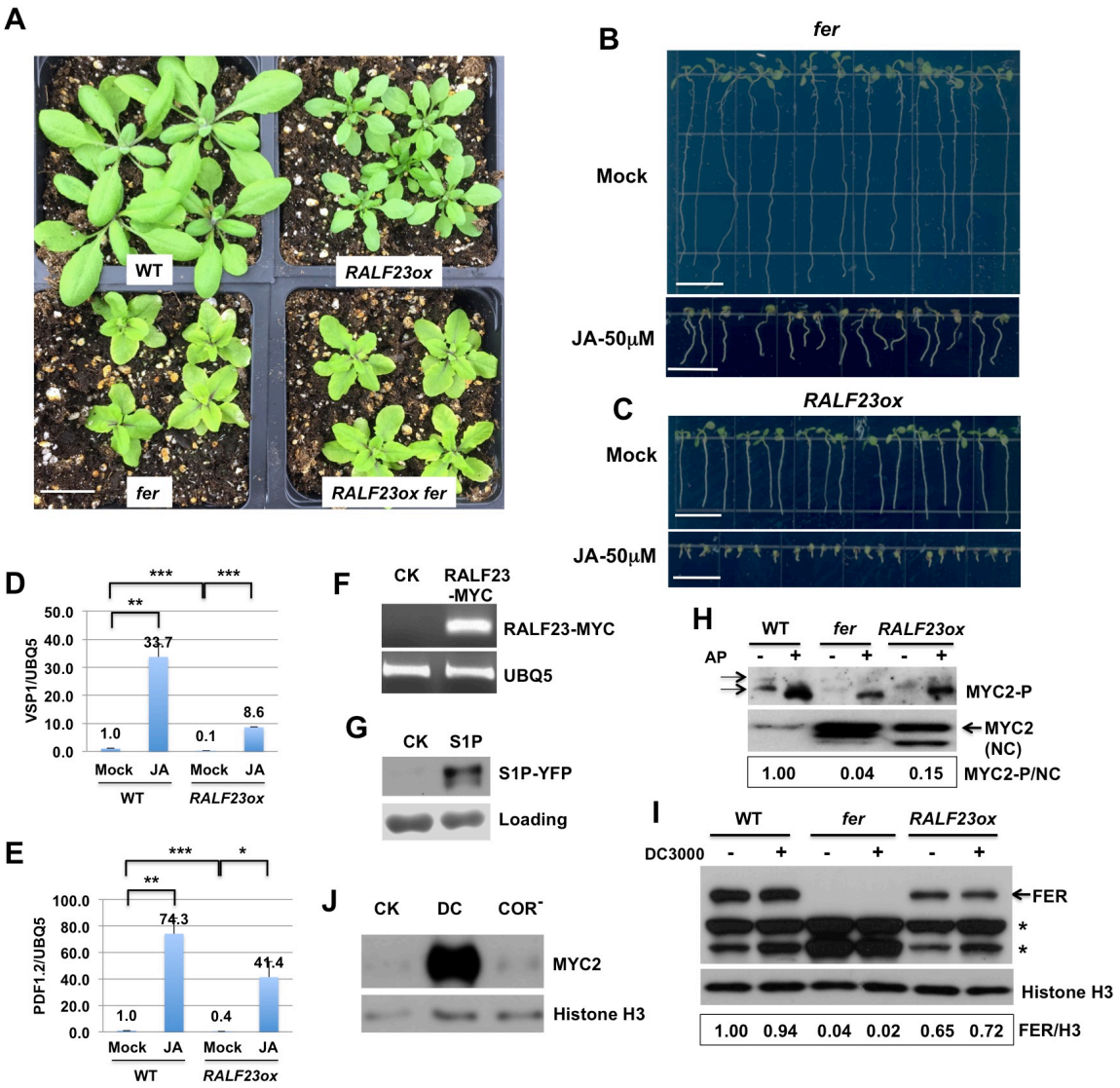

Figure 2S4. RALF23 functions through FER to positively regulate JA signaling. Related to Figure 2.4, Data S1 and Table 2S3. (**A)** Four-week-old plants show phenotypes of WT, *RALF23ox* [S3], *fer* and *RALF23ox fer*, supplemental to Figure 2.4A. Bar represents 2 cm. (**B** and **C**) *fer* and *RALF23ox* seeds germinated in the absence or presence of JA show that both *fer* and *RALF23ox* are hypersensitive to JA treatment in root growth, related to Figure 2.4B. Bars represent 1 cm. (**D** and **E)** JA target genes such as VSP1 and PDF1.2 have lower level expression in *RALF23ox* before and after 10 hours of JA treatment. However, the extent of the induction is much greater, related to Figures 2.4G and 2.4H. The experiment and data analysis were carried

out as in Figures 2.1B-D. (**F)** *RALF23ox-MYC* transcript was detected in infiltrated *N. benthamiana* leaves, using RT-PCR, Related to Figure 2.4I. (**G)** S1P-YFP [S4] expression was detected by anti-GFP in infiltrated *N. benthamiana* leaves, related to Figure 2.4I. (**H)** MYC2 is phosphorylated in vivo, which is reduced in *fer* and *RALF23ox*. MYC2 was immunoprecipitated from cytoplasmic protein of indicated genotypes and resolved on a Phos-tag gel (Top panel). MYC2 phosphorylation was observed in WT (arrows), and reduced in both *fer* and *RALF23ox*. The bottom panel indicated non-cytoplasmic MYC2 protein levels from indicated genotypes revealed by Western blot with anti-MYC2. The quantification was done by setting the ratio of phosphorylated MYC2 (MYC2-P) over non-cytoplasmic MYC2 (MYC2-NC) in WT to1, and the ratios in *fer* mutant and *RALF23ox* were then calculated by comparing to that of WT. The ratio was generated using blots with shorter exposure. (**I)** *RALF23* overexpression reduces FER protein levels. Total protein from leaves with and without 48 hours of pst DC3000 infection was extracted, resolved on SDS-PAGE and blotted with anti-FER or anti-Histone H3 antibodies. The * indicates non-specific background bands. (**J)** Nuclear MYC2 was extracted from plants infected by pst DC3000 or pst DC3000^{COR-} and resolved on SDS-PAGE, H2O only infiltration as control. MYC2 induction is much reduced by DC3000^{COR-}.

Phosphorylation Sites	Phosphorylated Residues	Peptide Sequence
S27	1	24 AFMSSSDISTLWPPASTTTTTATTE 48
S27 or S28 or S29	1	24 AFMSSSDISTLWPPASTTTTTATTE 48
S28 or S32 or T33	1	24 AFMSSSDISTLWPPASTTTTTATTE 48
S121 or S122 or S123 or S127	1	121 SSSPPFSTPADQEYR 135
S147 or S153	1	141ELNSLISGGVAPSDDAVDEEVTDTEWFFLVSMT QSFACGAGLAGK 185
T219	1	211 QGGVFGMHTIACIPSANGVVEVGSTEPIR 239
S308 or S315	1	308 SIQFENGSSSTITENPNLDPTPSPVHSQTQNPK 340
S315 or S316 or S317 or T318 or T320	1	313NGSSSTITENPNLDPTPSPVHSQTQNPKFNNTFSR E 348
T328 or S330 or S334 or T336	1	313NGSSSTITENPNLDPTPSPVHSQTQNPKFNNTFSR E 348
S352 or T353 or S354 or S355 or S356	1	349 LNFSTSSSTLVKPRSGE 365
S377 or S378	1	366 ILNFGDEGKRSSGNPDPSSYSGQTQFE 392
S383 or S384 or S386	1	376 SSGNPDPSSYSGQTQFENKR 395
T389	1	376 SSGNPDPSSYSGQTQFENK 394
S417	1	413 TAGESDHSDLEASVVK 428
S420	1	413 TAGESDHSDLEASVVK 428
S425	1	413 TAGESDHSDLEAsVVKEVAVEK 434

Table 2S1. FER phosphorylation sites of MYC2 identified by mass spectrometry. Related to Figure 2.2, Figure 2.3 and Table 2S2. Recombinant MYC2N and MYC2M were phosphorylated in vitro by GST-FERK and used to map the phosphorylation sites by Mass Spectrometry. The locations of potential phosphorylation sites and peptide sequences are included.

At. AA No.	27	28	29	33	147	219	328	386	389	417	420	425
AtMYC2	S	S	S	T	S	T	T	S	T	S	S	S
SlMYC2	S	S	S	S	S	T	Q	T	S	S	S	S
NtMYC2	S	S		S	S	T		S	S	S	S	S
GRMZM2G001930	A	S	A	T	S	T	P	S	T	S	S	S
GRMZM2G049229	A	S	A	A	S	T	P	S	Q	S	S	S
AtMYC2 codon	AGC	TCT	TCC	ACT	TCC	ACT	ACT	TCG	ACA	TCA	TCC	TCC
$AtMYC2^{A12}$ codon	GCT	GCT	GCA	GCT	GCT	GCT	GCT	GCG	GCA	GCA	GCC	GCT

Table 2S2. The 12 FER phosphorylation sites of MYC2 are mostly conserved in other species. Related to Figure 2.2, Figure 2.3 and Table 2S1. The 12 potential FER phosphorylation sites are mostly conserved among MYC2 proteins from Arabidopsis (At), Tomato (Sl), tobacco (Nt) and maize (GRMZM). The protein sequences were retrieved from NCBI and aligned with Clustal Omega from EMBL-EBI. The 12 codons that are mutated in $MYC2^{A12}$ are also shown.

Experiment	Oligo sequence 5'to 3'	Gene/region (relative to ATG +1)
		FER-GFP
Cloning	GACGGATCCACCATGAAGATCACAGAGGGACG	AT3G51550 CDS forward primer (nt1-20)
	GACGTCGACACGTCCCTTTGGATTCATGATCTG	AT3G51550 CDS reverse primer without stop codon
		Introducing K565R mutation
	CAA AGG TAG CCA TCA GGA GAG GCA ACC CAA TG	Introducing K565R mutation toAT3G51550 5'-3'
	CAT TGG GTT GCC TCT CCT GAT GGC TAC CTT TG	Introducing K565R mutation toAT3G51550 3'-5'
		MYC2-FLAG/GST-MYC2/MBP-MYC2
	GAC GGT ACC ACC ATG ACT GAT TAC CGG CTA CAA CC	AT1G32640 CDS forward primer (nt1-23)
	GACGGTACCACCGATTTTTGAAATCAAACTTGC	AT1G32640 CDS reverse primer without stop codon
		GST-FERK
	CAG GGA TCC TAC GCA GAC GTA AGC GTG GTG	FER kinase forward primer
	GCA GCG GCC GCC TAA CGT CCC TTT GGA TTC	FER kinase reverse primer including stop codon
		GST-MYC2-N/MBP-MYC2-N
	GAC GGT ACC ACC ATG ACT GAT TAC CGG CTA CAA CC	AT1G32640 CDS forward primer (nt1-23)
	TCA GGT ACC TCA AAG AAT TCG AAC CTT GTT AAT AAG G	MYC2-N reverse primer (nt729-753) with stop codon
		GST-MYC2-M/MBP-MYC2-M
	TCA GGT ACC TTC AAT TTC GAC GGC GGA GCT GG	MYC2-M forward primer (nt754-776)
	TCA GGT ACC TCA TCC TCG TTT CTT TGG ACG	MYC2-M reverse primer (nt1303-1320) with stop codon
		MBP-MYC2-C
	TCA GGT ACC AGA AAG CCA GCA AAC GGT AG	MYC2-C forward primer (nt1321-1340)
	GACGGTACCACCGATTTTTGAAATCAAACTTGC	AT1G32640 CDS reverse primer without stop codon
		MBP-MYC2-NM
	GAC GGT ACC ACC ATG ACT GAT TAC CGG CTA CAA CC	AT1G32640 CDS forward primer (nt1-23)
	TCA GGT ACC TCA TCC TCG TTT CTT TGG ACG	MYC2-M reverse primer (nt1303-1320) with stop codon
Genotyping	GGA AAA TGA GAG AAC AGA GAA CAA	GABI_106A06 forward primer
	CTT CTG TGA GTT CCT TGT CTC TCT C	GABI_106A06 reverse primer
	ATATTGACCATCATACTCATTGC	Left boarder primer for GABI T-DNA line
	CTC GAG CTG GTT CTT GAT TTG	Salk_061267 forward primer
	TGG TTT TTC TTG GTT TCG ATG	Salk_061267 reverse primer
	GGCAATCAGCTGTTGCCCGTCTCACTGGTG	Left boarder primer for SALK T-DNA line
RT-qPCR	TTATTGGAAAGCAACGGGTA	RD26 forward primer
	TCGTCAAGCTGTGATGAAGA	RD26 reverse primer
	TGG CTC TAG GGG CAG AGA AT	TAT forward primer
	CCT TGG AGA TGG CAT GAC GA	TAT reverse primer
	ACTGGTCGTGGTTAGAGTCC	VSP1 forward primer
	CTCCAATATTCCCAACGATG	VSP1 reverse primer
	AGTTTGCTTCCATCATCACC	PDF1.2 forward primer
	TAACAGATACACTTGTGTGC	PDF1.2 reverse primer
	AAGATCCAAGACAAGGAAGG	UBQ5 forward primer
	GAAGAACAGCGAGCTTAACC	UBQ5 reverse primer

Table 2S3: Oligonucleotides for cloning, genotyping and RT-qPCR. Related to Figures 2.1, 2.2, 2.3, 2.4, Figure 2S4.

2.11 Supplemental References

S1. Bailey, T.L. (2011). DREME: motif discovery in transcription factor ChIP-seq data. Bioinformatics *27*, 1653-1659.

S2. Guo, H., Li, L., Ye, H., Yu, X., Algreen, A., and Yin, Y. (2009). Three related receptor-like kinases are required for optimal cell elongation in Arabidopsis thaliana. Proc Natl Acad Sci U S A *106*, 7648-7653.

S3. Srivastava, R., Liu, J.X., Guo, H., Yin, Y., and Howell, S.H. (2009). Regulation and processing of a plant peptide hormone, AtRALF23, in Arabidopsis. Plant J *59*, 930-939.

S4. Liu, J.X., Srivastava, R., Che, P., and Howell, S.H. (2007). Salt stress responses in Arabidopsis utilize a signal transduction pathway related to endoplasmic reticulum stress signaling. Plant J *51*, 897-909.

CHAPTER 3

PROTEOMICS AND PHOSPHOPROTEOMICS REVEAL NOVEL FUNCTIONS OF FERONIA in *ARABIDOPSIS THALIANA*

Hongqing Guo[1], Gaoyuan Song[2], Trevor M. Nolan[1], Sean McLaughlin[1], Ping Wang[1], Ching-Yi Liao[1], Diane C. Bassham[1] Justin W. Walley[2] and Yanhai Yin[1]

[1]Department of Genetics, Development and Cell Biology; Iowa State University

[2]Department of Plant Pathology and Microbiology; Iowa State University

Keywords: FERONIA, ER body, NAI1, Glucosinolates, TOR, SnRK1, Autophagy, phosphorylation, Arabidopsis

3.1 Abstract

FERONIA (FER) receptor kinase plays versatile and critical roles in plant growth and development, biotic and abiotic stress responses and reproduction. Loss-of-function *fer* mutants display stunted growth, hypersensitivity to the stress hormones ABA and JA and bacterial pathogens, increased tolerance to fungal pathogen, and compromised female fertility. Progress has been made in understanding the underlying mechanisms, but much of them still remain elusive. In order to gain new insights into the molecular interplay of these processes and to identify new functions of FER, we carried out quantitative proteomics and phosphoproteomics of a *fer* mutant, *fer-4*. The analysis of *fer* omics data has validated previous findings. In agreement with FER's negative regulation in ABA, JA and fungal pathogen stress responses, the GO terms

in ABA, JA and fungal pathogen responses are significantly enriched in proteins with increased levels in *fer*. The GO terms in carbohydrate, lipid and peptide metabolism and energy reserves are enriched in proteins with reduced levels in *fer*, which suggests that FER is positively involved in nutrient and energy homeostasis, while functioning to suppress major stress responses. Interestingly, eight transcription factors (TFs) are identified as potential FER substrates, and exhibited reduced phosphorylation in the *fer* mutant. Some of the TFs or close homologs have been shown to play important roles in plant growth (e.g. BES1), ABA-mediated stress (e.g. ABF3) and dual roles by shuttling between cytoplasm and nucleus (e.g. OXS2). Furthermore, the omics data analyses have also revealed novel functions of FER. FER functions to suppress ER body formation likely through negatively regulating NAI1 and NAIP2. FER also negatively regulates autophagy conceivably by functioning in a complex with TOR and SnRK1. Our results provide new insights into the underlying mechanisms of FER function and reveal novel functions of FER, which together establish FER as a critical regulator in mediating plant growth and stress responses.

3.2 Introduction

3.2.1 Proteomics and Phosphoproteomics

FER receptor kinase plays important roles in plant growth and development, abiotic and biotic stress responses, and reproduction. Comparative transcriptome analysis has revealed that FER cross-talks with many phytohormones, such as growth hormone Brassinosteroids (BR) and stress hormones Abscisic acid (ABA) and Jasmonic Acid (JA) (Guo et al., 2018). We further established one of the underlying mechanisms of FER and JA interaction during bacterial

infection. FER phosphorylates and destabilizes MYC2, the master regulator in the JA pathway, thus down-regulating JA signaling and MYC2-mediated host susceptibility (Guo et al., 2018).

However, since transcription and translation are both heavily regulated and highly dynamic processes, transcript and protein levels of a certain gene are not always correlated (Liu et al., 2016). Furthermore, post-translational protein modifications such as phosphorylation are critical for a protein's function. For example, FER, as a Ser/Thr receptor kinase, has been shown to regulate JA pathway through phosphorylation modification (Guo et al., 2018). In order to gain new insights and a better understanding of FER function and its underlying molecular mechanisms, we carried out quantitative proteomics and phosphoproteomics of the *fer* mutant, using WT as control.

3.2.2 ER Body

ER bodies, the name first coined by Hayashi et al, are 1μm x10 μm membrane structures surrounded by ribosomes in the cytoplasm in *Arabidopsis* (Hayashi et al., 2001). They constitutively exist in epidermal cells of healthy seedlings, and have been shown to fuse with each other and the vacuole when the cells are damaged and deliver the precursors of a cysteine proteinase RD21 and a vacuolar processing enzyme (VPE) to the vacuole. In healthy adult plants, rosette leaves are free of ER bodies. Both GFP-HDEL (HDEL-ER retention signal) transgenic plants and electron microscopy showed that ER bodies are inducible in rosette leaves by methyl jasmonic acid (MeJA) and the induction was suppressed by ethylene treatment, which led the authors to speculate that ER bodies play a role in stress since JA and ethylene are known to be associated with wounding, defenses against fungal infection and herbivory (Hara-Nishimura and Matsushima, 2003; Matsushima et al., 2002). A genetic suppressor screen with

GFP-HDEL transgenic plants identified *NAI1*, later cloned and characterized as a bHLH transcription factor (Matsushima et al., 2004; Matsushima et al., 2003b). A *nai1* mutant is devoid of ER bodies even in healthy seedlings, suggesting NAI1 is required for ER body formation.

Many ER body-localized or -related proteins have been identified. PYK10 (BGLU23), a beta-glucosidase with ER retention signal, is localized in the ER bodies (Matsushima et al., 2003a) and involved in hydrolysis of glucosides and oligosaccharides. PBP1 (PYK10-binding protein 1), localized in the cytosol, binds to PYK10 and regulates its activity. PBP1 (JAL30, Jaclin-related lectin 30) has two repeated regions that are highly homologous to the alpha-chain of jaclin, a carbohydrate-binding protein (lectin) of jackfruit (Nagano et al., 2005). Two more beta-glucosidases (BGLU21, BGLU22), four more JAL proteins (JAL31, JAL33, JAL34, JAL35) and a GLL protein (GLL22, GDSL lipase-like) have been co-purified with PYK10 (Nagano et al., 2008). Moreover, NAI2, a membrane protein with 10 EFE repeats, also localizes in the ER bodies (Yamada et al., 2008). Loss-of-function of *NAI2* lacks regular ER bodies. BGLU18, an ER resident protein, accumulates only in the induced ER bodies by wounding (Ogasawara et al., 2009).

NAI1 regulates the expression of many genes including the ones encoding PYK10/BGLU23, JAL22, JAL23, JAL31, JAL33, PBP1/JAL30, GLL23, GLL25 and NAI2 (Yamada et al., 2008). Recently, NAIP1/2/3 (NAI2 interaction proteins 1,2,3), localized in ER bodies and ER-derived structures, have been shown to interact with NAI2 and are required for ER body biogenesis (Wang et al., 2019).

Glucosinolates (GSLs), the brassicales-specific beta-thiol-glucosides, along with their hydrolases, the myrosinases, are involved in plant defense responses (Wittstock and Burow, 2010). Recently, it has been shown that there is close correlation between ER bodies and GSL

biosynthesis and hydrolysis gene expression. The ER body resident protein PYK10 displayed myrosinase activity in vitro, and therefore can potentially hydrolyze GSLs in vivo (Nakano et al., 2017). Further more, Wang et al (2017) showed that MEcPP, a stress-specific retrograde signaling metabolite, promotes ER body formation while regulating glucosinolate metabolism. Although the biological significance of ER bodies is still unclear, it is conceivable that ER bodies are involved in biotic stress responses, at least partially through GSL metabolism.

3.2.3 SnRK1, TOR and Autophagy

SnRK1 (Sucrose non-fermenting-1-related protein kinase 1) is an Arabidopsis ortholog of yeast Snf1 (Sucrose non-fermenting-1) and mammalian AMPK (AMP-activated protein kinase), which serve as energy and nutrient sensors and can be activated by an energy- and nutrient-deprived state (Baena-Gonzalez et al., 2007). SnRK1 functions as a heterotrimeric complex, consisting of a kinase alpha subunit (KIN10/11/12) with KIN10/11 being the major functional isoforms, a regulatory beta subunit (KINβ1/2/3), and a plant-specific hybrid form beta-gamma subunit (KINβγ) (Darwin review 2016). The SnRK1 is related to SnRK2, which is well known for its positive role in the ABA signaling pathway although it doesn't function in a heterotrimeric manner.

KIN10/11/12 (Snf1 kinase homolog), the catalytic kinase subunit, consists of an N-terminal kinase domain and C-terminal regulatory domain (αCTD) that interacts with the KINβ and KINβγ subunits. A double mutant of *kin10kin11* appears to be lethal (Baena-Gonzalez et al., 2007).

KINβ (AKINβ1, 5'-AMP-activated protein kinase beta subunit) functions as the complex scaffold and typically consists of an undefined N-terminus, a central carbohydrate-binding motif

(CBM) that binds to glycogen in Snf1 and AMPK in yeast and mammals, and a C-terminal domain (βCTD) that interacts with alpha and betagamma subunits. The N-terminus has been shown to be Myristolated with a lipidation modification at the second amino acid Glycine (Pierre et al., 2007). The authors further showed that KINβ1-GFP is mainly localized near the plasmamembrane. With the Glycine mutated to Alanine that abolishes the myristolation modification, the protein has a significant nuclear localization, which correlated with increased transcripts of KINβ1 and elevated SnRK1 kinase activity.

The KINβγ subunit is shown to be the functional equivalent of gamma subunits in yeast and mammals (Gao et al., 2016), where they regulate the kinase activity through ATP/ADP/AMP binding. The four CBS (cystathione beta-synthase) domains at the C-terminus can generate four potential nucleotide-binding sites. The KINβγ has one CBM at the N-terminus. Similar to its counterparts in yeast and mammals, SnRK1 has been shown to positively regulate autophagy in Arabidopsis (Chen et al., 2017; Soto-Burgos and Bassham, 2017).

TOR (Target of rapamycin) is an atypical Ser/Thr kinase of the phosphatidylinositol 3-kinase-related lipid kinase family. Similar to its counterparts in yeast and mammals, TOR plays central roles in balancing nutrient, energy, and internal and external stimuli to regulate plant growth development and stress responses (Shi et al., 2018). Loss-of-function TOR mutants are embryonic lethal. TOR functions in a complex with RAPTOR1B (regulator associated protein of TOR) and LST8 (lethal with sec thirteen 8, a WD40 protein) (Liu and Bassham, 2012). RAPTOR1B binds to the N-terminus of TOR and LST8 binds to the kinase domain of TOR at the C-terminus. It has been shown that RAPTOR1B can be the point of entry for TOR regulation. SnRK1 was shown to interact with RAPTOR1B and directly phosphorylate RAPTOR1B in vivo, which likely in turn regulates TOR activity (Nukarinen et al., 2016). In agreement with the above

observation, KIN10, KIN11 and TOR were co-purified with RAPTOR1B in a purified protein complex (Van Leene et al., 2019). Similar to its orthologs in yeast and mammals, TOR has been shown to negatively regulate autophagy in Arabidopsis (Liu and Bassham, 2010).

Autophagy, self-eating, is a cellular recycling process critical for replenishing the nutrient sources for new growth. Cargoes such as single molecules, larger multi-molecular aggregates, damaged organelles or even whole organelles no longer in service can all be recycled through autophagy. There are three types of autophagy, microphagy, macrophagy and megaphagy. Microphagy is the direct engulfing process of the cytoplasmic materials by a vacuole. In macrophagy, the canonical autophagy, cargo is trapped by de novo synthesized double membrane-bound autophagosome that subsequently fuses with the vacuole. In the megaphagy, the vacuole contents are released to the cytoplasm to facilitate programmed cell death (Liu and Bassham, 2012; Marshall and Vierstra, 2018).

From cargo to its destination vacuole, the canonical autophagy involves many steps, including induction, membrane delivery, vesicle nucleation, phagophore expansion and closure, autophagosome delivery and fusion and digestion. SnRK1 and TOR have been shown to regulate autophagy at the induction step, where autophagy proteins ATG1 and ATG13 are involved. When there are sufficient nutrients, TOR is active and phosphorylates ATG13 to interfere with its complex formation with ATG1, which is required for autophagy (Suttangkakul et al., 2011). Under starvation condition, SnRK1 is activated, and TOR is inhibited and ATG1 is likely phosphorylated by SnRK1, which results in complex formation with ATG13 and activation of autophagy (Liu and Bassham, 2010; Signorelli et al., 2019; Soto-Burgos and Bassham, 2017).

In this study, we performed proteomics and phosphoproteomic studies with WT and *fer* mutants and found that FER is involved in ER body formation and autophagy regulation.

3.3 Results and Discussion

3.3.1 Proteomics Analysis of *fer*

The quantitative proteomics detected 7240 proteins and further analysis identified 3699 (q-value < 0.1) differentially expressed proteins (DEPs) in adult rosette leaves of the *fer* mutant. Among the DEPs, 1685 had increased and 2014 had decreased protein levels in the *fer* mutant. About 48% of the proteins were also differentially expressed in the *fer* transcriptome (Figure 3.1A), with most of the DEPs following the same direction of change as their transcript levels (Figure 3.1B). For example, 588 DEPs with increased protein levels in *fer* also showed increased levels of transcripts (Group1: G1), while only 179 DEPs with increased levels in *fer* showed decreased transcript levels (Group 2: G2). Likewise, 892 DEPs with decreased levels in *fer* also showed decreased levels of transcripts (Group 3: G3), but only 92 DEPs with decreased levels in *fer* showed increased transcript levels (Group 4: G4).

In the Gene Ontology analysis of proteins with increased levels in *fer*, there were 160 significantly enriched GO terms in biological processes (Table 3.1) and 56 in cellular components ($p<0.05$, fold enrichment>1.3) (Table 3.2). GO terms related to stress hormones were enriched. For example, GO terms related to ABA response (GO:0009737), and to JA biosynthesis (GO:0009695), JA metabolic process (GO:0009694), and JA responses (GO:0009753) were significantly enriched (Figure 3.1C), which corroborates the previous findings that FER inhibits both ABA and JA signaling pathways and loss of function *fer* mutants are hypersensitive to the hormones (Guo et al., 2018; Yu et al., 2012).

GO terms related to biotic stresses were also enriched, e.g. response to biotic stimulus (GO:0009607), innate immune response (GO:0045087), defense response to bacterium

(GO:0042742), and defense response to fungus (GO:0050832) (Figure 3.1C), which partially confirms the involvement of FER in fungal and bacterial defense responses (Guo et al., 2018; Masachis et al., 2016; Stegmann et al., 2017).

In the Gene Ontology analysis of proteins with decreased levels in *fer*, there were 281 significantly enriched GO terms in biological processes (Table 3.3) and 99 GO terms in cellular components ($p<0.05$, fold enrichment>1.3) (Table 3.4). Overwhelmingly large number of GO terms were related biosynthetic and metabolic pathways of important compounds, such as carbohydrate biosynthetic (GO:0016051) and catabolic (GO:0016052) processes, lipid biosynthetic (GO:0008610) and metabolic (GO:0006629) processes, and peptide biosynthetic (GO:0043043) and metabolic (GO:0006518) processes. GO terms related to energy reserves and maintenance were also significantly enriched, such as energy reserve metabolic process (GO:0006112), ATP biosynthetic process (GO:0006754), and ATP generation from ADP (GO:0006757) and ATP metabolic process (GO:0046034) (Figure 3.1D). The involvement of FER–regulated proteins in these pathways suggests an important role of FER in maintaining plant nutrient and energy homeostasis and survival, which is likely in part responsible for the observed growth defects of *fer* mutant (Guo et al., 2009).

It has been reported previously that FER positively regulates cold and heat stress and *fer* mutant is hypersensitive to cold and heat treatment compared to wildtype seedlings (Chen et al., 2016). In agreement with these findings, both response to cold (GO:0009409) and response to heat (GO:0009408) were enriched specifically in proteins decreased in *fer* (Figure 3.1D). A recent study showed that FER is important for sensing cell wall component pectin and regulates salt stress (Feng et al., 2018; Zhao et al., 2018) and *fer* mutant is hypersensitive to high salt

conditions. In agreement with the finding, the GO term response to salt stress (GO:0009651) was also enriched in the decreased proteins in *fer* (Figure 3.1D).

Interestingly, the GO term for defense response to bacterium (GO:0042742) was enriched in both groups of proteins (Figure 3.1C and 3.1D). Out of the 393 proteins in the GO term, 60 of them were decreased in protein levels in *fer* and 53 of them were increased in the mutant (Table 3.5), including commonly known defense related genes, such as positive immunity regulators EDS1 (Enhanced Disease Susceptibility) and PAD4 (Phytoalexin Deficient 4), and negative regulators such as RIN4 (RPM1 Interacting Protein 4). The above observation corroborates the previous reports that FER regulates bacterial pathogen response through different mechanisms. FER can serve as a scaffold protein for immune receptors FLS2 and EFR for their activity in PTI (Stegmann et al., 2017), and FER can also inhibit JA signaling through MYC2 to inhibit bacterial pathogen-mediated plant host susceptibility (Guo et al., 2018), both of which positively contribute to plant immunity.

It has been shown that *fer* is resistant to osmotic stress such as imposed by Mannitol (Chen et al., 2016). Although response to osmotic stress (GO:0006970) was enriched in both sets of proteins (Figure 3.1C and 3.1D), response to water deprivation (GO:0009611) was only enriched in proteins increased in *fer*, which supports that FER negatively regulates osmotic stress and likely drought responses. Consistent with these findings, *fer* mutant is more tolerant of drought in soil and FER overexpression *(FEROX)* plants are more susceptible to drought (Figure 3.1E).

3.3.2 Phosphoproteomic Analysis of *fer*

In the phosphoproteomic analysis, 11,579 phosphorylated peptides were detected and 350 individual proteins (q-value<0.1) had altered phosphorylation status. While 170 of the proteins had elevated phosphorylation, 172 of them had decreased phosphorylation and 8 have both up and down phosphorylation sites. When compared to the *fer* transcriptome and proteome results, 65.1% of the proteins with altered phosphorylation overlapped with either or both of them (Figure 3.2A), suggesting that the phosphoproteomic data are relevant to FER-mediated functions. For further analysis, we'll focus on the 180 proteins with under phosphorylated sites that are potentially FER substrates.

FER was found to be hypo-phosphorylated at S883 and S887 in the C-terminus of the protein. These sites are likely autophosphorylation sites; they are conserved in the two homologs THE1 and HERK1. THE1 and HERK1 were also hypo-phosphorylated. THE1 was under-phosphorylated at T665, S668 and T669 (Figure 3.2B), which therefore are likely transphosphorylation sites by FER. In agreement with the notion that FER may function together with THE1, a recent study showed that RLAF34-THE1 ligand and receptor interaction is at least partially dependent on FER (Gonneau et al., 2018). HERK1 was under-phosphorylated at S807, S813, S816 and S817 (Figure 3.2B). These results suggest that FER forms heterodimers with and phosphorylates HERK1/THE1. Further studies are needed to characterize the function of these phosphorylation events.

Another interesting finding from the phosphoproteomics analysis is the identification of eight transcription factors (TFs) that were hypo-phosphorylated in *fer* mutant, which makes them candidate substrates for FER (Table 3.6). Interestingly, BES1 (BRI1-EMS-Suppressor 1) and ABF3 (ABA responsive elements-Binding Factor 3), the major regulators in the BR and the

ABA signaling pathways respectively, are each responsible for regulating large numbers of BR- and ABA-regulated gene expression (Nolan et al., 2017; Song et al., 2016). FER has been shown to phosphorylate MYC2, the master TF in the JA signaling pathway, and to regulate JA signaling and MYC2-mediated host susceptibility (Guo et al., 2018). It is conceivable that FER regulates other TFs to regulate diverse biological processes that FER is involved in, such as plant growth and development and other stress responses.

In order to better understand the group of TFs, we extracted their regulons (a group of genes co-regulated with a TF) from the TINGe gene regulatory network consisting of all genes in the Arabidopsis genome (Chockalingam, 2017) and compared them to *fer*-regulated genes (Figure 3.2C). It is quite interesting that BES1-regulon formed tight cluster with genes down-regulated in *fer* (fer-Down). BES1 regulates BR-mediated plant growth, which suggests that FER might regulate plant growth partially through BES1. Interestingly, FER has been shown previously to be induced by BES1 at transcript level (Guo et al., 2009). HB34 (a Zinc Finger and Homeo domain family TF), AT3G51950 (a Zinc Finger family TF with a RNA recognition motif (RRM)) and bZIP61 (a bZIP family TF) are also clustered with fer-Down genes. HB34's close homolog HB23 has been shown to positively contribute to hypocotyl elongation (Perrella et al., 2018), and a close homolog of bZIP61, bZIP34, was shown to be required for pollen development (Gibalova et al., 2009). OXS2 (Oxidative Stress 2) regulon also showed moderate correlation with fer-Down genes. OXS2 has been shown to regulate both growth and oxidative stress, and a loss-of-function *oxs2* mutant displayed stunted growth under oxidizing agent Diamide treatment (Blanvillain et al., 2011). More interestingly, OXS2 localizes in the cytoplasm under normal growth, and shuttles to the nucleus upon stress (e.g., ABA or cold),

which provides a potentially novel mechanism for FER's regulation on both plant growth and stress responses.

Not surprisingly, ABF3 and FBH3 (Flowering BHLH 3), both of which are induced by ABA treatment, were closely clustered with genes up-regulated in *fer* (fer-Up) (Figure 3.2C), suggesting that FER can regulate ABA signaling directly through TFs. It has been shown that FER activates ABI2, the co-receptor and negative regulator in ABA signaling, to inhibit ABA responses (Chen et al., 2016; Yu et al., 2012). Our results suggest a possible second mechanism by which FER negatively regulates TFs involved in ABA responses.

ALY3 (Always Early 3) is an atypical transcription regulator required for nucleocytoplasmic mRNA transport. Loss-of-function quadruple mutant *aly1/2/3/4* displays a dwarf growth phenotype. The ALY3 regulon didn't shown significant correlation with FER-regulated genes, which may be partially due to the smaller gene numbers in the regulon.

In addition to the predicted regulons from TINGe network, direct gene targets have also been obtained by ChIP-chip and ChIP-seq for BES1, ABF3 and FBH3 (Song et al., 2016; Sun et al., 2010; Yu et al., 2011). Significant correlation was also observed when comparing fer-regulated genes and the direct target genes of those TFs (Figure 3.2D). Future studies will be carried out to elucidate the detailed regulation of FER on these TFs and their functional consequences.

In summary, from the Gene Ontology analysis of *fer* proteomics, we found that GO terms related to many abiotic and biotic stresses were significantly enriched among proteins increased in *fer* mutant, suggesting that FER functions to suppress those stress responses. In the meantime, GO terms such as the metabolisms of carbohydrates, lipids and peptides as well as energy reserves were enriched among proteins with decreased levels in *fer* mutant, suggesting that FER

functions to maintain nutrient and energy homeostasis and promote plant survival. From the analysis of the *fer* phosphoproteomics, we have identified a group of TFs that are likely phosphorylated by FER and function downstream of FER, which will open exciting new revenues for studying FER function and underlying molecular mechanisms.

In addition, we have identified two specific new pathways regulated by FER, ER body and autophagy. They will be detailed in the next two sections.

3.3.3 FER Negatively Regulates ER Body Formation

In the Gene Ontology analysis of *fer* proteomics data, ER body (GO:0010168) was the most enriched term in the cellular processes in the proteins increased in *fer* mutant (Table 3.2). A group of ER body-associated proteins has been identified (Wang et al., 2017). Out of the seventeen ER body-associated proteins (Table 3.7), 14 had increased protein levels (Figure 3.3A), and 16 of them had increased transcript levels. The results suggest that FER plays an important role in negatively regulating ER bodies. NAI1, a bHLH family transcription factor, induces the expression of many ER body-associated genes, including *PYK10, GLL23* and *NAI2*, and is required for ER body formation. Loss-of-function of *nai1* mutant fails to form ER bodies in response to inducers such as MeJA (Matsushima et al., 2004). *NAI1* has increased transcript level in *fer* although its protein was not detected. We hypothesize that FER regulates ER body by negatively regulating NAI1.

To examine the functional relationship between FER and NAI1, we extracted a regulon from the TINGe transcription regulation network (Chockalingam, 2017). 461 genes were identified in the NAI1 regulon and 43.4% of them were regulated in *fer* (Figure 3.3B). Gene Ontology analysis with the 171 genes up-regulated in *fer* revealed that the GO term ER body

(GO:0010168) was significantly enriched (Figure 3.3C), supporting the notion that FER and NAI1 regulate ER body.

We further test if the negative regulation of FER on NAI1 is also through protein abundance, in addition to transcript level. We generated a FLAG-tagged *NAI1* and transiently co-transformed with *FER-GFP* or *FERm-GFP* (K565R mutation disrupted the kinase activity) into the leaves of *Nicotiana benthamiana.* NAI1-FLAG protein was accumulated when co-expressed with FERm-GFP and NAI1-FLAG accumulation was decreased when co-expressed with FER-GFP, suggesting that FER negatively regulates NAI1 protein level to inhibit ER body formation (Figure 3.3D). Further studies will be carried out to elucidate the detailed regulatory mechanism of NAI1 by FER.

In the analysis of the *fer* phosphoproteomics data, NAIP2, an NAI2 interacting protein localized in the ER body, was found to be a potential FER substrate (Figure 3.3E). NAIP2 is required for ER body formation (Wang et al., 2019). There were four potential phosphorylation sites identified, two of them S213 and S217, are conserved in all three homologs while the other two S206 and S208 are less conserved. Genetics, molecular biology and biochemistry studies will be carried out to dissect the detailed regulatory mechanism.

Glucosinolates (GSLs) metabolism is closely correlated to the ER body formation (Wang et al., 2017). In *fer* proteome, 31 out of 63 GSLs-related proteins had altered levels (Figure 3.3F), suggesting a highly active GSL metabolism in *fer* mutant. Accordingly, the Gene Ontology analysis showed that glucosinolate catabolic process (GO:0019762) and glucosinolate metabolic process (GO:0019760) were specifically enriched in proteins with increased levels in *fer* (Table 3.1). GSL is an important metabolite for plant stress responses such as defense against herbivory.

In summary, our preliminary data indicated that FER negatively regulates ER body through destabilizing NAI1, the transcription factor that controls many ER body genes and is required for ER body formation. FER can also regulate ER body through the phosphorylation of NAIP2 (Figure 3.4G). The GSL metabolic pathway that is closely related to the ER body formation is also hyperactive in *fer* mutant, which confirms a known connection of ER body and GSL metabolism, and also opens doors to exciting possibilities that the FER regulates stress responses such as to herbivore attack through the regulation of ER bodies and glucosinolate metabolism.

3.3.4 FER Negatively Regulates Autophagy Pathway

KINβ functions in the same complex as KIN10/11, the kinase subunit of the SnRK1 and KINβγ, and regulates its kinase activity (Pierre et al., 2007). The domain structures of the three subunits are shown in Figure 3.4A. KIN10/11 have been shown to regulate many genes that are involved in plant metabolism, energy homeostasis and plant growth and development (Baena-Gonzalez et al., 2007). Overexpression of KIN10 resulted in semi-dwarf plants, suggesting KIN10 plays a negative role in growth. Comparison of the transcriptomes of *fer* mutant and KIN10 (Baena-Gonzalez et al., 2007) revealed more than 50% of KIN10-regulated genes were also regulated in *fer*, more than 60% of which were regulated in an antagonistic manner (Figure 3.4B). For example, in 506 KIN10-induced genes (KIN10-UP), 261 genes (51.6%) were regulated in *fer*, 161 out of the 261 (61.6%) were up-regulated in *fer* (conceptually repressed by FER). The growth phenotype and gene expression data support that FER and KIN10 function antagonistically in plant growth and other processes.

KIN10 has also been shown to positively regulate autophagy. While overexpression of KIN10 resulted in constitutive autophagy, a loss-of-function *kin10* mutant failed in abiotic stress-induced autophagy (Soto-Burgos and Bassham, 2017). This leads to our hypothesis that like KIN10, KINβ is also required for autophagy, and FER negatively regulates KINβ to suppress autophagy. To test the hypothesis, we obtained *kinβ1* homozygous T-DNA insertion mutant. Sucrose starvation followed by MDC (monodansylcadaverine) staining showed that compared to WT plants, *kinβ1* mutant didn't show sucrose starvation-induced autophagy, while *fer* mutant displayed constitutive autophagy, even under normal nutrition-rich condition (Figure 3.4C). These results led to the conclusion that KINβ1 is required for autophagy conceivably by functioning through KIN10 in the SnRK1 complex, and FER functions to suppress stress-mediated induction of autophagy.

In the effort to identify FER substrates via phosphoproteomics analysis, KINβ1 was found to be significantly phosphorylated at two Serine sites, S48 and S53. Our previous finding that FER negatively regulates transcription factor MYC2 (Guo et al., 2018) through phosphorylation and destabilization prompted us to test if the FER regulation on KINβ1 deploys similar mechanisms. We generated FLAG-tagged constructs of wildtype *KINβ1* (*KINβ1-FLAG*), and transiently co-expressed it with *FER-GFP* or *FERm-GFP* in *Nicotiana benthamiana*. The results demonstrated that while KINβ1-FLAG protein accumulated to high levels when co-expressed with FERm-GFP, KINβ1-FLAG level was much lower when co-expressed with FER-GFP (Figure 3.4D), suggesting that FER functions to destabilize KINβ1. Furthermore, we generated mutations with both S48 and S53 to Alanine (denoted as KINβ1^{A2}) and constructed FLAG-tagged mutant *KINβ1* (*KINβ1^{A2}-FLAG*) and transiently co-expressed it with *FER-GFP* in *Nicotiana benthamiana*, using *FLAG-GUS* as an internal control. The results showed that in

three separate leaves, the KINβ1^{A2}-FLAG protein accumulated to higher levels than that of KINβ1-FLAG, suggesting that FER phosphorylates and destabilizes KINβ1 (Figure 3.4E).

In order to gain more insights into the relationship of FER and KINβ1 in vivo, we generated double mutant *fer kinβ1*. To our surprise, the double mutant phenocopied *fer* mutant in both growth (Figure 3.4F) and sucrose starvation-induced autophagy (Figure 3.4G), suggesting that there is more to this regulation complex other than a FER to KINβ1 linear regulation. Although KINβ2, homolog of KINβ1, may function redundantly in these processes, but complete loss of sucrose starvation-induced autophagy in *kinβ1* suggests that this is not likely the case.

It has been shown that TOR positively regulates plant growth and negatively regulates autophagy (Liu and Bassham, 2010). Loss-of-function of TOR in *TOR RNAi* plants displayed reduced root length and fresh weight in 7-day old seedlings, and showed constitutive autophagy. Recently, it was shown that TOR functions downstream of SnRK1 in autophagy regulation (Soto-Burgos and Bassham, 2017). In addition, TOR can be directly activated by a small GTPase, ROP2 (Schepetilnikov et al., 2017) that has been shown to be activated by FER (Duan et al., 2010), suggesting that FER may function in the same complex with TOR. We hypothesize that FER and TOR function in the same complex and interact with SnRK1 to regulate plant growth and autophagy.

To test the hypothesis, we first compared the transcriptomes of TOR and FER. The TOR transcriptome was generated via AZD treatment, a TOR kinase inhibitor (Dong et al., 2015). The comparison revealed significant overlaps, with 54.7% AZD-induced and 65.4% AZD-repressed genes regulated in *fer* mutant (Figure 3.5A). Interestingly, majority of the co-regulated genes were regulated by FER and TOR in the same direction. For example, 1197 genes were repressed

by AZD (conceptually up-regulated by TOR), 65.4% (783) of those were also regulated in *fer*, with 89.8% (703) of the co-regulated (783) down-regulated in *fer* mutant (conceptually FER-induced). The comparison of TOR and KIN10-regulated genes showed significant overlap, and the regulation was in an antagonistic fashion (Figure 3.5B).

In order to understand the genetic interactions between *FER* and *TOR* , the double mutant of *fer TOROE* was constructed, where *TOROE* is a gain-of-function T-DNA mutant (Ren et al., 2011). The double mutant phenocopied *fer* mutant in both growth, and autophagy. As shown in Figure 3.5C, while *TOROE* mutant growth phenotype is similar to that of WT, *fer TOROE* mirrors *fer* mutant, suggesting that TOR activity is dependent on FER. Root growth inhibition assay was carried out to test TOR inhibitor AZD sensitivity of the different genotypes. Root growth of WT seedlings was inhibited by 1μM AZD, to 36% of the control treatment and *fer* is hypersensitive with the root growth inhibition to 27% of the control. While *TOROE* is less sensitive than that of WT as expected, *fer TOROE* is more sensitive to AZD inhibition, suggesting that TOR function is dependent on FER (Figure 3.5D). Consistent with the growth phenotype and responses to AZD, *fer TOROE* displays constitutive autophagy similar to *fer*, while sucrose starvation–induced autophagy in *TOROE* is completely abolished as expected (Figure 3.5E).

In summary, FER can inhibit SnRK1 activity through phosphorylating and destabilizing KINβ1. However, loss-of-function *kinβ1* mutant failed to rescue autophagy and growth defects of *fer*, indicating that the regulation of FER over SnRK1 is nonlinear. From both gene expression and genetic interactions, we identified TOR as the possible missing link. The fact that both growth phenotype and constitutive autophagy of *fer TOROE* double mutant mimic *fer* suggests that FER is required for TOR activity. Further genetics, biochemistry and cell biology studies

will be carried out to fully understand the functional interactions of FER, TOR and SnRK1 in the regulation of plant growth and autophagy.

Our data suggest the following model (Figure 3.5F). Under normal growth conditions, FER is active and phosphorylates and destabilizes KINβ1 to inhibit the activity of the heterotrimeric complex SnRK1, which in turn alleviates its inhibitory effect on TOR to facilitate plant growth. In the meantime, FER activates ROP2 to activate TOR, which results in plant growth and inhibited autophagy pathway. Under stress conditions, such as sucrose starvation, SnRK1 is activated, and TOR is inhibited subsequently. FER might also be inhibited under the stress conditions since it has been shown that bacterial pathogen infection and salt stress can promote functional mature peptide production (Stegmann et al., 2017; Zhao et al., 2018). The inactivation of FER can also lead to TOR inactivation through ROP2, which results in inhibited growth and activated autophagy likely through antagonistic co-regulation of SnRK1 and TOR on ATG1/ATG13 complex that is required for the early stage autophagy induction.

3.4 Conclusions

In conclusion, *fer* omics data analysis corroborates the previous findings that FERONIA receptor kinase plays a critical role in mediating plant growth development, and biotic and abiotic stress responses. The analysis also identifies several transcription factors that are potential FER substrates, which will help establish underlying molecular mechanisms of FER function. Moreover, it also reveals that FER regulates novel pathways. FER negatively regulates ER body formation, likely through negatively regulating the TF NAI1, and through the regulation of

NAIP2. FER also negatively regulates autophagy, conceivably through functioning in the same complex with SnRK1 and TOR.

3.5 Acknowledgments

HG would like to thank Prof. Jo Anne Powell-Coffman and Prof. Steve Whitham for guidance and encouragement. The research is supported by grants from NSF (IOS-1257631), NIH (1R01GM120316-01A1), and by Plant Sciences Institute at Iowa State University.

3.6 Author Contributions

HG and YY conceived the project. HG performed most of the genetic, molecular and biochemical experiments. GS and JWW performed the quantitative proteomics and phosphoproteomics. TN generated the heatmaps and the volcano plot. SM conducted most of the genotyping experiments. CL and PW performed MDC staining. All authors contributed to analysis of corresponding data. HG wrote the paper with edits from other co-authors.

3.7 Methods

Plant Materials and Growth Conditions

The Arabidopsis accession Columbia-0 was used as WT in all experiments. T-DNA insertion mutant *kinβ1* (GABI_235_B06) was obtained from the Arabidopsis Biological Resource Center (ABRC) (Alonso et al., 2003), and homozygous lines were selected by

genotyping. The *fer* mutant and *TOROE* mutant were described previously (Guo et al., 2018; Ren et al., 2011). The *fer kinβ1* double mutant was generated by crossing *fer* to *kinβ1* and *fer TOROE* double mutant was generated by crossing *fer* to *TOROE*. For all experiments involving Arabidopsis plants, seeds were sterilized with 70% ethanol containing 0.1% Triton and germinated on 1/2MS plates with 1% sucrose and 0.8% agar, with or without treatments as indicated when it is appropriate. 10-day old seedlings were transferred to soil to obtain 4-5 week adult plants.

Quantitative Proteomics and Phosphoproteomics

Protein Extraction and Digestion

The proteomics experiments were carried out based established methods as follows (Song et al., 2018a; Song et al., 2018b; Walley et al., 2018). Three biological replicate samples were collected from 5-week-old whole rosettes of both WT and *fer* mutant, with 4-5 WT rosettes and 8-10 *fer* rosettes in each sample. Lysis buffer consisting of 8M urea, 100mM Tris pH 7, 5mM TCEP and 1 X phosphatase inhibitor (2.5 mM sodium fluoride (NAF), 0.25 mM sodium vanadate ($NaVO_4$), 0.25 mM sodium pyrophosphate decahydrate ($NaPyroPO_4$), and 0.25 mM glycerophosphate (glycerol-P) in H_2O) was added to 250 mg tissue at a ratio of 1:2 sample:buffer (w:v). One mm zirconium oxide beads (Next Advance) were added to the sample at ratio of 1:1 (v:v) and then the samples were shaken using a GenoGrinder (SPEX) at 1,500 rpm for 3 minutes. The samples were centrifuged at 4,000 x g for 3 min. The shaking and centrifuge steps were repeated once. Samples were transferred to a new tube and 4 volumes of prechilled 100% acetone was added. Samples were precipitated at -20°C for >30 min followed by centrifugation at 4,500 x g for 10 min at 4°C. Eighty percent acetone was added to the pellet and the sample was probe sonicated to resuspend the pellet and shear DNA. Samples were incubated -20°C for >5 min and then

centrifuged at 4,500 x g for 10 min at 4°C. Precipitation and sonication in 80% acetone was repeated 3 times in total. Then prechilled 100% methanol was added to the pellet, sample was probe sonicated, and kept at -20°C for 30 min prior to centrifugation at 4,500 x g for 10 min at 4°C. Methanol precipitation was repeated once. The supernatant was discarded and the pellet was placed in a vacuum concentrator until nearly dry.

Protein was solubilized in 0.5 ml protein resuspension buffer (8 M Urea, 0.1 M Tris-HCl pH 7, 5mM TCEP, 1 X phosphatase inhibitor) and probe sonicated. The protein amount was evaluated by Bradford assay and ~ 1 mg worth was mixed with 3.5 ml urea solution (8 M Urea, 0.1 M Tris-HCl pH 8, 1 X phosphatase inhibitor). This solution was added to an Amicon Ultracel – 30K centrifugal filter (Cat # UFC803008) and centrifuged at 4,000 x g for 20-40 min. This step was repeated once. Then 4 ml of urea solution with 2mM TCEP was added to the filter unit and centrifuged at 4,000 x g for 20-40 min. Next, 2 ml IAM solution (50 mM IAM in 8 M urea solution) was added and incubated without mixing at room temperature for 30 min in the dark prior to centrifuging at 4,000 x g for 20-40 min. Two ml of urea solution was added to the filter unit, which was then centrifuged at 4,000 x g for 20-40 min. This step was repeated once. Two ml of 0.05 M NH_4HCO_3 with 1 X phosphatase inhibitor was added to the filter unit and centrifuged at 4,000 x g for 20-40 min. This step was repeated once. Then the filter unit was added to a new collection tube and 2 ml 0.05M NH_4HCO_3/1 X phosphatase inhibitor with trypsin (enzyme to protein ratio 1:100) was added. Samples were incubated at 37°C overnight. Undigested protein was estimated using Bradford assays then trypsin (1ug/µl) was added to a ratio of 1:100 and a equal volume of Lys-C (0.1 µg/µl) was added and incubated for an additional 4 hours at 37°C. The filter unit was centrifuged at 4,000 x g for 20-40 min. 1 ml 0.05M NH_4HCO_3 /1 X phosphatase inhibitor was added and centrifuged at 4,000 x g for 20-40

min. The samples were acidified to pH 2-3 with 100% formic acid and centrifuged at 21,000 x g for 20 min. Finally, samples were desalted using 50 mg Sep-Pak C18 cartridges (Waters). Eluted peptides were dried using a vacuum centrifuge (Thermo) and resuspended in 0.1% formic acid. Peptide amount was quantified using the Pierce BCA Protein assay kit.

Tandem Mass Tag (TMT) Labeling

TMTsixplex™ label reagents (ThermoFisher, Lot #SH254566) were used to label the samples according to manufacturer's recommended peptide-to-TMT reagent ratio. 400 µg of vacuum-dried peptides from each sample were resuspended with 400 µl 50 mM TEAB buffer and vortexed for 10 minutes at room temperature. 41 µl acetonitrile was added to each tube of TMT label (0.8 mg), then vortexed, and incubated at room temperature for 5 minutes to resuspend the labels. 4 tubes (4 X 41 µl) of each type of TMT labels were added to each tube of the peptide solutions, pipetted up and down several times and vortexed to mix them well. After 2 hours incubation at room temperature, 32 µl of 5% hydroxylamine were added to each tube, vortexed and incubated at room temperature for 15 minutes to quench the labeling reaction. Next, the six samples were mixed together, a 35 µg aliquot of peptides was reserved for protein abundance profiling, and the remaining peptides were used for for phosphopeptide enrichment, and stored at -80ºC.

Phosphopeptide enrichment

The TMT-labeled phosphopeptides were enriched using Titansphere Phos-TiO_2 beads (GL Sciences 5010–21315) based on previously published methods (Kettenbach and Gerber, 2011; Song et al., 2018a). The beads were prepared by resuspending in 1.5 ml wash and binding buffer (2 M lactic acid in 50% acetonitrile), vortexing, and then centrifuging at 3,000 g for 1 minute; this was repeated a total of three times. At the last step of washing, 5 mg and 11 mg TiO_2 beads were aliquoted to new tubes before centrifugation. After centrifugation, the wash and binding

buffer were removed and the TiO_2 beads were saved for the phosphopeptide enrichment. ~2.4 mg TMT6-labeled and vacuum dried peptides were resuspended with 2.4 ml wash and binding buffer and then added to the tube containing 11 mg TiO_2 beads, rotated at room temperature for 1 hour, and then centrifuged at 3,000 g for 1 minute. The supernatant was processed with a second round of enrichment using 5 mg of TiO_2 beads. 1.8 ml wash and binding buffers were added to each tube of the two enrichment steps, vortexed and centrifuged at 3,000 g for 1 minute. This wash was repeated once. Next, the TiO_2 beads were washed twice with 1.8 ml of 50% acetonitrile in 0.1% trifluoroacetic acid (TFA). After the wash steps, 500 µl of 3% ammonium hydroxide was added to each tube of the two enrichment steps, vortexed and centrifuged at 3,000 g for 1 minute. The eluted supernatants were combined. One more elution step was performed with 5% ammonium hydroxide. All the supernatants from the two elution steps were combined and dried in a speedvac, and then the phosphopeptides were resuspended in 0.1% FA, and stored at -80ºC until the LC/MS-MS run.

LC/MS-MS

An Agilent 1260 quaternary HPLC was used to deliver a flow rate of ~600 nL min-1 via a splitter. All columns were packed in house using a Next Advance pressure cell, and the nanospray tips were fabricated using a fused silica capillary that was pulled to a sharp tip using a laser puller (Sutter P-2000). 35 µg of TMT-labeled peptides (non-modified proteome), or 25 µg TiO_2 enriched peptides (phosphoproteome), were loaded onto 20 cm capillary columns packed with 5 µM Zorbax SB-C18 (Agilent), which was connected using a zero dead volume 1 µm filter (Upchurch, M548) to a 5 cm long strong cation exchange (SCX) column packed with 5 µm PolySulfoethyl (PolyLC). The SCX column was then connected to a 20 cm nanospray tip packed with 2.5 µM C18 (Waters). The 3 sections were joined and mounted on a custom electrospray

source for on-line nested peptide elution. A new set of columns was used for every sample. Peptides were eluted from the loading column onto the SCX column using a 0 to 80% acetonitrile gradient over 60 minutes. Peptides were then fractionated from the SCX column using a series of salt steps. For the non-modified proteome, the following ammonium acetate salt steps were used: 10, 25, 30, 32, 33, 34, 35, 36, 37, 38, 39, 40, 42, 45, 47, 50, 55, 65, 75, 90, 98, 100, 110, 130, 150, 200 and 1000 mM. For the phosphoproteome analysis, ammonium acetate steps of 6, 10, 12, 15, 18, 21, 30, 45, 70, 90, 100, 150, 500 and 1000 mM were used. For these analyses, buffers A (99.9% H_2O, 0.1% formic acid), B (99.9% ACN, 0.1% formic acid), C (100 mM ammonium acetate, 2% formic acid), and D (2 M ammonium acetate, 2% formic acid) were utilized. For each salt step, a 150-minute gradient program comprised of a 0–5 minute increase to the specified ammonium acetate concentration, 5–10 minutes hold, 10–14 minutes at 100% buffer A, 15–120 minutes 5–35% buffer B, 120–140 minutes 35–80% buffer B, 140–145 minutes 80% buffer B, and 145–150 minutes buffer A was employed.

Eluted peptides were analyzed using a Thermo Scientific Q-Exactive Plus high-resolution quadrupole Orbitrap mass spectrometer, which was directly coupled to the HPLC. Data dependent acquisition was obtained using Xcalibur 4.0 software in positive ion mode with a spray voltage of 2.00 kV and a capillary temperature of 275 °C and an RF of 60. MS1 spectra were measured at a resolution of 70,000, an automatic gain control (AGC) of 3e6 with a maximum ion time of 100 ms and a mass range of 400-2000 m/z. Up to 15 MS2 were triggered at a resolution of 17,500 with a fixed first mass of 120 m/z for phosphoproteome and 115 m/z for proteome. An AGC of 1e5 with a maximum ion time of 50 ms, an isolation window of 1.3 m/z for phosphoproteome and 1.2 m/z for proteome, and a normalized collision energy of 31 and 32 were used for non-modified and phospho- proteomes, respectively. Charge exclusion was set to

unassigned, 1, 5–8, and >8. MS1 that triggered MS2 scans were dynamically excluded for 25 or 30 s for non-modified and phospho proteomes, respectively.

Data Analysis

The raw data were analyzed using MaxQuant version 1.6.1.0 (Tyanova et al., 2016a). Spectra were searched, using the Andromeda search engine (Cox et al., 2011) against the Tair10 proteome file entitled "TAIR10_pep_20101214" that was downloaded from the TAIR website (https://www.arabidopsis.org/download/index-auto.jsp?dir=%2Fdownload_files%2FProteins%2FTAIR10_protein_lists) and was complemented with reverse decoy sequences and common contaminants by MaxQuant. Carbamidomethyl cysteine was set as a fixed modification while methionine oxidation and protein N-terminal acetylation were set as variable modifications. For the phosphoproteome "Phosho STY" was also set as a variable modification. The sample type was set to "Reporter Ion MS2" with "6plex TMT selected for both lysine and N-termini". TMT batch-specific correction factors were configured in the MaxQuant modifications tab (TMT Lot SH254566). Digestion parameters were set to "specific" and "Trypsin/P;LysC". Up to two missed cleavages were allowed. A false discovery rate, calculated in MaxQuant using a target-decoy strategy (Elias and Gygi, 2007) less than 0.01 at both the peptide spectral match and protein identification level was required. The 'second peptide' option identify co-fragmented peptides was not used. The match between runs feature of MaxQuant was not utilized.

Statistical analyses were carried out using Perseus (Tyanova et al., 2016). No imputation for missing values was performed. Statistical analyses to uncover differential accumulation were also performed in Perseus via two-sample *t*-tests and coupled with permutation-based false

discovery rate (FDR) correction. Proteins/phosphorylation sites were categorized as differentially accumulating if they had a *P*-value ≤ 0.05 and a *q*-value ≤ 0.1.

Data Analysis of Transcriptome, Proteome and Phosphoproteome:

Venn diagrams were generated using Venny (http://bioinfogp.cnb.csic.es/tools/venny/). Gene Ontology analysis was carried out through GO Term Enrichment for Plants at Tair, using all genes in the Arabidopsis genome as reference (https://www.arabidopsis.org/tools/go_term_enrichment.jsp).

Comparisons of regulons and *fer*-regulated genes were performed in R (version 3.3.0) using the *GeneOverlap* package (version 1.12.0; http://shenlab-sinai.github.io/shenlab-sinai/). P-values for intersections between gene lists were assessed using Fisher's exact test and visualized with ComplexHeatmap.

Clustering analysis of *fer* RNA-seq data and fer-proteome was performed using the 'aheatmap' function of the NMF package in R (https://cran.r-project.org/web/packages/NMF/index.html) using log2 fold change (*fer*/WT)

To visualize the proteomics data, volcano plot was constructed with ggplot2 (Wickham, 2016) in R using -log10 transformed q-values and log2 fold change (*fer*/WT) of protein expression values.

fer-regulated genes were described previously (Guo et al., 2018) and the fer-regulated proteins were generated in this study. The individual regulon of the 8 TFs were extracted from the TINGe gene regulatory network (Chockalingam, 2017) with all genes in the Arabidopsis genome. The direct target genes for FBH3 and ABF3 are described (Song et al., 2016) and BES1/BZR1 target genes were described (Sun et al., 2010; Yu et al., 2011) previously.

Transient Expression Assay

Nicotiana benthamiana (*N. benthamiana)* seeds were germinated in soil. About two-month old plants were used for the assays. Agrobacterial cultures carrying the genes of interest were grown in liquid LB medium with antibiotics in a 30°C shaker for 2 days. After collecting the agrobacteria, the cells were resuspended in infiltration buffer (10mM $MgCl_2$, 10mM MES pH 5.7, 200μM Acetosyringone). The density was measured at 600□nm wavelength and each culture was diluted to final concentration of OD600 0.3 for infiltration. The leaf infiltration was done with 1ml syringe without a needle on the abaxial side of the leaf. At least two biological replicates were examined for each target construct.

Total Protein Extraction and Western Blotting

For transient expression in *Nicotiana benthamiana*, 5 leaf discs (7mm in diameter) were collected for each sample and flash frozen in liquid nitrogen and ground directly in 200□l 2xSDS sample buffer. The samples were resolved on 8% SDS-PAGE, followed by immunoblotting using anti-GFP or anti-FLAG antibodies.

MDC Staining

The MDC (Monodansylcadaverine) staining and visualization were carried out as described (Wang, 2019). Briefly, seeds of different genotypes were germinated on 1/2MS plates with 1% sucrose for 7 days. Then the seedlings were transferreds to 1/2 MS plate with no sucrose, and with 1% sucrose as control, and were grown in the dark for 3 more days. The roots were then stained with MDC for 15 minutes. After washes with PBS buffer, the elongation zone of seedling roots was observed via epifluorescence microscope. The fluorescent puncta, representing the autophagosomes, were counted in each photo frame and 10-30 photo frames were generated from five seedling roots per treatment.

AZD8055 Response by Root Growth Inhibition

To assay the response to TOR kinase inhibitor AZD8055, seeds were sterilized and germinated on 1/2MS plate containing 1uM AZD8055, plates containing same volume of DMSO as control. The plates were scanned and the roots of these seedlings were measured at 8 days after germination. The measurement of the root length was carried out using ImageJ. Statistical significance was calculated using Tukey HSD test. P-values less than 0.05 were considered significant.

Drought Treatment in Soil

For the observation of the drought response, the seeds were presoaked in 0.1% agarose for 4 days at 4°C and then sprinkled to presoaked soil. The plants were watered regularly for 3 weeks, at which time watering was halted for half the pots, and the other half were watered regularly. The plants under water withdrawal were re-watered at 5 weeks when most of the WT started to wither. The plants shown in Figure 3.1E were 7 weeks old. The pots shown are representative of 4 pots per treatment.

3.8 References

Alonso, J.M., Stepanova, A.N., Leisse, T.J., Kim, C.J., Chen, H., Shinn, P., Stevenson, D.K., Zimmerman, J., Barajas, P., Cheuk, R.*, et al.* (2003). Genome-wide insertional mutagenesis of Arabidopsis thaliana. Science *301*, 653-657.

Baena-Gonzalez, E., Rolland, F., Thevelein, J.M., and Sheen, J. (2007). A central integrator of transcription networks in plant stress and energy signalling. Nature *448*, 938-942.

Blanvillain, R., Wei, S., Wei, P., Kim, J.H., and Ow, D.W. (2011). Stress tolerance to stress escape in plants: role of the OXS2 zinc-finger transcription factor family. EMBO J *30*, 3812-3822.

Chen, J., Yu, F., Liu, Y., Du, C., Li, X., Zhu, S., Wang, X., Lan, W., Rodriguez, P.L., Liu, X.*, et al.* (2016). FERONIA interacts with ABI2-type phosphatases to facilitate signaling cross-talk between abscisic acid and RALF peptide in Arabidopsis. Proc Natl Acad Sci U S A *113*, E5519-5527.

Chen, L., Su, Z.Z., Huang, L., Xia, F.N., Qi, H., Xie, L.J., Xiao, S., and Chen, Q.F. (2017). The AMP-Activated Protein Kinase KIN10 Is Involved in the Regulation of Autophagy in Arabidopsis. Front Plant Sci *8*, 1201.

Chockalingam, S.A., M .; Guo, H.; Yin, Y.; Aluru, S. (2017). Reverse engineering gene networks: An comparative study at genome-scale. In Proceedings of the 8th ACM International Conference on Bioinformatics, Computational Biology, and Health Informatics (ACM), pp. 480-490.

Cox, J., Neuhauser, N., Michalski, A., Scheltema, R.A., Olsen, J.V., and Mann, M. (2011). Andromeda: a peptide search engine integrated into the MaxQuant environment. J Proteome Res *10*, 1794-1805.

Dong, P., Xiong, F., Que, Y., Wang, K., Yu, L., Li, Z., and Ren, M. (2015). Expression profiling and functional analysis reveals that TOR is a key player in regulating photosynthesis and phytohormone signaling pathways in Arabidopsis. Front Plant Sci *6*, 677.

Duan, Q., Kita, D., Li, C., Cheung, A.Y., and Wu, H.M. (2010). FERONIA receptor-like kinase regulates RHO GTPase signaling of root hair development. Proc Natl Acad Sci U S A *107*, 17821-17826.

Elias, J.E., and Gygi, S.P. (2007). Target-decoy search strategy for increased confidence in large-scale protein identifications by mass spectrometry. Nat Methods *4*, 207-214.

Feng, W., Kita, D., Peaucelle, A., Cartwright, H.N., Doan, V., Duan, Q., Liu, M.C., Maman, J., Steinhorst, L., Schmitz-Thom, I.*, et al.* (2018). The FERONIA Receptor Kinase Maintains Cell-Wall Integrity during Salt Stress through Ca(2+) Signaling. Curr Biol *28*, 666-675 e665.

Gibalova, A., Renak, D., Matczuk, K., Dupl'akova, N., Chab, D., Twell, D., and Honys, D. (2009). AtbZIP34 is required for Arabidopsis pollen wall patterning and the control of several metabolic pathways in developing pollen. Plant Mol Biol *70*, 581-601.

Gonneau, M., Desprez, T., Martin, M., Doblas, V.G., Bacete, L., Miart, F., Sormani, R., Hematy, K., Renou, J., Landrein, B.*, et al.* (2018). Receptor Kinase THESEUS1 Is a Rapid Alkalinization Factor 34 Receptor in Arabidopsis. Curr Biol *28*, 2452-2458 e2454.

Guo, H., Li, L., Ye, H., Yu, X., Algreen, A., and Yin, Y. (2009). Three related receptor-like kinases are required for optimal cell elongation in Arabidopsis thaliana. Proc Natl Acad Sci U S A *106*, 7648-7653.

Guo, H., Nolan, T.M., Song, G., Liu, S., Xie, Z., Chen, J., Schnable, P.S., Walley, J.W., and Yin, Y. (2018). FERONIA Receptor Kinase Contributes to Plant Immunity by Suppressing Jasmonic Acid Signaling in Arabidopsis thaliana. Curr Biol *28*, 3316-3324 e3316.

Hara-Nishimura, I., and Matsushima, R. (2003). A wound-inducible organelle derived from endoplasmic reticulum: a plant strategy against environmental stresses? Curr Opin Plant Biol *6*, 583-588.

Hayashi, Y., Yamada, K., Shimada, T., Matsushima, R., Nishizawa, N.K., Nishimura, M., and Hara-Nishimura, I. (2001). A proteinase-storing body that prepares for cell death or stresses in the epidermal cells of Arabidopsis. Plant Cell Physiol *42*, 894-899.
Kettenbach, A.N., and Gerber, S.A. (2011). Rapid and reproducible single-stage phosphopeptide enrichment of complex peptide mixtures: application to general and phosphotyrosine-specific phosphoproteomics experiments. Anal Chem *83*, 7635-7644.

Liu, Y., and Bassham, D.C. (2010). TOR is a negative regulator of autophagy in Arabidopsis thaliana. PLoS One *5*, e11883.

Liu, Y., and Bassham, D.C. (2012). Autophagy: pathways for self-eating in plant cells. Annu Rev Plant Biol *63*, 215-237.

Liu, Y., Beyer, A., and Aebersold, R. (2016). On the Dependency of Cellular Protein Levels on mRNA Abundance. Cell *165*, 535-550.

Marshall, R.S., and Vierstra, R.D. (2018). Autophagy: The Master of Bulk and Selective Recycling. Annu Rev Plant Biol *69*, 173-208.

Masachis, S., Segorbe, D., Turra, D., Leon-Ruiz, M., Furst, U., El Ghalid, M., Leonard, G., Lopez-Berges, M.S., Richards, T.A., Felix, G.*, et al.* (2016). A fungal pathogen secretes plant alkalinizing peptides to increase infection. Nat Microbiol *1*, 16043.

Matsushima, R., Fukao, Y., Nishimura, M., and Hara-Nishimura, I. (2004). NAI1 gene encodes a basic-helix-loop-helix-type putative transcription factor that regulates the formation of an endoplasmic reticulum-derived structure, the ER body. Plant Cell *16*, 1536-1549.

Matsushima, R., Hayashi, Y., Kondo, M., Shimada, T., Nishimura, M., and Hara-Nishimura, I. (2002). An endoplasmic reticulum-derived structure that is induced under stress conditions in Arabidopsis. Plant Physiol *130*, 1807-1814.

Matsushima, R., Hayashi, Y., Yamada, K., Shimada, T., Nishimura, M., and Hara-Nishimura, I. (2003a). The ER body, a novel endoplasmic reticulum-derived structure in Arabidopsis. Plant Cell Physiol *44*, 661-666.

Matsushima, R., Kondo, M., Nishimura, M., and Hara-Nishimura, I. (2003b). A novel ER-derived compartment, the ER body, selectively accumulates a beta-glucosidase with an ER-retention signal in Arabidopsis. Plant J *33*, 493-502.

Nagano, A.J., Fukao, Y., Fujiwara, M., Nishimura, M., and Hara-Nishimura, I. (2008). Antagonistic jacalin-related lectins regulate the size of ER body-type beta-glucosidase complexes in Arabidopsis thaliana. Plant Cell Physiol *49*, 969-980.

Nagano, A.J., Matsushima, R., and Hara-Nishimura, I. (2005). Activation of an ER-body-localized beta-glucosidase via a cytosolic binding partner in damaged tissues of Arabidopsis thaliana. Plant Cell Physiol *46*, 1140-1148.

Nakano, R.T., Pislewska-Bednarek, M., Yamada, K., Edger, P.P., Miyahara, M., Kondo, M., Bottcher, C., Mori, M., Nishimura, M., Schulze-Lefert, P*., et al.* (2017). PYK10 myrosinase reveals a functional coordination between endoplasmic reticulum bodies and glucosinolates in Arabidopsis thaliana. Plant J *89*, 204-220.

Nolan, T., Chen, J., and Yin, Y. (2017). Cross-talk of Brassinosteroid signaling in controlling growth and stress responses. Biochem J *474*, 2641-2661.

Nukarinen, E., Nagele, T., Pedrotti, L., Wurzinger, B., Mair, A., Landgraf, R., Bornke, F., Hanson, J., Teige, M., Baena-Gonzalez, E*., et al.* (2016). Quantitative phosphoproteomics reveals the role of the AMPK plant ortholog SnRK1 as a metabolic master regulator under energy deprivation. Sci Rep *6*, 31697.

Ogasawara, K., Yamada, K., Christeller, J.T., Kondo, M., Hatsugai, N., Hara-Nishimura, I., and Nishimura, M. (2009). Constitutive and inducible ER bodies of Arabidopsis thaliana accumulate distinct beta-glucosidases. Plant Cell Physiol *50*, 480-488.

Perrella, G., Davidson, M.L.H., O'Donnell, L., Nastase, A.M., Herzyk, P., Breton, G., Pruneda-Paz, J.L., Kay, S.A., Chory, J., and Kaiserli, E. (2018). ZINC-FINGER interactions mediate transcriptional regulation of hypocotyl growth in Arabidopsis. Proc Natl Acad Sci U S A *115*, E4503-E4511.

Pierre, M., Traverso, J.A., Boisson, B., Domenichini, S., Bouchez, D., Giglione, C., and Meinnel, T. (2007). N-myristoylation regulates the SnRK1 pathway in Arabidopsis. Plant Cell *19*, 2804-2821.

Ren, M., Qiu, S., Venglat, P., Xiang, D., Feng, L., Selvaraj, G., and Datla, R. (2011). Target of rapamycin regulates development and ribosomal RNA expression through kinase domain in Arabidopsis. Plant Physiol *155*, 1367-1382.

Schepetilnikov, M., Makarian, J., Srour, O., Geldreich, A., Yang, Z., Chicher, J., Hammann, P., and Ryabova, L.A. (2017). GTPase ROP2 binds and promotes activation of target of rapamycin, TOR, in response to auxin. EMBO J *36*, 886-903.

Shi, L., Wu, Y., and Sheen, J. (2018). TOR signaling in plants: conservation and innovation. Development *145*.

Signorelli, S., Tarkowski, L.P., Van den Ende, W., and Bassham, D.C. (2019). Linking Autophagy to Abiotic and Biotic Stress Responses. Trends Plant Sci.

Song, G., Brachova, L., Nikolau, B.J., Jones, A.M., and Walley, J.W. (2018a). Heterotrimeric G-Protein-Dependent Proteome and Phosphoproteome in Unstimulated Arabidopsis Roots. Proteomics *18*, e1800323.

Song, G., Hsu, P.Y., and Walley, J.W. (2018b). Assessment and Refinement of Sample Preparation Methods for Deep and Quantitative Plant Proteome Profiling. Proteomics *18*, e1800220.
Song, L., Huang, S.C., Wise, A., Castanon, R., Nery, J.R., Chen, H., Watanabe, M., Thomas, J., Bar-Joseph, Z., and Ecker, J.R. (2016). A transcription factor hierarchy defines an environmental stress response network. Science *354*.

Soto-Burgos, J., and Bassham, D.C. (2017). SnRK1 activates autophagy via the TOR signaling pathway in Arabidopsis thaliana. PLoS One *12*, e0182591.

Stegmann, M., Monaghan, J., Smakowska-Luzan, E., Rovenich, H., Lehner, A., Holton, N., Belkhadir, Y., and Zipfel, C. (2017). The receptor kinase FER is a RALF-regulated scaffold controlling plant immune signaling. Science *355*, 287-289.

Sun, Y., Fan, X.Y., Cao, D.M., Tang, W., He, K., Zhu, J.Y., He, J.X., Bai, M.Y., Zhu, S., Oh, E.*, et al.* (2010). Integration of brassinosteroid signal transduction with the transcription network for plant growth regulation in Arabidopsis. Dev Cell *19*, 765-777.

Suttangkakul, A., Li, F., Chung, T., and Vierstra, R.D. (2011). The ATG1/ATG13 protein kinase complex is both a regulator and a target of autophagic recycling in Arabidopsis. Plant Cell *23*, 3761-3779.

Tyanova, S., Temu, T., Sinitcyn, P., Carlson, A., Hein, M.Y., Geiger, T., Mann, M., and Cox, J. (2016). The Perseus computational platform for comprehensive analysis of (prote)omics data. Nat Methods *13*, 731-740.

Van Leene, J., Han, C., Gadeyne, A., Eeckhout, D., Matthijs, C., Cannoot, B., De Winne, N., Persiau, G., Van De Slijke, E., Van de Cotte, B.*, et al.* (2019). Capturing the phosphorylation and protein interaction landscape of the plant TOR kinase. Nat Plants *5*, 316-327.

Walley, J.W., Shen, Z., McReynolds, M.R., Schmelz, E.A., and Briggs, S.P. (2018). Fungal-induced protein hyperacetylation in maize identified by acetylome profiling. Proc Natl Acad Sci U S A *115*, 210-215.

Wang, J.Z., Li, B., Xiao, Y., Ni, Y., Ke, H., Yang, P., de Souza, A., Bjornson, M., He, X., Shen, Z.*, et al.* (2017). Initiation of ER Body Formation and Indole Glucosinolate Metabolism by the Plastidial Retrograde Signaling Metabolite, MEcPP. Mol Plant *10*, 1400-1416.

Wang, P.N., T. M.; Yin, Y.; Bassham, D. (2019). Identification of transcription factors that regulate ATG8 expression and autophagy in Arabidopsis. Autophagy.

Wang, Z., Li, X., Liu, N., Peng, Q., Wang, Y., Fan, B., Zhu, C., and Chen, Z. (2019). A Family of NAI2-Interacting Proteins in the Biogenesis of the ER Body and Related Structures. Plant Physiol.

Wickham, H. (2016). ggplot2: Elegant Graphics for Data Analysis. Springer-Verlag New York.

Wittstock, U., and Burow, M. (2010). Glucosinolate breakdown in Arabidopsis: mechanism, regulation and biological significance. Arabidopsis Book *8*, e0134.

Yamada, K., Nagano, A.J., Nishina, M., Hara-Nishimura, I., and Nishimura, M. (2008). NAI2 is an endoplasmic reticulum body component that enables ER body formation in Arabidopsis thaliana. Plant Cell *20*, 2529-2540.

Yu, F., Qian, L., Nibau, C., Duan, Q., Kita, D., Levasseur, K., Li, X., Lu, C., Li, H., Hou, C.*, et al.* (2012). FERONIA receptor kinase pathway suppresses abscisic acid signaling in Arabidopsis by activating ABI2 phosphatase. Proc Natl Acad Sci U S A *109*, 14693-14698.

Yu, X., Li, L., Zola, J., Aluru, M., Ye, H., Foudree, A., Guo, H., Anderson, S., Aluru, S., Liu, P.*, et al.* (2011). A brassinosteroid transcriptional network revealed by genome-wide identification of BESI target genes in Arabidopsis thaliana. Plant J *65*, 634-646.

Zhao, C., Zayed, O., Yu, Z., Jiang, W., Zhu, P., Hsu, C.C., Zhang, L., Tao, W.A., Lozano-Duran, R., and Zhu, J.K. (2018). Leucine-rich repeat extensin proteins regulate plant salt tolerance in Arabidopsis. Proc Natl Acad Sci U S A *115*, 13123-13128.

3.9 Figures and Tables

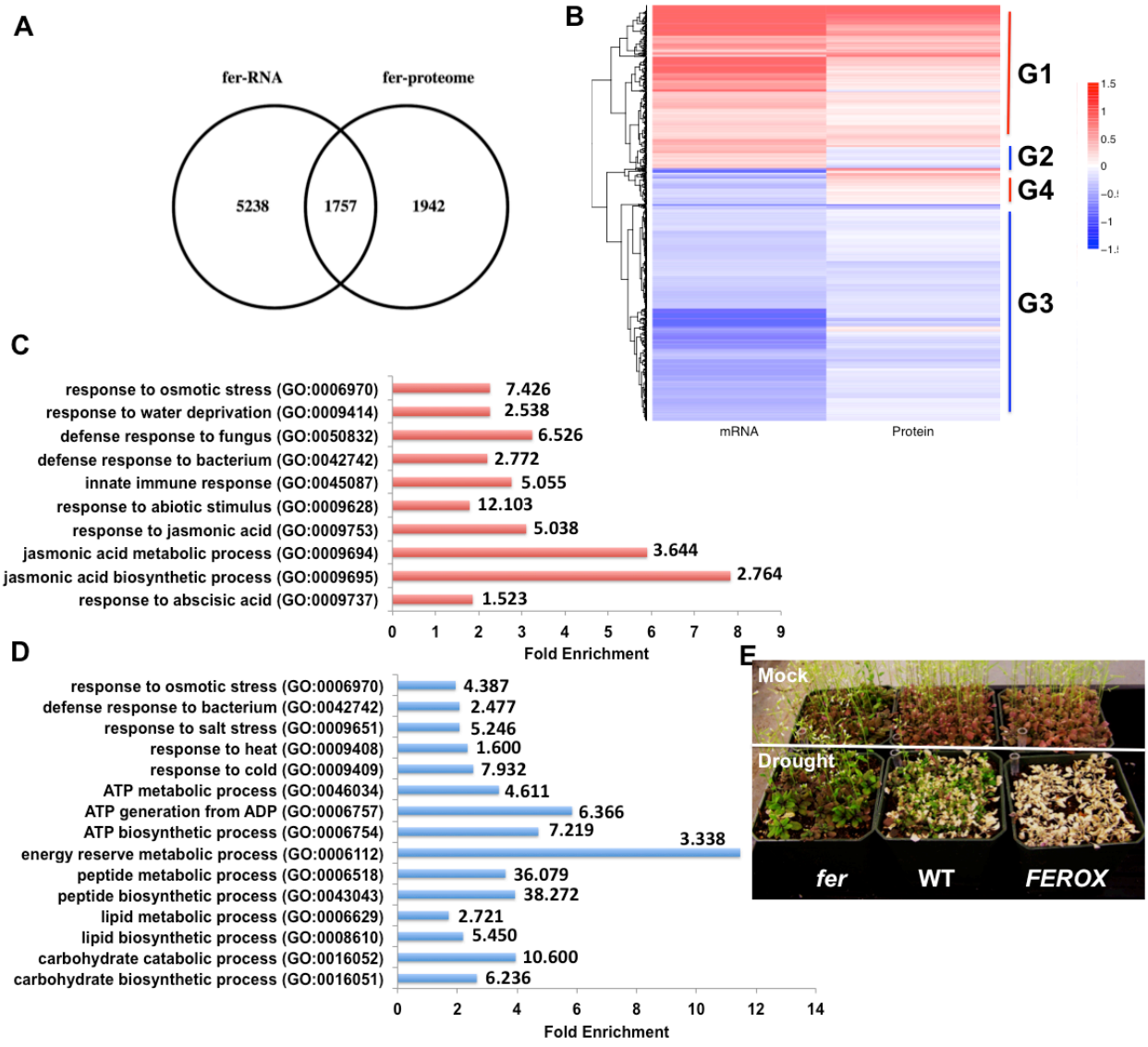

Figure 3.1: Analysis of *fer* Proteomics Data

(A) Venn diagram shows significant overlap of gene transcripts and proteins regulated in *fer* mutant. fer-RNA represents genes whose transcript levels changed in *fer*, described previously

(Guo et al., 2018); fer-proteome represents all proteins whose levels significantly changed in *fer*. (B) A clustering analysis displays that the RNA and protein levels change in the same direction (G1 (group 1) and G3 (group 3)) for most of the overlapped genes from Figure 3.1A, and small portion of the genes change in the opposite direction in RNA and protein levels (G2 (group 2) and G4 (group 4)). (C-D) Selected enriched GO terms in proteins with increased levels in *fer* (C) and decreased in *fer* (D) are presented; -log10 (pvalue) is also shown for each GO term. (E) Drought responses of WT, *fer* and *FEROX* plants.

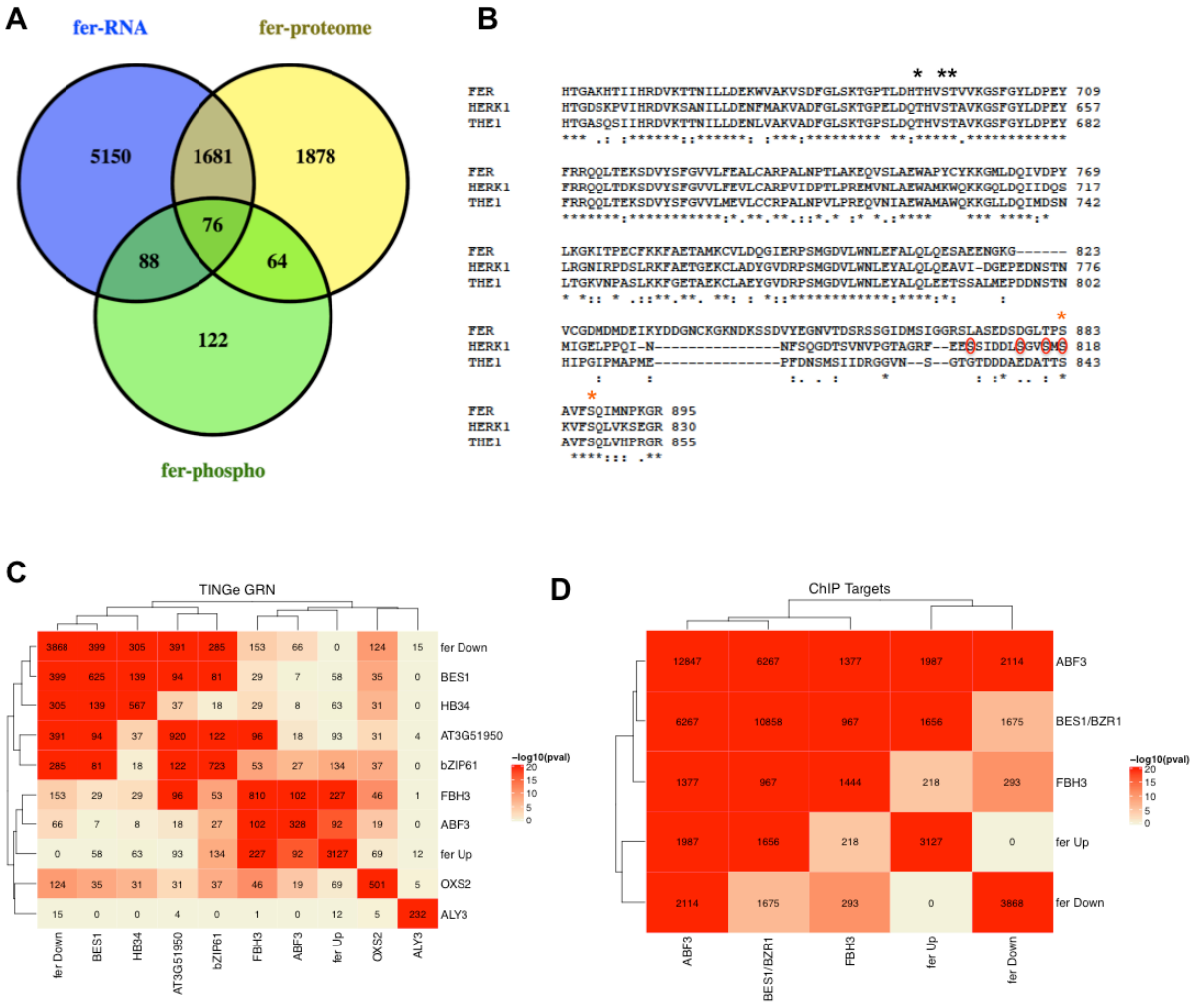

Figure 3.2: Analysis of *fer* Phosphoproteomics Data

(A) Venn diagram shows the overlap of the three sets of omics data, fer-RNA (transcriptome), fer-proteome and fer-phospho (phosphoproteome). (B) Partial alignment of protein sequences of FER, HERK1 and THE1, showing the phosphorylation sites in FER (red stars), HERK1 (red ovals) and THE1 (black stars) that hypo-phosphorylated in *fer* mutant. (C) Comparison of FER-regulated genes with the regulons of the eight TFs that are FER potential substrates, which were extracted from the TINGe network. The color represents –log10 (pvalue) from the overlaps calculated from Fisher's exact test by GeneOverlap.

(D) Comparison of fer-regulated genes and direct targets of ABF3, FBH3 and BES1 identified by ChIP-chip or ChIP-sequencing (Song et al., 2016; Sun et al., 2010; Yu et al., 2011).

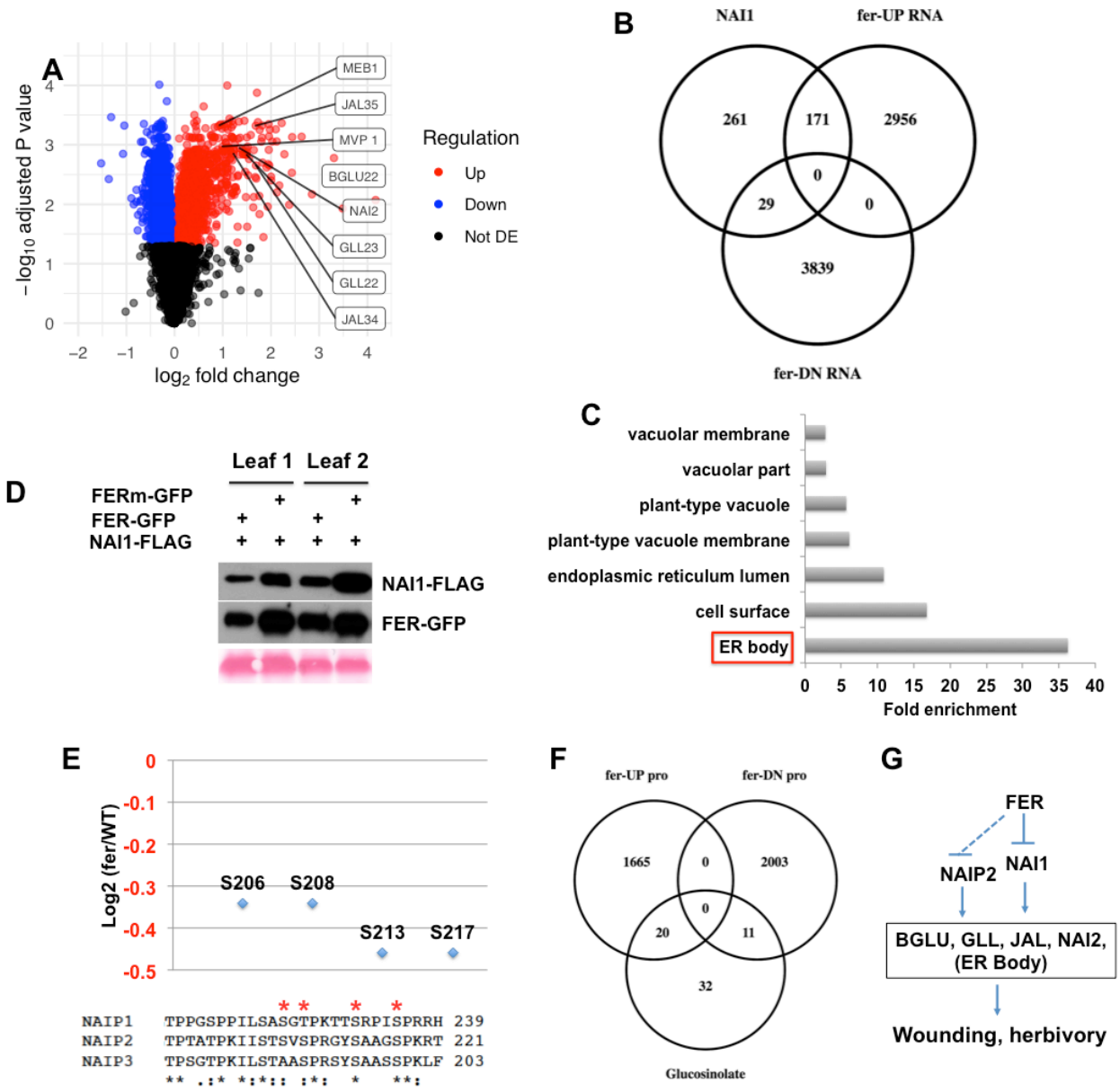

Figure 3.3: FER Negatively Regulates ER body Formation

(A) Volcano plot of the 7240 proteins that are detected in the proteomics. X-axis is the log2 fold change (*fer*/WT) and y-axis represents the –log10 pvalue. Selected ER body-associated proteins are labeled. (B) Venn diagram shows the overlap of the NAI1 regulon extracted from the TINGe network and FER-regulated genes. (C) The significantly enriched GO terms in the 171 genes that are up-regulated in *fer* and also present in the NAI1 regulon. The GO term ER body was

indicated. (D) Co-expression of *NAI1-FLAG* and *FER-GFP* or *FERm-GFP* in two individual *N. benthamiana* leaves. Proteins were extracted followed by western blotting 24 hours after the infiltration. (E) The four identified phosphosites in NAIP2. The top panel shows the Log2 fold change (*fer*/WT) showing all 4 sites are under-phosphorylated in *fer* mutant. The red stars in the bottom panel shows the phosphosites in NAIP2 and the conservation between the other two homologs. (F) Venn diagram shows that about half of the glucosinolate-related proteins (Wang et al., 2017) are regulated in *fer*. (G) A working model for how FER negatively regulates ER body formation and the potential outcomes.

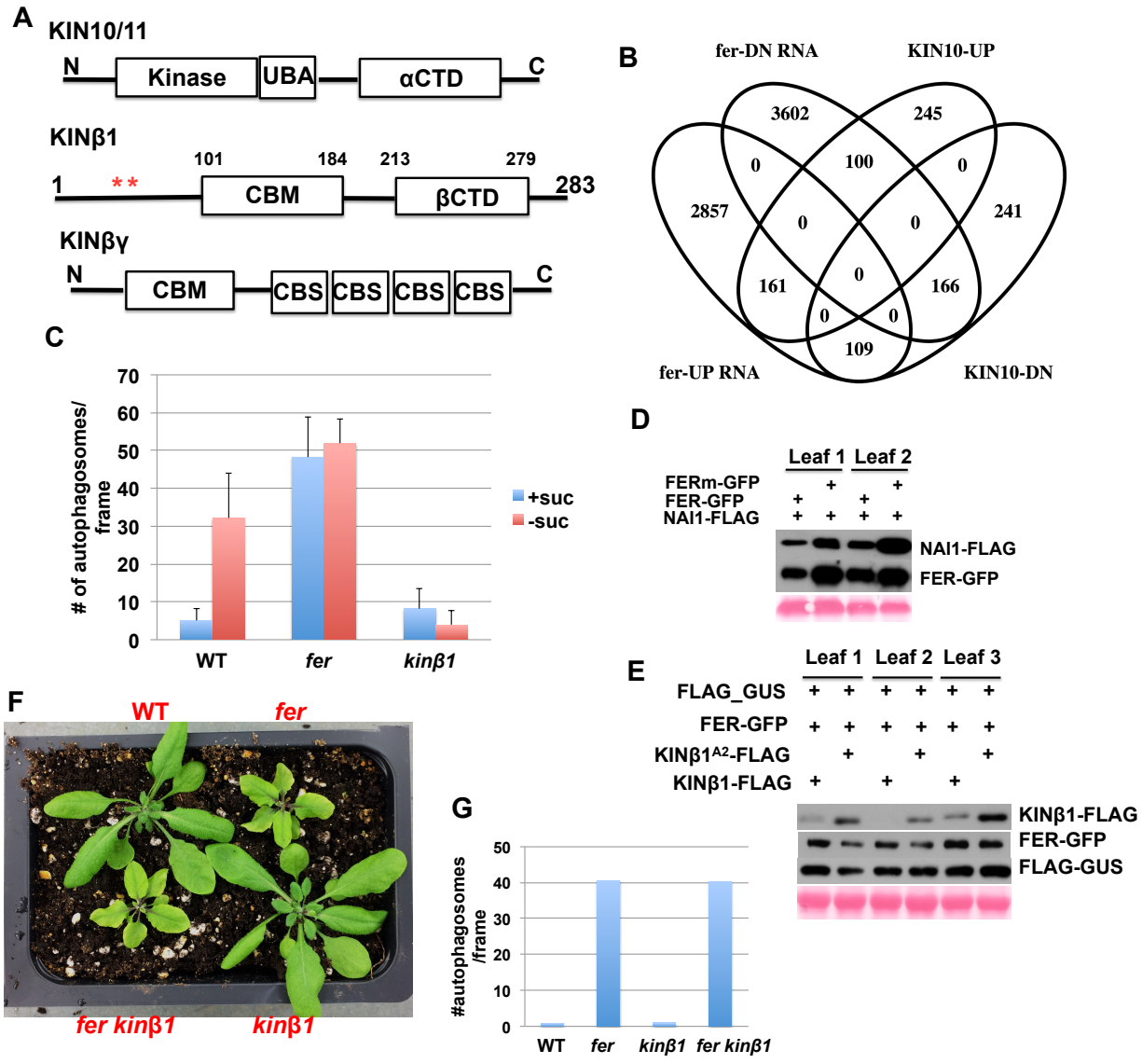

Figure 3.4: FER Phosphorylates KINβ1 and Negatively Regulates Autophagy

(A) A diagram to show KIN10/11, KINβ1 and KINβγ with conserved domains, and the red stars denote the FER phosphorylation sites on KINβ1. UBA: ubiquitin-associated domain; CTD: C-terminal domain; CBM: carbohydrate binding motif; CBS: cystathionine β-synthetase domain. (B) Venn diagram shows major overlap between KIN10-regulated genes and fer-regulated genes. (C) MDC staining of seedling roots of the indicated genotypes under sucrose starvation. Average and SD were generated from 10 individual seedlings (n=10). The experiment was repeated twice

with similar results. (D) Co-expression of *KINβ1-FLAG* and *FER-GFP* or *FERm-GFP* in two individual *N. benthamiana* leaves. Proteins were extracted followed by western blotting 24 hours after the infiltration. (E) Co-expression of *KINβ1-FLAG* or *KINβ1*^{A2}*-FLAG* and *FER-GFP* in three individual *N. benthamiana* leaves. Protein was extracted followed by western blotting 24 hours after the infiltration. FLAG-GUS was used as internal control. (F) Five-week old plants show that the growth phenotype of the double *fer kinβ1* mirrors *fer.* (G) MDC staining shows that similar to *fer*, the double mutant also displays constitutive autophagy (n=10-16).

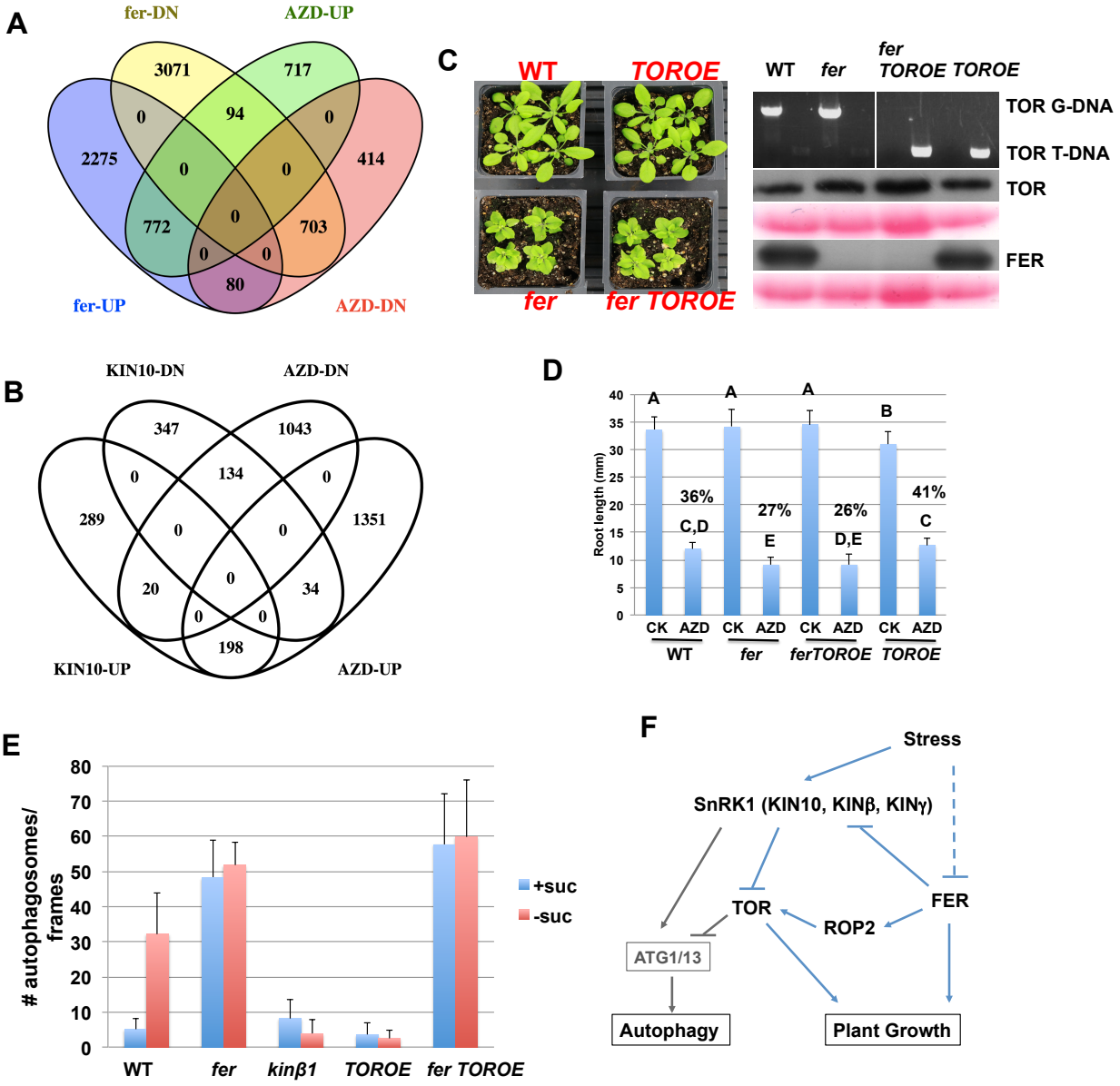

Figure 3.5: FER, KINβ1 and TOR Function in a Complex to Regulate Plant Growth and Autophagy

(A) Venn diagram shows significant overlap between AZD-regulated genes and FER-regulated genes, and FER and TOR regulate the genes in the same direction. (B) Venn diagram shows that AZD-regulated genes also overlap with KIN10-regulated genes, but in an antagonistic manner. (C) The left panel shows that five-week old *fer TOROE* double mutant mirrors *fer*

phenotypically. The right panel shows the genotyping results of the mutants, and FER and TOR proteins using western blotting and corresponding antibodies. (D) AZD response of different genotypes. Seeds were germinated on 1/2MS plates containing 1uM AZD, DMSO as control. Average and SD were generated from 12 seedling roots (n=12). The statistic significance was calculated using Tukey HSD test and p value less than 0.05 were considered significant. (E) MDC staining seedling roots of indicated genotypes under sucrose starvation. Average and SD were generated from 10 individual seedlings (n=10). The experiment was repeated twice with similar results. (F) A working model on how FER, SnRK1 complex and TOR function together to regulate growth and autophagy.

Table 3.1: List of Biological Process GO Term in Proteins with Increased Levels in *fer*

GO biological process complete	AT ref (27581)	fer_UP (1690)	expected	over/under	fold Enrichment	P-value
long-chain fatty acid metabolic process (GO:0001676)	13	8	0.8	+	10.04	3.41E-02
indolalkylamine metabolic process (GO:0006586)	29	14	1.78	+	7.88	1.89E-04
tryptophan metabolic process (GO:0006568)	29	14	1.78	+	7.88	1.89E-04
jasmonic acid biosynthetic process (GO:0009695)	25	12	1.53	+	7.83	1.72E-03
indolalkylamine biosynthetic process (GO:0046219)	23	11	1.41	+	7.81	5.20E-03
tryptophan biosynthetic process (GO:0000162)	23	11	1.41	+	7.81	5.20E-03
indole-containing compound biosynthetic process (GO:0042435)	50	22	3.06	+	7.18	1.47E-07
jasmonic acid metabolic process (GO:0009694)	47	17	2.88	+	5.9	2.27E-04
glucosinolate catabolic process (GO:0019762)	38	13	2.33	+	5.58	1.24E-02
glycosinolate catabolic process (GO:0019759)	38	13	2.33	+	5.58	1.24E-02
S-glycoside catabolic process (GO:0016145)	38	13	2.33	+	5.58	1.24E-02
indole-containing compound metabolic process (GO:0042430)	91	31	5.58	+	5.56	4.40E-09
glycosyl compound catabolic process (GO:1901658)	61	20	3.74	+	5.35	6.50E-05
sulfur compound catabolic process (GO:0044273)	53	17	3.25	+	5.23	9.33E-04
amine biosynthetic process (GO:0009309)	44	14	2.7	+	5.19	1.08E-02
cellular biogenic amine biosynthetic process (GO:0042401)	44	14	2.7	+	5.19	1.08E-02
cellular amine metabolic process (GO:0044106)	60	19	3.68	+	5.17	2.28E-04
cellular biogenic amine metabolic process (GO:0006576)	60	19	3.68	+	5.17	2.28E-04
response to endoplasmic reticulum stress (GO:0034976)	73	23	4.47	+	5.14	1.11E-05
flavonoid metabolic process (GO:0009812)	69	21	4.23	+	4.97	8.54E-05
toxin metabolic process (GO:0009404)	71	21	4.35	+	4.83	1.29E-04
aromatic amino acid family metabolic process (GO:0009072)	79	23	4.84	+	4.75	3.84E-05
lipid oxidation (GO:0034440)	55	16	3.37	+	4.75	6.00E-03
flavonoid biosynthetic process (GO:0009813)	59	17	3.62	+	4.7	3.25E-03
glutathione metabolic process (GO:0006749)	57	16	3.49	+	4.58	8.86E-03
monocarboxylic acid catabolic process (GO:0072329)	63	17	3.86	+	4.4	6.94E-03
carbohydrate derivative catabolic process (GO:1901136)	87	23	5.33	+	4.31	1.72E-04
plant-type hypersensitive response (GO:0009626)	57	15	3.49	+	4.29	3.44E-02
host programmed cell death induced by symbiont (GO:0034050)	58	15	3.55	+	4.22	4.10E-02
auxin metabolic process (GO:0009850)	62	16	3.8	+	4.21	2.20E-02
response to wounding (GO:0009611)	216	50	13.24	+	3.78	3.29E-10
sulfur compound biosynthetic process (GO:0044272)	142	32	8.7	+	3.68	1.43E-05
carboxylic acid catabolic process (GO:0046395)	139	31	8.52	+	3.64	3.05E-05
organic acid catabolic process (GO:0016054)	139	31	8.52	+	3.64	3.05E-05
glucosinolate metabolic process (GO:0019760)	137	30	8.39	+	3.57	7.45E-05
glycosinolate metabolic process (GO:0019757)	137	30	8.39	+	3.57	7.45E-05
S-glycoside metabolic process (GO:0016143)	137	30	8.39	+	3.57	7.45E-05
glycosyl compound metabolic process (GO:1901657)	207	45	12.68	+	3.55	3.42E-08
glycoprotein metabolic process (GO:0009100)	120	26	7.35	+	3.54	7.35E-04
secondary metabolic process (GO:0019748)	371	80	22.73	+	3.52	5.59E-16
response to fungus (GO:0009620)	310	65	18.99	+	3.42	4.42E-12
macromolecule glycosylation (GO:0043413)	107	22	6.56	+	3.36	1.24E-02
protein glycosylation (GO:0006486)	107	22	6.56	+	3.36	1.24E-02
secondary metabolite biosynthetic process (GO:0044550)	180	37	11.03	+	3.35	8.33E-06
glycoprotein biosynthetic process (GO:0009101)	108	22	6.62	+	3.32	1.42E-02
endoplasmic reticulum to Golgi vesicle-mediated transport (GO:0006888)	99	20	6.07	+	3.3	4.15E-02
cellular modified amino acid metabolic process (GO:0006575)	124	25	7.6	+	3.29	3.90E-03
small molecule catabolic process (GO:0044282)	214	43	13.11	+	3.28	8.35E-07
glycosylation (GO:0070085)	110	22	6.74	+	3.26	1.83E-02
defense response to fungus (GO:0050832)	232	46	14.22	+	3.24	2.98E-07
phenylpropanoid metabolic process (GO:0009698)	141	28	8.64	+	3.24	1.22E-03
sulfur compound metabolic process (GO:0006790)	378	75	23.16	+	3.24	3.98E-13
amine metabolic process (GO:0009308)	111	22	6.8	+	3.23	2.07E-02
monocarboxylic acid metabolic process (GO:0032787)	430	85	26.35	+	3.23	4.45E-15
response to jasmonic acid (GO:0009753)	216	41	13.24	+	3.1	9.17E-06
fatty acid metabolic process (GO:0006631)	212	40	12.99	+	3.08	1.64E-05
response to karrikin (GO:0080167)	129	24	7.9	+	3.04	2.09E-02
defense response, incompatible interaction (GO:0009814)	168	31	10.29	+	3.01	1.24E-03
monocarboxylic acid biosynthetic process (GO:0072330)	267	49	16.36	+	3	7.67E-07

Table 3.1. (continued)

Golgi vesicle transport (GO:0048193)	179	32	10.97	+	2.92	1.51E-03
alpha-amino acid metabolic process (GO:1901605)	271	48	16.61	+	2.89	3.25E-06
carbohydrate catabolic process (GO:0016052)	182	32	11.15	+	2.87	2.07E-03
cellular amino acid biosynthetic process (GO:0008652)	202	35	12.38	+	2.83	8.72E-04
alpha-amino acid biosynthetic process (GO:1901607)	180	31	11.03	+	2.81	4.50E-03
innate immune response (GO:0045087)	296	50	18.14	+	2.76	8.81E-06
organic hydroxy compound metabolic process (GO:1901615)	286	48	17.52	+	2.74	2.08E-05
response to biotic stimulus (GO:0009607)	989	164	60.6	+	2.71	1.15E-23
response to external biotic stimulus (GO:0043207)	988	164	60.54	+	2.71	1.09E-23
response to other organism (GO:0051707)	988	164	60.54	+	2.71	1.09E-23
immune response (GO:0006955)	302	50	18.5	+	2.7	1.28E-05
vesicle-mediated transport (GO:0016192)	453	75	27.76	+	2.7	1.52E-09
immune system process (GO:0002376)	359	58	22	+	2.64	1.48E-06
regulation of defense response (GO:0031347)	249	40	15.26	+	2.62	8.44E-04
defense response to other organism (GO:0098542)	682	109	41.79	+	2.61	7.12E-14
organic acid metabolic process (GO:0006082)	1032	165	63.23	+	2.61	3.06E-22
oxoacid metabolic process (GO:0043436)	1030	165	63.11	+	2.61	1.72E-22
carboxylic acid metabolic process (GO:0019752)	882	140	54.04	+	2.59	2.60E-18
carboxylic acid biosynthetic process (GO:0046394)	521	82	31.92	+	2.57	1.68E-09
hormone metabolic process (GO:0042445)	254	40	15.56	+	2.57	1.26E-03
organic acid biosynthetic process (GO:0016053)	521	82	31.92	+	2.57	1.68E-09
response to toxic substance (GO:0009636)	207	32	12.68	+	2.52	2.46E-02
carbohydrate derivative metabolic process (GO:1901135)	716	110	43.87	+	2.51	7.44E-13
cellular amino acid metabolic process (GO:0006520)	377	58	23.1	+	2.51	7.57E-06
small molecule metabolic process (GO:0044281)	1587	239	97.24	+	2.46	2.46E-30
response to metal ion (GO:0010038)	478	71	29.29	+	2.42	5.80E-07
response to bacterium (GO:0009617)	493	72	30.21	+	2.38	1.06E-06
response to external stimulus (GO:0009605)	1388	200	85.05	+	2.35	1.37E-22
small molecule biosynthetic process (GO:0044283)	670	96	41.05	+	2.34	2.36E-09
response to cadmium ion (GO:0046686)	345	49	21.14	+	2.32	1.46E-03
response to salt stress (GO:0009651)	590	82	36.15	+	2.27	4.18E-07
response to osmotic stress (GO:0006970)	665	92	40.75	+	2.26	3.75E-08
response to water deprivation (GO:0009414)	346	48	21.2	+	2.26	2.90E-03
carbohydrate derivative biosynthetic process (GO:1901137)	413	57	25.31	+	2.25	3.40E-04
defense response (GO:0006952)	1147	158	70.28	+	2.25	1.34E-15
regulation of response to stress (GO:0080134)	359	49	22	+	2.23	4.23E-03
response to water (GO:0009415)	353	48	21.63	+	2.22	5.99E-03
defense response to bacterium (GO:0042742)	393	53	24.08	+	2.2	1.69E-03
response to inorganic substance (GO:0010035)	945	126	57.9	+	2.18	7.09E-11
multi-organism process (GO:0051704)	1482	196	90.81	+	2.16	3.39E-18
response to oxidative stress (GO:0006979)	424	56	25.98	+	2.16	1.52E-03
intracellular protein transport (GO:0006886)	560	73	34.31	+	2.13	5.53E-05
cellular catabolic process (GO:0044248)	1308	170	80.15	+	2.12	1.11E-14
establishment of protein localization (GO:0045184)	707	92	43.32	+	2.12	6.97E-07
protein transport (GO:0015031)	699	91	42.83	+	2.12	8.91E-07
catabolic process (GO:0009056)	1486	192	91.05	+	2.11	9.06E-17
intracellular transport (GO:0046907)	683	88	41.85	+	2.1	2.69E-06
nucleobase-containing small molecule metabolic process (GO:0055086)	450	58	27.57	+	2.1	1.95E-03
organic substance catabolic process (GO:1901575)	1317	169	80.7	+	2.09	4.03E-14
response to acid chemical (GO:0001101)	1178	150	72.18	+	2.08	5.34E-12
cellular macromolecule localization (GO:0070727)	678	86	41.54	+	2.07	9.46E-06
cellular lipid metabolic process (GO:0044255)	675	85	41.36	+	2.06	1.47E-05
cofactor metabolic process (GO:0051186)	499	63	30.58	+	2.06	1.49E-03
protein localization (GO:0008104)	780	98	47.79	+	2.05	1.05E-06
regulation of hormone levels (GO:0010817)	406	51	24.88	+	2.05	1.82E-02
amide transport (GO:0042886)	785	98	48.1	+	2.04	1.83E-06
drug metabolic process (GO:0017144)	543	68	33.27	+	2.04	6.70E-04
peptide transport (GO:0015833)	768	96	47.06	+	2.04	2.04E-06
lipid metabolic process (GO:0006629)	831	103	50.92	+	2.02	8.43E-07
carbohydrate metabolic process (GO:0005975)	810	100	49.63	+	2.01	2.07E-06
cellular localization (GO:0051641)	901	111	55.21	+	2.01	1.85E-07
organonitrogen compound catabolic process (GO:1901565)	845	104	51.78	+	2.01	8.04E-07
cellular protein localization (GO:0034613)	646	79	39.58	+	2	1.85E-04
macromolecule localization (GO:0033036)	1037	127	63.54	+	2	1.03E-08

Table 3.1. (continued)

establishment of localization in cell (GO:0051649)	737	90	45.16	+	1.99	2.41E-05
organic substance transport (GO:0071702)	1210	147	74.14	+	1.98	3.19E-10
nitrogen compound transport (GO:0071705)	970	114	59.44	+	1.92	1.76E-06
response to stress (GO:0006950)	3158	366	193.5	+	1.89	3.12E-27
response to alcohol (GO:0097305)	558	64	34.19	+	1.87	2.09E-02
response to abscisic acid (GO:0009737)	554	63	33.95	+	1.86	3.00E-02
regulation of response to stimulus (GO:0048583)	679	77	41.61	+	1.85	4.51E-03
response to abiotic stimulus (GO:0009628)	2098	230	128.55	+	1.79	7.89E-13
organonitrogen compound biosynthetic process (GO:1901566)	1384	151	84.8	+	1.78	2.78E-07
oxidation-reduction process (GO:0055114)	937	102	57.41	+	1.78	4.04E-04
response to oxygen-containing compound (GO:1901700)	1596	174	97.79	+	1.78	9.92E-09
aromatic compound biosynthetic process (GO:0019438)	816	88	50	+	1.76	5.55E-03
regulation of biological quality (GO:0065008)	1129	122	69.18	+	1.76	3.55E-05
organic cyclic compound biosynthetic process (GO:1901362)	930	100	56.98	+	1.75	1.05E-03
response to chemical (GO:0042221)	2777	296	170.16	+	1.74	6.50E-16
cellular response to stress (GO:0033554)	924	98	56.62	+	1.73	2.07E-03
biosynthetic process (GO:0009058)	2823	294	172.98	+	1.7	1.54E-14
transport (GO:0006810)	2194	228	134.44	+	1.7	2.23E-10
organic substance biosynthetic process (GO:1901576)	2706	280	165.81	+	1.69	2.74E-13
establishment of localization (GO:0051234)	2238	230	137.13	+	1.68	5.10E-10
localization (GO:0051179)	2382	245	145.95	+	1.68	6.06E-11
cellular biosynthetic process (GO:0044249)	2576	258	157.84	+	1.63	2.24E-10
response to stimulus (GO:0050896)	5731	565	351.16	+	1.61	4.06E-28
organonitrogen compound metabolic process (GO:1901564)	4315	414	264.4	+	1.57	2.93E-16
response to endogenous stimulus (GO:0009719)	1615	155	98.96	+	1.57	4.65E-04
response to organic substance (GO:0010033)	1916	184	117.4	+	1.57	3.04E-05
response to hormone (GO:0009725)	1599	152	97.98	+	1.55	1.23E-03
organic substance metabolic process (GO:0071704)	7417	690	454.47	+	1.52	1.10E-29
metabolic process (GO:0008152)	8211	745	503.12	+	1.48	7.21E-30
cellular response to stimulus (GO:0051716)	2335	211	143.07	+	1.47	1.80E-04
cellular metabolic process (GO:0044237)	7157	631	438.54	+	1.44	6.97E-20
organic cyclic compound metabolic process (GO:1901360)	2724	236	166.91	+	1.41	6.39E-04
cellular aromatic compound metabolic process (GO:0006725)	2612	224	160.05	+	1.4	2.81E-03
primary metabolic process (GO:0044238)	6707	576	410.97	+	1.4	6.93E-15
nitrogen compound metabolic process (GO:0006807)	5875	499	359.99	+	1.39	4.38E-11
cellular nitrogen compound metabolic process (GO:0034641)	2986	250	182.96	+	1.37	3.41E-03
cellular process (GO:0009987)	10295	859	630.82	+	1.36	2.46E-24

Table 3.2: List of Cellular Process GO Terms in Proteins with Increased Levels in *fer*

GO cellular component complete	AT ref (27581)	fer_UP (1690)	expected	over/under	fold Enrichment	P-value
ER body (GO:0010168)	10	7	0.61	+	11.42	1.60E-02
endoplasmic reticulum lumen (GO:0005788)	39	23	2.39	+	9.62	1.24E-10
lytic vacuole (GO:0000323)	56	15	3.43	+	4.37	6.89E-03
integral component of endoplasmic reticulum membrane (GO:0030176)	70	18	4.29	+	4.2	1.52E-03
intrinsic component of endoplasmic reticulum membrane (GO:0031227)	72	18	4.41	+	4.08	2.14E-03
vacuole (GO:0005773)	1091	239	66.85	+	3.58	2.34E-55
microbody (GO:0042579)	255	55	15.62	+	3.52	5.85E-11
peroxisome (GO:0005777)	255	55	15.62	+	3.52	5.85E-11
endoplasmic reticulum part (GO:0044432)	514	110	31.49	+	3.49	3.19E-23
endoplasmic reticulum (GO:0005783)	1028	212	62.99	+	3.37	5.98E-45
vacuolar part (GO:0044437)	627	123	38.42	+	3.2	3.07E-23
vacuolar membrane (GO:0005774)	624	121	38.24	+	3.16	1.90E-22
endoplasmic reticulum membrane (GO:0005789)	459	86	28.12	+	3.06	1.16E-14
nuclear outer membrane-endoplasmic reticulum membrane network (GO:0042175)	463	86	28.37	+	3.03	1.84E-14
whole membrane (GO:0098805)	964	168	59.07	+	2.84	3.99E-27
cell junction (GO:0030054)	953	162	58.39	+	2.77	5.96E-25
cell-cell junction (GO:0005911)	953	162	58.39	+	2.77	5.96E-25
plasmodesma (GO:0009506)	953	162	58.39	+	2.77	5.96E-25
symplast (GO:0055044)	953	162	58.39	+	2.77	5.96E-25
plant-type vacuole (GO:0000325)	160	27	9.8	+	2.75	6.83E-03
plant-type cell wall (GO:0009505)	373	62	22.86	+	2.71	3.48E-08
coated vesicle (GO:0030135)	139	23	8.52	+	2.7	3.91E-02
trans-Golgi network (GO:0005802)	317	52	19.42	+	2.68	1.86E-06
bounding membrane of organelle (GO:0098588)	1266	204	77.57	+	2.63	1.71E-29
Golgi subcompartment (GO:0098791)	368	59	22.55	+	2.62	4.57E-07
cell wall (GO:0005618)	756	121	46.32	+	2.61	2.34E-16
external encapsulating structure (GO:0030312)	758	121	46.45	+	2.61	4.40E-16
integral component of plasma membrane (GO:0005887)	177	28	10.85	+	2.58	1.67E-02
endomembrane system (GO:0012505)	2245	353	137.56	+	2.57	1.55E-52
endosome (GO:0005768)	431	63	26.41	+	2.39	2.61E-06
Golgi apparatus (GO:0005794)	1199	175	73.47	+	2.38	1.41E-20
cytoplasmic vesicle (GO:0031410)	598	85	36.64	+	2.32	2.29E-08
intracellular vesicle (GO:0097708)	599	85	36.7	+	2.32	2.35E-08
organelle membrane (GO:0031090)	1811	250	110.97	+	2.25	2.20E-27
Golgi apparatus part (GO:0044431)	614	84	37.62	+	2.23	1.26E-07
cytoplasmic vesicle part (GO:0044433)	250	34	15.32	+	2.22	3.61E-02
cytosol (GO:0005829)	2290	308	140.32	+	2.2	7.06E-33
vesicle (GO:0031982)	662	86	40.56	+	2.12	8.92E-07
Golgi membrane (GO:0000139)	376	47	23.04	+	2.04	1.30E-02
apoplast (GO:0048046)	488	56	29.9	+	1.87	2.37E-02
cell periphery (GO:0071944)	4199	451	257.29	+	1.75	1.06E-28
intracellular organelle part (GO:0044446)	5375	550	329.35	+	1.67	1.06E-31
organelle part (GO:0044422)	5381	551	329.72	+	1.67	7.58E-32
plasma membrane (GO:0005886)	3572	359	218.87	+	1.64	5.44E-17
membrane (GO:0016020)	7769	721	476.04	+	1.51	5.70E-32
intracellular organelle lumen (GO:0070013)	1245	114	76.29	+	1.49	4.03E-02
membrane-enclosed lumen (GO:0031974)	1245	114	76.29	+	1.49	4.03E-02
organelle lumen (GO:0043233)	1245	114	76.29	+	1.49	4.03E-02
cytoplasmic part (GO:0044444)	12257	1096	751.04	+	1.46	2.12E-57
cytoplasm (GO:0005737)	14521	1254	889.76	+	1.41	4.99E-67
integral component of membrane (GO:0016021)	4315	364	264.4	+	1.38	4.38E-07
membrane part (GO:0044425)	5102	431	312.62	+	1.38	4.15E-09
plastid (GO:0009536)	5292	443	324.26	+	1.37	6.43E-09
chloroplast (GO:0009507)	5248	438	321.57	+	1.36	1.33E-08
intrinsic component of membrane (GO:0031224)	4577	380	280.45	+	1.35	1.07E-06
extracellular region (GO:0005576)	3169	255	194.18	+	1.31	9.58E-03

Table 3.3: List of Biological Process GO Term in Proteins with Decreased Levels in *fer*

GO biological process complete	AT ref (27581)	fer_UP (1690)	expected	over/under	fold Enrichment	P-value
energy reserve metabolic process (GO:0006112)	13	11	0.96	+	11.47	4.59E-04
glycogen metabolic process (GO:0005977)	13	11	0.96	+	11.47	4.59E-04
chloroplast rRNA processing (GO:1901259)	16	13	1.18	+	11.02	4.73E-05
reductive pentose-phosphate cycle (GO:0019253)	13	10	0.96	+	10.43	3.10E-03
photosystem II repair (GO:0010206)	15	11	1.11	+	9.94	1.25E-03
photosynthesis, dark reaction (GO:0019685)	14	10	1.03	+	9.69	4.98E-03
chlorophyll biosynthetic process (GO:0015995)	37	26	2.73	+	9.53	3.94E-11
carbon fixation (GO:0015977)	20	14	1.47	+	9.49	5.08E-05
starch catabolic process (GO:0005983)	17	11	1.25	+	8.77	3.05E-03
plastid translation (GO:0032544)	14	9	1.03	+	8.72	3.06E-02
gluconeogenesis (GO:0006094)	22	14	1.62	+	8.63	1.21E-04
tetrapyrrole biosynthetic process (GO:0033014)	50	31	3.69	+	8.41	1.50E-12
protein repair (GO:0030091)	21	13	1.55	+	8.39	4.68E-04
hexose biosynthetic process (GO:0019319)	26	16	1.92	+	8.34	1.88E-05
photosystem II assembly (GO:0010207)	22	13	1.62	+	8.01	6.97E-04
porphyrin-containing compound biosynthetic process (GO:0006779)	46	27	3.39	+	7.96	3.03E-10
monosaccharide catabolic process (GO:0046365)	24	14	1.77	+	7.91	2.71E-04
glucose metabolic process (GO:0006006)	45	26	3.32	+	7.83	1.13E-09
chlorophyll metabolic process (GO:0015994)	56	32	4.13	+	7.75	2.89E-12
photosynthetic electron transport chain (GO:0009767)	39	21	2.88	+	7.3	5.42E-07
glyceraldehyde-3-phosphate metabolic process (GO:0019682)	36	19	2.65	+	7.16	5.08E-06
branched-chain amino acid biosynthetic process (GO:0009082)	21	11	1.55	+	7.1	1.42E-02
protein import into chloroplast stroma (GO:0045037)	23	12	1.7	+	7.07	5.46E-03
tetrapyrrole metabolic process (GO:0033013)	71	37	5.24	+	7.07	1.67E-13
monosaccharide biosynthetic process (GO:0046364)	43	22	3.17	+	6.94	4.27E-07
porphyrin-containing compound metabolic process (GO:0006778)	69	35	5.09	+	6.88	2.16E-12
photosynthesis, light reaction (GO:0019684)	127	62	9.37	+	6.62	8.29E-23
thylakoid membrane organization (GO:0010027)	48	23	3.54	+	6.5	4.51E-07
carotenoid biosynthetic process (GO:0016117)	23	11	1.7	+	6.49	2.77E-02
tetraterpenoid biosynthetic process (GO:0016109)	23	11	1.7	+	6.49	2.77E-02
photosynthesis (GO:0015979)	189	89	13.94	+	6.39	9.70E-33
glucan catabolic process (GO:0009251)	30	14	2.21	+	6.33	2.18E-03
galactose metabolic process (GO:0006012)	28	13	2.06	+	6.3	5.64E-03
starch metabolic process (GO:0005982)	54	25	3.98	+	6.28	1.30E-07
protein refolding (GO:0042026)	50	23	3.69	+	6.24	8.46E-07
heme metabolic process (GO:0042168)	24	11	1.77	+	6.21	3.79E-02
hexose metabolic process (GO:0019318)	86	39	6.34	+	6.15	9.21E-13
ADP metabolic process (GO:0046031)	60	27	4.42	+	6.1	3.68E-08
purine nucleoside diphosphate metabolic process (GO:0009135)	60	27	4.42	+	6.1	3.68E-08
purine ribonucleoside diphosphate metabolic process (GO:0009179)	60	27	4.42	+	6.1	3.68E-08
glucose 6-phosphate metabolic process (GO:0051156)	29	13	2.14	+	6.08	7.65E-03
pentose-phosphate shunt (GO:0006098)	27	12	1.99	+	6.03	1.98E-02
nucleoside diphosphate phosphorylation (GO:0006165)	59	26	4.35	+	5.98	1.26E-07
pyruvate biosynthetic process (GO:0042866)	59	26	4.35	+	5.98	1.26E-07
pyruvate metabolic process (GO:0006090)	75	33	5.53	+	5.97	3.34E-10
amino acid activation (GO:0043038)	55	24	4.06	+	5.92	8.16E-07
tRNA aminoacylation (GO:0043039)	55	24	4.06	+	5.92	8.16E-07
tRNA aminoacylation for protein translation (GO:0006418)	55	24	4.06	+	5.92	8.16E-07
ribonucleoside diphosphate metabolic process (GO:0009185)	62	27	4.57	+	5.91	6.67E-08
establishment of protein localization to chloroplast (GO:0072596)	46	20	3.39	+	5.9	2.56E-05
protein targeting to chloroplast (GO:0045036)	46	20	3.39	+	5.9	2.56E-05
cellular polysaccharide catabolic process (GO:0044247)	30	13	2.21	+	5.88	1.03E-02
ATP generation from ADP (GO:0006757)	58	25	4.28	+	5.84	4.30E-07
glycolytic process (GO:0006096)	58	25	4.28	+	5.84	4.30E-07
cellular aldehyde metabolic process (GO:0006081)	73	31	5.38	+	5.76	3.83E-09
nucleoside diphosphate metabolic process (GO:0009132)	66	28	4.87	+	5.75	4.68E-08
monosaccharide metabolic process (GO:0005996)	116	49	8.55	+	5.73	1.56E-15
carotenoid metabolic process (GO:0016116)	31	13	2.29	+	5.69	1.37E-02
tetraterpenoid metabolic process (GO:0016108)	31	13	2.29	+	5.69	1.37E-02

Table 3.3. (continued)

plastid membrane organization (GO:0009668)	55	23	4.06	+	5.67	3.67E-06
protein localization to chloroplast (GO:0072598)	48	20	3.54	+	5.65	4.52E-05
nucleotide phosphorylation (GO:0046939)	63	26	4.65	+	5.6	3.96E-07
photosynthesis, light harvesting (GO:0009765)	46	19	3.39	+	5.6	1.15E-04
nucleoside phosphate catabolic process (GO:1901292)	66	27	4.87	+	5.55	2.06E-07
pyridine-containing compound biosynthetic process (GO:0072525)	79	32	5.83	+	5.49	4.61E-09
neurotransmitter metabolic process (GO:0042133)	30	12	2.21	+	5.42	4.61E-02
nucleotide catabolic process (GO:0009166)	65	26	4.79	+	5.42	6.81E-07
regulation of generation of precursor metabolites and energy (GO:0043467)	30	12	2.21	+	5.42	4.61E-02
translational elongation (GO:0006414)	48	19	3.54	+	5.37	1.97E-04
nicotinamide nucleotide biosynthetic process (GO:0019359)	69	27	5.09	+	5.31	4.60E-07
pyridine-containing compound metabolic process (GO:0072524)	116	45	8.55	+	5.26	5.46E-13
nicotinamide nucleotide metabolic process (GO:0046496)	104	40	7.67	+	5.22	3.17E-11
ribosomal large subunit assembly (GO:0000027)	42	16	3.1	+	5.17	3.15E-03
water-soluble vitamin metabolic process (GO:0006767)	63	24	4.65	+	5.17	7.21E-06
pyridine nucleotide biosynthetic process (GO:0019363)	71	27	5.24	+	5.16	7.69E-07
water-soluble vitamin biosynthetic process (GO:0042364)	50	19	3.69	+	5.15	3.30E-04
NADP metabolic process (GO:0006739)	37	14	2.73	+	5.13	1.56E-02
pyridine nucleotide metabolic process (GO:0019362)	106	40	7.82	+	5.12	5.26E-11
aspartate family amino acid biosynthetic process (GO:0009067)	48	18	3.54	+	5.08	8.28E-04
pigment biosynthetic process (GO:0046148)	107	40	7.89	+	5.07	6.75E-11
nucleobase-containing small molecule biosynthetic process (GO:0034404)	86	32	6.34	+	5.05	2.82E-08
cofactor biosynthetic process (GO:0051188)	252	92	18.58	+	4.95	4.28E-27
purine nucleoside triphosphate biosynthetic process (GO:0009145)	99	36	7.3	+	4.93	2.54E-09
oxidoreduction coenzyme metabolic process (GO:0006733)	124	45	9.14	+	4.92	4.02E-12
aspartate family amino acid metabolic process (GO:0009066)	64	23	4.72	+	4.87	3.75E-05
generation of precursor metabolites and energy (GO:0006091)	330	118	24.34	+	4.85	1.01E-34
purine ribonucleoside triphosphate biosynthetic process (GO:0009206)	98	35	7.23	+	4.84	7.95E-09
nucleoside triphosphate biosynthetic process (GO:0009142)	108	38	7.96	+	4.77	1.37E-09
purine nucleotide biosynthetic process (GO:0006164)	145	51	10.69	+	4.77	1.52E-13
'de novo' protein folding (GO:0006458)	57	20	4.2	+	4.76	4.46E-04
ATP biosynthetic process (GO:0006754)	95	33	7.01	+	4.71	6.04E-08
response to cytokinin (GO:0009735)	231	80	17.04	+	4.7	4.66E-22
ribosome assembly (GO:0042255)	84	29	6.19	+	4.68	1.09E-06
dicarboxylic acid metabolic process (GO:0043648)	91	31	6.71	+	4.62	3.60E-07
ribonucleoside triphosphate biosynthetic process (GO:0009201)	103	35	7.6	+	4.61	2.51E-08
purine ribonucleotide biosynthetic process (GO:0009152)	136	46	10.03	+	4.59	1.66E-11
pigment metabolic process (GO:0042440)	128	43	9.44	+	4.56	1.52E-10
purine-containing compound biosynthetic process (GO:0072522)	158	53	11.65	+	4.55	1.95E-13
plastid organization (GO:0009657)	285	95	21.02	+	4.52	1.44E-25
ribonucleotide biosynthetic process (GO:0009260)	153	51	11.28	+	4.52	9.21E-13
vitamin metabolic process (GO:0006766)	81	27	5.97	+	4.52	8.09E-06
ribose phosphate biosynthetic process (GO:0046390)	158	52	11.65	+	4.46	7.30E-13
chaperone-mediated protein folding (GO:0061077)	61	20	4.5	+	4.45	1.09E-03
alpha-amino acid biosynthetic process (GO:1901607)	180	59	13.27	+	4.44	8.51E-15
cellular amino acid biosynthetic process (GO:0008652)	202	66	14.9	+	4.43	9.84E-17
vitamin biosynthetic process (GO:0009110)	68	22	5.01	+	4.39	3.53E-04
glutamine family amino acid metabolic process (GO:0009064)	62	20	4.57	+	4.37	1.35E-03
nucleoside phosphate biosynthetic process (GO:1901293)	202	65	14.9	+	4.36	3.63E-16
organophosphate catabolic process (GO:0046434)	94	30	6.93	+	4.33	2.57E-06
chloroplast organization (GO:0009658)	217	69	16	+	4.31	4.69E-17
nucleotide biosynthetic process (GO:0009165)	200	63	14.75	+	4.27	3.16E-15
response to cadmium ion (GO:0046686)	345	108	25.44	+	4.24	1.88E-27
serine family amino acid biosynthetic process (GO:0009070)	48	15	3.54	+	4.24	4.83E-02
serine family amino acid metabolic process (GO:0009069)	61	19	4.5	+	4.22	4.00E-03
coenzyme biosynthetic process (GO:0009108)	193	59	14.23	+	4.15	1.24E-13
coenzyme metabolic process (GO:0006732)	278	83	20.5	+	4.05	1.82E-19
cellular amino acid metabolic process (GO:0006520)	377	111	27.8	+	3.99	2.32E-26
carbohydrate catabolic process (GO:0016052)	182	53	13.42	+	3.95	2.54E-11
translation (GO:0006412)	554	161	40.86	+	3.94	7.26E-39

Table 3.3. (continued)

peptide biosynthetic process (GO:0043043)	559	162	41.22	+	3.93	5.34E-39
cofactor metabolic process (GO:0051186)	499	144	36.8	+	3.91	3.68E-34
amide biosynthetic process (GO:0043604)	617	172	45.5	+	3.78	9.83E-40
small molecule biosynthetic process (GO:0044283)	670	187	49.41	+	3.78	1.45E-43
alpha-amino acid metabolic process (GO:1901605)	271	75	19.99	+	3.75	8.38E-16
carboxylic acid biosynthetic process (GO:0046394)	521	141	38.42	+	3.67	7.23E-31
organic acid biosynthetic process (GO:0016053)	521	141	38.42	+	3.67	7.23E-31
sulfur compound biosynthetic process (GO:0044272)	142	38	10.47	+	3.63	1.15E-06
peptide metabolic process (GO:0006518)	635	169	46.83	+	3.61	8.34E-37
protein import (GO:0017038)	125	33	9.22	+	3.58	2.10E-05
fatty acid biosynthetic process (GO:0006633)	129	34	9.51	+	3.57	1.30E-05
nucleoside triphosphate metabolic process (GO:0009141)	160	42	11.8	+	3.56	2.34E-07
organophosphate biosynthetic process (GO:0090407)	339	89	25	+	3.56	7.34E-18
tRNA metabolic process (GO:0006399)	160	42	11.8	+	3.56	2.34E-07
purine nucleoside triphosphate metabolic process (GO:0009144)	149	39	10.99	+	3.55	1.17E-06
ribosomal large subunit biogenesis (GO:0042273)	92	24	6.78	+	3.54	2.66E-03
ribose phosphate metabolic process (GO:0019693)	264	68	19.47	+	3.49	8.44E-13
purine nucleotide metabolic process (GO:0006163)	226	58	16.67	+	3.48	1.46E-10
carboxylic acid metabolic process (GO:0019752)	882	226	65.04	+	3.47	4.08E-48
cellular glucan metabolic process (GO:0006073)	160	41	11.8	+	3.47	7.25E-07
organonitrogen compound biosynthetic process (GO:1901566)	1384	353	102.07	+	3.46	3.38E-78
purine ribonucleoside triphosphate metabolic process (GO:0009205)	145	37	10.69	+	3.46	5.84E-06
cellular amide metabolic process (GO:0043603)	757	192	55.83	+	3.44	9.81E-40
response to metal ion (GO:0010038)	478	121	35.25	+	3.43	6.62E-24
nucleotide metabolic process (GO:0009117)	337	85	24.85	+	3.42	4.89E-16
ATP metabolic process (GO:0046034)	140	35	10.32	+	3.39	2.45E-05
glucan metabolic process (GO:0044042)	168	42	12.39	+	3.39	8.39E-07
nucleoside phosphate metabolic process (GO:0006753)	340	85	25.07	+	3.39	7.80E-16
cellular nitrogen compound biosynthetic process (GO:0044271)	1272	316	93.81	+	3.37	8.07E-67
electron transport chain (GO:0022900)	101	25	7.45	+	3.36	3.62E-03
ribonucleotide metabolic process (GO:0009259)	234	58	17.26	+	3.36	5.09E-10
monocarboxylic acid biosynthetic process (GO:0072330)	267	66	19.69	+	3.35	1.24E-11
purine ribonucleotide metabolic process (GO:0009150)	215	53	15.86	+	3.34	6.61E-09
ribonucleoside triphosphate metabolic process (GO:0009199)	150	37	11.06	+	3.34	1.27E-05
cellular response to oxidative stress (GO:0034599)	86	21	6.34	+	3.31	2.95E-02
intracellular protein transmembrane transport (GO:0065002)	82	20	6.05	+	3.31	4.81E-02
nuclear transport (GO:0051169)	116	28	8.55	+	3.27	1.33E-03
nucleocytoplasmic transport (GO:0006913)	116	28	8.55	+	3.27	1.33E-03
nucleobase-containing small molecule metabolic process (GO:0055086)	450	106	33.19	+	3.19	1.32E-18
oxoacid metabolic process (GO:0043436)	1030	242	75.96	+	3.19	4.09E-46
organic acid metabolic process (GO:0006082)	1032	242	76.11	+	3.18	5.48E-46
ribosome biogenesis (GO:0042254)	381	89	28.1	+	3.17	4.52E-15
cell redox homeostasis (GO:0045454)	99	23	7.3	+	3.15	2.31E-02
purine-containing compound metabolic process (GO:0072521)	259	60	19.1	+	3.14	2.33E-09
ribonucleoprotein complex assembly (GO:0022618)	170	39	12.54	+	3.11	2.76E-05
ribonucleoprotein complex subunit organization (GO:0071826)	179	41	13.2	+	3.11	1.22E-05
energy derivation by oxidation of organic compounds (GO:0015980)	136	31	10.03	+	3.09	9.76E-04
monocarboxylic acid metabolic process (GO:0032787)	430	98	31.71	+	3.09	3.52E-16
microtubule cytoskeleton organization (GO:0000226)	125	28	9.22	+	3.04	4.73E-03
heterocycle biosynthetic process (GO:0018130)	716	160	52.8	+	3.03	3.83E-27
ncRNA metabolic process (GO:0034660)	401	89	29.57	+	3.01	6.99E-14
small molecule metabolic process (GO:0044281)	1587	351	117.04	+	3	6.53E-64
rRNA processing (GO:0006364)	214	47	15.78	+	2.98	3.02E-06
protein folding (GO:0006457)	266	58	19.62	+	2.96	4.55E-08
fatty acid metabolic process (GO:0006631)	212	46	15.63	+	2.94	6.29E-06
drug metabolic process (GO:0017144)	543	116	40.04	+	2.9	1.94E-17
establishment of protein localization to organelle (GO:0072594)	258	55	19.03	+	2.89	3.14E-07
ribonucleoprotein complex biogenesis (GO:0022613)	463	98	34.14	+	2.87	3.45E-14
rRNA metabolic process (GO:0016072)	227	48	16.74	+	2.87	5.89E-06
cellular polysaccharide metabolic process (GO:0044264)	238	50	17.55	+	2.85	3.32E-06

Table 3.3. (continued)

organelle assembly (GO:0070925)	171	36	12.61	+	2.85	6.31E-04
cellular protein-containing complex assembly (GO:0034622)	434	90	32.01	+	2.81	1.81E-12
organophosphate metabolic process (GO:0019637)	555	115	40.93	+	2.81	1.49E-16
cellular carbohydrate metabolic process (GO:0044262)	344	71	25.37	+	2.8	2.77E-09
aromatic compound biosynthetic process (GO:0019438)	816	168	60.18	+	2.79	4.53E-25
carbohydrate derivative biosynthetic process (GO:1901137)	413	85	30.46	+	2.79	1.66E-11
cellular biosynthetic process (GO:0044249)	2576	518	189.97	+	2.73	2.45E-86
ncRNA processing (GO:0034470)	323	65	23.82	+	2.73	5.96E-08
membrane organization (GO:0061024)	228	45	16.81	+	2.68	1.19E-04
nucleobase-containing compound biosynthetic process (GO:0034654)	506	100	37.32	+	2.68	9.78E-13
organic cyclic compound biosynthetic process (GO:1901362)	930	184	68.58	+	2.68	6.55E-26
organic substance biosynthetic process (GO:1901576)	2706	530	199.56	+	2.66	5.08E-85
carbohydrate biosynthetic process (GO:0016051)	317	62	23.38	+	2.65	5.81E-07
protein-containing complex assembly (GO:0065003)	486	94	35.84	+	2.62	1.80E-11
protein-containing complex subunit organization (GO:0043933)	570	110	42.04	+	2.62	1.20E-13
biosynthetic process (GO:0009058)	2823	544	208.19	+	2.61	2.40E-85
response to cold (GO:0009409)	428	80	31.56	+	2.53	1.17E-08
protein localization to organelle (GO:0033365)	302	55	22.27	+	2.47	5.03E-05
protein targeting (GO:0006605)	225	41	16.59	+	2.47	3.00E-03
response to temperature stimulus (GO:0009266)	622	113	45.87	+	2.46	1.48E-12
cellular carbohydrate biosynthetic process (GO:0034637)	205	37	15.12	+	2.45	1.24E-02
cytoskeleton organization (GO:0007010)	224	40	16.52	+	2.42	9.31E-03
polysaccharide metabolic process (GO:0005976)	302	54	22.27	+	2.42	1.06E-04
response to inorganic substance (GO:0010035)	945	167	69.69	+	2.4	1.25E-18
carbohydrate derivative metabolic process (GO:1901135)	716	126	52.8	+	2.39	3.12E-13
oxidation-reduction process (GO:0055114)	937	165	69.1	+	2.39	3.01E-18
gene expression (GO:0010467)	1525	268	112.46	+	2.38	1.32E-31
macromolecule biosynthetic process (GO:0009059)	1266	222	93.36	+	2.38	3.11E-25
carbohydrate metabolic process (GO:0005975)	810	140	59.73	+	2.34	2.04E-14
cellular component assembly (GO:0022607)	706	122	52.06	+	2.34	3.75E-12
cellular macromolecule biosynthetic process (GO:0034645)	1218	210	89.82	+	2.34	5.34E-23
response to heat (GO:0009408)	220	38	16.22	+	2.34	2.51E-02
small molecule catabolic process (GO:0044282)	214	37	15.78	+	2.34	3.38E-02
cellular component biogenesis (GO:0044085)	1176	201	86.73	+	2.32	2.57E-21
heterocycle catabolic process (GO:0046700)	235	40	17.33	+	2.31	1.74E-02
cellular nitrogen compound catabolic process (GO:0044270)	238	40	17.55	+	2.28	3.11E-02
intracellular protein transport (GO:0006886)	560	91	41.3	+	2.2	2.74E-07
lipid biosynthetic process (GO:0008610)	501	81	36.95	+	2.19	3.55E-06
sulfur compound metabolic process (GO:0006790)	378	61	27.88	+	2.19	4.58E-04
intracellular transport (GO:0046907)	683	110	50.37	+	2.18	5.55E-09
cellular nitrogen compound metabolic process (GO:0034641)	2986	473	220.21	+	2.15	3.51E-49
establishment of localization in cell (GO:0051649)	737	116	54.35	+	2.13	4.62E-09
organelle organization (GO:0006996)	1602	250	118.14	+	2.12	2.98E-22
protein transport (GO:0015031)	699	108	51.55	+	2.1	7.12E-08
embryo development ending in seed dormancy (GO:0009793)	559	86	41.22	+	2.09	9.20E-06
establishment of protein localization (GO:0045184)	707	109	52.14	+	2.09	5.88E-08
defense response to bacterium (GO:0042742)	393	60	28.98	+	2.07	3.33E-03
response to salt stress (GO:0009651)	590	90	43.51	+	2.07	5.67E-06
embryo development (GO:0009790)	575	87	42.4	+	2.05	1.50E-05
response to bacterium (GO:0009617)	493	74	36.36	+	2.04	3.60E-04
cellular macromolecule localization (GO:0070727)	678	101	50	+	2.02	1.75E-06
cellular protein localization (GO:0034613)	646	96	47.64	+	2.02	6.67E-06
cellular component organization (GO:0016043)	2490	369	183.63	+	2.01	4.82E-31
cellular component organization or biogenesis (GO:0071840)	2845	421	209.81	+	2.01	2.84E-36
protein localization (GO:0008104)	780	114	57.52	+	1.98	4.35E-07
response to light stimulus (GO:0009416)	739	108	54.5	+	1.98	1.38E-06
cellular lipid metabolic process (GO:0044255)	675	97	49.78	+	1.95	2.21E-05
response to abiotic stimulus (GO:0009628)	2098	302	154.72	+	1.95	1.54E-22
cellular localization (GO:0051641)	901	129	66.45	+	1.94	7.53E-08
heterocycle metabolic process (GO:0046483)	2465	352	181.78	+	1.94	1.95E-26

Table 3.3. (continued)

peptide transport (GO:0015833)	768	110	56.64	+	1.94	2.82E-06
response to osmotic stress (GO:0006970)	665	95	49.04	+	1.94	4.10E-05
response to radiation (GO:0009314)	760	109	56.05	+	1.94	2.49E-06
amide transport (GO:0042886)	785	112	57.89	+	1.93	1.92E-06
seed development (GO:0048316)	725	102	53.47	+	1.91	2.14E-05
organonitrogen compound metabolic process (GO:1901564)	4315	603	318.22	+	1.89	9.60E-49
cellular aromatic compound metabolic process (GO:0006725)	2612	362	192.63	+	1.88	3.34E-25
organic cyclic compound metabolic process (GO:1901360)	2724	376	200.89	+	1.87	4.49E-26
fruit development (GO:0010154)	756	103	55.75	+	1.85	8.74E-05
cellular metabolic process (GO:0044237)	7157	964	527.8	+	1.83	9.68E-85
RNA processing (GO:0006396)	733	99	54.06	+	1.83	2.58E-04
response to chemical (GO:0042221)	2777	368	204.79	+	1.8	2.14E-22
metabolic process (GO:0008152)	8211	1076	605.53	+	1.78	1.95E-93
macromolecule localization (GO:0033036)	1037	134	76.48	+	1.75	1.54E-05
nucleobase-containing compound metabolic process (GO:0006139)	2156	279	159	+	1.75	1.40E-14
lipid metabolic process (GO:0006629)	831	105	61.28	+	1.71	1.90E-03
organic substance metabolic process (GO:0071704)	7417	938	546.98	+	1.71	2.35E-67
response to endogenous stimulus (GO:0009719)	1615	202	119.1	+	1.7	1.52E-08
nitrogen compound metabolic process (GO:0006807)	5875	730	433.26	+	1.68	4.67E-44
primary metabolic process (GO:0044238)	6707	832	494.62	+	1.68	8.60E-53
response to hormone (GO:0009725)	1599	198	117.92	+	1.68	6.21E-08
cellular process (GO:0009987)	10295	1258	759.22	+	1.66	2.07E-99
nitrogen compound transport (GO:0071705)	970	117	71.53	+	1.64	3.34E-03
response to organic substance (GO:0010033)	1916	229	141.3	+	1.62	3.30E-08
response to external stimulus (GO:0009605)	1388	165	102.36	+	1.61	4.47E-05
response to biotic stimulus (GO:0009607)	989	116	72.94	+	1.59	1.33E-02
response to external biotic stimulus (GO:0043207)	988	116	72.86	+	1.59	1.31E-02
response to other organism (GO:0051707)	988	116	72.86	+	1.59	1.31E-02
catabolic process (GO:0009056)	1486	173	109.59	+	1.58	8.96E-05
organic substance catabolic process (GO:1901575)	1317	153	97.12	+	1.58	6.78E-04
cellular catabolic process (GO:0044248)	1308	151	96.46	+	1.57	1.09E-03
RNA metabolic process (GO:0016070)	1286	148	94.84	+	1.56	1.57E-03
phosphorus metabolic process (GO:0006793)	1735	198	127.95	+	1.55	3.21E-05
response to stress (GO:0006950)	3158	360	232.89	+	1.55	4.71E-12
cellular protein metabolic process (GO:0044267)	2874	327	211.95	+	1.54	1.61E-10
response to stimulus (GO:0050896)	5731	651	422.64	+	1.54	1.73E-26
protein metabolic process (GO:0019538)	3199	361	235.91	+	1.53	1.57E-11
organic substance transport (GO:0071702)	1210	134	89.23	+	1.5	3.31E-02
cellular macromolecule metabolic process (GO:0044260)	3861	424	284.73	+	1.49	1.90E-12
phosphate-containing compound metabolic process (GO:0006796)	1695	185	125	+	1.48	1.48E-03
response to oxygen-containing compound (GO:1901700)	1596	172	117.7	+	1.46	8.20E-03
macromolecule metabolic process (GO:0043170)	5021	534	370.28	+	1.44	1.72E-14

Table 3.4: List of Cellular Process GO Term in Proteins with Decreased Levels in *fer*

GO cellular component complete	AT ref (27581)	fer_UP (1690)	expected	over/under	fold Enrichment	P-value
tubulin complex (GO:0045298)	12	11	0.88	+	12.43	6.36E-05
endopeptidase Clp complex (GO:0009368)	10	9	0.74	+	12.2	1.07E-03
chloroplastic endopeptidase Clp complex (GO:0009840)	8	7	0.59	+	11.86	1.83E-02
stromule (GO:0010319)	35	28	2.58	+	10.85	8.73E-14
plastid small ribosomal subunit (GO:0000312)	13	9	0.96	+	9.39	4.77E-03
cytoplasmic chromosome (GO:0000229)	18	12	1.33	+	9.04	1.87E-04
NAD(P)H dehydrogenase complex (plastoquinone) (GO:0010598)	12	8	0.88	+	9.04	1.90E-02
plastid chromosome (GO:0009508)	18	12	1.33	+	9.04	1.87E-04
photosystem II oxygen evolving complex (GO:0009654)	22	13	1.62	+	8.01	1.67E-04
plastid ribosome (GO:0009547)	28	16	2.06	+	7.75	9.90E-06
chloroplast stroma (GO:0009570)	769	428	56.71	+	7.55	3.14E-197
thylakoid lumen (GO:0031977)	97	54	7.15	+	7.55	2.75E-22
plastid stroma (GO:0009532)	779	430	57.45	+	7.48	3.62E-197
chloroplast photosystem II (GO:0030095)	19	10	1.4	+	7.14	8.88E-03
chloroplast thylakoid lumen (GO:0009543)	82	42	6.05	+	6.95	5.24E-16
plastid thylakoid lumen (GO:0031978)	82	42	6.05	+	6.95	5.24E-16
plastid nucleoid (GO:0042646)	53	26	3.91	+	6.65	4.67E-09
chloroplast nucleoid (GO:0042644)	47	23	3.47	+	6.64	7.81E-08
thylakoid (GO:0009579)	595	283	43.88	+	6.45	2.67E-113
plastoglobule (GO:0010287)	79	37	5.83	+	6.35	5.66E-13
chloroplast thylakoid (GO:0009534)	519	241	38.27	+	6.3	7.88E-94
plastid thylakoid (GO:0031976)	520	241	38.35	+	6.28	1.08E-93
thylakoid membrane (GO:0042651)	428	198	31.56	+	6.27	4.79E-76
photosynthetic membrane (GO:0034357)	429	198	31.64	+	6.26	6.56E-76
chloroplast thylakoid membrane (GO:0009535)	408	188	30.09	+	6.25	8.56E-72
plastid thylakoid membrane (GO:0055035)	409	188	30.16	+	6.23	1.17E-71
thylakoid part (GO:0044436)	471	213	34.73	+	6.13	1.08E-80
chloroplast part (GO:0044434)	1452	641	107.08	+	5.99	2.52E-263
chloroplast thylakoid membrane protein complex (GO:0098807)	34	15	2.51	+	5.98	3.73E-04
nucleoid (GO:0009295)	59	26	4.35	+	5.98	3.03E-08
plastid part (GO:0044435)	1469	644	108.33	+	5.94	2.32E-263
proton-transporting two-sector ATPase complex, catalytic domain (GO:0033178)	23	10	1.7	+	5.9	3.19E-02
plastid envelope (GO:0009526)	700	303	51.62	+	5.87	2.44E-113
chloroplast envelope (GO:0009941)	681	293	50.22	+	5.83	8.21E-109
chloroplast inner membrane (GO:0009706)	83	33	6.12	+	5.39	7.52E-10
plastid inner membrane (GO:0009528)	86	34	6.34	+	5.36	3.91E-10
photosystem (GO:0009521)	90	31	6.64	+	4.67	6.89E-08
organelle subcompartment (GO:0031984)	896	290	66.08	+	4.39	3.13E-83
photosystem II (GO:0009523)	65	21	4.79	+	4.38	1.65E-04
small ribosomal subunit (GO:0015935)	129	39	9.51	+	4.1	7.80E-09
envelope (GO:0031975)	1189	358	87.68	+	4.08	4.44E-97
organelle envelope (GO:0031967)	1189	358	87.68	+	4.08	4.44E-97
cytosolic small ribosomal subunit (GO:0022627)	104	31	7.67	+	4.04	1.29E-06
cytosolic ribosome (GO:0022626)	309	91	22.79	+	3.99	8.00E-22
cytosolic part (GO:0044445)	351	102	25.88	+	3.94	2.81E-24
apoplast (GO:0048046)	488	135	35.99	+	3.75	7.04E-31
ribosome (GO:0005840)	466	127	34.37	+	3.7	2.10E-28
chloroplast membrane (GO:0031969)	255	69	18.81	+	3.67	1.45E-14
plastid membrane (GO:0042170)	262	70	19.32	+	3.62	1.49E-14
ribosomal subunit (GO:0044391)	319	85	23.53	+	3.61	6.32E-18
organellar ribosome (GO:0000313)	69	18	5.09	+	3.54	1.40E-02
cytosolic large ribosomal subunit (GO:0022625)	137	34	10.1	+	3.37	1.11E-05
oxidoreductase complex (GO:1990204)	150	37	11.06	+	3.34	3.05E-06
large ribosomal subunit (GO:0015934)	190	46	14.01	+	3.28	7.26E-08
mitochondrial matrix (GO:0005759)	161	36	11.87	+	3.03	4.20E-05
cytosol (GO:0005829)	2290	473	168.88	+	2.8	1.09E-81
chloroplast (GO:0009507)	5248	1049	387.02	+	2.71	1.36E-213
plastid (GO:0009536)	5292	1052	390.27	+	2.7	9.76E-213
ribonucleoprotein complex (GO:1990904)	910	175	67.11	+	2.61	8.28E-24

Table 3.4. (continued)

intracellular organelle part (GO:0044446)	5375	1006	396.39	+	2.54	1.59E-181
organelle part (GO:0044422)	5381	1007	396.83	+	2.54	9.37E-182
cell wall (GO:0005618)	756	137	55.75	+	2.46	3.53E-16
external encapsulating structure (GO:0030312)	758	137	55.9	+	2.45	4.01E-16
organelle inner membrane (GO:0019866)	393	70	28.98	+	2.42	4.33E-07
membrane protein complex (GO:0098796)	666	116	49.12	+	2.36	2.69E-12
polymeric cytoskeletal fiber (GO:0099513)	205	35	15.12	+	2.32	1.73E-02
supramolecular complex (GO:0099080)	205	35	15.12	+	2.32	1.73E-02
supramolecular fiber (GO:0099512)	205	35	15.12	+	2.32	1.73E-02
supramolecular polymer (GO:0099081)	205	35	15.12	+	2.32	1.73E-02
cell junction (GO:0030054)	953	161	70.28	+	2.29	8.52E-17
cell-cell junction (GO:0005911)	953	161	70.28	+	2.29	8.52E-17
plasmodesma (GO:0009506)	953	161	70.28	+	2.29	8.52E-17
symplast (GO:0055044)	953	161	70.28	+	2.29	8.52E-17
plant-type cell wall (GO:0009505)	373	59	27.51	+	2.14	2.78E-04
intracellular non-membrane-bounded organelle (GO:0043232)	1672	262	123.3	+	2.12	2.45E-24
non-membrane-bounded organelle (GO:0043228)	1672	262	123.3	+	2.12	2.45E-24
mitochondrial part (GO:0044429)	542	82	39.97	+	2.05	9.39E-06
cytoskeletal part (GO:0044430)	302	45	22.27	+	2.02	2.58E-02
vacuole (GO:0005773)	1091	161	80.46	+	2	5.71E-12
protein-containing complex (GO:0032991)	3159	461	232.96	+	1.98	1.35E-39
vacuolar membrane (GO:0005774)	624	91	46.02	+	1.98	8.46E-06
trans-Golgi network (GO:0005802)	317	46	23.38	+	1.97	3.87E-02
vacuolar part (GO:0044437)	627	91	46.24	+	1.97	9.49E-06
cytoskeleton (GO:0005856)	381	55	28.1	+	1.96	8.97E-03
whole membrane (GO:0098805)	964	139	71.09	+	1.96	1.76E-09
endosome (GO:0005768)	431	59	31.78	+	1.86	1.85E-02
organelle membrane (GO:0031090)	1811	245	133.55	+	1.83	3.97E-15
cytoplasmic part (GO:0044444)	12257	1584	903.91	+	1.75	1.27E-191
cytoplasmic vesicle (GO:0031410)	598	77	44.1	+	1.75	8.97E-03
intracellular vesicle (GO:0097708)	599	77	44.17	+	1.74	9.13E-03
bounding membrane of organelle (GO:0098588)	1266	155	93.36	+	1.66	6.32E-06
cytoplasm (GO:0005737)	14521	1686	1070.87	+	1.57	1.65E-166
catalytic complex (GO:1902494)	1110	128	81.86	+	1.56	2.55E-03
Golgi apparatus (GO:0005794)	1199	131	88.42	+	1.48	1.94E-02
intracellular organelle lumen (GO:0070013)	1245	136	91.81	+	1.48	1.31E-02
membrane-enclosed lumen (GO:0031974)	1245	136	91.81	+	1.48	1.31E-02
organelle lumen (GO:0043233)	1245	136	91.81	+	1.48	1.31E-02
membrane (GO:0016020)	7769	820	572.94	+	1.43	8.28E-27
cell periphery (GO:0071944)	4199	434	309.66	+	1.4	1.23E-09

Table 3.5: List of Genes that are UP or DN in *fer* from the GO Term Defense Response to Bacterium (GO:0042742)

UP in fer	UP in fer	DN-in fer	DN-in fer
AT1G02920	AT5G06320	AT1G06680	AT4G11150
AT1G02930	AT5G24530	AT1G09340	AT4G15900
AT1G08450	AT5G28040	AT1G20020	AT4G20260
AT1G09770	AT5G36890	AT1G26630	AT4G23100
AT1G19670	AT5G42000	AT1G32060	AT4G24670
AT1G24100	AT5G44030	AT1G52740	AT4G26850
AT1G31280	AT5G46050	AT1G53240	AT4G30440
AT1G51890	AT5G46180	AT1G64550	AT4G32260
AT1G55020	AT5G48380	AT1G65930	AT4G33220
AT1G59870	AT5G48810	AT1G80600	AT4G35230
AT1G69370	AT5G53120	AT2G27040	AT4G36690
AT1G80460	AT5G56360	AT2G33340	AT5G06290
AT2G22240	AT5G58430	AT2G34690	AT5G08280
AT2G22300	AT5G59890	AT2G37660	AT5G11270
AT2G22330	AT5G67330	AT2G37710	AT5G14740
AT2G23810		AT2G39730	AT5G15090
AT2G30860		AT2G39770	AT5G18525
AT2G32680		AT2G39940	AT5G24400
AT2G43790		AT2G41560	AT5G66190
AT2G45220		AT2G43710	AT5G66570
AT2G47130		AT2G44490	AT5G67385
AT3G21630		AT3G01480	ATCG00120
AT3G25070		AT3G01500	
AT3G43300		AT3G04790	
AT3G44880		AT3G11630	
AT3G48090		AT3G14150	
AT3G49120		AT3G14210	
AT3G52430		AT3G14420	
AT3G54640		AT3G15020	
AT3G57330		AT3G16640	
AT4G00990		AT3G27890	
AT4G02520		AT3G52960	
AT4G08900		AT3G55800	
AT4G11850		AT3G62030	
AT4G12720		AT3G63190	
AT4G23250		AT4G01050	
AT4G31500		AT4G03280	
AT4G39090		AT4G09650	

Table 3.6: The Eight TFs that are Candidate Substrates of FER

Gene ID	
AT1G19350	BES1
AT4G34000	ABF3
AT3G28920	HB34
AT3G51950	
AT3G58120	BZIP61
AT2G41900	OXS2
AT1G51140	FBH3
AT3G21430	ALY3

Table 3.7: ER Body-associated Genes (FC: fold change; RPM: reads per million)

		Protein	Transcripts	
Gene ID	**Name**	**FC (fer/WT)**	**fer (RPM)**	**WT (RPM)**
AT3G09260	PYK10/BGLU23	2.29	215	10
AT1G66270	BGLU21	ND	0.17	0
AT1G66280	BGLU22	9.89	3	0.05
AT3G16420	PBP1/JAL30	1.76	168	39
AT3G16430	JAL31	1.76	0.9	0.1
AT3G16450	JAL33	1.9	13	0.8
AT3G16460	JAL34	2.33	190	29
AT3G16470	JAL35	3.21	1130	218
AT1G54000	GLL22	3.22	*5	3.4
AT2G22770	NAI1	ND	5	1.2
AT4G27860	MEB1	1.91	95	14
AT5G24290	MEB2	ND	11	2.1
AT1G52400	BGLU18	4.28	1450	214
AT5G23820	ML3	2.27	137	26
AT1G54010	GLL23	2.82	87	8
AT1G54030	MVP 1	1.99	107	60
AT3G15950	NAI2	2.54	28	6.5

* not significant
ND: not detected

CHAPTER 4

DISCUSSION AND FUTURE DIRECTIONS

4.1 Discussion and Future Directions

4.1.1 FER and Jasmonic Acid (JA) Signaling

This dissertation summarizes my work on elucidating FERONIA functions and the underlying mechanisms. FER has been shown to play important roles in plant growth, and loss of function of *fer* mutant has severe dwarf phenotype (Guo et al., 2009). In the subsequent transcriptome analysis, FER was found to be a major negative regulator of JA signaling (Guo et al., 2018a). The G-Box (CACA/GT/CG) promoter element was enriched in FER-regulated genes and G-Box is a known binding site for transcription factor MYC2 that mediates JA signaling and plays a positive role in bacterial host susceptibility. Further genetics, cell biological and biochemical studies showed that FER phosphorylates and destabilizes MYC2 to down-regulate MYC2-mediated JA signaling and host susceptibility, which establishes FER as a positive regulator in bacterial pathogen defense. RALF23, a rapid alkalization factor and a peptide ligand for FER, functions through FER to negatively contribute to bacterial defense. Another study corroborates the positive role of FER and negative role of RALF23 in this process but through a different molecular mechanism, in that FER is required for immune receptors FLS2/EFR-mediated PAMP-triggered immunity (Stegmann et al., 2017).

The discovery that a plasmamembrane-localized receptor kinase FER directly regulates a transcription factor MYC2 that in turn, regulates MYC2-mediated nuclear events provides a new paradigm for future studies of FER signaling. Corroborating our findings, a recent study has

shown that FER can directly interact with and phosphorylate a nuclear DNA binding protein EBP1 (ErbB3-binding protein1), which results in the EBP1 nuclear accumulation and subsequent transcriptional regulation, likely leading to a feedback inhibition loop to down-regulate RALF1/FER signaling (Li et al., 2018).

My work on FER-MYC2 prompts another question: Does FER regulate other JA signaling components? Our previous study showed that MYC2 was not able to fully rescue all aspects of *fer* mutant phenotypes (Guo et al., 2018a). There are more JA signaling components such as co-receptors COI1 and JAZ family proteins, as well as other TFs homologous to MYC2 (e.g. MYC3, MYC4, MYC5). It is possible that MYC3/4/5 also function down-stream of FER redundantly (Qi et al., 2015). Similar experiments can be conducted to characterize FER regulation on MYC3/4/5.

Alternatively or additionally, JAZ may be a target of FER signaling. The JAZ repressor proteins are highly functionally redundant in suppressing JA signaling by interacting with MYC TFs to inhibit their regulatory activity. Recently, the transcriptome and proteome of a JAZ decuple mutant, *jazD* (defective in JAZ1-7, -9, -10 and -13), were reported (Guo et al., 2018b). The omics data comparison revealed that more than 50% of the genes regulated in *jazD* are regulated in *fer* mutant, and more than 80% of the co-regulated genes are regulated in the same direction by FER and JAZ (Figure 4.1A). Over 70% of the genes regulated in *jazD* are also regulated in *fer* mutant, and 94% of the co-regulated proteins are regulated in the same direction by FER and JAZ (Figure 4.1B). More interestingly, similar to *fer* mutant, *jazD* displays compromised growth and resistance to fungal pathogen and insect herbivores. The above analysis strongly suggests that FER may also regulate JA pathway through JAZ proteins. Further research can be carried out to test the hypothesis.

4.1.2 FER and Candidate Substrate Transcription Factors

To better understand FER function and the underlying mechanisms, we carried out quantitative proteomics and phosphoproteomics of *fer* mutant. The Gene Ontology analysis supports previous findings that FER plays important roles in stress hormone (e.g. JA, ABA) signaling (Chen et al., 2016; Guo et al., 2018a; Yu et al., 2012), plant immunity against bacterial and fungal pathogens (Guo et al., 2018a; Masachis et al., 2016; Stegmann et al., 2017), and the data also suggest an important role for FER in nutrient and energy homeostasis.

More interestingly, a group of transcription factors are identified as potential FER substrates. They belong to different families of TFs, basic Helix-Loop-Helix/bHLH (BES1, FBH3), basic Leucine Zipper/bZIP (bZIP61, ABF3), Zinc Finger (OXS2, AT3G51950), Zinc Finger-Homeo Domain (HB34) and SANT/MYB-like (ALY3). Some of the TFs have well defined functions. BES1 is the major TF in BR signaling pathway and positively regulates BR-mediated plant growth (Yin et al., 2002). BES1 was also shown to induce FER transcript level (Guo et al., 2009). It is conceivable that FER partially functions through BES1 to regulate plant growth. ABF3 is induced by ABA and regulates ABA-mediated leaf senescence (Gao et al., 2016) and drought-accelerated flowering (Hwang et al., 2019). FER has been shown to activate ABI2, the ABA co-receptor and negative regulator in ABA signaling, to inhibit ABA pathway. It is also conceivable that FER regulates ABA signaling directly through down-stream TFs. OXS2 has been shown to regulate both growth and oxidative stress by shuttling from cytoplasm to nucleus (Blanvillain et al., 2011), which may also partially account for FER's dual role in growth and stress responses.

This part of the study will bring about a series of interesting research topics, and will provide a more comprehensive understanding on how receptor kinase FER regulates nuclear events directly through transcription factors. Further work can be conducted to dissect the functions of these TFs and their regulation by FER, which will broaden our understanding of FER function and the underlying mechanisms.

4.1.3 FER and ER Body

ER body was first described almost two decades ago (Hayashi et al., 2001) and more than a dozen of associated genes/proteins have been identified (Wang et al., 2017), including the TF NAI1 that regulates the expression of many ER body-related genes and is required for ER body formation (Matsushima et al., 2004). However, the biological significance of the phenomena is still unclear. It has been shown that ER-Body formation is closely related to glucosinolate (GSL) metabolism, and the ER body resident protein PYK10 can potentially function as a Myrosinase to hydrolyze GSLs (Nakano et al., 2017). GSL metabolism is known to play important roles in plant defense responses such as defense against herbivory (Wittstock and Burow, 2010), which suggests that ER body may function in plant defense against insect herbivore. The omics data supports that FER negatively regulates ER body formation through NAI1 and NAIP2, and GSL metabolism is hyperactive in *fer* mutant, which suggests that FER possibly regulates herbivore defense through the regulation of ER body and GSLs metabolism.

To follow up on this line of research, the detailed regulation of FER on NAI1 and NAIP2 will need to be carried out. The biological output of the ER body and closely correlated glucosinolate metabolism in the context of FER regulation can be tested by responses to herbivory.

4.1.4 FER and Autophagy

Autophagy plays fundamental roles all through a plant's life to recycle and reuse cellular nutrients for critical developmental stages and survival, especially under stress conditions such as starvation (Liu and Bassham, 2012; Marshall and Vierstra, 2018). Similar to their counterparts in yeast and mammals, TOR kinase and SnRK1 kinase complex have been shown to play important roles in autophagy regulation (Liu and Bassham, 2010; Soto-Burgos and Bassham, 2017). TOR negatively and SnRK1 positively regulates autophagy (Liu and Bassham, 2010; Soto-Burgos and Bassham, 2017). Our phosphoproteomics data analysis and subsequent experiments reveal that FER phosphorylates and destabilizes KINβ1 and likely down-regulates SnRK1 complex activity. Further transcriptome and genetic analyses show that FER, TOR and SnRK1 likely function in the same complex to regulate plant growth and autophagy in response to different stimuli.

To follow up with this study, extensive genetic, biochemistry and cell biology experiments will be needed to test the potential interactions among the three proteins and the functional consequences of the interactions in plant growth and autophagy.

4.1.5 FER and Arabidopsides

In order to better understand FER function, secondary metabolites were partially analyzed (Appendix). Arabidopsides, a family of oxylipins, were found to be enriched in *fer* mutant (Hansen et al., 2019), and wounding also increased Arabidopside levels, in agreement with previous findings (Vu et al., 2012). Some oxylipins such as JA function as signaling

molecules and are involved in plant stress responses (Mosblech et al., 2009). However, functional role of Arabidopsides is not clear.

Hansen et al. (2019) found that the purified Arabidopside A inhibited root growth at 20 μM concentration in WT while *fer* was not sensitive to the inhibition. These results lead to the interesting question: Are the Arabidopsides signaling molecules that function through receptor kinase FERONIA? This question can be answered by a survey of the transcriptome change upon treatment of Arabidopside A in WT and *fer* mutant. We are currently testing this, and if the change is significant in WT but reduced in *fer*, we will carry out follow-up experiments to establish a ligand/receptor relationship.

4.2 References

Blanvillain, R., Wei, S., Wei, P., Kim, J.H., and Ow, D.W. (2011). Stress tolerance to stress escape in plants: role of the OXS2 zinc-finger transcription factor family. EMBO J *30*, 3812-3822.

Chen, J., Yu, F., Liu, Y., Du, C., Li, X., Zhu, S., Wang, X., Lan, W., Rodriguez, P.L., Liu, X*., et al.* (2016). FERONIA interacts with ABI2-type phosphatases to facilitate signaling cross-talk between abscisic acid and RALF peptide in Arabidopsis. Proc Natl Acad Sci U S A *113*, E5519-5527.

Gao, S., Gao, J., Zhu, X., Song, Y., Li, Z., Ren, G., Zhou, X., and Kuai, B. (2016). ABF2, ABF3, and ABF4 Promote ABA-Mediated Chlorophyll Degradation and Leaf Senescence by Transcriptional Activation of Chlorophyll Catabolic Genes and Senescence-Associated Genes in Arabidopsis. Mol Plant *9*, 1272-1285.

Guo, H., Li, L., Ye, H., Yu, X., Algreen, A., and Yin, Y. (2009). Three related receptor-like kinases are required for optimal cell elongation in Arabidopsis thaliana. Proc Natl Acad Sci U S A *106*, 7648-7653.

Guo, H., Nolan, T.M., Song, G., Liu, S., Xie, Z., Chen, J., Schnable, P.S., Walley, J.W., and Yin, Y. (2018a). FERONIA Receptor Kinase Contributes to Plant Immunity by Suppressing Jasmonic Acid Signaling in Arabidopsis thaliana. Curr Biol *28*, 3316-3324 e3316.

Guo, Q., Yoshida, Y., Major, I.T., Wang, K., Sugimoto, K., Kapali, G., Havko, N.E., Benning, C., and Howe, G.A. (2018b). JAZ repressors of metabolic defense promote growth and reproductive fitness in Arabidopsis. Proc Natl Acad Sci U S A *115*, E10768-E10777.

Hansen, R.L., Guo, H., Yin, Y., and Lee, Y.J. (2019). FERONIA mutation induces high levels of chloroplast-localized Arabidopsides which are involved in root growth. Plant J *97*, 341-351.

Hayashi, Y., Yamada, K., Shimada, T., Matsushima, R., Nishizawa, N.K., Nishimura, M., and Hara-Nishimura, I. (2001). A proteinase-storing body that prepares for cell death or stresses in the epidermal cells of Arabidopsis. Plant Cell Physiol *42*, 894-899.

Hwang, K., Susila, H., Nasim, Z., Jung, J.Y., and Ahn, J.H. (2019). Arabidopsis ABF3 and ABF4 Transcription Factors Act with the NF-YC Complex to Regulate SOC1 Expression and Mediate Drought-Accelerated Flowering. Mol Plant *12*, 489-505.

Li, C., Liu, X., Qiang, X., Li, X., Li, X., Zhu, S., Wang, L., Wang, Y., Liao, H., Luan, S.*, et al.* (2018). EBP1 nuclear accumulation negatively feeds back on FERONIA-mediated RALF1 signaling. PLoS Biol *16*, e2006340.

Liu, Y., and Bassham, D.C. (2010). TOR is a negative regulator of autophagy in Arabidopsis thaliana. PLoS One *5*, e11883.

Liu, Y., and Bassham, D.C. (2012). Autophagy: pathways for self-eating in plant cells. Annu Rev Plant Biol *63*, 215-237.

Marshall, R.S., and Vierstra, R.D. (2018). Autophagy: The Master of Bulk and Selective Recycling. Annu Rev Plant Biol *69*, 173-208.

Masachis, S., Segorbe, D., Turra, D., Leon-Ruiz, M., Furst, U., El Ghalid, M., Leonard, G., Lopez-Berges, M.S., Richards, T.A., Felix, G.*, et al.* (2016). A fungal pathogen secretes plant alkalinizing peptides to increase infection. Nat Microbiol *1*, 16043.

Matsushima, R., Fukao, Y., Nishimura, M., and Hara-Nishimura, I. (2004). NAI1 gene encodes a basic-helix-loop-helix-type putative transcription factor that regulates the formation of an endoplasmic reticulum-derived structure, the ER body. Plant Cell *16*, 1536-1549.

Mosblech, A., Feussner, I., and Heilmann, I. (2009). Oxylipins: structurally diverse metabolites from fatty acid oxidation. Plant Physiol Biochem *47*, 511-517.

Nakano, R.T., Pislewska-Bednarek, M., Yamada, K., Edger, P.P., Miyahara, M., Kondo, M., Bottcher, C., Mori, M., Nishimura, M., Schulze-Lefert, P.*, et al.* (2017). PYK10 myrosinase reveals a functional coordination between endoplasmic reticulum bodies and glucosinolates in Arabidopsis thaliana. Plant J *89*, 204-220.

Qi, T., Huang, H., Song, S., and Xie, D. (2015). Regulation of Jasmonate-Mediated Stamen Development and Seed Production by a bHLH-MYB Complex in Arabidopsis. Plant Cell *27*, 1620-1633.

Soto-Burgos, J., and Bassham, D.C. (2017). SnRK1 activates autophagy via the TOR signaling pathway in Arabidopsis thaliana. PLoS One *12*, e0182591.

Stegmann, M., Monaghan, J., Smakowska-Luzan, E., Rovenich, H., Lehner, A., Holton, N., Belkhadir, Y., and Zipfel, C. (2017). The receptor kinase FER is a RALF-regulated scaffold controlling plant immune signaling. Science *355*, 287-289.

Vu, H.S., Tamura, P., Galeva, N.A., Chaturvedi, R., Roth, M.R., Williams, T.D., Wang, X., Shah, J., and Welti, R. (2012). Direct infusion mass spectrometry of oxylipin-containing Arabidopsis membrane lipids reveals varied patterns in different stress responses. Plant Physiol *158*, 324-339.

Wang, J.Z., Li, B., Xiao, Y., Ni, Y., Ke, H., Yang, P., de Souza, A., Bjornson, M., He, X., Shen, Z*., et al.* (2017). Initiation of ER Body Formation and Indole Glucosinolate Metabolism by the Plastidial Retrograde Signaling Metabolite, MEcPP. Mol Plant *10*, 1400-1416.

Wittstock, U., and Burow, M. (2010). Glucosinolate breakdown in Arabidopsis: mechanism, regulation and biological significance. Arabidopsis Book *8*, e0134.

Yin, Y., Wang, Z.Y., Mora-Garcia, S., Li, J., Yoshida, S., Asami, T., and Chory, J. (2002). BES1 accumulates in the nucleus in response to brassinosteroids to regulate gene expression and promote stem elongation. Cell *109*, 181-191.

Yu, F., Qian, L., Nibau, C., Duan, Q., Kita, D., Levasseur, K., Li, X., Lu, C., Li, H., Hou, C*., et al.* (2012). FERONIA receptor kinase pathway suppresses abscisic acid signaling in Arabidopsis by activating ABI2 phosphatase. Proc Natl Acad Sci U S A *109*, 14693-14698.

4.3 Figures

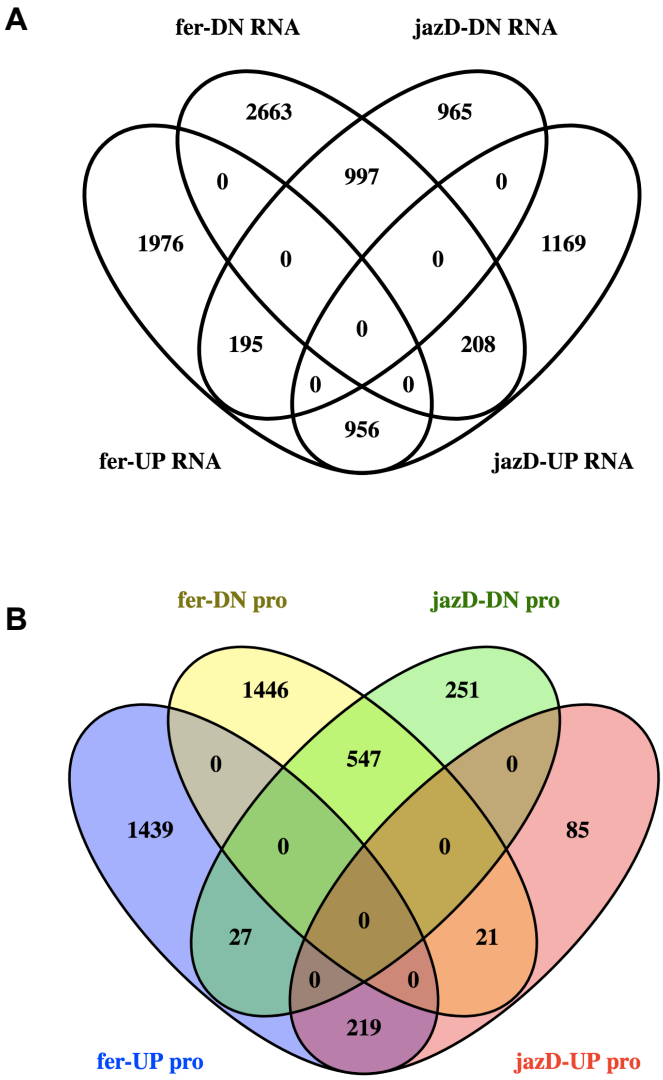

Figure 4.1: Comparisons of Transcriptomes and Proteomes of *fer* and *jazD*

(A) Transcriptome comparison of *fer* and *jazD*, using Venny 2.1.0.

(B) Proteome comparison of *fer* and *jazD*, using Venny 2.1.0.

APPENDIX

CHLOROPLAST LOCALIZED ARABIDOPSIDES ARE INVOLVED IN FERONIA-REGULATED ROOT GROWTH

A paper published in The Plant Journal

Rebecca L. Hansen[1], Hongqing Guo[2], Yanhai Yin[2], Young Jin Lee[1,*]

[1]Department of Chemistry, Iowa State University, Ames, IA 50011, USA
[2]Department of Genetics, Development, and Cell Biology, Iowa State University, Ames, IA 50011, USA

Address reprint requests to Dr. Young Jin Lee
35A Roy J Carver Co-Lab
1111 WOI Road
Ames, IA 50011-3650
Tel: 515-294-1235
Email: yjlee@iastate.edu

Running Title: Arabidopsides as Biomarker related to FERONIA

Abstract

The FERONIA signaling pathway is known to have diverse roles in *Arabidopsis thaliana*, such as growth, reproduction, and defense, but how this receptor-kinase regulates various biological processes is not well established. In this work, we applied multiple mass spectrometry techniques to identify metabolites involved in the FERONIA signaling pathway and to understand their biological roles. A direct infusion Fourier transform ion cyclotron resonance (FTICR)-MS approach was used for initial screening of wild-type and *feronia (fer)* mutant plant extracts, and Arabidopsides were found to be significantly enriched in the mutant.

As Arabidopsides are known to be induced by wounding, further experiments on wounded and non-wounded leaf samples were carried out to investigate these oxylipins as well as related phytohormones using a quadrupole time-of-flight (Q-TOF) MS by direct injection and LC-MS/MS. In a root growth bioassay with Arabidopside A isolated from *fer* mutants, the wild-type showed significant root growth inhibition compared to the *fer* mutant. Our results thus implicated Arabidopsides, and Arabidopside A specifically, in FER functions and/or signaling. Finally, matrix-assisted laser desorption/ionization MS imaging (MALDI-MSI) was used to visualize the localization of Arabidopsides, and we confirmed that Arabidopsides are highly abundant at wounding sites in both wild-type and *fer* mutant plants. More significantly, five micron high-spatial resolution MALDI-MSI revealed that Arabidopsides are localized to the chloroplasts where many stress signaling molecules are made.

Significance Statement

Arabidopside A is identified as a biomarker for the FER signaling pathway and is shown to inhibit root growth. Additionally, Arabidopside A was determined to be co-localized with pheophytin *a*, indicating that it is present in photosynthetic cells.

Key Words: Arabidopside A, FERONIA, mass spectrometry imaging, wounding, mass spectrometry, *Arabidopsis thaliana*.

Introduction

FERONIA (FER) is a receptor-like kinase in *Arabidopsis thaliana* that functions broadly throughout plant development and has critical roles in controlling fertilization, vegetative growth, and defense responses (Escobar-Restrepo *et al.*, 2007, Guo *et al.*, 2009a, Guo *et al.*, 2009b, Deslauriers and Larsen, 2010, Duan *et al.*, 2010, Keinath *et al.*, 2010, Kessler *et al.*,

2010, Yu *et al.*, 2012) as well as root growth and interactions with other plant hormones (Mao *et al.*, 2015, Yang *et al.*, 2015, Du *et al.*, 2016, Liao *et al.*, 2017). FER is a plasma membrane-localized transmembrane protein (Escobar-Restrepo *et al.*, 2007) and the extracellular domain contains motifs that share homology with malectin. The homology with malectin suggests that FERONIA may sense changes in the cell wall and signal for cellular responses (Hématy and Höfte, 2008), and also that a sugar-containing species may be involved in FER functions. The loss-of-function mutant of FER, *feronia (fer*), displays a defect in fertilization (Escobar-Restrepo *et al.*, 2007), reduced plant growth (Guo et al., 2009a), and has reduced susceptibility to bacterial pathogens (Stegmann *et al.*, 2017). FER's involvement in many diverse functions in Arabidopsis suggests the complex and interconnected nature of signaling pathways. One important balance in plants is the coordination of growth and stress responses, of which FER has distinct roles, and so the study of this signaling pathway is critical to our understanding of how plants effectively manage these functions.

Some components of the FER signaling pathway have been identified, including RALF1 (Haruta *et al.*, 2014) and RALF23 (Stegmann *et al.*, 2017) that function as ligands for FER, LLG1 acting as a FER co-receptor (Li *et al.*, 2015), ROP/RAC GTPases, (Yu *et al.*, 2012), and phosphatase ABI2 (Chen *et al.*, 2016). However, the metabolite changes in *fer* mutants have not yet been reported. Here, we identified metabolite biomarkers which were found to be more highly abundant in *fer* mutants. Such metabolites may help to explain some of the functions of FER. In addition, the multi-functionality of FER suggests that other ligands could be possible in addition to those previously reported. We presumed the loss of FERONIA would result in the accumulation of any possible ligands due to feedback mechanisms, and so we were specifically

interested in features increased in *fer* mutant plants. To this end we compared metabolite profiles of wild-type (WT) and *fer* mutant plants using various mass spectrometry techniques.

Gas chromatography-mass spectrometry (GC-MS) or liquid chromatography-tandem mass spectrometry (LC-MS/MS) experiments are most commonly used for metabolomics profiling. One significant limitation of these methods is the low throughput, typically taking half to one hour per sample. Additionally, there will be bias for certain compounds depending on the mode of separation. Direct infusion mass spectrometry has become a popular method for targeted and untargeted lipidomics profiling as it allows for high-throughput screening and has a wide metabolite coverage that is not limited by the separation device (González-Domínguez, 2017, Gang *et al.*, 2018). Here, we adopt direct infusion high-resolution mass spectrometry (HRMS) as a high-throughput screening method to identify biomarkers highly enriched in *fer* mutants. Arabidopsides, an oxylipin class previously known for its wounding response (Hisamatsu *et al.*, 2003, Hisamatsu *et al.*, 2005, Andersson *et al.*, 2006, Kourtchenko *et al.*, 2007, Ibrahim *et al.*, 2011), were found to be highly enriched in *fer*, among others. The possible roles of Arabidopsides in FERONIA are discussed in relation to wounding response and other oxylipins and phytohormones. Finally, matrix-assisted laser desorption/ionization (MALDI)-mass spectrometry imaging (MSI) was used to obtain cellular and subcellular level localization information of Arabidopsides.

Results

High-throughput Direct Infusion Biomarker Screening

A direct infusion high-resolution mass spectrometry approach was adopted as a high-throughput screening method to identify metabolite changes in *fer* mutant plants. Polar (water/methanol) and nonpolar (chloroform) leaf extracts from both the wild-type and *fer* mutant were analyzed in both positive and negative ion modes using a 7T Bruker SolariX FTICR-MS. Figure AS1A compares spectra from a representative biological replicate of the wild-type and *fer* mutant for the nonpolar extract in positive ion mode. As expected, most peaks are consistent between the two genotypes, such as *m/z* 871.57 (pheophytin *a*) and *m/z* 893.55, as well as other peaks in the low mass region. Monogalactosyldiacylglycerol (MGDG) species were also detected as shown in Figure AS2 for the narrow mass range corresponding to MGDG (18:3/18:3) and MGDG (18:3/16:3). There are a couple of readily apparent differences in the spectra of the two genotypes, such as the consistently greater abundance of *m/z* 797.45, 813.42, and 825.48 in the *fer* mutant (Figure AS1A). Closer inspection of the *fer* mutant spectra reveals a series of seemingly related peaks as indicated in Figure AS3 and Appendix S1. The apparent structural relationships in this series of peaks indicate the compounds might be sugar-containing lipid species. In the nonpolar extract in negative ion mode (Figure S1B), similarly, there are many peaks in common between the genotypes, such as *m/z* 582.50 and 937.53, among others. There are also several significant differences between the two genotypes, such as the higher abundance of *m/z* 755.45, 847.49, and 1009.54 in the *fer* mutant consistently across the biological replicates (Figure AS1B).

Statistical analysis was performed for four biological replicates of each genotype using the Plant/Eukaryotic and Microbial Systems Resource (PMR) database (data publically available at http://metnetweb.gdcb.iastate.edu/PMR/experiments/?expid=256). Figure A1A shows a volcano plot comparing the fold change of the signal intensity vs p-value for various *m/z* values between wild-type and *fer* for the nonpolar leaf extracts in positive and negative mode. A total of 68 and 52 peaks in positive and negative mode, respectively, were identified to have significant differences according to the volcano plot with a minimum fold change of 2 and maximum p-value of 0.01, as summarized in Table AS1. There are several interesting *m/z* peaks that display a high fold change and a significant p-value. For example, from the nonpolar positive mode data, *m/z* 797.45 (indicated with a green circle in Figure A1A) has a fold change of 71 and p-value of 0.0018, and *m/z* 825.48 (orange circle) has a fold change of 31 and a p-value of 0.0067. In negative ion mode, several noteworthy peaks include *m/z* 847.49 (pink circle) with a fold change of 79 and a p-value of 0.0027, and *m/z* 1009.54 (purple circle) with a fold change of 70 and a p-value of 0.0012.

The series of features in the nonpolar positive mode data that were significantly increased in the *fer* mutant were identified as Arabidopsides according to their chemical compositions from the high-resolution mass spectra and MS/MS performed using a Q-TOF MS. Figure A1B shows the MS/MS spectra for three potential biomarkers, *m/z* 797.45, 825.48, and 987.53, which are assigned as sodium ion adducts of Arabidopside A, Arabidopside B, and Arabidopside D, respectively. One can readily observe many similarities between the three spectra, again signifying their structural relationship (see Appendix S2 for detailed annotation). MGDG (18:3/18:3) has the same nominal mass as Arabidopside A, but it is clearly distinguished using HRMS (Figure AS2), and fragment ions from both species are observed (Figure A1B; asterisk

indicates a 18:3 fatty acid loss from the MGDG species). The fragments of Arabidopside A are consistent with previous reports in literature (Ibrahim *et al.*, 2011). In the nonpolar extract in negative mode, *m/z* 819.45, 847.49, and 1009.54 are assigned as formate ion adducts of Arabidopside A, B, and D, respectively. The MS/MS spectra of these species are shown in Figure AS4.

Wounding Experiments

In our experiments, Arabidopsides, which are known to be induced upon wounding in wild-type *Arabidopsis* plants (Buseman *et al.*, 2006, Kourtchenko *et al.*, 2007, Vu *et al.*, 2015), showed increased abundances in non-wounded *fer* mutants compared to the wild-type; however the effect of wounding in *fer* mutants is unknown. Therefore it is essential to study the effect of wounding on the levels of Arabidopsides in both genotypes in order to explore the significance of Arabidopsides in the FERONIA pathway. Additionally, OPDA (12-oxo-phytodienoic acid) and dnOPDA (dinor-oxo-phytodienoic acid), which are precursors of phytohormone jasmonic acid (JA) and essential components of Arabidopsides, were also studied. These subsequent experiments were performed with Q-TOF MS as it provides sufficient mass resolution for the purpose. The Arabidopside family of metabolites were further investigated using a Q-TOF MS with direct injection, and OPDA, dnOPDA, and JA were studied using LC-Q-TOF MS. The Arabidopside family and OPDA/dnOPDA/JA were compared with and without wounding in both genotypes. Figure AS5 shows representative mass spectra from the nonpolar leaf extracts in the high mass range comparing the Arabidopside levels in the *fer* and wild-type genotypes both without wounding and 15 minutes post-wounding in positive mode. Wounding was accomplished by crimping the leaf with a tweezers 3-4 times across the midvein of the leaf (see

the photo in Figure A2A) and then harvesting the leaves after 15 minutes. For each sample, several leaves were combined and the dried extract from each biological replicate was re-suspended to the same final concentration before analysis.

In all four spectra of Figure AS5 (*fer*, wild-type, *fer* wounded, and wild-type wounded), the signal intensity of pheophytin *a* (*m/z* 871.57), chlorophyll *a* which loses Mg^{2+} during analysis, remains relatively unchanged and was used to normalize Arabidopside signals. The signal intensities of the Arabidopside compounds vary across the samples. As previously observed, the levels of Arabidopsides A, B, and D in the *fer* mutants are significantly increased compared to the wild-type, although the signal ratios for these compounds are not exactly the same as Figure AS1 due to experimental variations. This is attributed to the hypersensitive response of Arabidopsides to stress conditions. The levels of Arabidopsides A, B, and D increase in the wounded *feronia* and wild-type leaves compared to the unwounded leaves of the same genotype. As summarized in Figure A2B, for the post-wounding Arabidopside signals with normalization to pheophytin *a*, there is a significant increase of Arabidopsides A, B and D from non-wounded to wounded samples in both genotypes. The amount of increase is especially significant for Arabidopside A (p-value < 0.001 for WT and < 0.01 for *fer*), followed by Arabidopside B (p-value < 0.01 for both WT and *fer*) and Arabidopside D (p-value < 0.05 for both WT and *fer*). A slight decrease is observed for Arabidopsides E and G after wounding, although not statistically significant. Despite differences in the initial amounts of Arabidopside A and B in the wild-type and *feronia* mutant, the amount of increase between *fer* to *fer* wounded and wild-type to wild-type wounded is similar.

A similar trend is found in the negative mode nonpolar extracts (Figure AS6). The most apparent differences after wounding in both genotypes are Arabidopside A (*m/z* 819.49),

Arabidopside B (*m/z* 847.49), and Arabidopside D (*m/z* 1009.54), present as formate adducts. In addition to the nonpolar extract, the polar extract was analyzed in both ion modes (Figure AS7), and there are only minor differences between the two genotypes with and without wounding. Specifically, we could not find any meaningful changes for OPDA, dnOPDA, and JA (based on exact mass) in the negative mode polar extracts using this direct injection analysis, presumably due to significant chemical or spectral interference, suggesting the limitation of direct injection analysis for small, low abundance metabolite molecules.

Further study of the Arabidopside-related metabolites, OPDA, dnOPDA, and JA, were explored using liquid chromatographic separation combined with Q-TOF MS analysis. Figure A2C displays the quantification results for OPDA, dnOPDA, and JA in wounded and non-wounded leaves of both genotypes. As JA is synthesized in response to wounding, no JA is detected when the leaves are not wounded. After wounding, levels of JA increase in both genotypes. Slightly more JA (p-value 0.016) is produced in the wounded *fer* mutant than in the wounded wild-type, which may be due to a higher stress state of the mutant. Before wounding, statistically higher levels of OPDA and dnOPDA are present in *fer* than in the wild-type, especially for dnOPDA where the level in the mutant is approximately 1.5 times higher than in the wild-type (p-value 0.005). In both genotypes there is a decrease in the amounts of OPDA and dnOPDA present after wounding. This decrease is especially significant for *fer* as the levels of dnOPDA and OPDA decrease by about 3.4 (p-value 0.00035) and 2.6 fold (p-value 0.00025), respectively, compared to the non-wounded samples. In the wild-type, the decrease in the levels of dnOPDA and OPDA after wounding is about 1.3 (p-value 0.061) and 1.8 times (p-value 0.0046), respectively.

Overall, dnOPDA and OPDA are much more abundant in *fer* than in the wild-type before wounding, but the levels of these compounds generally decrease and become similar after wounding. This is in contrast to Arabidopsides, which although are also more abundant in *fer* than in the wild-type before wounding, the amount of these metabolites further increases in both genotypes after wounding.

Biological Assay

Biological activity of Arabidopside A is not known nor suggested, as far as we are aware. As an initial study whether Arabidopside A has any distinct biological activity or is merely a consequence of a stress response, we have performed an experiment to test its effect on plant growth. Arabidopside A was isolated from approximately two hundred *fer* plants using a preparative-LC. The purified Arabidopside A was dissolved in methanol and added to 1/2MS medium (Murashige and Skoog medium) to a final concentration of 20 μM. The MGDG lipid mixture (containing 66.8% MGDG (16:3-18:3)) was also added to 1/2MS medium to a final concentration of 20 μM to be used as a negative control. Wild-type and *fer* plants were germinated in 1/2MS medium for 4 days and then transferred to 1/2MS medium containing Arabidopside A, MGDG, or plain medium for another 4 days. The root lengths were measured for each of 13-16 plants per treatment. When grown in regular medium (denoted by control in figure), wild-type plants have longer root lengths compared to the *feronia* plants (p-value of 0.000191). For the roots grown in MGDG, in both cases there was no significant difference compared to the control (p-value of 0.101 for *fer* and p-value of 0.134 for wild-type). Inhibition of root growth was observed in the wild-type plants that were exposed to Arabidopside A (p-value < 0.00001), whereas *feronia* did not display any inhibition of growth (p-value 0.472)

(Figure A3A and A3B). The decrease in root length in wild-type plants suggests growth suppression by Arabidopside A. However, the is no significant effect of Arabidopside A on *feronia* indicating that the *fer* mutant is less sensitive to the presence of Arabidopside A during root growth compared to the wild-type plant.

MALDI-MSI of Arabidopsides

Although it is well-known that Arabidopsides are induced by wounding, specific localization of these metabolites to the wounded area has not yet been shown. To this end we performed MALDI-MSI to visualize Arabidopside distributions in fractured leaves (see methods section for fracturing sample preparation details). Figure A4A shows low-resolution MS images (pixel size of 100 μm) for the Arabidopside compounds in *fer* and wild-type whole leaves after wounding. The fracturing method, which we previously developed, was used in this experiment, and allows the internal leaf layers to be exposed for MS imaging studies (Klein *et al.*, 2015). Images of pheophytin *a* showed that the thylakoid membrane-associated metabolite is homogenously localized throughout the leaf, which indicated that adequate signal is present throughout the tissue. The images were all normalized to the TIC (total ion count) and set to the same maximum and minimum values to facilitate comparison.

In all cases, the highest Arabidopside signal intensity is localized to the wound sites (Figure A4A, red boxes on leaf images). Arabidopsides A, B and D are easily visualized in both genotypes, but Arabidopsides E and G were not successfully imaged in the wild-type, presumably due to their lower abundances. The localization of the Arabidopside compounds to the wounded areas is reproducible across multiple biological replicates of each genotype. MS images obtained at a higher spatial resolution of 30 μm for a portion of the leaves (Figure AS8)

showed a similar result, although the images for the wild-type are not as clear due to low ion signals with a small sampling size.

Finally, in an effort to obtain cellular or subcellular level localization information, 5 μm high-resolution MS images were acquired for cross-sections of non-wounded *fer* leaves. Figure A4B displays the localizations of Arabidopside A (shown in false color blue) and pheophytin *a* (in false color green) signal intensities overlaid with a microscope image. Single pixel spectra demonstrate the apparent co-localization of the two metabolites, although Arabidopside A is not present at every pixel where the pheophytin *a* is present. For example, in the top single pixel spectrum which corresponds to a green-colored pixel in the MS image, only pheophytin *a* is present. In the middle spectrum (a cyan pixel) both Arabidopside A and pheophytin *a* are present. Finally, in the bottom spectrum, even though the pixel color is dark blue, both Arabidopside A and pheophytin *a* are present, although Arabidopside A does have a higher signal intensity. As pheophytin *a* is present in the thylakoid membrane of photosynthetic cells, this co-localization suggests that Arabidopside A is also present in the chloroplast thylakoid membrane. It also demonstrates that even in the non-wounded *fer* leaves, Arabidopsides are present, although at lower abundances compared to wounded leaves, consistent with the direct infusion ESI-MS data.

Discussion

Arabidopsides are well known to be induced by wounding (Buseman *et al.*, 2006, Kourtchenko *et al.*, 2007, Vu *et al.*, 2012, Vu *et al.*, 2015), especially in *Arabidopsis* from which the name originates. One study found very low levels of Arabidopsides are present in unwounded wild-type leaves, but the levels of Arabidopsides A, B, and D, increased 200- to

1,000-fold 15 minutes after wounding (Buseman *et al.*, 2006). Another study reported increases of ~100 and ~50 fold 45 minutes after wounding for Arabidopside A and B, respectively (Vu *et al.*, 2015). Arabidopsides E and G, containing an additional OPDA attached to the galactose group, have also been reported to be induced by abiotic stress (Kourtchenko *et al.*, 2007, Nilsson *et al.*, 2012, Vu *et al.*, 2012). For example, Nilsson et al. demonstrated that during freeze-thaw stress Arabidopsides A, B, E, and G all accumulate; however, Arabidopsides E and G increased more slowly than Arabidopsides A or B (Nilsson *et al.*, 2012). In another study, oxidized MGDG species (e.g., Arabidopside A and B) were found to predominate in wounding stress, whereas oxidized acylated MGDGs (e.g. Arabidopside E and G) predominated during pathogen infection, although both types were present in both stress conditions (Vu *et al.*, 2012). Therefore, Arabidopsides also have roles in biotic stress, in addition to abiotic stress. It was also demonstrated that Arabidopside E was induced after recognition of avirulence proteins AvrRpm1 and AvrRpt2 in *Arabidopsis* transgenic lines using [^{14}C]acetate labeling (Andersson *et al.*, 2006). In addition, Arabidopside E was found to inhibit *P. syringae* growth by 60% (Andersson *et al.*, 2006). Levels of Arabidopsides have also been studied during hypersensitive response (HR) (Andersson *et al.*, 2006, Kourtchenko *et al.*, 2007, Vu *et al.*, 2012, Nilsson *et al.*, 2014). In addition to *Arabidopsis thaliana*, Arabidopsides have also been found in other species, such as *Cirsium avrvense* (Creeping thistle) (Hartley *et al.*, 2015), *Ipomoea tricolor* (Ohashi et al., 2005), and *Melissa officinalis* (Zábranská et al., 2012), as well as in other plant species of the Brassicaceae family. Despite evidence of a significant stress response, the biological role of Arabidopsides is largely unknown in regard to its relationship with biotic or abiotic stress.

In our study, Arabidopsides A and B significantly increase 15 minutes post-wounding compared to basal levels in similarity to many other studies (Figure A2B). Although

Arabidopsides E and G appear to decrease upon wounding, in apparent contradiction to other studies where increases were detected, it is important to note that this decrease is not statistically significant. Kourtchenko et al. found Arabidopsides A, B, E, and G all increased upon wounding, with Arabidopsides E and G levels peaking around one hour post-wounding (Kourtchenko *et al.*, 2007). The steep accumulation and assumed linearity of accumulation does not necessarily contradict our finding of no statistical difference between basal and wounded levels at a much earlier time point. Furthermore, several papers have noted Arabidopsides E and G increase slower than non-head group acylated species (e.g., Arabidopsides A and B) (Nilsson *et al.*, 2012, Vu *et al.*, 2012). Vu et al. reports increased accumulation of Arabidopsides at 15 minutes post-wounding, with A and B accumulating to a greater extent (Vu *et al.*, 2012). Compared to Kourtchenko et al. who found steep accumulation between time zero and one hour post-wounding, Vu et al. showed similar levels of accumulation at 15 minutes, 45 minutes, and 6 hours post-wounding time points (Kourtchenko *et al.*, 2007, Vu *et al.*, 2012). This difference could be explained by considering, as Vu et al. points out, that "variation in plant growth conditions can affect basal levels of some ox-lipid compounds" (Vu *et al.*, 2012). Indeed, Vu et al. uses 14 hour light/10 hour dark growth conditions while Kourtchenko et al. and our study used short day conditions (i.e. 8 hour light/16 hour dark). Therefore with the growth conditions utilized in our experiments there may be minimal change in Arabidopside E and G levels at early time points, and any deviations from published trends may be simply due to time point variations and/or differing growth conditions between the studies.

Interestingly, the Arabidopside lipid family contains 12-oxo-phytodienoic acid (OPDA) and dinor-oxo-phytodienoic acid (dnOPDA) side chains. OPDA, and possibly dnOPDA, are precursors of jasmonic acid (JA) through the octadecanoid pathway; and JA is an important plant

hormone for stress response against herbivores (Koo *et al.*, 2009). It has also been shown that OPDA itself has roles in plant defense (Stintzi *et al.*, 2001). Due to the connections between these metabolites, it is important that the results from the phytohormone and Arabidopside wounding experiments be considered in conjunction. One of the striking findings of this study is that Arabidopsides are significantly increased in *fer* mutants even without wounding, although wounding resulted in additional accumulation of Arabidopsides in both wild-type and *fer* mutant plants. This suggests that FER functions to repress production of Arabidopsides under normal conditions.

Overall, dnOPDA and OPDA are much more abundant in *feronia* than in the wild-type before wounding, but the levels of these compounds generally decrease and become similar after wounding (Figure A2C). This is in contrast to the increase of Arabidopsides after wounding, suggesting that dnOPDA and OPDA might have been used to produce Arabidopsides. Considering OPDA is a known precursor for JA biosynthesis (and also possibly dnOPDA, although this pathway has not yet been confirmed), it is also possible OPDA and dnOPDA are used to produce JA. However, the increase of JA after wounding, 8.6 and 16.8 nmol/gram for wild-type and *fer*, respectively, is much lower than the decrease of OPDA, 40 and 76 nmol/gram for wild-type and *fer*, respectively, although some JA derivatives such as methyl jasmonate were hard to quantify due to their volatile nature. Furthermore, the high abundance of both OPDA and dnOPDA without wounding in *fer* and their sharp decrease after wounding is particularly well correlated with Arabidopside A, which has both OPDA and dnOPDA side chains. Arabidopside A has a relatively high abundance initially in *feronia* and significantly increases with wounding, further supporting the hypothesis that free OPDA and dnOPDA might be precursors of Arabidopsides, especially Arabidopside A.

The above hypothesis, however, is not without contradiction. A previous study involving ^{18}O-labelled water determined that the biosynthesis of OPDA and dnOPDA occurs while the fatty acid precursors are esterified to membrane lipids in wild-type plants (Nilsson *et al.*, 2012). In other words, the fatty acids on MGDG or digalactosyldiacylglycerol (DGDG) lipids are directly converted to dnOPDA or OPDA to form Arabidopsides, and it is not necessary for free fatty acids to be enzymatically cyclized to dnOPDA or OPDA before being attached to sugar-containing glycerol backbones to form Arabidopsides. This conclusion is also supported in our data for the wild-type where the levels of dnOPDA only slightly decrease after wounding, despite a significant increase in Arabidopsides, while the more significant decrease in OPDA can be at least partially attributed to JA synthesis. Although not analyzed in this experiment, the formation of amino acid conjugates of JA or other derivatives of JA and/or OPDA could also account for the decreased OPDA levels.

Alternatively, pathways might exist to synthesize Arabidopsides from both free OPDA/dnOPDA and membrane bound galactosyl lipids. The latter pathway might be dominant in the wild-type, but in the case of the *fer* mutant, the much higher initial levels of both OPDA and dnOPDA and their more significant decrease after wounding suggests that free OPDA/dnOPDA are utilized for the rapid synthesis of Arabidopsides. Additionally, OPDA and dnOPDA are known to be induced by wounding on their own, which may explain the more significant change of these metabolites after wounding stress in the *fer* mutant (Stintzi *et al.*, 2001). Overall, we hypothesize that *fer* is in a higher stress state and can therefore more rapidly respond to stress using a pathway involving free dnOPDA/OPDA. This also suggests that the initial accumulation of Arabidopsides, and specifically Arabidopside A, in *fer* is not due to a simple stress response, and that this lipid may play an important role through FERONIA.

The distinct post-wounding decrease of OPDA in both genotypes and dnOPDA in *fer* in our data (Figure A2C) is in contrast with the increased accumulation of OPDA and dnOPDA after wounding reported by Stintzi et al. (Stintzi *et al.*, 2001). However, there is a significant time difference between the two experiments; they collected samples 90 minutes or later after wounding whereas we collected after 15 minutes. In fact, other studies indicate that OPDA decreases initially before increasing at longer time frames. In both Stelmach et al. and Koo et al., OPDA appears to decrease around 15 minutes post-wounding before increasing (Stelmach *et al.*, 2001) (Koo *et al.*, 2009). Hence, our data agrees with other reports, although it is not clear why OPDA decreases at early time points after wounding.

Our finding that Arabidopside inhibits root growth in wild-type plants (Figure A3) supports the possibility that Arabidopsides, and specifically Arabidopside A, may play an important role through FERONIA. The fact that the *fer* mutant is much less sensitive to the Arabidopside A suggests that Arabidopsides may function through FERONIA either directly or indirectly, to regulate plant growth. It has been previously demonstrated that *fer* is hypersensitive to JA, thereby showing a different trend than that of Arabidopside A (Guo *et al.*, 2018). Therefore the effect of Arabidopside A does not likely arise from liberated OPDA that is further metabolized to OPDA. The growth inhibition of Arabidopside A revealed here is a novel function of the Arabidopside family, beyond the general wound response for which they are currently known. In other words, Arabidopside A, accumulated through a wounding response, may potentially signal through the FERONIA pathway to suppress growth and promote stress responses.

The use of MS imaging revealed the previously unknown cellular/subcellular localization of Arabidopside A, which would be unavailable using extraction based experiments. This

localization information allows for deeper insight into metabolism. In our experiments, Arabidopsides were found to be co-localized with pheophytin *a,* which is a chloroplast thylakoid membrane associated compound, demonstrating that Arabidopsides are also localized to the chloroplasts. Chloroplasts also have roles in plant immune response in addition to photosynthesis. For example, many important defense signaling molecules are biosynthesized in the chloroplast, such as salicylic acid (Dempsey *et al.*, 2011), JA (Wasternack, 2007), and reactive oxygen species (Asada, 2006). It has also been demonstrated that chloroplastic stromules, critical connections to the membranes of other organelles such as the nucleus, are induced during immune responses (Caplan *et al.*, 2015). Therefore, both the previously known and the demonstrated roles of Arabidopsides in abiotic/biotic stress responses correlates well with this localization.

Experimental Procedures

Materials

The organic MALDI matrix 2,5-dihydroxybenzoic acid (DHB, 98%) was purchased from Sigma-Aldrich (St. Louis, MO, USA). Iron oxide nanoparticles (NPs) (Fe_3O_4, 11 nm, no organic capping) were synthesized according to a previously published method (Berger *et al.*, 1999). The NPs were suspended in isopropyl alcohol to a final concentration of 5 mM. Isopropyl alcohol (LCMS Chromasolv), chloroform (Chromasolv Plus), and methanol (LCMS Chromasolv) were purchased from Sigma-Aldrich (St. Louis, MO, USA). Water (Optima LCMS) was purchased from Fisher Scientific (Hampton, NH, USA). Ethyl acetate (OmniSolv) was purchased from EMD Millipore Corporation (Billerica, MA, USA). Gelatin from porcine skin (300 bloom) was purchased from Electron Microscopy Sciences (Hatfield, PA, USA).

Formic acid (98%, Fluka LC-MS) was purchased from Sigma-Aldrich (St. Louis, MO, USA). MGDG lipid mixture standard was purchased from Avanti Polar Lipids, Inc. (Alabaster, AL, USA).

Plant Growth and the feronia Mutant

Wild-type (Columbia-0) and *feronia* mutant seeds were germinated on 1/2MS medium for 10 days and then seedlings were transferred to soil and grown for another three weeks before harvesting. The plants were grown under short day conditions (8 hours light and 16 hours dark cycle) at 23 °C in a growth chamber. The FERONIA mutant is a tDNA insertion mutant, *fer-4* (GABI_106A06), as described elsewhere (Duan *et al.*, 2010), and seeds were obtained from the Arabidopsis Biological Resource Center (ABRC).

Metabolite Extractions for Biomarker Determination

The extraction procedure utilized was based on the Bligh/Dyer method (Bligh and Dyer, 1959). Approximately 40 mg of leaf tissue was frozen in liquid nitrogen, ground in a mortar and pestle, and extracted using a solvent mixture of chloroform:60°C methanol:water (47:33:20). After the addition of the hot methanol (0.5 mL), samples were incubated at 60 °C for 10 minutes before being briefly vortexed and then sonicated for 15 minutes. Then, chloroform (0.7 mL) and water (0.3 mL) were added with 30 seconds of vortexing after each addition. Finally the samples were centrifuged at 10000 rpm for 5 minutes and then separated into polar (methanol/water) and nonpolar (chloroform) fractions. Extracts were stored at -80 °C until analysis.

Direct Infusion Mass spectrometry (FT-ICR)

For the initial biomarker discovery experiments, samples were prepared as discussed above. Before analysis, all leaf extracts were diluted 1:10 in methanol and either 0.1% formic acid (final concentration) in positive mode or 10 mM ammonium formate in negative mode (final

concentration) were added based on additive testing. Other additives tested included acetic acid, ammonium acetate, ammonium hydroxide, and sodium hydroxide. Samples were analyzed using direct infusion at a flow rate of 2 μL/min with a 7.0 T SolariX FT-ICR MS (Bruker). Data analysis was done using DataAnalysis (Bruker).

MS/MS Analysis (Q-TOF)

Structural analysis was performed with MS/MS using extracts prepared as indicated above. MS/MS spectra were collected using a 6540 quadrupole-time of flight (Q-TOF) mass spectrometer (Agilent) with an isolation window of 1.5 Da. Collision energies were individually optimized for each metabolite.

Wounding Experiments (Q-TOF)

Leaves from both the wild-type and *feronia* plants were wounded 3-4 times across the midvein of the leaves (Figure A2A). The leaves were harvested 15 minutes post-wounding and extracted as discussed above. For comparison, non-wounded leaves were also harvested and extracted. Dried extracts were weighed and re-suspended to a stock solution of 1.0 mg/mL with methanol. Prior to analysis, the leaf extracts were diluted 1:10 using methanol. In positive mode formic acid was added at a 0.1% final concentration and 10 mM ammonium formate was added to negative mode samples. The extracts (10 μL for each injection) were analyzed using a 6540 quadrupole-time of flight (Q-TOF) mass spectrometer (Agilent) in both positive and negative ion mode. Water/methanol (0.1% formic acid) 50:50 was used as the effluent solvent at a flow rate of 0.7 mL/min. MassHunter Quantitative Analysis (Agilent) was used for data analysis.

OPDA, dnOPDA, and JA Analysis (LC-MS)

Leaf extracts, combining several leaves per sample, were prepared similarly to Chung et al. with minor modifications (Chung *et al.*, 2008). Briefly, approximately 200 to 300 mg of leaf tissue was frozen in liquid nitrogen and a mortar and pestle was used to ground to the tissue to a powder. Then, after 1.25 mL of ethyl acetate was added to each vial the samples were briefly vortexed before being centrifuged at 10000 rpm for 10 minutes. The supernatant of each sample was transferred to a new separate microcentrifuge tube and the remaining pellets were re-extracted with 1 mL of ethyl acetate including the vortexing and centrifuging steps as before. Finally, the supernatants for each sample were combined and the solvent evaporated at 55 °C. The dried samples were stored at -80 °C until analysis. Before analysis all the samples were dissolved in 800 µL of 10% methanol:water (v/v).

These extracts (10 µL per injection) were analyzed in negative ion mode on an Agilent LC 1200 series system with a 6540 quadrupole-time of flight (Q-TOF) mass spectrometer. An Agilent Zorbax Eclipse XBD C18 column (1.8 µm, 4.6 x 150 mm) was used for the separation. A gradient from 10% to 90% methanol/0.1% formic acid (solvent B) was used with a flow rate of 0.4 mL/min over 12 minutes and then 90% solvent B was maintained for 10 minutes before 10% solvent B was reestablished. Peak areas for each analyte of interest were integrated and peak areas used for quantification. Jasmonic acid was calibrated using a jasmonic acid external calibration curve. OPDA and dnOPDA were calibrated using an OPDA external calibration curve. MassHunter Quantitative Analysis (Agilent) was used for data analysis.

Leaf Preparation for MALDI Mass Spectrometry Imaging

For fractured leaf samples (Klein *et al.*, 2015), leaves were placed on packing tape and dried under vacuum. Once dry, the tape is folded, enclosing the leaf between the tape, and passed through a rolling press. The tape pieces are pulled apart resulting in the leaf fracturing open to expose internal metabolites. The tape pieces were aligned on glass slides for analysis. Matrices were applied as follows: DHB was sublimated for 5 minutes at 140°C and the binary matrix DHB:Fe_3O_4 (75 mM:5 mM in IPA) was sprayed using an oscillating capillary nebulizer (OCN) (Korte *et al.*, 2015).

To obtain cross-sectional images, leaf pieces were embedded by placing them in a cryo-mold containing 10% w/v gelatin. Molds were transferred to a cryostat (CM1850; Leica Microsystems, Buffalo Grove, IL, USA) prechilled to -22 °C and allowed to equilibrate. Sections of 10 µm thickness were collected on tape windows (Leica Biosystems, Buffalo Grove, IL) and then taped to chilled plain glass slides. Samples were stored at -80 °C until needed. Before analysis, the slides were lyophilized under vacuum before matrix application. Matrices were applied as for fractured leaves.

Data was acquired using a MALDI-linear ion trap (LIT)-Orbitrap mass spectrometer (MALDI-LTQ-Orbitrap Discovery; Thermo Finnigan, San Jose, CA, USA) with an external frequency-tripled Nd:YAG laser (UVFQ; Elforlight Ltd., Daventry, UK). The laser energy was optimized for each matrix and 10 laser shots were used for every raster step. Raster steps of 100 µm or 30 µm were used for imaging of fractured leaves, and a raster step of 5 µm was used for the high-spatial resolution cross-sections.

All images shown were generated using ImageQuest (Thermo) with a ±0.01 Da mass tolerance with normalization to the TIC. The maximum and minimum values for a particular

metabolite in all sample types were set to the same values to facilitate comparisons. Peak assignments were made using accurate mass.

Isolating Arabidopside A and Bioassay

Arabidopside A was isolated from scaled up *feronia* nonpolar leaf extracts (as previously discussed) using an Agilent PrepStar SD-1 HPLC system. These extracts (2 mL per injection) were separated and collected using an Agilent Zorbax Eclipse XDB C18 column (21.1 mm x 250 mm x 7 μm) was used for the separation. A gradient using 80% methanol/20% water (solvent B) with a flow rate of 15 mL/min was employed to isolate the compound of interest. The solvent from the isolated Arabidopside A was evaporated under vacuum and the solid was stored at -84 °C until added to growth medium.

Four-day old wild-type and *feronia* mutant seedlings were transferred to petri dishes containing 1/2MS medium, medium containing 20 μM purified Arabidopside A dissolved in methanol, or medium containing 20 μM MGDG lipid standard in methanol. After four days, the roots from each genotype with each treatment were measured and compared. Root lengths measurements were carried out using ImageJ.

Acknowledgements

This work was supported by Iowa State University College of Liberal Arts and Sciences (LAS) Signature Research Initiative.

Short Legends for Supporting Information

Figure AS1. Comparison of representative mass spectra from wild-type and *fer* leaf nonpolar extracts using direct infusion FT-ICR MS

Figure AS2. Representative spectra from *feronia* mutant nonpolar leaf extracts displaying MGDG species

Figure AS3. Zoomed spectra of the nonpolar extract of *fer* mutant in positive mode showing structural relation of features

Figure AS4. MS/MS of three compounds significantly enriched in the nonpolar extract in negative mode

Figure AS5. Comparison of representative positive mode mass spectra from nonpolar leaf extracts with and without wounding obtained with direct injection Q-TOF MS

Figure AS6. Comparison of negative mode mass spectra from nonpolar leaf extracts with and without wounding obtained with direct injection Q-TOF MS

Figure AS7. Comparison of representative spectra from *fer* and wild-type leaf polar extracts in positive and negative ion mode using direct injection QTOF MS

Figure AS8. Mass spectrometry images of Arabidopsides in fractured *fer* and wild-type leaves

Table AS1. Mass lists corresponding to the PMR volcano plot in Figure A1A for wild-type and *feronia* nonpolar leaf extracts in positive and negative modes

Appendix S1. A series of biomarker peaks in the nonpolar positive mode precursor spectrum

Appendix S2. MS/MS characterization of Arabidopsides

References

Andersson, M.X., Hamberg, M., Kourtchenko, O., Brunnström, Å., McPhail, K.L., Gerwick, W.H., Göbel, C., Feussner, I. and Ellerström, M. (2006) Oxylipin Profiling of the Hypersensitive Response in Arabidopsis thaliana: FORMATION OF A NOVEL OXO-PHYTODIENOIC ACID-CONTAINING GALACTOLIPID, ARABIDOPSIDE E. *Journal of Biological Chemistry*, 281, 31528-31537.

Asada, K. (2006) Production and Scavenging of Reactive Oxygen Species in Chloroplasts and Their Functions. *Plant Physiology*, 141, 391.

Berger, P., Adelman, N.B., Beckman, K.J., Campbell, D.J., Ellis, A.B. and Lisensky, G.C. (1999) Preparation and Properties of an Aqueous Ferrofluid. *Journal of Chemical Education*, 76, 943.

Bligh, E.G. and Dyer, W.J. (1959) A RAPID METHOD OF TOTAL LIPID EXTRACTION AND PURIFICATION. *Canadian Journal of Biochemistry and Physiology*, 37, 911-917.

Buseman, C.M., Tamura, P., Sparks, A.A., Baughman, E.J., Maatta, S., Zhao, J., Roth, M.R., Esch, S.W., Shah, J., Williams, T.D. and Welti, R. (2006) Wounding Stimulates the Accumulation of Glycerolipids Containing Oxophytodienoic Acid and Dinor-Oxophytodienoic Acid in Arabidopsis Leaves. *Plant Physiology*, 142, 28.

Caplan, Jeffrey L., Kumar, Amutha S., Park, E., Padmanabhan, Meenu S., Hoban, K., Modla, S., Czymmek, K. and Dinesh-Kumar, Savithramma P. (2015) Chloroplast Stromules Function during Innate Immunity. *Developmental Cell*, 34, 45-57.

Chen, J., Yu, F., Liu, Y., Du, C., Li, X., Zhu, S., Wang, X., Lan, W., Rodriguez, P.L., Liu, X., Li, D., Chen, L. and Luan, S. (2016) FERONIA interacts with ABI2-type phosphatases to facilitate signaling cross-talk between abscisic acid and RALF peptide in Arabidopsis. *Proc Natl Acad Sci U S A*, 113, E5519-5527.

Chung, H.S., Koo, A.J.K., Gao, X., Jayanty, S., Thines, B., Jones, A.D. and Howe, G.A. (2008) Regulation and Function of Arabidopsis JASMONATE ZIM-Domain Genes in Response to Wounding and Herbivory. *Plant Physiology*, 146, 952-964.

Dempsey, D.M.A., Vlot, A.C., Wildermuth, M.C. and Klessig, D.F. (2011) Salicylic Acid Biosynthesis and Metabolism. *The Arabidopsis Book / American Society of Plant Biologists*, 9, e0156.

Deslauriers, S.D. and Larsen, P.B. (2010) FERONIA is a key modulator of brassinosteroid and ethylene responsiveness in Arabidopsis hypocotyls. *Mol Plant*, 3, 626-640.

Du, C., Li, X., Chen, J., Chen, W., Li, B., Li, C., Wang, L., Li, J., Zhao, X., Lin, J., Liu, X., Luan, S. and Yu, F. (2016) Receptor kinase complex transmits RALF peptide signal to inhibit root growth in Arabidopsis. *Proc Natl Acad Sci U S A*, 113, E8326-E8334.

Duan, Q., Kita, D., Li, C., Cheung, A.Y. and Wu, H.M. (2010) FERONIA receptor-like kinase regulates RHO GTPase signaling of root hair development. *Proc Natl Acad Sci U S A*, 107, 17821-17826.

Escobar-Restrepo, J.-M., Huck, N., Kessler, S., Gagliardini, V., Gheyselinck, J., Yang, W.-C. and Grossniklaus, U. (2007) The FERONIA Receptor-like Kinase Mediates Male-Female Interactions during Pollen Tube Reception. *Science*, 317, 656-660.

Gang, K.-Q., Zhou, D.-Y., Lu, T., Liu, Z.-Y., Zhao, Q., Xie, H.-K., Song, L. and Shahidi, F. (2018) Direct infusion mass spectrometric identification of molecular species of glycerophospholipid in three species of edible whelk from Yellow Sea. *Food Chemistry*, 245, 53-60.

González-Domínguez, R. (2017) Metabolomic Fingerprinting of Blood Samples by Direct Infusion Mass Spectrometry: Application in Alzheimer's Disease Research. *Journal of Analysis and Testing*, 1, 1-9.

Guo, H., Li, L., Ye, H., Yu, X., Algreen, A. and Yin, Y. (2009a) Three related receptor-like kinases are required for optimal cell elongation in Arabidopsis thaliana. *Proc Natl Acad Sci U S A*, 106, 7648-7653.

Guo, H., Nolan, T.M., Song, G., Liu, S., Xie, Z., Chen, J., Schnable, P.S., Walley, J.W. and Yin, Y. (2018) FERONIA Receptor Kinase Contributes to Plant Immunity by Suppressing Jasmonic Acid Signaling in *Arabidopsis thaliana*. *Current Biology 28*, 3316-3324 e3316.

Guo, H., Ye, H., Li, L. and Yin, Y. (2009b) A family of receptor-like kinases are regulated by BES1 and involved in plant growth in Arabidopsis thaliana. *Plant Signal Behav*, 4, 784-786.

Hartley, S.E., Eschen, R., Horwood, J.M., Gange, A.C. and Hill, E.M. (2015) Infection by a foliar endophyte elicits novel arabidopside-based plant defence reactions in its host, Cirsium arvense. *New Phytologist*, 205, 816-827.

Haruta, M., Sabat, G., Stecker, K., Minkoff, B.B. and Sussman, M.R. (2014) A Peptide Hormone and Its Receptor Protein Kinase Regulate Plant Cell Expansion. *Science*, 343, 408.

Hisamatsu, Y., Goto, N., Hasegawa, K. and Shigemori, H. (2003) Arabidopsides A and B, two new oxylipins from Arabidopsis thaliana. *Tetrahedron Letters*, 44, 5553-5556.

Hisamatsu, Y., Goto, N., Sekiguchi, M., Hasegawa, K. and Shigemori, H. (2005) Oxylipins Arabidopsides C and D from Arabidopsis thaliana. *Journal of Natural Products*, 68, 600-603.

Hématy, K. and Höfte, H. (2008) Novel receptor kinases involved in growth regulation. *Current Opinion in Plant Biology*, 11, 321-328.

Ibrahim, A., Schütz, A.-L., Galano, J.-M., Herrfurth, C., Feussner, K., Durand, T., Brodhun, F. and Feussner, I. (2011) The Alphabet of Galactolipids in Arabidopsis thaliana. *Frontiers in Plant Science*, 2, 95.

Keinath, N.F., Kierszniowska, S., Lorek, J., Bourdais, G., Kessler, S.A., Shimosato-Asano, H., Grossniklaus, U., Schulze, W.X., Robatzek, S. and Panstruga, R. (2010) PAMP (pathogen-associated molecular pattern)-induced changes in plasma membrane compartmentalization reveal novel components of plant immunity. *J Biol Chem*, 285, 39140-39149.

Kessler, S.A., Shimosato-Asano, H., Keinath, N.F., Wuest, S.E., Ingram, G., Panstruga, R. and Grossniklaus, U. (2010) Conserved molecular components for pollen tube reception and fungal invasion. *Science*, 330, 968-971.

Klein, A.T., Yagnik, G.B., Hohenstein, J.D., Ji, Z., Zi, J., Reichert, M.D., MacIntosh, G.C., Yang, B., Peters, R.J., Vela, J. and Lee, Y.J. (2015) Investigation of the Chemical Interface in the Soybean–Aphid and Rice–Bacteria Interactions Using MALDI-Mass Spectrometry Imaging. *Analytical Chemistry*, 87, 5294-5301.

Koo, A.J.K., Gao, X., Daniel Jones, A. and Howe, G.A. (2009) A rapid wound signal activates the systemic synthesis of bioactive jasmonates in Arabidopsis. *The Plant Journal*, 59, 974-986.

Korte, A.R., Yagnik, G.B., Feenstra, A.D. and Lee, Y.J. (2015) Multiplex MALDI-MS Imaging of Plant Metabolites Using a Hybrid MS System. In *Mass Spectrometry Imaging of Small Molecules* (He, L. ed. New York, NY: Springer New York, pp. 49-62.

Kourtchenko, O., Andersson, M.X., Hamberg, M., Brunnström, Å., Göbel, C., McPhail, K.L., Gerwick, W.H., Feussner, I. and Ellerström, M. (2007) Oxo-Phytodienoic Acid-Containing Galactolipids in Arabidopsis: Jasmonate Signaling Dependence. *Plant Physiology*, 145, 1658.

Li, C., Yeh, F.L., Cheung, A.Y., Duan, Q., Kita, D., Liu, M.C., Maman, J., Luu, E.J., Wu, B.W., Gates, L., Jalal, M., Kwong, A., Carpenter, H. and Wu, H.M. (2015) Glycosylphosphatidylinositol-anchored proteins as chaperones and co-receptors for FERONIA receptor kinase signaling in Arabidopsis. *Elife*, 4.

Liao, H., Tang, R., Zhang, X., Luan, S. and Yu, F. (2017) FERONIA Receptor Kinase at the Crossroads of Hormone Signaling and Stress Responses. *Plant Cell Physiol*, 58, 1143-1150.

Mao, D., Yu, F., Li, J., Van de Poel, B., Tan, D., Li, J., Liu, Y., Li, X., Dong, M., Chen, L., Li, D. and Luan, S. (2015) FERONIA receptor kinase interacts with S-adenosylmethionine synthetase and suppresses S-adenosylmethionine production and ethylene biosynthesis in Arabidopsis. *Plant Cell Environ*, 38, 2566-2574.

Nilsson, A.K., Fahlberg, P., Ellerström, M. and Andersson, M.X. (2012) Oxo-phytodienoic acid (OPDA) is formed on fatty acids esterified to galactolipids after tissue disruption in Arabidopsis thaliana. *FEBS Letters*, 586, 2483-2487.

Nilsson, A.K., Johansson, O.N., Fahlberg, P., Steinhart, F., Gustavsson, M.B., Ellerström, M. and Andersson, M.X. (2014) Formation of oxidized phosphatidylinositol and 12-oxo-phytodienoic acid containing acylated phosphatidylglycerol during the hypersensitive response in Arabidopsis. *Phytochemistry*, 101, 65-75.

Ohashi, T., Ito, Y., Okada, M. and Sakagami, Y. (2005) Isolation and stomatal opening activity of two oxylipins from Ipomoea tricolor. *Bioorganic & Medicinal Chemistry Letters*, 15, 263-265.

Stegmann, M., Monaghan, J., Smakowska-Luzan, E., Rovenich, H., Lehner, A., Holton, N., Belkhadir, Y. and Zipfel, C. (2017) The receptor kinase FER is a RALF-regulated scaffold controlling plant immune signaling. *Science*, 355, 287-289.

Stelmach, B.A., Müller, A., Hennig, P., Gebhardt, S., Schubert-Zsilavecz, M. and Weiler, E.W. (2001) A Novel Class of Oxylipins,sn1-O-(12-Oxophytodienoyl)-sn2-O-(hexadecatrienoyl)-monogalactosyl Diglyceride, from Arabidopsis thaliana. *Journal of Biological Chemistry*, 276, 12832-12838.

Stintzi, A., Weber, H., Reymond, P., Browse, J. and Farmer, E.E. (2001) Plant defense in the absence of jasmonic acid: The role of cyclopentenones. *Proceedings of the National Academy of Sciences*, 98, 12837-12842.

Vu, H.S., Roston, R., Shiva, S., Hur, M., Wurtele, E.S., Wang, X., Shah, J. and Welti, R. (2015) Modifications of membrane lipids in response to wounding of Arabidopsis thaliana leaves. *Plant Signaling & Behavior*, 10, e1056422.

Vu, H.S., Tamura, P., Galeva, N.A., Chaturvedi, R., Roth, M.R., Williams, T.D., Wang, X., Shah, J. and Welti, R. (2012) Direct Infusion Mass Spectrometry of Oxylipin-Containing Arabidopsis Membrane Lipids Reveals Varied Patterns in Different Stress Responses. *Plant Physiology*, 158, 324.

Wasternack, C. (2007) Jasmonates: An Update on Biosynthesis, Signal Transduction and Action in Plant Stress Response, Growth and Development. *Annals of Botany*, 100, 681-697.

Yang, T., Wang, L., Li, C., Liu, Y., Zhu, S., Qi, Y., Liu, X., Lin, Q., Luan, S. and Yu, F. (2015) Receptor protein kinase FERONIA controls leaf starch accumulation by interacting with glyceraldehyde-3-phosphate dehydrogenase. *Biochem Biophys Res Commun*, 465, 77-82.

Yu, F., Qian, L., Nibau, C., Duan, Q., Kita, D., Levasseur, K., Li, X., Lu, C., Li, H., Hou, C., Li, L., Buchanan, B.B., Chen, L., Cheung, A.Y., Li, D. and Luan, S. (2012) FERONIA receptor kinase pathway suppresses abscisic acid signaling in Arabidopsis by activating ABI2 phosphatase. *Proc Natl Acad Sci U S A*, 109, 14693-14698.

Zábranská, M., Vrkoslav, V., Sobotníková, J. and Cvačka, J. (2012) Analysis of plant galactolipids by reversed-phase high-performance liquid chromatography/mass spectrometry with accurate mass measurement. *Chemistry and Physics of Lipids*, 165, 601-607.

Figures

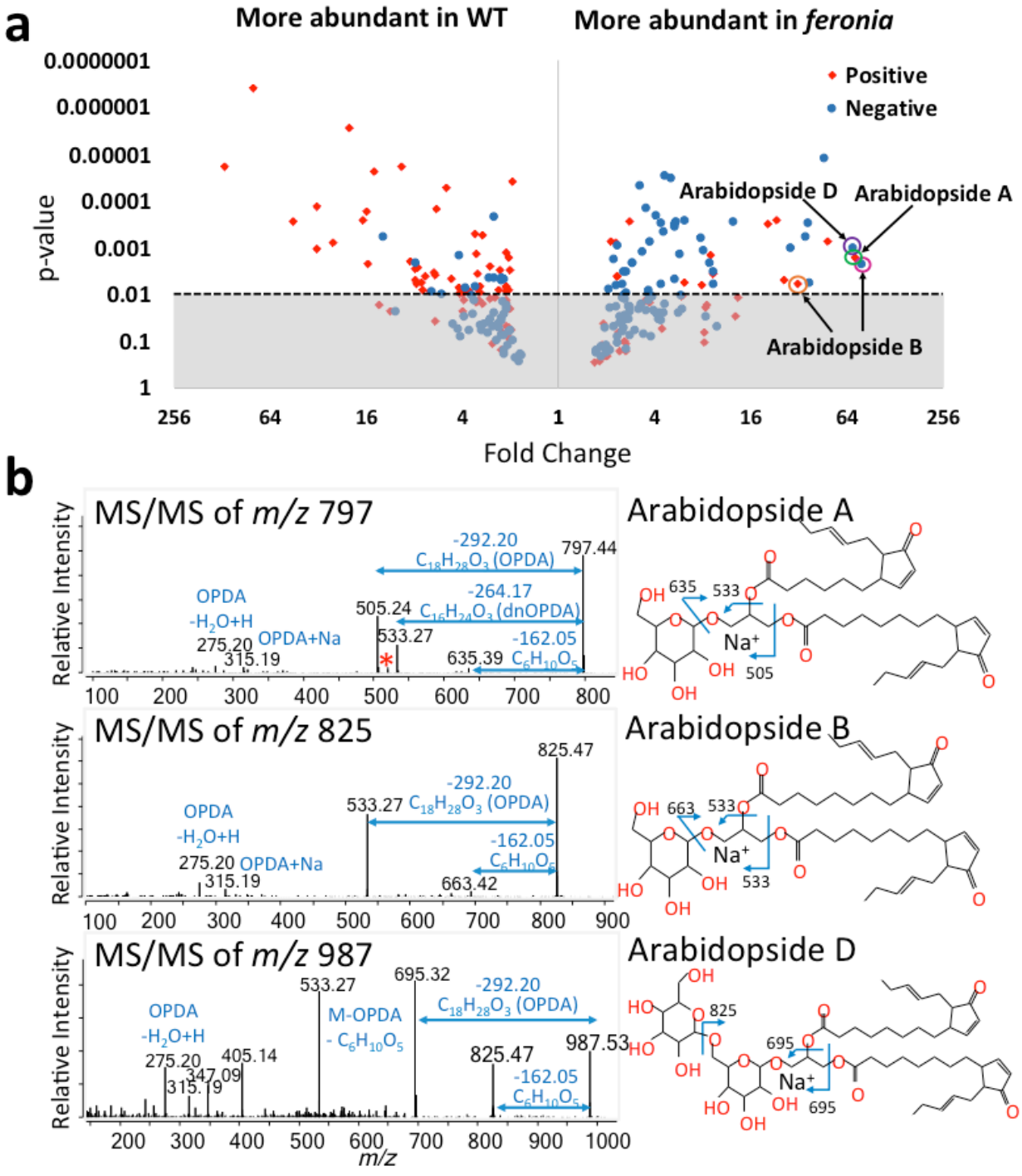
a
More abundant in WT
More abundant in feronia
Positive
Negative
Arabidopside D
Arabidopside A
Arabidopside B
p-value
0.0000001
0.000001
0.00001
0.0001
0.001
0.01
0.1
1
256
64
16
4
1
4
16
64
256
Fold Change
b
MS/MS of m/z 797
Relative Intensity
-292.20
C18H28O3 (OPDA)
797.44
OPDA
-H2O+H
275.20
315.19
OPDA+Na
505.24
-264.17
C16H24O3 (dnOPDA)
533.27
-162.05
C6H10O5
635.39
Arabidopside A
635
533
505
Na+
MS/MS of m/z 825
825.47
533.27
663.42
Arabidopside B
663
MS/MS of m/z 987
695.32
M-OPDA
- C6H10O5
987.53
405.14
347.09
315.19
695
m/z

Figure A1. a) Volcano plot displaying the p-value versus fold change for *m/z* values in the mass spectra of the nonpolar leaf extracts in both ion modes. Points on the left-hand side of the chart indicate the signal intensity of the metabolite is greater in the wild-type leaves whereas points on the right-hand side indicate metabolites whose signal intensity is greater in *feronia* leaves. Colored circles represent potentially important metabolites: green circle – *m/z* 797.45, fold change 71, p-value 0.0018; orange circle – *m/z* 825.48, fold change 31, p-value 0.0067; pink circle – *m/z* 847.49, fold change 79, p-value 0.0027; purple circle – *m/z* 1009.54, fold change 70, p-value 0.0012. The remaining data points are noted in Table AS1. This volcano plot was produced using The Plant/Eukaryotic and Microbial Systems Resource (PMR) database. **b) MS/MS of three Arabidopside compounds in positive ion mode.** All species are seen as sodiated adducts. Some fragments are annotated on the Arabidopside structures as well as in the MS/MS spectra. * = MGDG (18:3/18:3) fragment corresponding to the loss of 18:3 fatty acid.

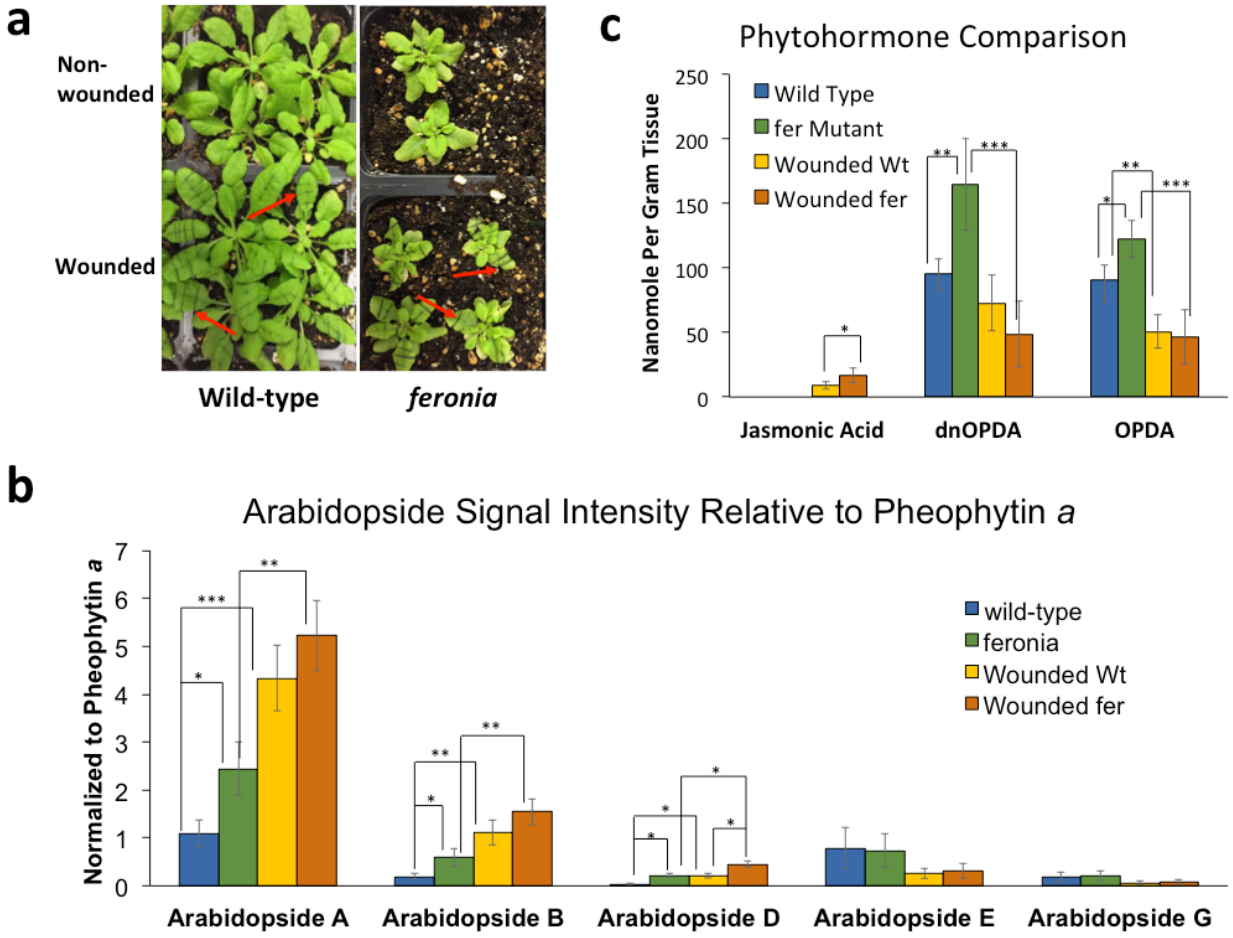

Figure A2. a) Photo of wild-type and *feronia* leaves after wounding 3-4 times across the midvein. Red arrows indicate example wounding sites. **b) Arabidopside signal intensities relative to pheophytin a signal in *feronia* mutant and wild-type leaf extracts with and without wounding**. Error bars indicate standard deviation, and n=6 for all samples. **c) Quantification of jasmonic acid, dinor-oxo-phytodienoic acid (dnOPDA), and oxo-phytodienoic acid (OPDA) using LC-Q-TOF MS.** The levels of JA, OPDA and dnOPDA are compared in wild-type and *feronia* wounded and non-wounded nonpolar leaf extracts. Error bars indicate standard deviation, and n=4 for all samples. In both panels B and C, * signifies p-value < 0.05, ** signifies p-value < 0.01, *** signifies p-value < 0.001.

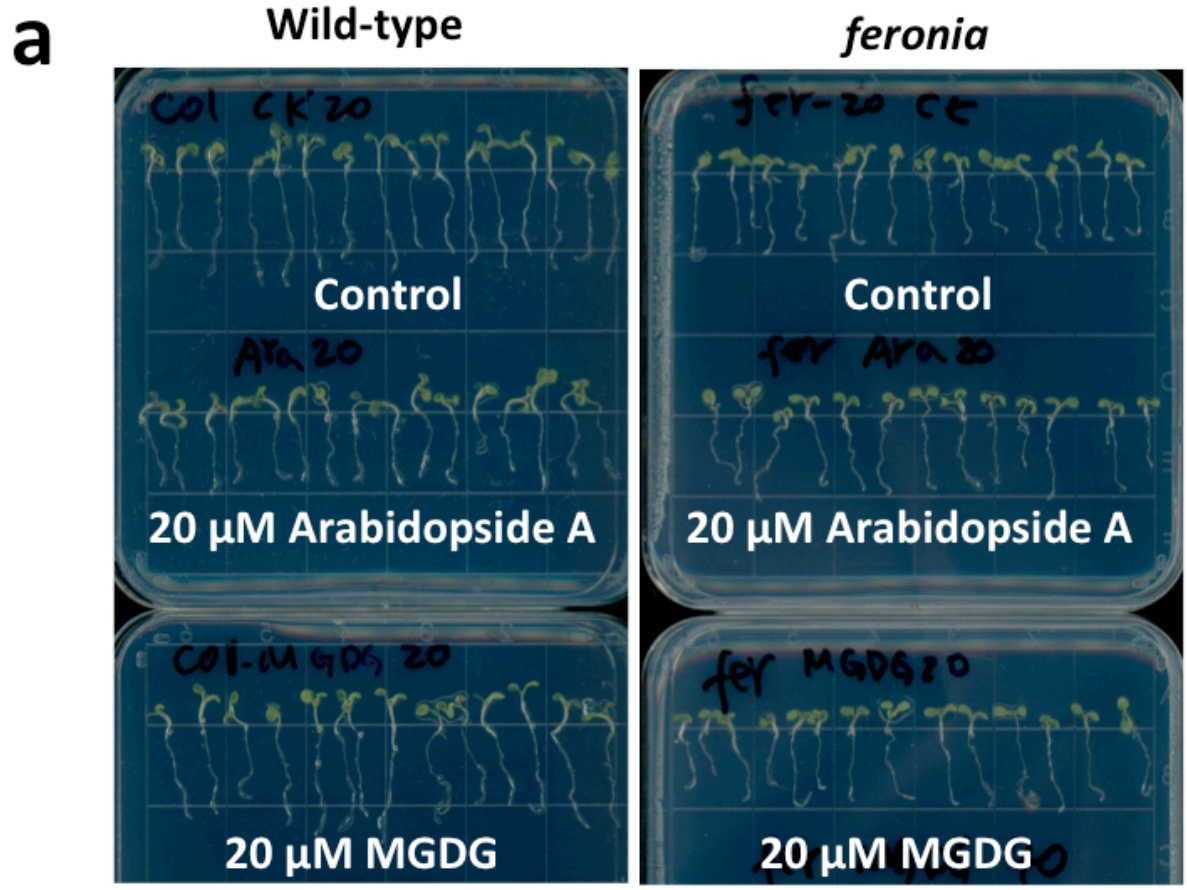
a
Wild-type
feronia
Control
20 µM Arabidopside A
20 µM MGDG
Control
20 µM Arabidopside A
20 µM MGDG

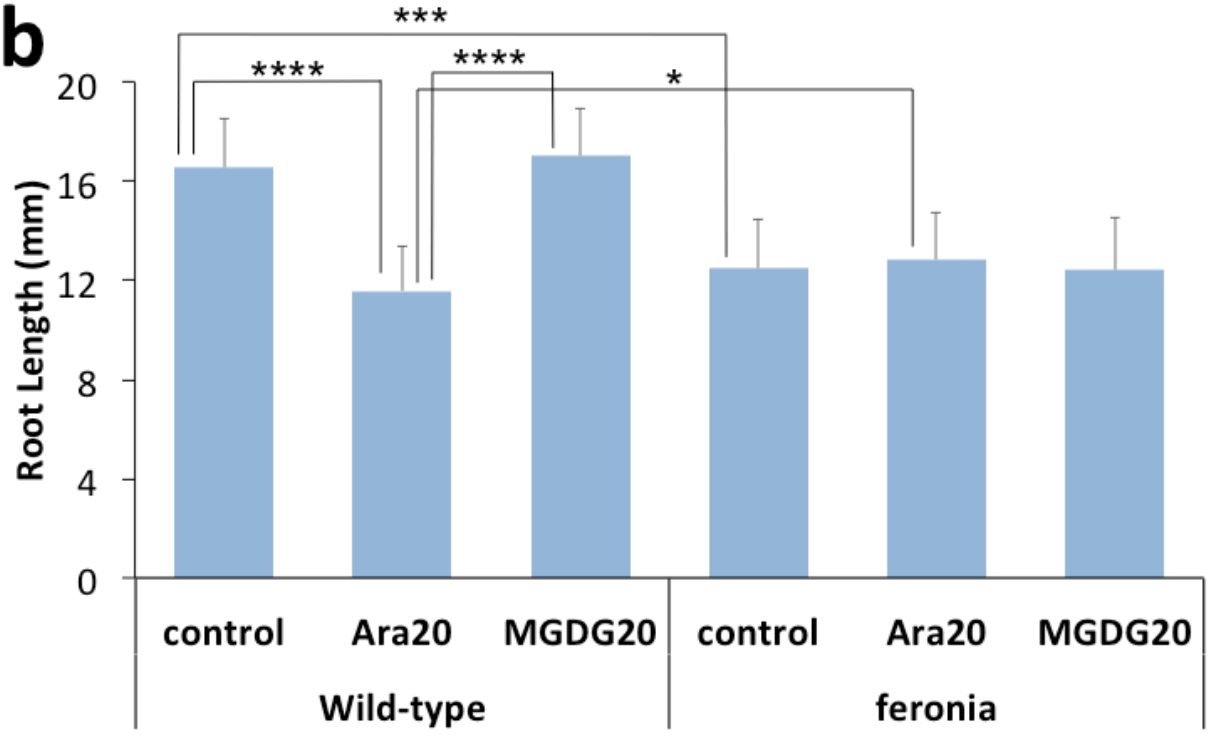
b
***
****
****
*
Root Length (mm)
0
4
8
12
16
20
control
Ara20
MGDG20
control
Ara20
MGDG20
Wild-type
feronia

Figure A3. a) Photo of roots from biological assay. b) Comparison of root length for wild-type and feronia mutant plants with and without exposure to Arabidopside A or MGDG. Control = grown in medium, Ara20 = grown in medium with 20μM Arabidopside A. MGDG 20 = grown in medium with 20μM MGDG. * signifies p-value < 0.05, ** signifies p-value < 0.01, *** signifies p-value < 0.001., **** signifies p-value < 0.0001. Error bars indicate standard deviation and n=13-16.

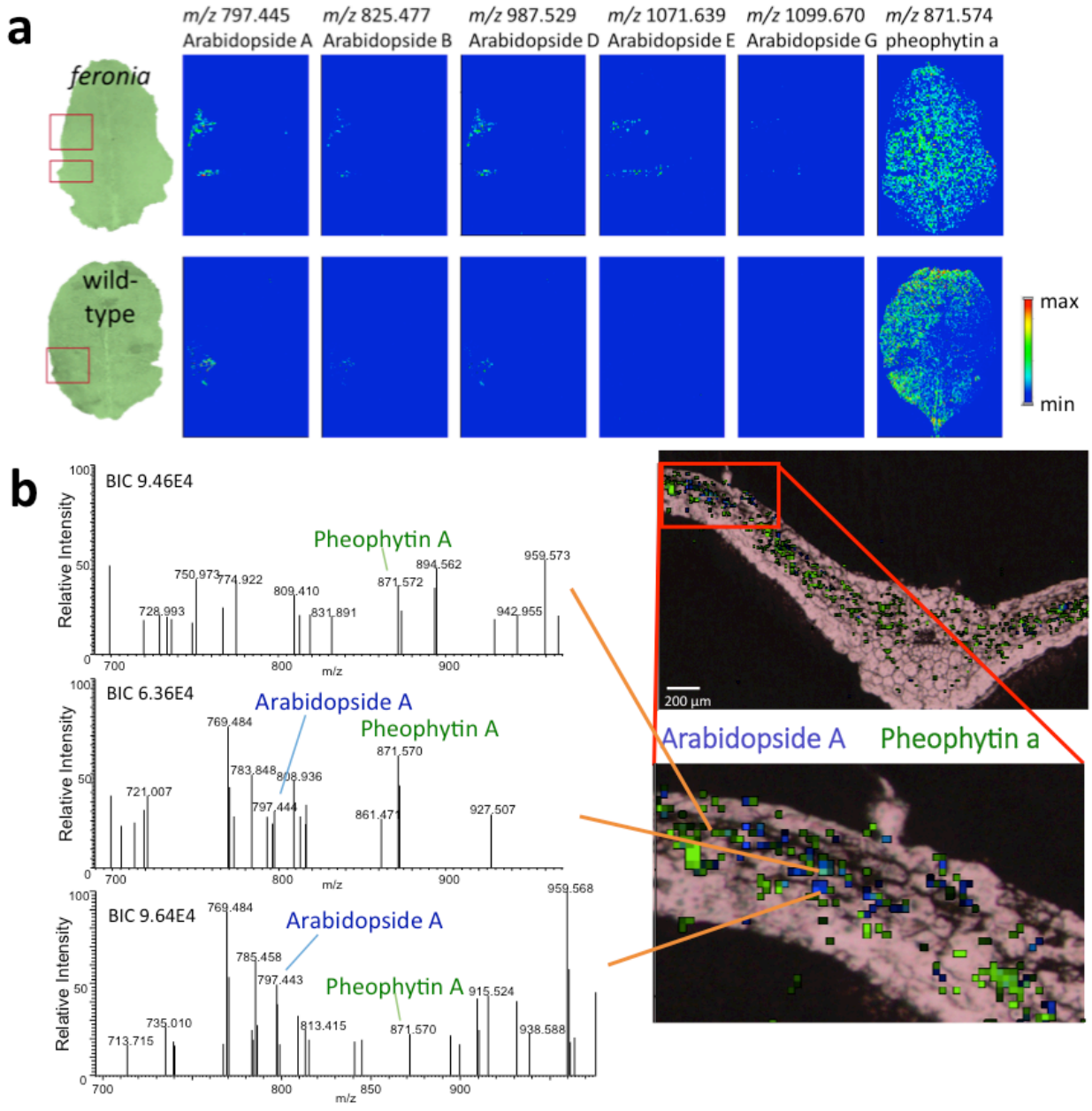

Figure A4. a) Mass spectrometry images of Arabidopsides in fractured *feronia* and wild-type leaves. The family of Arabidopside compounds show localizations in wounded areas. The top row displays images of a *feronia* leaf and the bottom row images of a wild-type leaf. Samples were imaged at 100 µm spatial resolution using DHB as a matrix. Red boxes indicate mechanical wounding locations. **b) High-resolution MSI of a non-wounded *feronia* mutant leaf cross-section.** Single spectra on the left correspond to single pixels in the MSI overlay of

pheophytin a (green) and Arabidopside A (blue). The single pixel spectra suggest that Arabidopsides (when present) are co-localized with pheophytin a, a chloroplast-related compound. Samples were imaged at 5 μm spatial resolution using a binary Fe_3O_4:DHB matrix.

Supplementary Discussion

Appendix S1. A series of biomarker peaks in the nonpolar positive mode precursor spectra

The mass spectrum of the feronia mutant nonpolar leaf extract is closely interpreted in Figure AS2.

In the case of m/z 813.42 and 797.45, there is a mass difference of 15.97 Da, the same mass difference between K and Na, suggesting the two are potassium and sodium adducts, respectively of the same compound. Between m/z 797.45 and 825.48, as well as m/z 1071.64 and 1099.67, there is a mass difference of 28.03 Da corresponding to C2H4, which is typically seen for a series of lipid species (e.g., palmitic (16:0) vs stearic (18:0) acid). Additionally, there is a mass difference of 274.19 Da (C18H26O2) between m/z 1071.64 and 797.45, and between m/z 1099.67 and 825.48, suggesting both metabolites have a common side chain. Finally there is a mass difference of 162.05 Da (C6H10O5) between m/z 987.53 and 825.48, which matches the chemical composition of a glucosyl/galactosyl group. Theapparent structural relationships in this series of peaks indicate they might be a series of sugarcontaining lipid species, and potentially related to FERONIA.

Appendix S2. MS/MS characterization of Arabidopside.

In the three MS/MS spectra of Arabidopside A, B, and D (Figure A1B), commonalities include neutral losses of 162.05 Da (C6H10O5, galactosyl) and 292.20 (C18H28O3, 12-oxo-

phytodienoic acid (OPDA)). Additionally, m/z 275.20 and 315.19 are present in all three MS/MS spectra which correspond to OPDA related peaks. Finally, m/z 533.27 is present in all the spectra and are annotated as a loss of dinor-OPDA (dnOPDA, 264.17 Da) in Arabidopside A, a loss of OPDA in Arabidopside B (292.20 Da), and a loss of OPDA and galactosyl group (454.25 Da) in Arabidopside D. In the MS/MS spectrum of m/z 797, the mass difference of 28.03 Da between m/z 533.27 and 505.24 corresponds to the two carbon chain length difference between OPDA and dnOPDA. In negative ion mode, the formate adducts of these three Arabidopsides can also be found (Figure AS3). All have the characteristic peak at m/z 291.20 which corresponds to OPDA, as well as the neutral loss of formic acid, resulting in the deprotonated molecules, [M-H]-. Assignments of other fragments are shown in Figure AS3.

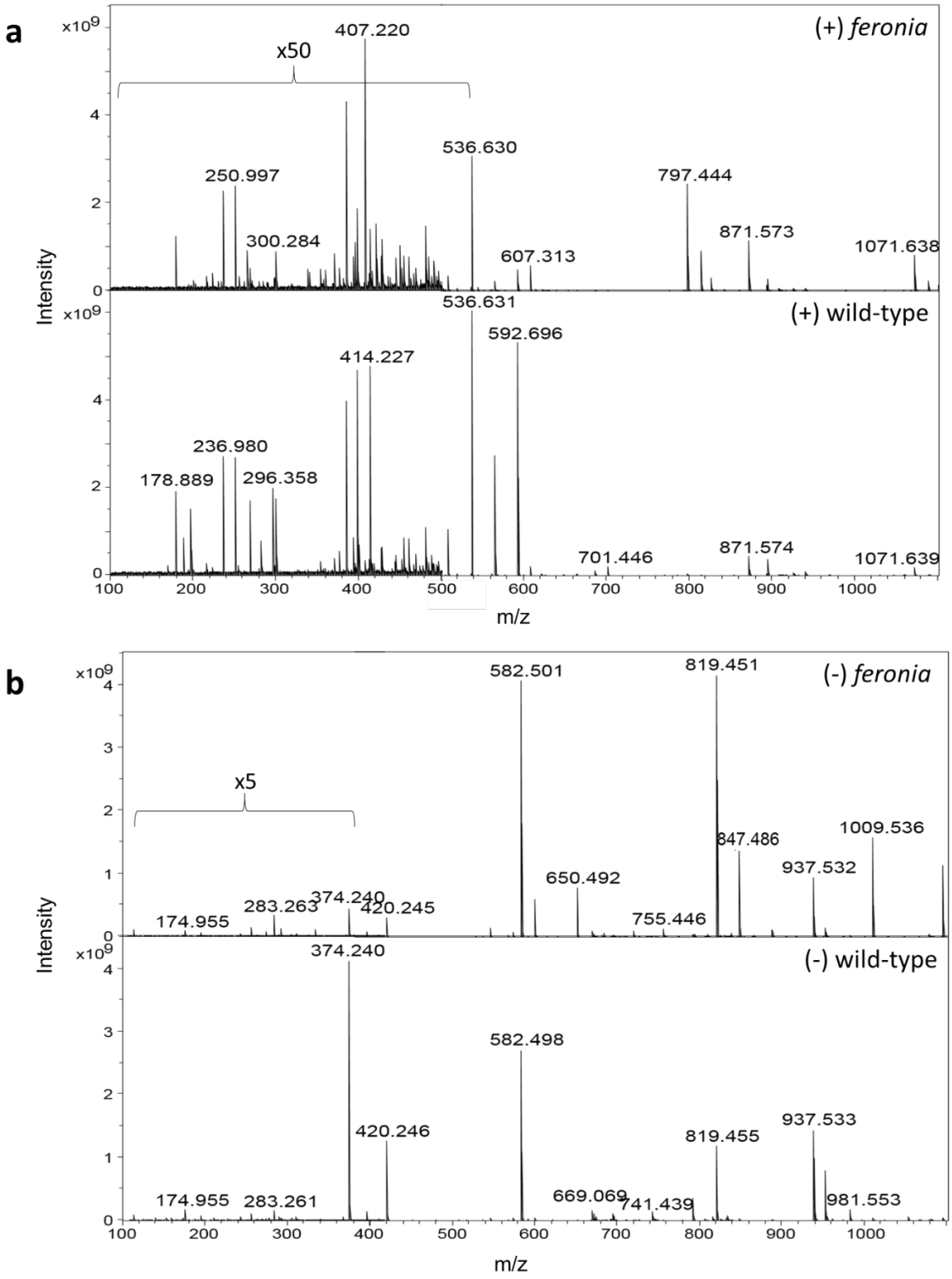

Figure AS1. Comparison of representative mass spectra from wild-type and *fer* leaf nonpolar extracts using direct infusion FT-ICR MS. a) Positive ion mode spectra of *fer*

mutant (top) and wild-type (bottom) and b) negative ion mode spectra of *fer* (top) and wild-type (bottom).

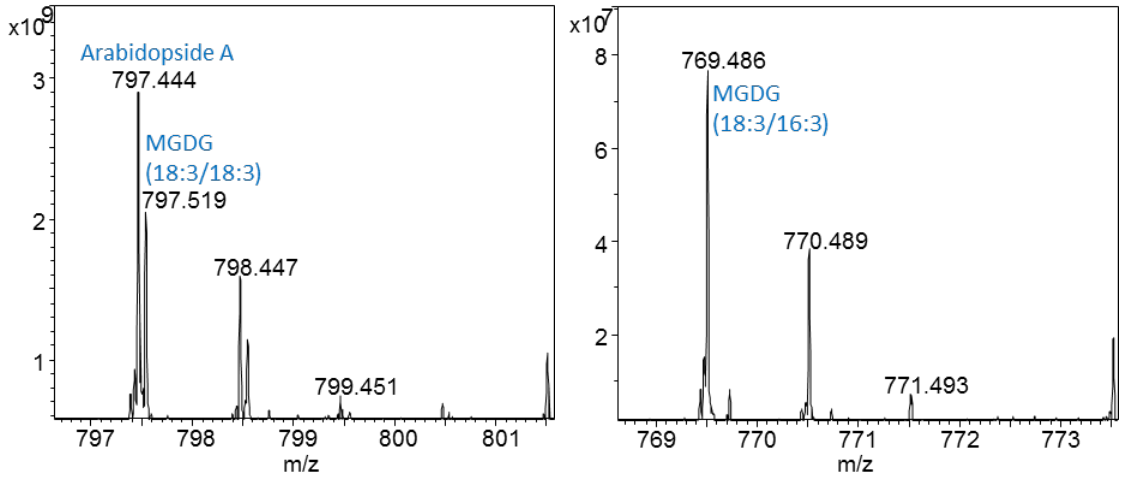

Figure AS2. Representative spectra from *feronia* mutant nonpolar leaf extracts displaying MGDG species. a) Zoomed in spectrum showing Arabidopside A (m/z 797.444) and MGDG (18:3/18:3) (m/z 797.519) are both present and b) MGDG (16:3/18:3) (m/z 769.486). MGDG species are detected, although not easily visualized in spectra covering a wide mass range.

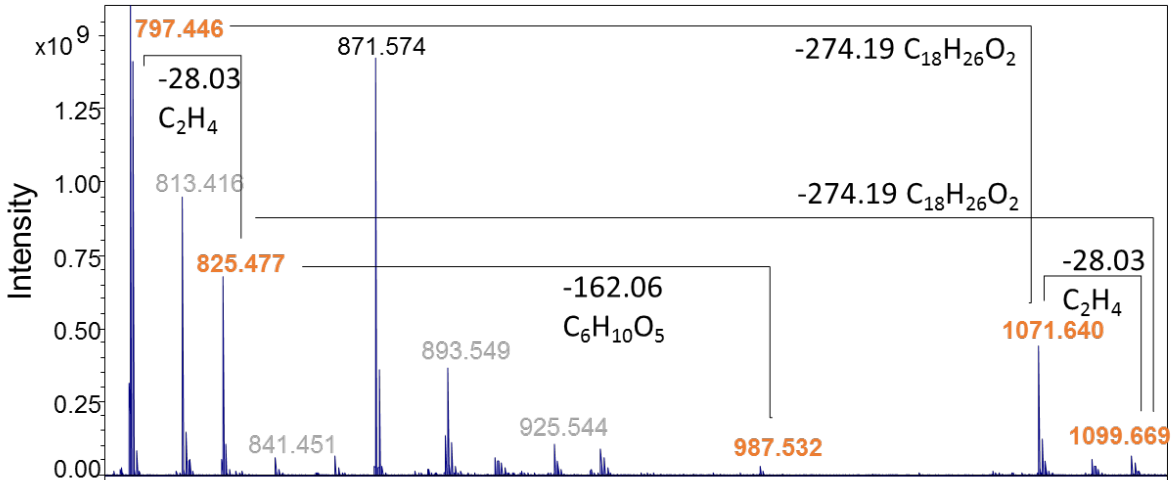

Figure AS3. Zoomed spectra of the nonpolar extract of *fer* mutant in positive mode showing structural relation of features. A series of peaks that are more abundant in the *fer* mutant includes repeating differences of C_2H_4 (28.03 Da), $C_6H_{10}O_5$ (162.06 Da, a monosaccharide), and $C_{18}H_{26}O_2$ (274.19 Da).

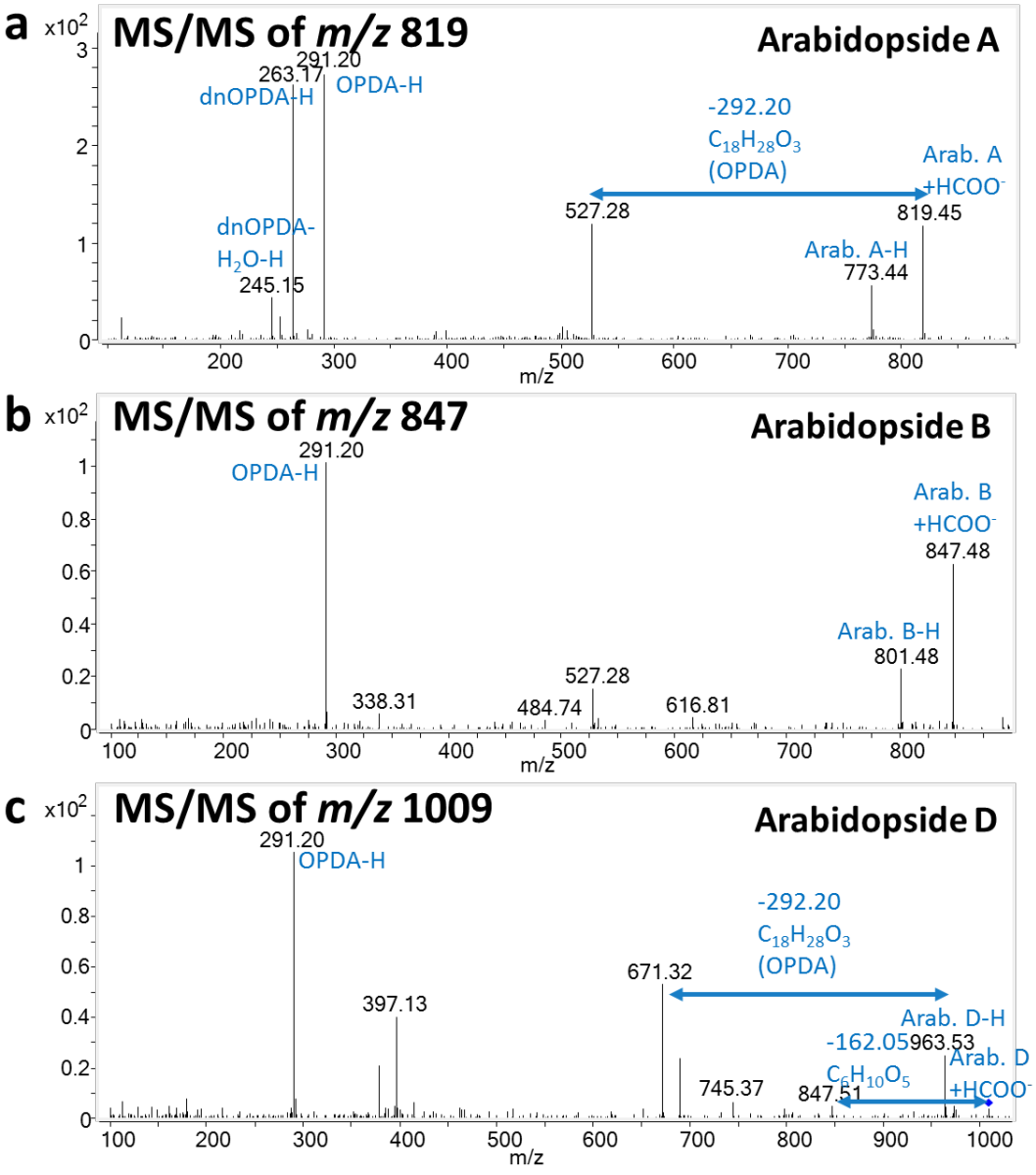

Figure AS4. MS/MS of three compounds significantly enriched in the nonpolar extract in

negative mode. All species are formate ($HCOO^-$) adducts. a) Arabidopside A, b) Arabidopside B, and c) Arabidopside D.

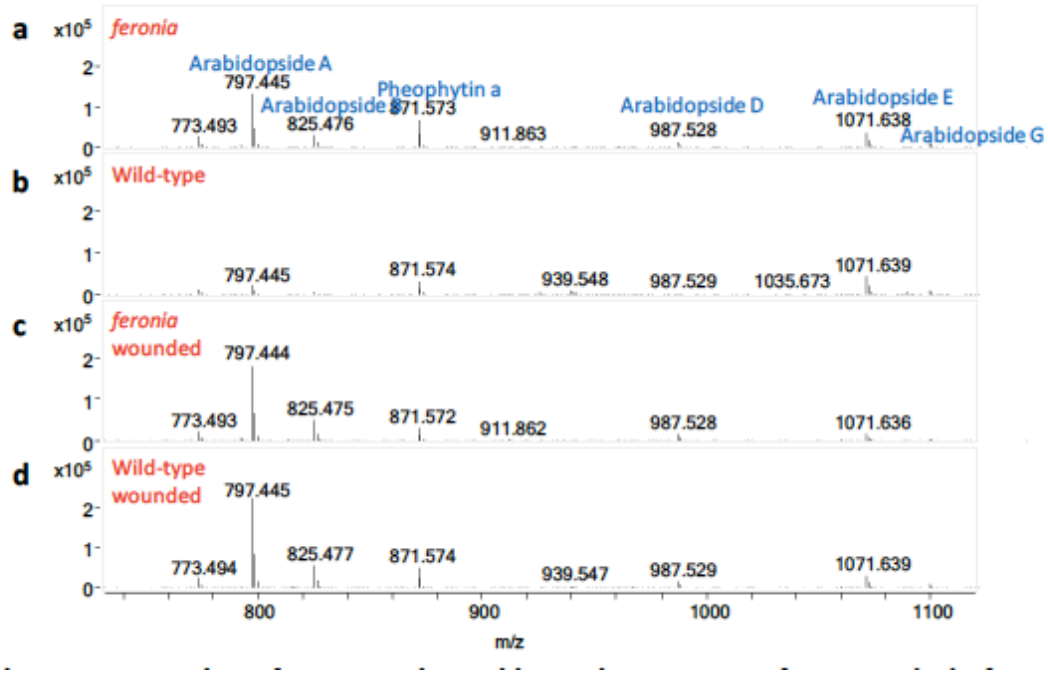

Figure AS5. Comparison of representative positive mode mass spectra from nonpolar leaf extracts with and without wounding obtained with direct injection Q-TOF MS. a) *fer* non-wounded, b) wild-type non-wounded, c) *fer* 15-minutes post-wounding, and d) wild-type 15-minutes post-wounding. Multiple Arabidopsides were detected as labeled in panel A.

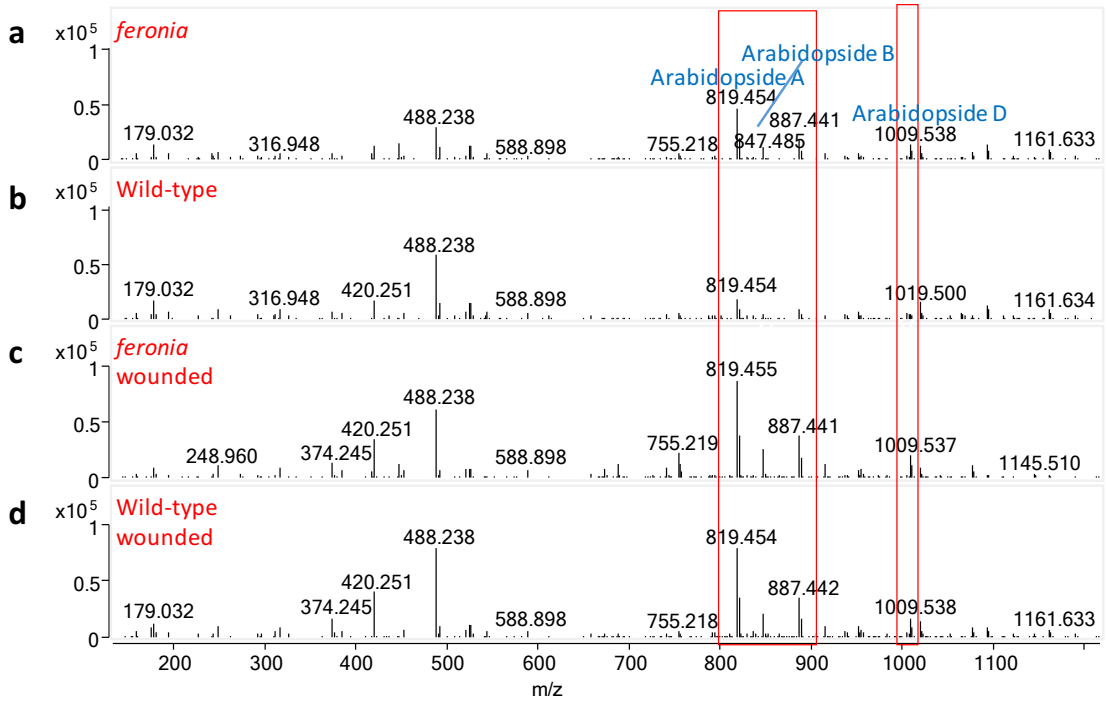

Figure AS6. Comparison of negative mode mass spectra from nonpolar leaf extracts with and without wounding obtained with direct injection Q-TOF MS. a) *fer* non-wounded, b) wild-type non-wounded, c) *fer* 15-minutes post-wounding, and d) wild-type 15-minutes post-wounding. Red boxes indicate metabolites that increase in both genotypes after wounding.

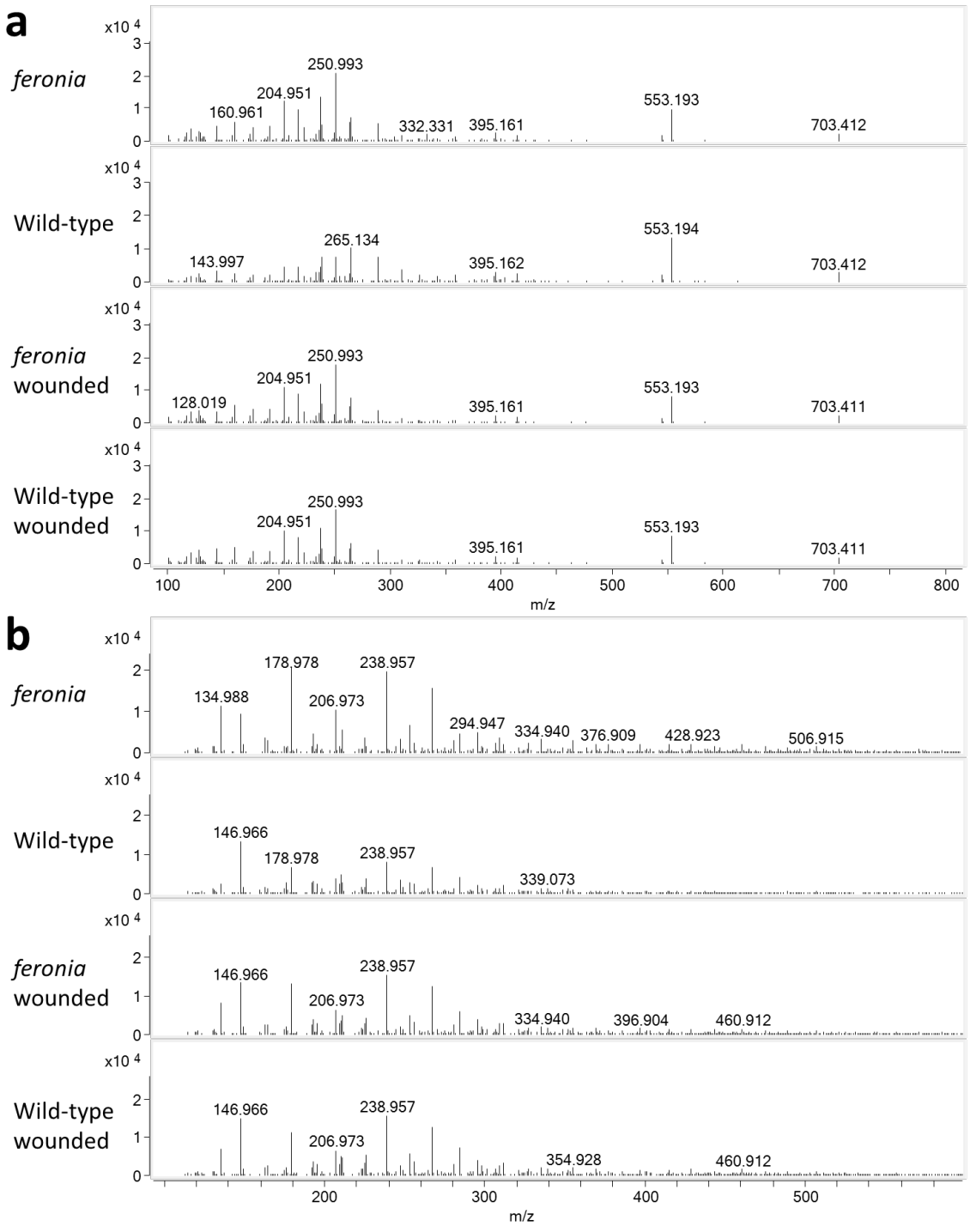

Figure AS7. Comparison of representative spectra from *fer* and wild-type leaf polar extracts in a) positive and b) negative ion mode using direct injection QTOF MS.

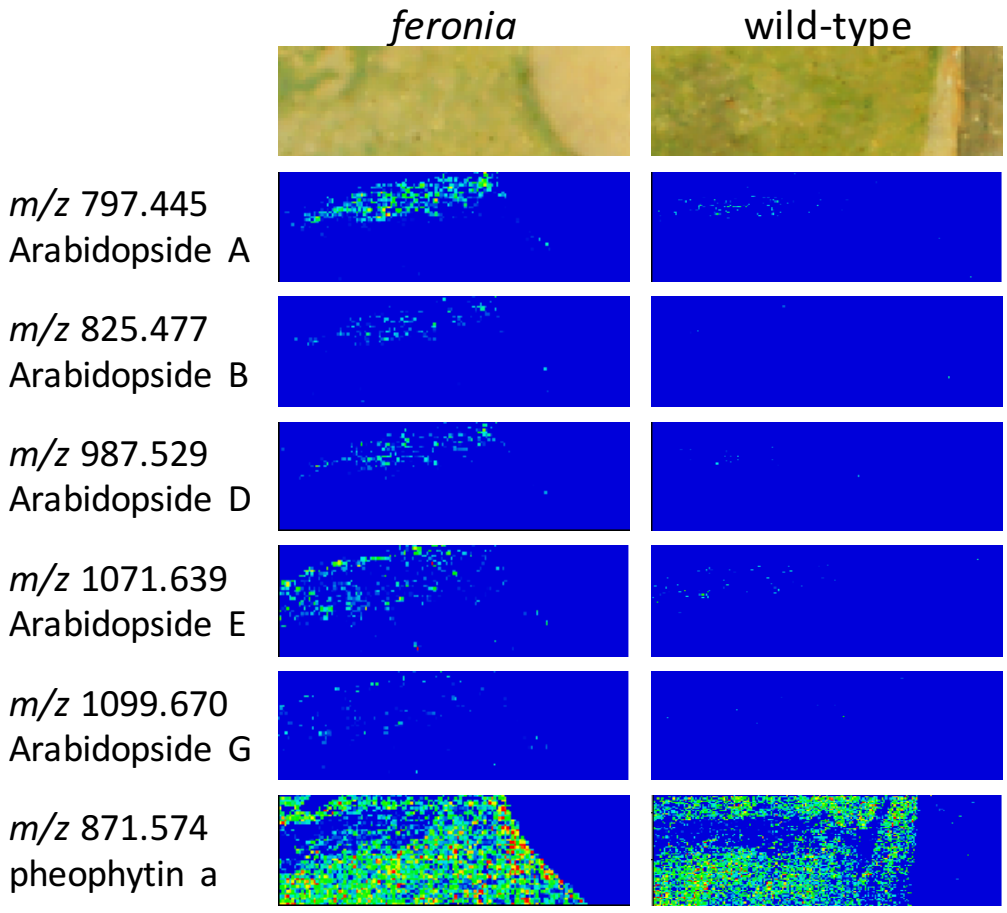

Figure AS8. Mass spectrometry images of Arabidopsides in fractured *fer* and wild-type leaves. The family of Arabidopside compounds show localizations in wounded areas. Samples were imaged at 30 μm spatial resolution using Fe_3O_4 nanoparticles as a matrix.

Table AS1A-D. Mass lists corresponding to the PMR volcano plot in Figure A1A for wild-type and *feronia* nonpolar leaf extracts in positive and negative modes. Colored m/z values correspond to colored circles in the volcano plot.

A: More Abundant in Wild-Type (+)

m/z	Fold Change	p-value
1255.298	125.6	1.86E-05
1256.292	82.37	3.78E-07
1200.211	46.49	0.000275
1199.356	33.36	0.000131
1199.208	33.17	0.001025
593.703	26.21	0.0008
1227.281	20.86	2.75E-06
1199.865	17.14	0.00026
1228.285	16.1	0.000168
593.665	15.83	0.00221
1198.870	14.41	2.40E-05
565.673	9.795	1.82E-05
593.620	8.533	0.001927
1199.049	7.934	0.002805
592.614	7.923	0.004911
564.589	7.846	0.005999
1200.042	7.653	0.002566
564.665	7.362	0.005502
1172.014	7.126	0.007877
592.696	6.912	0.004001
1255.902	6.422	0.008704
592.657	6.067	0.003443
592.736	6	0.00381
1255.097	5.86	0.000152
1257.273	5.112	5.08E-05
564.629	4.757	0.004674
620.738	4.272	0.007156
685.477	4.211	0.009542
537.567	4.193	0.009185
592.774	4.064	0.009781
537.603	3.711	0.00909
537.634	3.688	0.008408
537.667	3.671	0.008405
967.987	3.394	0.000503
594.713	3.333	0.001307
268.323	3.258	0.007743
621.744	3.22	0.003504
536.530	3.114	0.006691
592.576	3.114	0.008782
509.581	2.996	0.000523
915.594	2.698	0.002491
911.932	2.405	0.008129
649.781	2.339	0.002953
536.564	2.163	0.00656
300.285	2.157	0.00853
916.593	2.144	0.001286
536.598	2.136	0.007052
648.504	2.063	0.001657
939.955	2.056	0.008154
1061.755	2.017	0.003029
1057.825	1.947	3.81E-05

B: More Abundant in *feronia* (+)

m/z	Fold Change	p-value
797.445	71.11	0.001827
798.499	48.03	0.000848
825.477	31.3	0.006665
813.471	25.32	0.005377
797.419	23.13	0.000316
797.568	20.14	0.000368
814.479	9.12	0.004178
593.303	8.815	0.001695
502.270	7.873	0.006919
799.503	6.042	0.006257
1116.707	2.774	0.00034
623.513	2.328	0.004517
538.543	2.294	0.004504
539.548	2.25	0.00091
622.506	2.107	0.000875

Table AS1 (continued)

C: More Abundant in Wild-Type (-)

m/z	Fold Change	p-value
374.242	12.62	0.000621
420.248	7.852	0.002239
375.245	6.233	0.009256
815.485	5.344	0.009913
938.532	4.144	0.001534
815.523	3.829	0.007508
951.504	3.304	0.006983
667.448	2.715	0.00464
939.516	2.537	0.004673
1079.702	2.502	0.000234
1844.715	2.267	0.005241
952.486	2.261	0.004543
1080.699	2.175	0.004741

D: More Abundant in *feronia* (-)

m/z	Fold Change	p-value
847.483	79.23	0.002719
1009.537	69.45	0.001224
1010.536	46.3	1.65E-05
820.446	37.3	0.006509
821.456	36.35	0.000377
848.483	35.26	0.000699
887.444	28.25	0.001258
755.442	12.48	0.000343
836.463	9.376	0.003806
719.384	9.331	0.007214
837.462	8.803	0.002531
809.431	8.112	0.001359
1077.559	7.841	0.000765
865.453	6.143	0.000333
1011.564	5.728	0.001716
757.432	5.476	0.000354
1078.571	5.4	0.000443
849.502	5.322	0.005512
1011.494	5.318	0.000401
757.472	5.067	4.22E-05
756.456	4.649	3.86E-05
756.417	4.528	0.000562
819.199	4.42	0.000375
822.475	4.374	0.006913
720.410	4.127	0.000252
739.426	3.776	0.000894
735.361	3.665	0.009314
720.377	3.578	0.000181
773.463	3.35	0.00145
973.599	3.229	6.06E-05
974.607	2.906	0.002565
838.482	2.898	0.002534
865.395	2.641	0.00381
829.442	2.565	0.003856
845.492	2.54	0.00719
973.536	2.369	0.00107
830.498	2.321	0.007507
830.446	2.216	0.002178
853.476	2.073	0.009164